

## **Copyright Warning & Restrictions**

The copyright law of the United States (Title 17, United States Code) governs the making of photocopies or other reproductions of copyrighted material.

Under certain conditions specified in the law, libraries and archives are authorized to furnish a photocopy or other reproduction. One of these specified conditions is that the photocopy or reproduction is not to be “used for any purpose other than private study, scholarship, or research.” If a user makes a request for, or later uses, a photocopy or reproduction for purposes in excess of “fair use” that user may be liable for copyright infringement,

This institution reserves the right to refuse to accept a copying order if, in its judgment, fulfillment of the order would involve violation of copyright law.

**Please Note: The author retains the copyright while the New Jersey Institute of Technology reserves the right to distribute this thesis or dissertation**

Printing note: If you do not wish to print this page, then select “Pages from: first page # to: last page #” on the print dialog screen

The Van Houten library has removed some of the personal information and all signatures from the approval page and biographical sketches of theses and dissertations in order to protect the identity of NJIT graduates and faculty.

66-11,393

EISENBERG, Lawrence, 1933-  
DESIGN OF FEEDBACK CONTROL SYSTEMS WITH  
TRANSPORT LAG BY PARAMETER PLANE TECHNIQUES.

Newark College of Engineering, D. Eng., Sc., 1966  
Engineering, electrical

University Microfilms, Inc., Ann Arbor, Michigan

DESIGN OF FEEDBACK CONTROL SYSTEMS WITH TRANSPORT  
LAG BY PARAMETER PLANE TECHNIQUES

BY

LAWRENCE EISENBERG

A DISSERTATION  
PRESENTED IN PARTIAL FULFILLMENT OF  
THE REQUIREMENTS FOR THE DEGREE  
OF  
DOCTOR OF ENGINEERING SCIENCE  
ELECTRICAL ENGINEERING  
AT  
NEWARK COLLEGE OF ENGINEERING

This dissertation is to be used only with due regard to the rights of the author. Bibliographical references may be noted, but passages must not be copied without permission of the College and without credit being given in subsequent written or published work.

Newark, New Jersey

1966

## ABSTRACT

A method is presented for the exact determination of absolute and relative stability of linear feedback control systems containing transport or distributed lag. All results are in terms of two variable system parameters. The method utilizes an extension of modern parameter plane techniques that allows for the inclusion of transcendental functions in the system characteristic equation. The design of controllers in linear systems containing transport lag is then considered. A design technique is proposed that allows for the systematic determination of two variable controller parameters in order to meet frequency or time domain design specifications.

The design technique is formulated in terms of the familiar "dominant root" concept for systems that do *not* contain transport lag. The proposed design technique gives the system designer "at least" as much control over the system response as conventional design procedures for systems without transport lag.

The investigation of absolute and relative stability, as well as the proposed method for controller design, is no more complicated for multiloop feedback control systems than for single loop systems. This is because the characteristic equation of the closed-loop system transfer function is utilized rather than the conventional open-loop methods. Further, if a digital computer is used, high-order systems are dealt with as easily as low-order systems.

A method of constructing the root-locus of systems containing transport lag is then proposed so that this familiar engineering tool can be utilized in conjunction with the proposed analysis and design technique.

Finally, nonlinear systems containing transport lag are considered where describing function analysis is applicable. It is shown that the amplitude and frequency of limit cycles can be predicted where the describing function is real and is dependent upon the amplitude of the input signal to the nonlinearity.

APPROVAL OF DISSERTATION  
DESIGN OF FEEDBACK CONTROL SYSTEMS WITH TRANSPORT  
LAG BY PARAMETER PLANE TECHNIQUES  
BY  
LAWRENCE EISENBERG  
FOR  
DEPARTMENT OF ELECTRICAL ENGINEERING  
NEWARK COLLEGE OF ENGINEERING

BY  
FACULTY COMMITTEE

APPROVED: \_\_\_\_\_ CHAIRMAN

\_\_\_\_\_  
\_\_\_\_\_  
\_\_\_\_\_

NEWARK, NEW JERSEY

JUNE, 1966

DEDICATION

To my wife Brenda for her patience, help and encouragement.



#### ACKNOWLEDGMENTS

The author is indebted to Dr. J. J. Padalino, Dr. F. A. Russell, Dr. P. Fox and Dr. P. Goodman for their helpful suggestions and encouragement.

The author is also indebted to the National Science Foundation for the Fellowship which helped to make this work a pleasurable and successful venture.

TABLE OF CONTENTS

CHAPTER	PAGE
1 THE PARAMETER PLANE . . . . .	1
1.1 Introduction. . . . .	1
1.2 Historical Development of the Parameter Plane . . . . .	3
2 REVIEW OF PARAMETER PLANE METHODS . . . . .	9
2.1 Vishnegradski Curves. . . . .	9
2.2 D-Partition Boundaries. . . . .	11
2.2.1 The Construction of Stability Regions in the Plane of One Parameter--Neimark's Technique. . . . .	12
2.2.2 The Construction of Stability Regions in the Plane of Two Parameters--Neimark's Technique. . . . .	14
2.3 Mitrović's Method . . . . .	17
2.4 The Generalized Mitrović's Method-Siljak's Method . . . . .	22
3 TRANSPORT LAG--CONVENTIONAL SOLUTIONS . . . . .	34
3.1 Introduction. . . . .	34
3.2 Approximation Techniques. . . . .	37
3.3 Nyquist Diagrams. . . . .	41
3.4 Bode Plots. . . . .	42
3.5 Root-Locus. . . . .	43
4 ABSOLUTE AND RELATIVE STABILITY OF SYSTEMS WITH TRANSPORT LAG . . . . .	59
4.1 Derivation of Parameter Plane Equations . . . . .	59

CHAPTER	PAGE
4.2 Distributed Lags. . . . .	66
4.3 Example of Absolute and Relative Stability of a Linear Feedback Control System . . . . .	66
4.4 Relative Stability with Respect to Finite Semicircular Regions. . . . .	73
4.5 Relative Stability with Respect to Constant Settling Time Lines . . . . .	75
4.6 Real Roots. . . . .	77
4.7 Real Root Boundaries. . . . .	80
5 CONTROLLER DESIGN FOR SYSTEMS WITH TRANSPORT LAG. . . . .	97
5.1 Introduction. . . . .	97
5.2 Controller Design for Systems with Transport Lag. . . . .	99
5.3 Integral-Proportional Controller. . . . .	101
5.4 Proportional Controller . . . . .	108
5.5 Derivative-Proportional Controller. . . . .	111
5.6 Tachometric Feedback Control. . . . .	120
6 ROOT-LOCUS FOR SYSTEMS WITH TRANSPORT LAG . . . . .	147
6.1 Introduction. . . . .	147
6.2 Complex Root-Locus. . . . .	148
6.3 Real Root-Locus . . . . .	151
7 NONLINEAR SYSTEMS . . . . .	162
7.1 Introduction. . . . .	162
7.2 Describing Functions. . . . .	163

CHAPTER	PAGE
7.3 Systems Containing a Single Nonlinearity with a Real Amplitude Dependent Describing Function. . .	166
8 CONCLUSIONS . . . . .	178
9 SUGGESTIONS FOR FUTURE INVESTIGATIONS . . . . .	180
APPENDIX I Tables of $T_k(\zeta)$ and $U_k(\zeta)$ . . . . .	184
APPENDIX II $\alpha$ - $\beta$ Curves for $\zeta = \pm 1$ . . . . .	185
APPENDIX III Constant Settling Time Lines. . . . .	189
APPENDIX IV Real Root Determination . . . . .	193
APPENDIX V Relationships Between Root Locations and System Response . . . . .	196
REFERENCES. . . . .	203

LIST OF FIGURES

FIGURE	PAGE
2.1.1 Vishnegradski Curve . . . . .	29
2.2.1 s-Plane Root Locations and the Coefficient Space. . . . .	30
2.2.2 D-Partition Boundaries. . . . .	31
2.3.1 Representation of the Characteristic Equation on the s-Plane . . . . .	32
2.3.2 $\alpha$ - $\beta$ Curve for $\zeta = 0$ Where $F(s) = s^3 + 5s^2 + \alpha s + \beta$ . . . . .	33
3.1.1 Distributed Parameter Transmission Lines. . . . .	48
3.1.2 Block Diagram of a Feedback Control System with Transport Lag. . . . .	49
3.2.1 Stability Diagram . . . . .	50
3.2.2 Impulse Response. . . . .	51
3.3.1 Nyquist Diagram of $G(s)\epsilon^{-sT} = K\epsilon^{-sT}/s(s + 1)$ . . . . .	52
3.4.1 Gain and Phase Curve for the Open-Loop Transfer Function $\epsilon^{-sT}/s(s + 1)$ . . . . .	53
3.5.1 The Root-Locus for $G(s) = K(s + 0.3)/s^2$ . . . . .	54
3.5.2 Phase-Angle Loci for $G(s) = K(s + 0.3)/s^2$ . . . . .	55
3.5.3 Transport Lag Phase-Angle Loci. . . . .	56
3.5.4 Construction of the Required Locus with Transport Lag . . . . .	57
3.5.5 Three Branches of the Required Locus with Transport Lag . . . . .	58
4.1.1 Control System with a Transport Lag . . . . .	83
4.1.2 s-Plane Contours. . . . .	84
4.3.1 Control System with Integral-Proportional Controller. . . . .	85

FIGURE	PAGE
4.3.2 $\alpha$ - $\beta$ Plot for $\zeta = 0$ , $T = 1$ sec. . . . .	86
4.3.3 $\alpha$ - $\beta$ Plot for $\zeta = 0.2$ , $T = 1$ sec. . . . .	87
4.3.4 Root Locations. . . . .	88
4.4.1 $\alpha$ - $\beta$ Plot for a Semicircle of Radius $\omega_n = 5$ rad./sec. . .	89
4.4.2 $\alpha$ - $\beta$ Plot for a Semicircle of Radius $\omega_n = 10$ rad./sec. . .	90
4.4.3 Fundamental, Secondary and Real Root-Loci . . . . .	91
4.5.1 $\alpha$ - $\beta$ Plot for a Constant Settling Time Contour of $\sigma = -0.5$	92
4.6.1 $\alpha$ - $\beta$ Plot for Lines of Constant $\sigma$ . . . . .	93
4.6.2 $\alpha$ - $\beta$ Plot for $\zeta = \pm 1$ , $T = 1$ sec. . . . .	94
4.7.1 $\alpha$ - $\beta$ Plot for $\zeta = -1$ , $T = 1$ sec. . . . .	95
4.7.2 $\alpha$ - $\beta$ Plot for $\zeta = 0$ and $\zeta = -1$ , $T = 1$ sec. . . . .	96
5.1.1 The Desired Response. . . . .	123
5.1.2 Pattern of Root-Zero Configuration of the Desired Response	124
5.3.1 Integral-Proportional Control . . . . .	125
5.3.2 $\alpha$ - $\beta$ Plot for $\zeta = 0.3$ (First Quadrant). . . . .	126
5.3.3 $\alpha$ - $\beta$ Plot for $0 \leq \zeta \leq 1$ (First Traversal). . . . .	127
5.3.4 $\alpha$ - $\beta$ Plot for $0 \leq \zeta \leq 0.5$ (Second Traversal) . . . . .	128
5.3.5 $\alpha$ - $\beta$ Plot for $0.1 \leq \zeta \leq 0.3$ (Third Traversal). . . . .	129
5.3.6 $\alpha$ - $\beta$ Plot for a Constant Settling Time Line of $\sigma = -2.5$ . .	130
5.3.7 $\alpha$ - $\beta$ Plot for $\zeta = \pm 1$ . . . . .	131
5.3.8 $\alpha$ - $\beta$ Plot for Lines of Constant $\sigma$ . . . . .	132
5.3.9 Root-Zero Locations . . . . .	133
5.3.10 Output Response Curves. . . . .	134
5.4.1 Proportional Controller . . . . .	135

FIGURE	PAGE
5.5.1 Derivative-Proportional Controller. . . . .	136
5.5.2 $\alpha$ - $\beta$ Plot for $0 \leq \zeta \leq 0.9$ (First Traversal). . . . .	137
5.5.3 $\alpha$ - $\beta$ Plot for $0 \leq \zeta \leq 0.35$ (Second Traversal). . . . .	138
5.5.4 $\alpha$ - $\beta$ Plot for $0 \leq \zeta \leq 0.3$ (Third Traversal). . . . .	139
5.5.5 $\alpha$ - $\beta$ Plot for $\zeta = \pm 1$ . . . . .	140
5.5.6 $\alpha$ - $\beta$ Plot for Lines of Constant $\sigma$ . . . . .	141
5.5.7 $\alpha$ - $\beta$ Plot for $\zeta = 0.5$ (First Quadrant) . . . . .	142
5.5.8 $\alpha$ - $\beta$ Plot for a Constant Settling Time Contour of $\sigma = -2.25$ . . . . .	143
5.5.9 Root-Zero Locations . . . . .	144
5.5.10 Output Response Curves. . . . .	145
5.6.1 Tachometric Feedback Control System . . . . .	146
6.2.1 Feedback Control System . . . . .	153
6.2.2 $\alpha$ - $\beta$ Plot for $\zeta = +0.35$ . . . . .	154
6.2.3 $\alpha$ - $\beta$ Plot for $\zeta = -0.35$ . . . . .	155
6.2.4 $\alpha$ - $\beta$ Plot for $0 \leq \zeta \leq 0.9$ (First Traversal). . . . .	156
6.2.5 $\alpha$ - $\beta$ Plot for $0 \leq \zeta \leq 0.35$ (Second Traversal). . . . .	157
6.2.6 $\alpha$ - $\beta$ Plot for $-0.1 \leq \zeta \leq -0.7$ (First Traversal). . . . .	158
6.2.7 $\alpha$ - $\beta$ Plot for $-0.1 \leq \zeta \leq -0.4$ (Second Traversal) . . . . .	159
6.2.8 Root-Locus for $\tau = 0.5$ sec. . . . .	160
6.3.1 $\alpha$ - $\beta$ Plot for $\zeta = \pm 1$ . . . . .	161
7.3.1 A Nonlinear Feedback Control System with Transport Lag. . . . .	172
7.3.2 $\alpha$ - $\beta$ Plot for $\zeta = 0$ with Describing Function Loci. . . . .	173
7.3.3 Inverse Nyquist Plot and Describing Function Loci for $\tau = 0.227$ . . . . .	174

FIGURE	PAGE
7.3.4 Inverse Nyquist Plot and Describing Function Loci for $\tau = 0.1314$ . . . . .	175
7.3.5 Input Waveform to the Nonlinearity for $\tau = 0.227$ and Disturbance $\frac{X}{D} = 1.5$ . . . . .	176
7.3.6 Steady State Input Waveform to the Nonlinearity for $\tau = 0.227$ and Disturbance $\frac{X}{D} = 3$ and $10$ . . . . .	177
9.1 Comparison of a High-Order System Response to a Second-Order Response with Transport Lag. . . . .	182
9.2 Predictor Method of Control . . . . .	183



LIST OF SYMBOLS

SYMBOL	DEFINITION	PAGE OF FIRST APPEARANCE
$A_n$	Fourier coefficient . . . . .	165
$B_n$	Fourier coefficient . . . . .	165
$J$	Jacobian determinant. . . . .	64
$K$	System gain . . . . .	37
$M$	Peak overshoot. . . . .	112
$N$	Number of oscillations. . . . .	112
$N$	Describing function . . . . .	164
$T$	Delay time or lag . . . . .	35
$T_p$	Peak time . . . . .	112
$T_s$	Settling time . . . . .	112
$Y_1$	$\sqrt{A_1^2 + B_1^2}$ . . . . .	166
$s$	Complex variable ( $\sigma + j\omega$ ) . . . . .	1
$t$	Time. . . . .	35
$I_k(\zeta)$	Modified Mitrović function defined as $-\sqrt{1 - \zeta^2} \phi_k(\zeta)$ . . . . .	23
$P_k(\sigma, \omega_n^2)$	Modified Chebyshev function defined as $(-1)^k \omega_n^k T_k(\zeta)$ . . . . .	189
$Q_k(\sigma, \omega_n^2)$	Modified Chebyshev function defined as $(-1)^{k+1} \omega_n^{k-1} U_k(\zeta)$ . . . . .	189
$R_k(\zeta)$	Modified Mitrović function defined as $\phi_{k-1}(\zeta) + \zeta \phi_k(\zeta)$ . . . . .	23
$T_k(\zeta)$	Chebyshev function of the first kind. . . . .	26

SYMBOL	DEFINITION	PAGE OF FIRST APPEARANCE
$U_k(\zeta)$	Chebyshev function of the second kind . . . . .	26
$\alpha$	Variable system parameter . . . . .	10
$\beta$	Variable system parameter . . . . .	10
$\gamma$	$\tan^{-1} \left( \frac{A_1}{B_1} \right)$ . . . . .	166
$\zeta$	Dimensionless damping ratio . . . . .	19
$\theta$	Defined as $\omega_n \sqrt{1 - \zeta^2} T$ . . . . .	20
$\phi$	Phase angle . . . . .	62
$\sigma$	Defined as $-\zeta \omega_n$ . . . . .	47
$\tau$	System time constant. . . . .	37
$\omega$	Defined as $\omega_n \sqrt{1 - \zeta^2}$ or the natural frequency	13
$\omega_n$	Undamped natural frequency. . . . .	19
$\bar{\theta}$	Defined as $\text{Im} [\sqrt{sT}]$ . . . . .	66
$\bar{\phi}$	Defined as $\text{Re} [\sqrt{sT}]$ . . . . .	66
$\phi(\zeta)$	Mitrović function . . . . .	21
$\Delta$	System determinant. . . . .	16

## CHAPTER 1

### THE PARAMETER PLANE

#### 1.1 Introduction

The object of this work is to develop a systematic design and analysis technique for feedback control systems whose transfer functions contain transcendental functions. Transcendental functions appear in all feedback control systems that, for one reason or another, exhibit the phenomenon of a pure time lag somewhere between the input and the output of the system. The transcendental function,  $\epsilon^{-sT}$  in the case of transport lag and  $\epsilon^{-\sqrt{s}T}$  for distributed lag, generates an infinite number of roots in the characteristic equation of the system transfer function thereby making it extremely unwieldy to analyze. An analog simulation of the system is difficult since the transcendental function can, at best, only be approximated by using a Padé approximation or some analogous representation. Frequency domain approaches via the Nyquist criterion are *one* parameter techniques and only information with respect to absolute stability is obtained.

Work has been performed by many researchers [3, 21, 23, 27] in connection with the absolute stability of second-order and third-order control systems with transport lags for systems containing *one* free parameter. Y. Chu [2] has presented a phase-angle loci method that can be used on systems with *one* free parameter, usually the gain, as in the normal root-locus method. However, Chu's method becomes

increasingly difficult for higher order systems, as do all root-locus methods, since the determination of the root-locus is accomplished by first determining the phase-angle loci for all angles, not merely for the angle  $-180^\circ$ .

In this work a method is presented for analyzing systems with transport lag or distributed lag in terms of *two* free parameters where high-order systems are dealt with as easily as low-order systems. This two parameter method is first used to formulate a systematic technique for the investigation of *relative* stability as well as *absolute* stability of linear feedback control systems. Next a formal technique for the design of controllers is proposed. The method is then used to yield a new method for determining the root-locus for systems containing transport lag. Finally, the existence of limit cycles in nonlinear systems is examined where describing function analysis is applicable.

The basic approach is the parameter plane representation of the characteristic equation of the system transfer function as introduced by Mitrović [16] and generalized by Siljak [25, 26]. This method deviates from Siljak's by representing the coefficients of the characteristic equation in a new manner in order to incorporate transcendental functions into the equation. The result is a useful technique for the investigation of linear and nonlinear feedback systems containing transport or distributed lag.

## 1.2 Historical Development of the Parameter Plane

A general and straightforward method for factoring polynomials has been long recognized as a central problem in feedback control theory. This is true since an interpretation of control systems design as an adjustment of the root locations of the relevant characteristic equations permits the designer to readily obtain information about, and control over, the system stability and other pertinent characteristics of the system responses. However, in all but the simplest systems, difficulties arise due to the absence of an explicit correlation between the root locations and the adjustable parameters that appear in the coefficients of the characteristic equation.

From the classical point of view, a central problem of linear feedback control theory could be identified as the stability problem. Numerous criteria [9, 12, 16, 18, 19, 20, 24, 25] have been developed for investigations of absolute, as well as relative, stability of linear control systems. On the basis of these criteria, it is possible to design control systems for dynamic performance specified by a certain degree of stability. However, the stability criteria do not constitute a complete and satisfactory theory for the design of control systems. This is because in a wide variety of control problems, the designer is interested not only in the stability of the system, but also in numerous other essential features of the system response. Thus, in control theory there has been a strong emphasis on the development of refined techniques for the analysis and synthesis

of control systems in terms of the system response to typical or test input signals.

In general, there are three approaches to the synthesis and analysis of linear control systems: frequency characteristics, algebraic domain, and integral criteria. In synthesizing control systems each of these approaches has certain advantages and disadvantages, and the proper approach should be chosen depending upon the nature of the control problem and specifications which must be satisfied. Thus, the integral criteria [29] are particularly suitable for investigations of the statistical properties of control systems, while the frequency and algebraic domain approaches are more convenient for the synthesis of control systems excited by deterministic input signals.

The frequency domain approach which is based upon the work of Nyquist [20], Bode [1], and Nichols [29], permits the designer to modify, in a simple manner, the open-loop system in order to obtain appropriate closed-loop frequency characteristics. However, at the very outset of the design, the complex variable  $s$  is replaced by its imaginary part  $j\omega$ , and the entire  $s$ -plane is, in effect, reduced to the imaginary axis. Therefore, only unwieldy relationships exist between the frequency and transient responses. For example, the time-domain characteristics such as the overshoot, the rise time, the settling time, etc., can hardly be recognized from frequency characteristics such as the bandwidth, the zero frequency behavior, etc. Moreover, the frequency response tech-

niques are not suitable for the design of multiloop control systems, particularly in the cases when a system has more than one adjustable parameter.

Since the correlation between the frequency and transient responses is absolutely essential in the vast majority of control systems, the Laplace transform with the concept of complex frequency  $s$  has become a powerful mathematical tool in the analysis and synthesis of feedback controls. One direct consequence of the Laplace transform applications has been a strong effort on the development of synthesis techniques in the algebraic domain where the characteristics of both the transient and the frequency responses are evident.

The term "algebraic domain" is fundamentally the modern "pole-zero" approach to linear automatic control systems. However, a pertinent distinction should be made between the voluminous works produced in this country, where root-locus techniques are generally employed, and the European investigations where a slightly different approach has been largely utilized in the investigation of parameter variations. The root-locus method is basically a one parameter variation method where the *open-loop* system is the basis for analysis and synthesis. In eastern Europe the *closed-loop* system is the basic structure where one or two variable parameters may appear in many or all of the coefficients. That is, the emphasis has been upon the investigation of the *characteristic equation* of the *closed-loop* system with respect to parameter variations.

The idea of investigating the transient response of feedback control systems in the closed-loop algebraic domain was first introduced by Vishnegradski [30]. Vishnegradski assumed that the two middle coefficients of the characteristic equation of a third-order system could be considered as variables. In the plane of the variable coefficients, a diagram was plotted which enabled the determination of these coefficients with respect to both the stability and the nature of the system transient response.

An extension of Vishnegradski's work was presented in 1948 by Neimark [18] in his D-partition method for the stability analysis of control systems. By utilizing this procedure, the designer may assume two system parameters, which appear linearly in the coefficients of the  $n^{\text{th}}$  order characteristic equation, to be variables. Then, the mapping of the imaginary axis of the  $s$ -plane onto the plane of the variable parameters (or the parameter plane) permits the designer to determine the number of left-hand-plane roots of the characteristic equation. Attempts to apply the D-partition method to the design of control systems in terms of transient response generate difficulties since the method essentially belongs to frequency response techniques. By applying the D-partition method, the designer is unable to obtain information about, or control over, the root locations of the characteristic equation. See Polack [22] for a comprehensive discussion and proof of this technique.

In 1948, Evans [7] presented his root-locus technique for the synthesis of control systems in the  $s$ -plane. The root-locus technique readily provides information about all the roots of the characteristic



equation and permits a simple numerical evaluation of these roots for different values of the open-loop gain and, usually less simply, for other single variable parameters. Applying the full potential of the Laplace Transform, the procedure proposed by Evans admits control over both the time-domain and the frequency domain characteristics. However, the root-locus method has two significant limitations: First, it is basically a one parameter method, and second, it makes the synthesis of multiloop systems inconvenient in much the same manner as do the frequency response techniques. Thus the root-locus method suffers from the same difficulties experienced in applying frequency response techniques to the design of multiloop structures with more than one adjustable parameter.

The algebraic problem of control system synthesis was partially solved by Mitrović [16] in 1958. Mitrović's method designates that the first two coefficients of an  $n^{\text{th}}$  order characteristic equation may be considered as variables. Then, by a proposed graphical procedure, which utilizes the concept of a parameter plane, the variable coefficients are chosen so that the characteristic equation has prescribed root values. Hence, this method permits the design to be guided by the behavior of both transient and frequency responses. Limitations of the method arise due to the fact that only the first two coefficients representing two parameters may be considered as variables. Unfortunately, the adjustable system parameters frequently appear in more than two coefficients of the characteristic equation. In such cases, by

applying Mitrović's method, it is not possible to adjust the system parameters without the applications of approximations, limitations and transformations.

In 1964 Siljak [25] generalized Mitrović's method to the point where two variable parameters could appear linearly in *any two* coefficients of the characteristic equation. A second generalized Mitrović's method was proposed by Siljak in 1964 [26] that greatly increased the effectiveness of the parameter plane techniques. This second generalized method allows two variable system parameters to appear linearly in *all* the coefficients of an  $n^{\text{th}}$  order characteristic equation, eliminating a fundamental disadvantage in Mitrović's method. Further, the introduction of Chebyshev functions in this work greatly simplifies the proposed procedure and makes simulation more convenient on both analog and digital computers.

## CHAPTER 2

### REVIEW OF PARAMETER PLANE METHODS

#### 2.1 Vishnegradski Curve

A detailed discussion of the concept of the parameter plane logically begins with the work of Vishnegradski. I. A. Vishnegradski [30] considered the general third order characteristic equation of the form  $Z^3 + \alpha Z^2 + \beta Z + 1 = 0$ , and, in the co-ordinate system of the parameters  $\alpha$  and  $\beta$ , plotted curves which divide the plane into stable and unstable regions. The parameters  $\alpha$  and  $\beta$  are functions of the coefficients of the equation and are known as the Vishnegradski parameters and the curves mentioned above are called the Vishnegradski curves. In general, a cubic equation can be reduced to a form in which it depends on the parameters  $\alpha$  and  $\beta$ . This is shown as follows, consider a third order equation,

$$F(s) = a_0 s^3 + a_1 s^2 + a_2 s + a_3 = 0 \quad (2.1.1)$$

Dividing the whole equation by  $a_3$  and introducing the notation,

$$b_0 = \frac{a_0}{a_3}, \quad b_1 = \frac{a_1}{a_3}, \quad b_2 = \frac{a_2}{a_3} \quad (2.1.2)$$

gives,

$$F(s) = b_0 s^3 + b_1 s^2 + b_2 s + 1 = 0 \quad (2.1.3)$$

Carrying out the following substitution of variables,

$$s = \frac{Z}{\sqrt[3]{b_0}} \quad (2.1.4)$$

gives

$$F(Z) = Z^3 + \frac{b_1}{\sqrt[3]{b_0^2}} Z^2 + \frac{b_2}{\sqrt[3]{b_0}} Z + 1 = 0 \quad (2.1.5)$$

Defining

$$\frac{b_1}{\sqrt[3]{b_0^2}} = \alpha, \quad \frac{b_2}{\sqrt[3]{b_0}} = \beta \quad (2.1.6)$$

and substituting (2.1.6) into (2.1.5) gives the Vishnegradski form

$$F(Z) = Z^3 + \alpha Z^2 + \beta Z + 1 \quad (2.1.7)$$

If  $\alpha > 0$  and  $\beta > 0$ , the Routh-Hurwitz criterion gives the stability conditions for equation (2.1.7) to be

$$\alpha\beta - 1 > 0 \quad (2.1.8)$$

The equation of the stability boundary is obtained if, instead of the inequality sign in (2.1.8), the equality sign is introduced, whence

$$\alpha\beta = 1 \quad (2.1.9)$$

This is the equation of a hyperbola, which divides the  $\alpha$ - $\beta$  plane into the stable and unstable regions, and was the starting point for the parameter plane concept. The Vishnegradski curve is shown in Figure 2.1.1, where the regions of stability and instability are easily determined from the inequality of equation (2.1.8).

## 2.2 D<sup>1</sup>-Partition Boundaries

The concept of D-partition boundaries was formulated by Neimark [18] and, as will be seen, is the basis for modern parameter plane techniques. Consider the general characteristic equation.

$$F(s) = a_n s^n + a_{n-1} s^{n-1} + \dots + a_1 s + a_0 = 0 \quad (2.2.1)$$

The aggregate of values  $a_0, a_1, a_2, \dots, a_n$  may be interpreted geometrically as a point in an  $(n+1)$ -dimensional space. To each point of this space there correspond definite values of the coefficients and consequently definite values of the roots  $s_1, s_2, s_3, \dots, s_n$  of the characteristic equation. Thus, if a region,  $R$ , exists in this space such that all the roots of (2.2.1) lie to the left of the imaginary axis in the  $s$ -plane, then the hypersurface bounding  $R$  is called the *boundary of the region of stability*. When there are only two independent coefficients, this region is bounded by a plane; when there are three, by a three-dimensional surface, etc.

Since the coefficients,  $a_k$ , are functions of the system parameters, such as gains and time constants, stability regions can be plotted in terms of these system parameters. For example, consider a characteristic equation in which all the coefficients except  $a_0$  and  $a_n$  are known. Suppose that for some definite values of  $a_0$  and  $a_n$  the characteristic

---

<sup>1</sup>The symbol  $D$  represents the usual operational notation of differential equations, i.e.,  $d/dt$  or  $s$ .

equation has  $k$  roots lying to the left and  $n-k$  roots lying to the right of the imaginary axis in the  $s$ -plane (see Figure 2.2.1a). It follows that there is a curve on the  $a_0$ - $a_n$  plane that bounds a region in which each point defines a polynomial also having  $k$  roots lying to the left and  $n-k$  roots to the right of the imaginary axis (see Figure 2.2.1b). Neimark denoted this region by  $D(k,n-k)$  where, for example, if (2.2.1) is of third order ( $n=3$ ), then in general the regions  $D(0,3)$ ,  $D(1,2)$ ,  $D(2,1)$  and  $D(3,0)$  can be found in the  $a_0$ - $a_n$  plane. The region  $D(3,0)$  is the region of stability in the  $a_0$ - $a_n$  plane. The partition of the  $a_0$ - $a_n$  plane of (2.2.1) into regions corresponding to the same number of roots lying to the left of the imaginary axis is called the  $D$ -partition.

It is obvious that the imaginary axis of the  $s$ -plane is the reflection of the boundary of the  $D$ -partition, and the crossing of the latter in the  $a_0$ - $a_n$  plane is represented by the roots in the  $s$ -plane crossing the imaginary axis. This suggests the method for determining the  $D$ -partition boundary: its equation is found in parametric form by replacing  $s$  by  $j\omega$  in the given polynomial (where  $\omega$  is the variable). From this equation the boundary may be constructed by varying  $\omega$  from  $-\infty$  to  $+\infty$ .

2.2.1 The construction of stability regions in the plane of one parameter--Neimark's technique. Define  $\alpha$  to be a complex parameter whose value is varied in order to investigate stability and assume that the characteristic equation can be reduced to the form

$$Q(s) + \alpha R(s) = 0 \text{ or } \alpha = -\frac{Q(s)}{R(s)} \quad (2.2.2)$$

Thus, for example, in the case of the equation

$$s^2 + s + \alpha = 0 \quad (2.2.3)$$

it follows that

$$Q(s) = s^2 + s, \quad R(s) = 1 \quad (2.2.4)$$

Only real values of  $\alpha$  have any practical value. However, for now assume that  $\alpha$  is complex and transform the imaginary axis in the  $s$ -plane into the  $\alpha$ -plane. To do this set  $s=j\omega$  in (2.2.2) giving

$$\alpha(j\omega) = -\frac{Q(j\omega)}{R(j\omega)} \quad (2.2.5)$$

Separating real and imaginary parts gives

$$\alpha(j\omega) = u(\omega) + jv(\omega) \quad (2.2.6)$$

By giving  $\omega$  values from  $-\infty$  to  $+\infty$  a curve is constructed which is the transformation of the imaginary axis of the  $s$ -plane on the  $\alpha$ -plane, i.e. the boundary of the D-partition in the  $\alpha$ -plane.

If  $\omega$  varies from  $-\infty$  to  $+\infty$  in the  $s$ -plane (Figure 2.2.2a) then the region of stability will always be on the left (the shaded side of Figure 2.2.2a). Since the mapping is conformal, the region to the left in the  $s$ -plane maps into the region in the  $\alpha$ -plane that is to the left of the D-partition when  $\omega$  varies from  $-\infty$  to  $+\infty$ . Thus, proceeding along

the boundary curve of the D-partition from the point corresponding to  $\omega = -\infty$  to the point corresponding to  $\omega = +\infty$ , the curve is shaded on the left (Figure 2.2.2b). If  $\alpha$  takes on a series of values such that the boundary of the D-partition in the  $\alpha$ -plane is crossed from the shaded to the unshaded side, then in the  $s$ -plane one root has crossed the imaginary axis, passing from the left-hand plane to the right-hand plane.

Thus it is sufficient to know the distribution of the roots relative to the imaginary axis for any one arbitrary value of  $\alpha$  ( $\alpha$  is usually set to zero for this determination) in order to determine the distribution for any other value of  $\alpha$ .

2.2.2 The construction of stability regions in the plane of two parameters--Neimark's Technique. Neimark extended his technique discussed in the previous section to account for the variation of two system parameters [13]. Since this is basically an extension of Vishnegradski's method, the resulting curves are called the generalized Vishnegradski diagrams. A Vishnegradski diagram is a plane of any two real parameters of a system in which the lines separating the region of stability are plotted. The Vishnegradski diagram may thus be obtained by constructing the D-partition of the plane of two parameters.

Suppose that the coefficients of the characteristic equation (2.2.1) of the system depend on two parameters,  $\alpha$  and  $\beta$ , and further assume that the parameters enter into the equation linearly, so that



this equation can be reduced to the form

$$\alpha Q(s) + \beta P(s) + R(s) = 0 \quad (2.2.7)$$

For example, the equation

$$(\alpha s + 1)(5s + 1) + 3\beta = 0 \quad (2.2.8)$$

can be reduced to the form

$$\alpha(5s^2 + s) + 3\beta + (5s + 1) = 0 \quad (2.2.9)$$

So that in this case

$$\begin{aligned} Q(s) &= 5s^2 + s \\ P(s) &= 3 \\ R(s) &= 5s + 1 \end{aligned} \quad (2.2.10)$$

Further, substituting  $s = j\omega$  into (2.2.7) gives

$$\alpha Q(j\omega) + \beta P(j\omega) + R(j\omega) = 0 \quad (2.2.11)$$

Now denoting

$$\begin{aligned} Q(j\omega) &= Q_1(\omega) + jQ_2(\omega) \\ P(j\omega) &= P_1(\omega) + jP_2(\omega) \\ R(j\omega) &= R_1(\omega) + jR_2(\omega) \end{aligned} \quad (2.2.12)$$

equation (2.2.11) can be written in the following form

$$[\alpha Q_1(\omega) + \beta P_1(\omega) + R_1(\omega)] + j[\alpha Q_2(\omega) + \beta P_2(\omega) + R_2(\omega)] = 0 \quad (2.2.13)$$

This yields two equations for the determination of  $\alpha$  and  $\beta$  which satisfy equation (2.2.11), namely,

$$\begin{aligned}\alpha Q_1(\omega) + \beta P_1(\omega) + R_1(\omega) &= 0 \\ \alpha Q_2(\omega) + \beta P_2(\omega) + R_2(\omega) &= 0\end{aligned}\tag{2.2.14}$$

Solving equations (2.2.14) for  $\alpha$  and  $\beta$ , gives,<sup>2</sup>

$$\alpha = \frac{\begin{vmatrix} -R_1(\omega) & P_1(\omega) \\ -R_2(\omega) & P_2(\omega) \end{vmatrix}}{\begin{vmatrix} Q_1(\omega) & P_1(\omega) \\ Q_2(\omega) & P_2(\omega) \end{vmatrix}}, \quad \beta = \frac{\begin{vmatrix} Q_1(\omega) & -R_1(\omega) \\ Q_2(\omega) & -R_2(\omega) \end{vmatrix}}{\begin{vmatrix} Q_1(\omega) & P_1(\omega) \\ Q_2(\omega) & P_2(\omega) \end{vmatrix}}\tag{2.2.15}$$

Equations (2.2.14) are valid only for those values of  $\omega$  at which equations (2.2.14) remain linearly independent and compatible. See Reference 13 for a complete discussion of this point. The shading rule now involves the following procedure. For all  $\omega$  values, at which:

$$\Delta = \begin{vmatrix} Q_1(\omega) & P_1(\omega) \\ Q_2(\omega) & P_2(\omega) \end{vmatrix} > 0\tag{2.2.16}$$

the left-hand side of the boundary is shaded; when  $\Delta < 0$  the right-hand side of the boundary is shaded [13]. Hence, if  $\alpha$  or  $\beta$  takes on a

---

<sup>2</sup>It will become obvious that this manner of representing the variable parameters motivated much of the work of D. D. Siljak to be discussed below.

series of values such that the boundary of the D-partition in the  $\alpha$ - $\beta$  plane is crossed from a shaded side to an unshaded side, then in the s-plane one<sup>3</sup> root has crossed the imaginary axis from the left-hand-plane to the right-hand-plane. See Figure 4.3.2 for an example of an  $\alpha$ - $\beta$  plane.

Having obtained regions with an equal number of roots to the left of the imaginary axis, it is then necessary to establish whether a region of stability does or does not exist. This is accomplished by choosing an arbitrary point in a region and verifying the stability of the original equation in which the co-ordinates of the chosen points have been substituted for  $\alpha$  and  $\beta$ . This stability verification can be performed by using any one of the standard stability tests.

### 2.3 Mitrović's Method

Mitrović utilized the general concept of the parameter plane and the basic theorem of Cauchy. His contribution was to depart from the  $j\omega$  axis and move out into the entire s-plane. The method is explained as follows.<sup>4</sup> Consider the equation

---

<sup>3</sup>In most practical systems the  $\alpha$ - $\beta$  plot for negative values of  $\omega$  will lie directly over the plot for positive values of  $\omega$ . However, the sign of  $\Delta$  will usually be such that the shading of the plot will always be on the same side. The result is a doubly shaded plot indicating that two roots leave the left-hand s-plane when the D-partition is crossed from a shaded side to an unshaded side. This is the case when, for example, a pair of complex conjugate roots crosses the imaginary axis in the s-plane.

<sup>4</sup>This section follows Thaler's interpretation of Mitrović's work as presented in Chapter 10 of Reference 28.

$$F(s) = a_n s^n + a_{n-1} s^{n-1} + \dots + a_2 s^2 + a_1 s + a_0 = 0 \quad (2.3.1)$$

which may be considered the characteristic equation of a closed-loop system. Assume that all the roots are in the left-hand half of the  $s$ -plane so that equation (2.3.1) may be factored to give

$$F(s) = a_n (s + r_1)(s + r_2)(s + r_3) \dots (s + r_n) = 0 \quad (2.3.2)$$

Figure 2.3.1 shows a few of these roots plotted on the  $s$ -plane and indicates the vectors which represent the factors of equation (2.3.2). Note that in (2.3.2) the angle associated with  $F(s)$  is the sum of the angles of all the factors and is therefore the algebraic sum of all the angles associated with the vectors in Figure 2.3.1.

It is apparent that if the point  $s$  is allowed to move along any selected path, the angles of all the vectors will change as  $s$  moves. If any path is selected which is a closed path enclosing all the roots, then each of the vectors makes a complete revolution as  $s$  traverses this path. Assume counterclockwise movement of  $s$  along such a closed path; then the vectors rotate counterclockwise and the angle of  $F(s)$  goes through a total positive angle of  $n(2\pi)$ , where  $n$  is the number of roots encircled. In order to check absolute stability the selected contour of the  $s$ -plane must encircle the entire left-hand plane. Since the order of the equation is known to be  $n$ , the number of roots is also known to be  $n$  and the  $F(s)$  curve on the  $F(s)$  plane must encircle the origin  $n$  times if all the roots are enclosed by the contour. If there are fewer than  $n$  encirclements, some roots lie outside the contour,

which means they are in the right-hand half-plane, and the system is therefore absolutely unstable.

In a like manner the contour on the  $s$ -plane may follow a locus of constant  $\zeta \neq 0$  (radial lines on Figure 2.3.1) and close with a circular arc of very large radius (often infinity). Note that when the contour is the imaginary axis the value of  $\zeta$  is zero. A constant  $\zeta \neq 0$  contour does not enclose the entire left half of the  $s$ -plane, but may enclose all the roots, in which case the number of encirclements by the  $F(s)$  curve is once again the number  $n$ . In addition, if all the roots are thus enclosed, it guarantees that no roots have a value of  $\zeta$  less than the value specified by the mapping contour. If the selected contour on the  $s$ -plane passes through a root, then for that particular value of  $s$ ,  $F(s) = 0$ . This means that the polar plot on the  $F(s)$  plane must pass through the origin for such values. It should be noted that the contour on the  $s$ -plane for  $\zeta = 1.0$  is the negative real axis and must pass through all the negative real roots of  $F(s)$ .

The concept of mapping constant  $\zeta$  lines is the basic contribution of Mitrović's method and the algebraic manipulations arising out of this method are as follows. Let the contours selected for mapping be radial straight lines in the left-hand  $s$ -plane for any and all values of  $0 \leq \zeta \leq 1$ . Since the radial distance from the origin to any point on such a radial line is  $\omega_n$ , then the values of  $s$  which are to be substituted in  $F(s)$  in the process of mapping are given by

$$s = -\omega_n \sin\theta + j\omega_n \cos\theta = -\zeta\omega_n + j\omega_n\sqrt{1-\zeta^2} \quad (2.3.3)$$

where  $\theta$  is the angle of the line  $\zeta = \text{constant}$  (see Figure 2.3.1) and the values of  $s$  are in the second quadrant. Substituting equation (2.3.3) in equation (2.3.1),  $F(s)$  can be written in the following form.

$$F(s) = a_n\omega_n^n(-\zeta + j\sqrt{1-\zeta^2})^n + a_{n-1}\omega_n^{n-1}(-\zeta + j\sqrt{1-\zeta^2})^{n-1} + \dots \\ + a_2\omega_n^2(-\zeta + j\sqrt{1-\zeta^2})^2 + a_1\omega_n(-\zeta + j\sqrt{1-\zeta^2}) + a_0 = 0 \quad (2.3.4)$$

Mitrović designates that coefficients  $a_1$  and  $a_0$  be considered variables where by definition  $a_1$  is the  $\alpha$  and  $a_0$  is the  $\beta$  of Section 2.1.2.

If, for example, the characteristic equation is of sixth-order, equation (2.3.4) can be written as two simultaneous equations since the summation of the reals and imaginaries must go to zero independently. Solving these two equations for  $\alpha$  and  $\beta$  gives

$$\alpha = a_2\omega_n(2\zeta) + a_3\omega_n^2(1 - 4\zeta^2) + a_4\omega_n^3(-4\zeta + 8\zeta^3) \\ + a_5\omega_n^4(-1 + 12\zeta^2 - 16\zeta^4) + a_6\omega_n^5(6\zeta - 32\zeta^3 + 32\zeta^5) \quad (2.3.5)$$

$$\beta = a_2\omega_n^2 + a_3\omega_n^3(-2\zeta) + a_4\omega_n^4(-1 + 4\zeta^2) + a_5\omega_n^5(4\zeta - 8\zeta^3) \\ + a_6\omega_n^6(1 - 12\zeta^2 + 16\zeta^4) \quad (2.3.6)$$

The functions which appear in the coefficients do not depend on the order of the equation; i.e., for a fourth-order equation merely discard all the terms above the  $a_4$  terms, etc. This means that these

coefficients may be computed and tabulated for selected values of  $\zeta$ ; then the tables are used when applying this method. Furthermore, a general formula may be obtained for each coefficient so that the coefficients of high-order terms are readily obtained as needed. To obtain the formula for the coefficients, it is first desirable to rearrange (2.3.6) by factoring out  $-\omega_n^2$ :

$$\begin{aligned} \beta = & -\omega_n^2 [a_2(-1) + a_3\omega_n(2\zeta) + a_4\omega_n^2(1 - 4\zeta^2) \\ & + a_5\omega_n^3(-4\zeta + 8\zeta^3) + a_6\omega_n^4(-1 + 12\zeta^2 - 16\zeta^4)] \end{aligned} \quad (2.3.7)$$

Comparison of equation (2.3.7) with (2.3.5) shows that identical  $\zeta$  functions appear in both. Thus it is convenient to define

$$\left. \begin{aligned} \phi_0(\zeta) &= 0, & \phi_1(\zeta) &= -1, & \phi_2(\zeta) &= 2\zeta \\ \phi_3(\zeta) &= 1 - 4\zeta^2, & \phi_4(\zeta) &= -4\zeta + 8\zeta^3 \\ \phi_5(\zeta) &= -1 + 12\zeta^2 - 16\zeta^4 \end{aligned} \right\} \quad (2.3.8)$$

From equation (2.3.8) it is readily seen that each successive  $\phi(\zeta)$  may be obtained from the two preceding  $\phi(\zeta)$ 's, according to the general formula

$$\phi_k(\zeta) = - [2\zeta\phi_{k-1}(\zeta) + \phi_{k-2}(\zeta)] \quad \text{for } k \geq 2 \quad (2.3.9)$$

The equations for  $\alpha$  and  $\beta$  for application to any order equation are then:

$$\alpha = a_2 \omega_n \phi_2(\zeta) + a_3 \omega_n^2 \phi_3(\zeta) + a_4 \omega_n^3 \phi_4(\zeta) + \dots + a_n \omega_n^{n-1} \phi_n(\zeta) \quad (2.3.10)$$

$$\beta = -\omega_n^2 [a_2 \phi_1(\zeta) + a_3 \omega_n \phi_2(\zeta) + a_4 \omega_n^2 \phi_3(\zeta) + \dots + a_n \omega_n^{n-2} \phi_{n-1}(\zeta)] \quad (2.3.11)$$

Equations (2.3.10) are the fundamental tools in Mitrović's method. The characteristic equation to be analyzed is used only to read off the values of its coefficients, which are then substituted into equations (2.3.10) and (2.3.11). The value of  $\zeta$  is selected as desired;  $\phi_k(\zeta)$  values are read from a previously tabulated table of  $\phi_k(\zeta)$  functions and substituted into the equations. Thus all values in the equations are defined numerically except  $\alpha$ ,  $\beta$  and  $\omega_n$ , so it is a simple matter to insert a sequence of values of  $\omega_n$  and plot a curve of  $\alpha$  versus  $\beta$ . The points of the  $\alpha$ - $\beta$  curve define regions of absolute and relative stability in the  $\alpha$ - $\beta$  plane corresponding to regions of absolute and relative stability in the  $s$ -plane. Figure 2.3.2 shows a typical region of absolute stability for a given characteristic equation.

#### 2.4 The Generalized Mitrović's Method-Siljak's Method

In 1964, D. D. Siljak<sup>5</sup> extended Mitrović's method so that the variable parameters  $\alpha$  and  $\beta$  could appear as coefficients of *any* two terms of the system characteristic equation [25]. Thus, the limitation that only the coefficients  $a_0$  and  $a_1$  of the characteristic

---

<sup>5</sup>This section follows the derivation presented by Siljak in References 25 and 26.



equation be variable was removed. This work was then generalized once again by Siljak [26] in 1964 by developing a method whereby the two variable parameters  $\alpha$  and  $\beta$  could appear linearly in all the coefficients of the characteristic equation, i.e., for example in the form,

$$F(s) = (\alpha b_0 + \beta c_0 + d_0) + (\alpha b_1 + \beta c_1 + d_1)s + \dots + (\alpha b_n + \beta c_n + d_n)s^n = 0 \quad (2.4.1)$$

The first generalization proceeds as follows. Consider the characteristic equation

$$F(s) = \sum_{k=0}^n a_k s^k = 0 \quad (2.4.2)$$

Let  $s^k$  in the above equation be expressed as

$$s^k = \omega^k [R_k(\zeta) + jI_k(\zeta)] , \quad k = 0, 1, 2, \dots, n \quad (2.4.3)$$

where  $R_k(\zeta)$  and  $I_k(\zeta)$  are functions of  $\zeta$ . Then, by applying the conditions that the summation of reals and summation of imaginaries must go to zero independently, the characteristic equation may be rewritten as two simultaneous equations

$$\sum_{k=0}^n a_k \omega_n^k R_k(\zeta) = 0 \quad (2.4.4)$$

$$\sum_{k=0}^n a_k \omega_n^k I_k(\zeta) = 0$$

As shown in Reference 25, both the functions  $R_k(\zeta)$  and  $I_k(\zeta)$  can be expressed by the Mitrović's functions as follows

$$\begin{aligned} R_k(\zeta) &= \phi_{k-1}(\zeta) + \zeta\phi_k(\zeta) \\ I_k(\zeta) &= -\sqrt{1-\zeta^2} \phi_k(\zeta) \end{aligned} \quad (2.4.5)$$

Substituting (2.4.5) into (2.4.4), gives

$$\sum_{k=0}^n a_k \omega_n^k [\phi_{k-1}(\zeta) + \zeta\phi_k(\zeta)] = 0 \quad (2.4.6)$$

$$\sum_{k=0}^n a_k \omega_n^k \phi_k(\zeta) = 0$$

Combining the above equations gives

$$\sum_{k=0}^n a_k \omega_n^k \phi_{k-1}(\zeta) = 0 \quad (2.4.7)$$

$$\sum_{k=0}^n a_k \omega_n^k \phi_k(\zeta) = 0$$

These equations allow an *arbitrary* pair of coefficients to be considered variable. Now, select two coefficients  $a_p$  and  $a_q$  ( $n \geq p > q \geq 0$ ) and rewrite the equations (2.4.7) as

$$a_p \omega_n^p \phi_{p-1}(\zeta) + a_q \omega_n^q \phi_{q-1}(\zeta) = - \sum_{\substack{k=0 \\ k \neq p, q}}^n a_k \omega_n^k \phi_{k-1}(\zeta) \quad (2.4.8)$$

$$a_p \omega_n^p \phi_p(\zeta) + a_q \omega_n^q \phi_q(\zeta) = - \sum_{\substack{k=0 \\ k \neq p, q}}^n a_k \omega_n^k \phi_k(\zeta)$$

Considering the coefficients  $a_p$  and  $a_q$  in the above equations (2.4.8) as variables  $\alpha$  and  $\beta$  respectively, there remain two equations in two unknowns which may be solved for  $\alpha$  and  $\beta$ . (Note the similarity between the linear simultaneous equations (2.4.8) and the equations (2.2.14) proposed by Neimark in his D-partition method.) Solving equations (2.4.8) for  $\alpha$  and  $\beta$  gives

$$\alpha = \sum_{\substack{k=0 \\ k \neq p}}^n a_k \omega_n^{k-p} \frac{\phi_k(\zeta) \phi_{q-1}(\zeta) - \phi_{k-1}(\zeta) \phi_k(\zeta)}{\phi_q(\zeta) \phi_{p-1}(\zeta) - \phi_{q-1}(\zeta) \phi_p(\zeta)} \quad (2.4.9)$$

$$\beta = \sum_{\substack{k=0 \\ k \neq q}}^n a_k \omega_n^{k-q} \frac{\phi_k(\zeta) \phi_{p-1}(\zeta) - \phi_{k-1}(\zeta) \phi_p(\zeta)}{\phi_p(\zeta) \phi_{q-1}(\zeta) - \phi_q(\zeta) \phi_{p-1}(\zeta)}$$

The equations (2.4.9) may be further simplified. If the Mitrovič's functions  $\phi_k(\zeta)$  are defined for negative values of subscript  $k$  as

$$\phi_{-k}(\zeta) = -\phi_k(\zeta) \quad (2.4.10)$$

it can be proven that (see Reference 25)

$$\phi_i(\zeta) \phi_{j-1}(\zeta) - \phi_{i-1}(\zeta) \phi_j(\zeta) = \phi_{i-j}(\zeta) \quad (2.4.11)$$

for any integer values of  $i$  and  $j$ . The equations (2.4.9) may then be

rewritten as

$$\alpha = \frac{1}{\phi_{q-p}(\zeta)} \sum_{\substack{k=0 \\ k \neq p}}^n a_k \omega_n^{k-p} \phi_{k-q}(\zeta) \quad (2.4.12)$$

$$\beta = \frac{1}{\phi_{p-q}(\zeta)} \sum_{\substack{k=0 \\ k \neq q}}^n a_k \omega_n^{k-q} \phi_{k-p}(\zeta)$$

The generalized equations (2.4.12) represent the loci of points in the  $\alpha$ - $\beta$  plane with constant  $\zeta$  or  $\omega_n$  in the same sense as do the fundamental equations (2.3.5) for the specific case  $a_1 = \alpha$  and  $a_0 = \beta$ . Plotting of the aforementioned loci corresponding to the generalized case is similar to the plotting of the loci corresponding to the original Mitrović's method. Further, the application of the generalized method is the same as the application of Mitrović's method.

In 1964, Siljak further generalized Mitrović's method (the second generalized method) by showing that (2.4.3) could be expressed as [26]

$$s^k = \omega_n^k [T_k(-\zeta) + j\sqrt{1-\zeta^2} U_k(-\zeta)] \quad (2.4.13)$$

where

$$T_k(-\zeta) = (-1)^k T_k(\zeta) \quad \text{and} \quad U_k(-\zeta) = (-1)^{k+1} U_k(\zeta) \quad (2.4.14)$$

The  $T_k(\zeta)$  and  $U_k(\zeta)$  are Chebyshev functions of the first and the second kind, respectively. The argument  $\zeta$  of these functions is  $0 \leq |\zeta| \leq 1$ , but for stable systems  $0 \leq \zeta \leq 1$ . The functions  $T_k(\zeta)$  and  $U_k(\zeta)$  may be

obtained by applying the recurrence formulae

$$\begin{aligned} T_{k+1}(\zeta) - 2\zeta T_k(\zeta) + T_{k-1}(\zeta) &= 0 \\ U_{k+1}(\zeta) - 2\zeta U_k(\zeta) + U_{k-1}(\zeta) &= 0 \end{aligned} \quad (2.4.15)$$

with  $T_0(\zeta) = 1$ ,  $T_1(\zeta) = \zeta$ ,  $U_0(\zeta) = 0$ , and  $U_1(\zeta) = 1$ . Since the functions  $T_k(\zeta)$  and  $U_k(\zeta)$  play an important role in future developments, their numerical values for pertinent values of  $\zeta$  are given in Appendix I. Substituting (2.4.13) into (2.4.2), and then applying the condition that the summation of the reals and the summation of the imaginaries must go to zero independently, gives

$$\sum_{k=0}^n a_k \omega_n^k T_k(-\zeta) = 0 \quad (2.4.16)$$

$$\sum_{k=0}^n a_k \omega_n^k U_k(-\zeta) = 0$$

Now, consider the coefficients  $a_k$  to be linear functions of variable system parameters  $\alpha$  and  $\beta$  as follows

$$a_k = \alpha b_k + \beta c_k + d_k \quad (2.4.17)$$

Then equations (2.4.16) may be rewritten as

$$\alpha B_1(\zeta, \omega_n) + \beta C_1(\zeta, \omega_n) + D_1(\zeta, \omega_n) = 0 \quad (2.4.18)$$

$$\alpha B_2(\zeta, \omega_n) + \beta C_2(\zeta, \omega_n) + D_2(\zeta, \omega_n) = 0$$

where (omitting the arguments  $\zeta, \omega_n$ )

$$\begin{aligned}
 B_1 &= \sum_{k=0}^n (-1)^k b_k \omega_n^k U_{k-1}(\zeta) , & B_2 &= \sum_{k=0}^n (-1)^k b_k \omega_n^k U_k(\zeta) \\
 C_1 &= \sum_{k=0}^n (-1)^k c_k \omega_n^k U_{k-1}(\zeta) , & C_2 &= \sum_{k=0}^n (-1)^k c_k \omega_n^k U_k(\zeta) \\
 D_1 &= \sum_{k=0}^n (-1)^k d_k \omega_n^k U_{k-1}(\zeta) , & D_2 &= \sum_{k=0}^n (-1)^k d_k \omega_n^k U_k(\zeta)
 \end{aligned} \tag{2.4.19}$$

Equations (2.4.18) are simultaneous equation in two unknowns,  $\alpha$  and  $\beta$ , which may be solved thus:

$$\alpha = \frac{C_1 D_2 - C_2 D_1}{B_1 C_2 - B_2 C_1} , \quad \beta = \frac{B_2 D_1 - B_1 D_2}{B_1 C_2 - B_2 C_1} \tag{2.4.20}$$

The application of the second generalized method is identical to the original Mitrović's method. The second generalization, however, is the most useful since the variable parameters,  $\alpha$  and  $\beta$ , can appear in the coefficients of the characteristic equation in the least restrictive manner (see equation (2.4.17)).

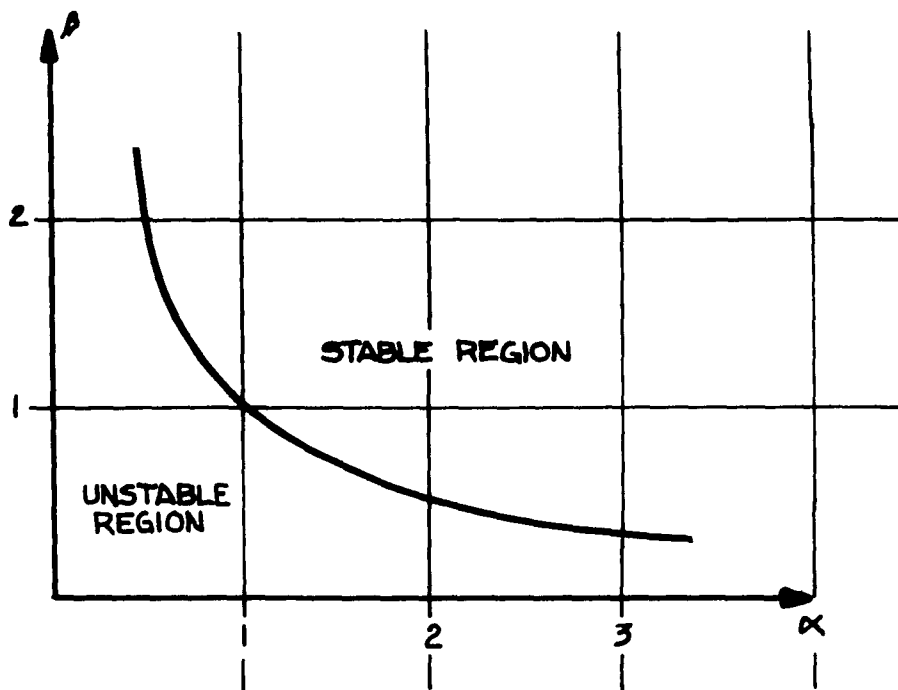
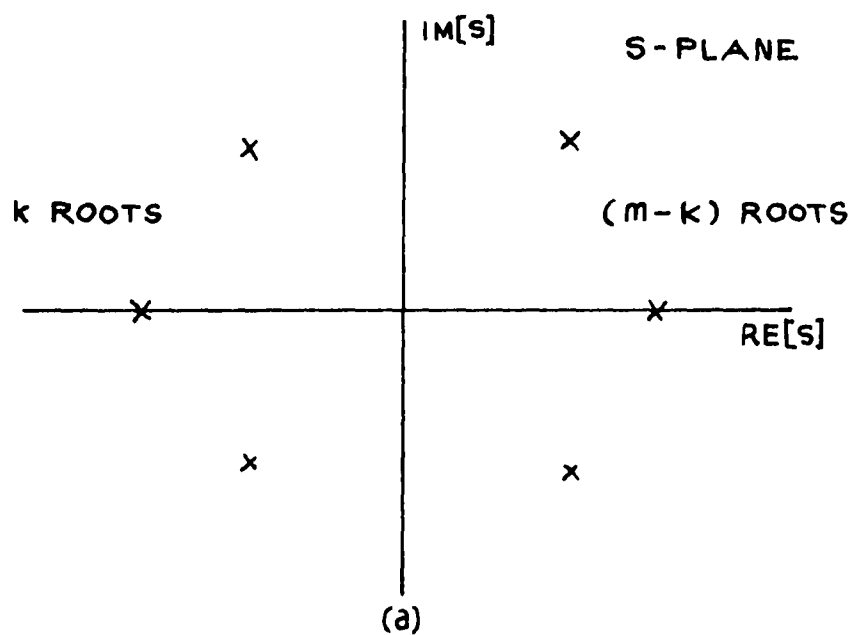
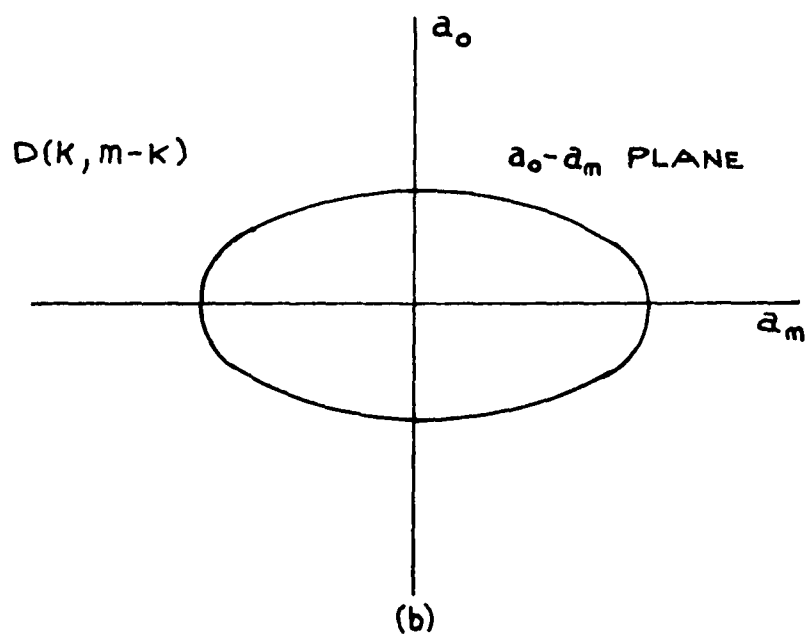


Fig. 2.1.1 Vishnegradski Curve.



S-PLANE ROOT LOCATIONS



COEFFICIENT SPACE

Fig. 2.2.1 s-Plane Root Locations and the Coefficient Space.



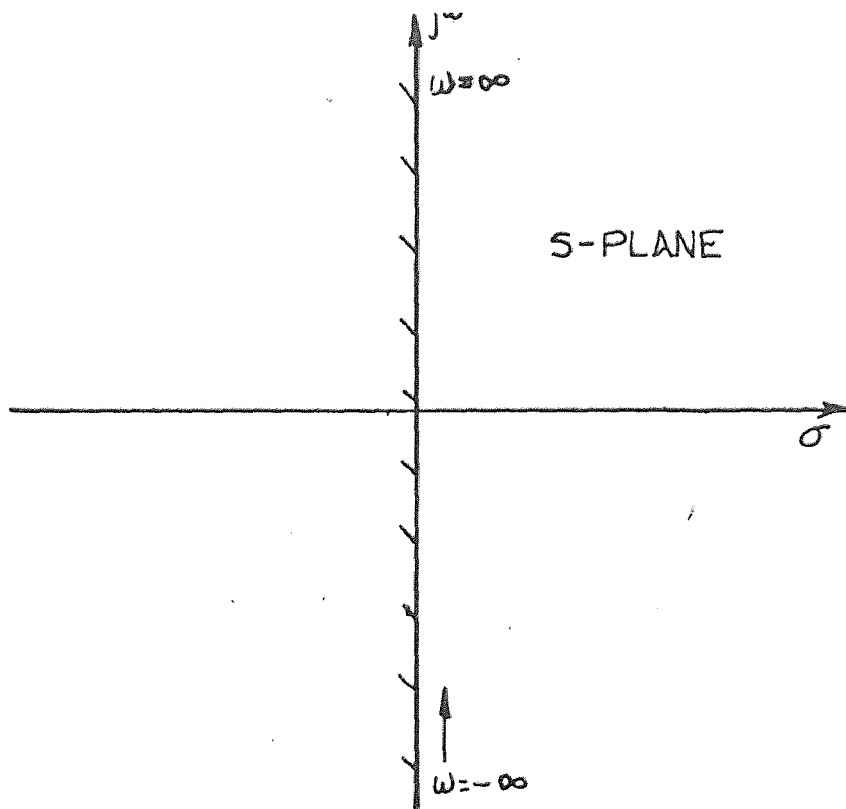


FIG. 2.2.2a

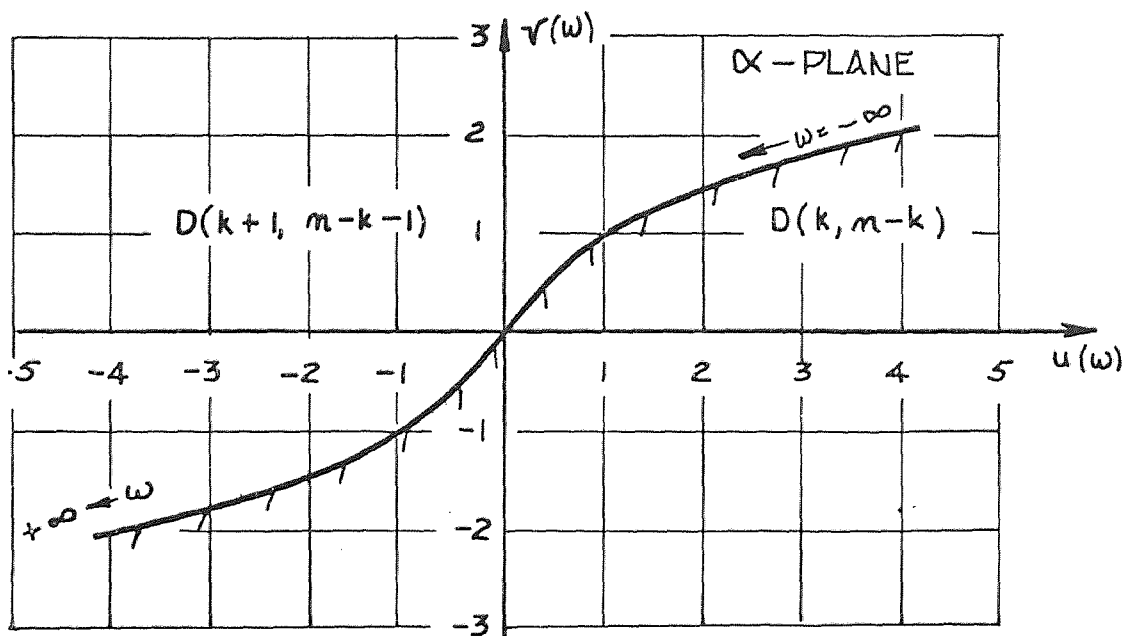


FIG. 2.2.2 b

Fig. 2.2.2 D-Partition Boundaries.

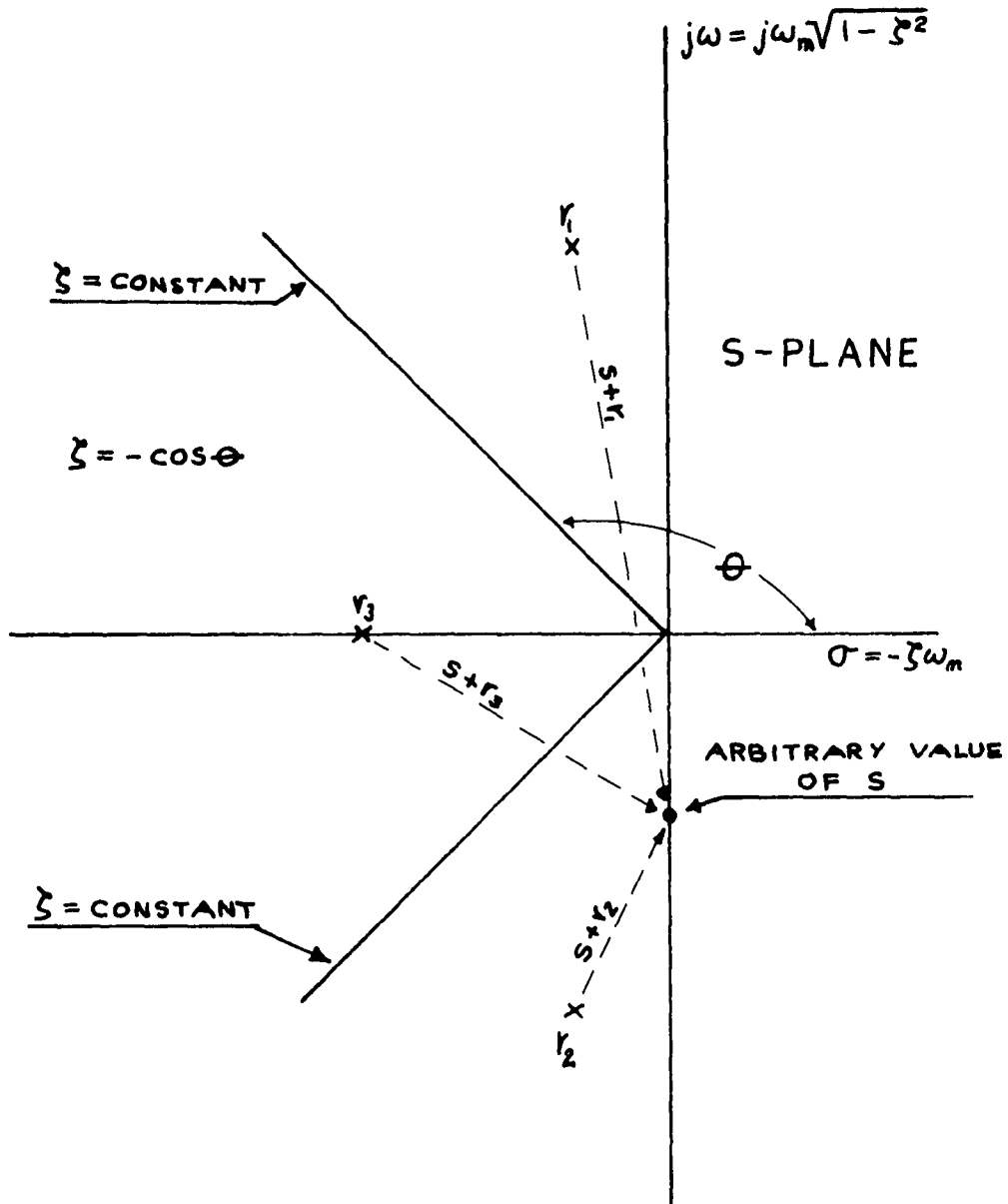


Fig. 2.3.1 Representation of the Characteristic Equation on the s-Plane.

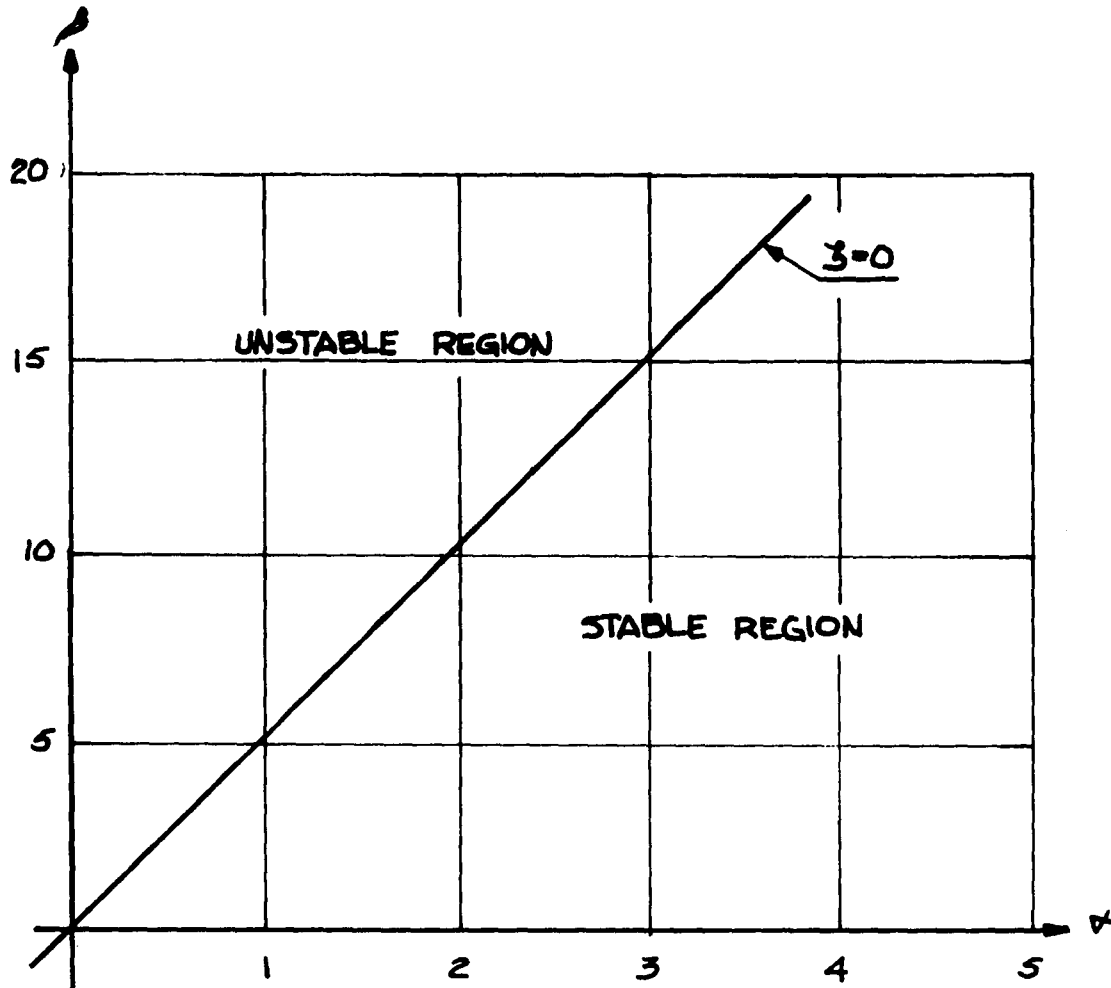


Fig. 2.3.2  $\alpha$ - $\beta$  Curve for  $\zeta = 0$  Where  $F(s) = s^3 + 5s^2 + \alpha s + \beta$ .  
 (From Fig. 9 in Ref. 16.)


## CHAPTER 3

### TRANSPORT LAG--CONVENTIONAL SOLUTIONS

#### 3.1 Introduction

In order to introduce the phenomenon of transport lag, which is sometimes referred to as "dead-time or distance-velocity lag," a practical example is given. Consider a person controlling the temperature of the hot water for a shower. Because of the flow time between the valve and the person (a transport lag), a change in valve setting is not immediately sensed, and the user does not know how much change he has made. After waiting until the change is sensed, he then tries another "blind" adjustment. If he is in a hurry, the sequence of adjustments may become oscillatory, with unfortunate results. It is obvious that high gain in a control loop with a transport lag can be unstable. In this instance the man is the controller and the difference in the temperature of the water from the desired temperature is the error upon which the man acts. The transport lag is the time taken for the water to flow from the valve to the man. If the man turns the valve too quickly and too much in one direction, implying a large gain within the control loop, he will overcompensate and eventually either scald or freeze.

An important point to be made for systems with transport lag is that the output of the device producing the lag is identical to the input except for the fact that it is delayed in time. This constant



time delay can be readily incorporated into the mathematical formulation of the system transfer function. For example, consider that the output from the fixed delay component is equal to the input delayed by  $T$  sec. Mathematically this can be expressed as follows

$$c_o(t) = c_i(t - T) \quad (3.1.1)$$

Taking the Laplace transform of both sides and dividing by  $C_i(s)$  yields

$$\frac{C_o(s)}{C_i(s)} = e^{-sT} \quad (3.1.2)$$

Thus the transfer function for a constant transportation lag is the transcendental function  $e^{-sT}$ .

The phenomenon of transport lag occurs in many areas of engineering: for example, in certain types of transmission lines, long pneumatic control lines, the time of motion of a relay armature in an on-off servomechanism, the flow of chemicals through pipes, etc. In order to exemplify the existence of transport lag in an electrical system, consider a transmission line that is terminated in its characteristic impedance (see Figure 3.1.1a). The ratio of the output voltage to the input voltage is [21]

$$\frac{V_o(s)}{V_i(s)} = e^{-sT_L} \quad (3.1.3)$$

where  $T_L$  is the transport lag which is a result of the finite propaga-

tion velocity  $u = \ell/\sqrt{L_0 C_0}$  of the voltage wave along the transmission line. The transport lag time  $T_L$  thus depends on the length  $\ell$  and the velocity  $u$ . Or

$$T_L = \frac{\ell}{u} \quad (3.1.4)$$

Figure 3.1.2 shows a typical block diagram representation of a feedback control system containing a transport lag in the forward path.

A second type of lag that also occurs in engineering systems, though less frequently, is the so called distributed lag. For example, distributed lag occurs in certain types of transmission lines, in thermal heat flow through solids and in acoustic lines with a large ratio of acoustic capacity to inductance [27]. The transmission line shown in Figure 3.1.1b exhibits the property of distributed lag. The ratio of the output voltage to the input voltage is [21]

$$\frac{V_o(s)}{V_i(s)} = e^{-\sqrt{sT_L}} \quad (3.1.5)$$

where  $T_L = R_0 C_0 \ell^2$ .

The following sections of this chapter will review some of the more popular techniques utilized in analyzing feedback control systems containing transport lag. Further, since systems containing distributed lag are less common than systems containing transport lag, the emphasis in what follows will be on the latter. However, reference to distributed

lag systems will be made where applicable.

### 3.2 Approximation Techniques

The open-loop transfer function of Figure 3.1.2 is given by

$$\frac{C_o(s)}{E(s)} = G(s)\epsilon^{-sT} \quad (3.2.1)$$

where  $G(s)$  is an algebraic rational function. Equation (3.2.1) contains the transcendental lag term,  $\epsilon^{-sT}$ , so that analysis is difficult. A popular analytical procedure is to convert the transcendental transfer function into a rational function by approximating the exponential term by a polynomial or ratio of polynomials in  $s$ , and then the usual techniques of analysis can be applied. For example, suppose the  $G(s)$  of Figure 3.1.2 is

$$G(s) = \frac{K}{s(1 + \tau_1 s)(1 + \tau_2 s)} \quad (3.2.2)$$

and the absolute stability of the system is to be examined in terms of the direct transmission gain,  $K$ , the time constants,  $\tau_1$  and  $\tau_2$ , and the time delay,  $T$ . The characteristic equation for this system is given by

$$1 + \frac{K\epsilon^{-sT}}{s(1 + \tau_1 s)(1 + \tau_2 s)} = 0 \quad (3.2.3)$$

The Routh criterion is the standard test for the absolute stability of linear systems, but it only applies to finite polynomials in  $s$ . Since

the transcendental term,  $\epsilon^{-sT}$ , is an infinite polynomial in  $s$ , it is approximated for small  $T$ , and low frequency, by

$$\epsilon^{-sT} \cong 1 - sT \quad (3.2.4)$$

Thus the characteristic equation becomes

$$\tau_1\tau_2s^3 + (\tau_1 + \tau_2)s^2 + (1 - KT)s + K = 0 \quad (3.2.5)$$

This is a cubic equation so the Routh criterion gives the condition for absolute stability in terms of the coefficients as (assuming that all the coefficients are positive)

$$(1 - KT)(\tau_1 + \tau_2) > K\tau_1\tau_2 \quad (3.2.6)$$

Rearranging (3.2.6) yields the condition for stability as

$$K < \frac{1}{\tau_1\tau_2/(\tau_1 + \tau_2) + T} \quad (3.2.7)$$

The boundary between stability and instability occurs when

$$K = \left( \frac{\tau_1\tau_2}{\tau_1 + \tau_2} + T \right)^{-1} \quad (3.2.8)$$

Equation (3.2.8) is graphed in Figure 3.2.1, where  $K$  is plotted versus  $T$  for constant  $\tau_1$  and  $\tau_2$ . For any given value of transport lag the system is stable if the gain  $K$  lies below the critical curve and unstable if  $K$  lies above it. The closer  $K$  lies to the curve, the more



likely the system is to become unstable for any unfavorable variations of the time constants,  $\tau_1$  and  $\tau_2$ . It must be emphasized that the stability condition of (3.2.8) depends upon the accuracy of the approximation of (3.2.4). If the exponential is expanded to include more terms of the series and the Routh criterion is then applied, a more exact statement of the stability condition is obtained.

Another approximation to the transcendental function is sometimes obtained from the fact that

$$\epsilon^{-sT} = \lim_{n \rightarrow \infty} \left( \frac{1}{1 + \frac{sT}{n}} \right)^n \quad (3.2.9)$$

If a finite value of  $n$  is used, the transcendental function is approximated by a pole of order  $n$  located at  $-n/T$  on the negative real axis in the  $s$ -plane. For example, an  $n$  of 3 yields

$$\epsilon^{-sT} \cong \left( \frac{1}{1 + \frac{sT}{3}} \right)^3 \quad (3.2.10)$$

The impulse response of the actual function and that of the approximation are sketched in Figure 3.2.2. The approximation is not particularly good, with the maximum value of the impulse response occurring at  $2T/3$ .

A third approach to the approximation of the exponential function is to utilize a rational algebraic function approximation. One such function is the Padé approximant. The Padé approximation is a rational algebraic function, with numerator polynomial of degree  $n$  and denominator

of degree  $m$ , such that the maximum number of terms in the Maclaurin expansion of the approximating function agree with similar terms in the expansion of the exponential function. Thus if  $\epsilon^{-sT}$  is to be approximated by the ratio of cubic to quadratic polynomials, there are six coefficients which can be selected arbitrarily:

$$\epsilon^{-sT} \cong \frac{1 + a_1s + a_2s^2 + a_3s^3}{b_0 + b_1s + b_2s^2} \quad (3.2.11)$$

These six coefficients can be chosen such that at least the first six terms are equal in the two Maclaurin expansions. In this specific example, the appropriate rational algebraic function is<sup>1</sup>

$$\epsilon^{-sT} \cong \frac{1 - \frac{3}{5}Ts + \frac{3}{20}T^2s^2 - \frac{1}{60}T^3s^3}{1 + \frac{2}{5}Ts + \frac{1}{20}T^2s^2} \quad (3.2.12)$$

The Maclaurin expansion of the fraction is

$$1 - Ts + \frac{1}{2}T^2s^2 - \frac{1}{6}T^3s^3 + \frac{1}{24}T^4s^4 - \frac{1}{120}T^5s^5 + \left[ \frac{1}{800}T^6s^6 - + \dots \right] \quad (3.2.13)$$

The first six terms are simply those of the expansion of  $\epsilon^{-sT}$ ; the last term given is the first one to differ. The Padé approximant technique, although better than the two previously mentioned techniques, is still an approximation and therefore limited in its application.

---

<sup>1</sup>Reference 5 shows a general method for constructing Padé approximants.

### 3.3 Nyquist Diagrams

Because of the disadvantages associated with approximations to the transcendental function, a graphical procedure often provides a much simpler approach to problems involving transportation lags. If the substitution  $s = j\omega$  is made, the transcendental term of the transfer function becomes  $\epsilon^{-j\omega T}$  and is readily interpreted in terms of either the Nyquist diagram or the Bode plot. In this instance no approximation is necessary, but the result is a frequency response analysis of the system with all the limitations thereof. In either the Nyquist plots or the Bode plots, multiplication of a transfer function by  $\epsilon^{-j\omega T}$  represents merely a phase shift varying linearly with frequency. This is because

$$\epsilon^{-j\omega T} = |\epsilon^{-j\omega T}| \angle -\omega T = 1 \angle -\omega T \text{ rad.} \quad (3.3.1)$$

In terms of the Nyquist diagram, each point on the diagram is rotated through an angle of  $-\omega T$  rad., where  $\omega$  is the angular frequency corresponding to the point on the original locus. For example, in the system of Figure 3.1.2, the transfer function  $G(s)$  is given by

$$G(s) = \frac{K}{s(s + 1)}$$

The Nyquist plots for the open-loop transfer function of the system for various values of time lag ( $T = 0, 0.5, 1.0, 1.5$  sec.) and  $K = 1$  are constructed in Figure 3.3.1. From this plot it is seen that the closed-loop system is always stable when the time-lag is zero, but the stability

deteriorates as the time-lag is increased, and for large values of lag the system is unstable since the  $(-1.0, 0)$  point is encircled.

The multiplication of  $G(s)$  by  $\epsilon^{-j\omega T}$  simply rotates each point on the  $G(s)$  curve by an angle of  $\omega T$  rad. in the clockwise direction (see Figure 3.3.1). Therefore, in this case, the Nyquist plots of the system with transportation lag spiral towards the origin as the frequency  $\omega$  approaches infinity. From the plots in Figure 3.3.1 it appears that the marginal value of  $T$  for stability lies somewhere between 1.0 and 1.5 sec. The exact value of  $T$  that will make the Nyquist plot go through the point  $(-1, 0)$  can be determined by trial and error or algebraically.

### 3.4 Bode Plots

The Bode plot, or the logarithmic gain and phase plots, permit a convenient method of analysis of the closed-loop system with a transportation lag. The gain curve is unchanged by the introduction of the lag factor, but the phase lag is increased proportional to frequency. Figure 3.4.1 presents the change caused by the introduction of the  $\epsilon^{-sT}$  factor in the  $\frac{K}{s(s+1)}$  transfer function considered previously. The allowable gain,  $K$ , for a stable system is rapidly determined. The gain of the  $\frac{1}{s(s+1)}$  plot at the frequency at which the phase shift of the total open-loop transfer function is  $-180^\circ$  is  $-1.1\text{db.}$ , if  $T$  is 1 sec.  $K$  can then be as high as  $+1.1\text{db.}$  or 1.14. The desirable characteristic of this approach to the problem of transportation lag is that the situation is not particularly complicated by increased complexity in the rest of the open-loop transfer function.

### 3.5 Root-Locus

The popular root-locus technique can be applied to control systems exhibiting transport lag. In order to appreciate the concept as applied to systems with transport lag, a brief discussion of the conventional root-locus technique is first given. In the root-locus method the locus of the roots of the characteristic equation of a feedback system are plotted, the gain usually being the variable parameter. Thus the locus gives a representation of these roots simultaneously with their corresponding values of gain. Transient solutions can be worked out once these roots are determined.

Consider again the feedback control system shown in Figure 3.1.2 where, if  $T = 0$ , the system reduces to a conventional feedback control system without transport lag. The characteristic equation of this system can be expressed as

$$G(s) = -1 \quad (3.5.1)$$

This equation is complex and may be rewritten as two equations by equating magnitudes and phase angles on both sides of (3.5.1) to each other. Thus, the magnitude equation is

$$|G(s)| = 1 \quad (3.5.2)$$

and the phase angle equation is

$$\angle G(s) = \pm 180 \text{ degrees (for the principal plane)} \quad (3.5.3)$$

The plot for the phase angle equation is called the root-locus (since the roots of the characteristic equation are points on the locus), while the magnitude equation gives the value of the gain on each point of the locus. Figure 3.5.1 illustrates the root-locus for the transfer function

$$G(s) = \frac{K(s + 0.3)}{s^2} \quad (3.5.4)$$

This particular transfer function will be used as an example in later work so the discussion of this function will be given in detail. Note that the locus is symmetrical with respect to the real axis. Equation (3.5.3) indicates that the root-locus is a curve on which every point has a phase angle of  $\pm 180$  degrees.

This concept has been generalized by Chu<sup>2</sup> by considering loci with other values of phase angle. Equation (3.5.3) is then expressed as  $\angle G(s) = \phi$  where  $\phi$  is a constant phase angle. Thus, a family of loci can be plotted for various values of  $\phi$ . Figure 3.5.2 illustrates a family of constant phase-angle root loci for the transfer function  $G(s)$  of equation (3.5.4). Such a family of curves for a given transfer function is called "the phase-angle loci." Since the locus with phase angle  $\phi$  is symmetrical to that with phase angle  $(-\phi)$  with respect to the real axis, only the loci on the upper half plane are shown. If the feedback control system contains a transport lag  $e^{-sT}$ , then the characteristic

---

<sup>2</sup>This section follows the derivation presented by Chu in Reference 2.

equation is (see Figure 3.1.2)

$$G(s)e^{-sT} = -1 \quad (3.5.5)$$

The phase angle equation is accordingly

$$\angle G(s) + \angle e^{-sT} = \pm 180 \text{ degrees} \quad (3.5.6)$$

where the phase angle equation can be simplified into

$$\angle G(s) - \omega T = \pm 180 \text{ degrees} \quad (3.5.7)$$

The technique for constructing the root-locus for a feedback control system with transport lag is based on (3.5.7). First the family of root-loci (or phase-angle loci) are constructed for

$$\angle G(s) = \phi_1 \quad (3.5.8)$$

Next, another family of root-loci is constructed for the transport lag term of (3.5.7), (sometimes referred to as the transport lag phase-angle loci) from the relation

$$-\omega T = \phi_2 \quad (3.5.9)$$

Then by superimposing these two families of loci, the points of intersection of the corresponding curves where the sum of phase angles  $\phi_1$ , and  $\phi_2$  equal to  $\pm 180$  degrees are the points of the locus required. The curve drawn through all these points of intersection is the required root-locus. The determination of the gain can then be carried out by

the criterion used in the conventional root-locus method. The magnitude equation is from (3.5.2)

$$K = \frac{1}{|G(s)\epsilon^{-sT}|} \quad (3.5.10)$$

which will give the gain  $K$  of any point on the required root-locus.

To illustrate this method, an example is selected with the transfer function previously discussed, namely

$$G(s) = \frac{(s + 0.3)}{s^2} \epsilon^{-sT} \quad (3.5.11)$$

For convenience, it is separated into two transfer functions

$$G_1(s) = \frac{(s + 0.3)}{s^2}, \quad G_2(s) = \epsilon^{-s} \quad (3.5.12)$$

where  $G(s) = G_1(s)G_2(s)$  and  $T$  is assumed to be unity. By following the previously mentioned procedure, a family of root-loci of the following equation is constructed

$$\angle G_1(s) = \phi_1$$

This family of root-loci has been shown in Figure 3.5.2. Next a family of transport lag loci is constructed from the relation

$$-\omega = \phi_2 \quad (3.5.13)$$

This family of loci is shown in Figure 3.5.3. Finally, these two families of loci are superimposed on the same  $s$ -plane. The required



root-locus is the points of intersection of every two loci with the sum  $\phi_1$  and  $\phi_2$  equal to  $\pm 180$  degrees as shown in Figure 3.5.4. The points of the required root-locus in the upper half plane are those with a phase angle of  $-180$  degrees. Since the locus is symmetrical with respect to the real axis, only those in the upper half plane are shown.

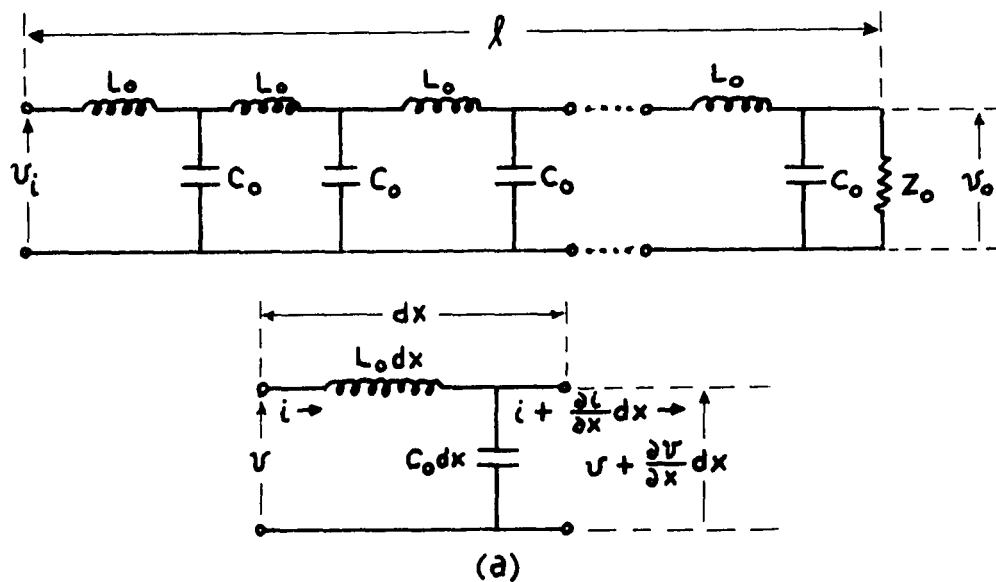
As an example, the points on Figure 3.5.4 which give unity gain are from equation (3.5.10)

$$\sigma_0 = -0.41, \sigma_1 \pm j\omega_1 = -0.17 \pm j1.17 \quad (3.5.14)$$

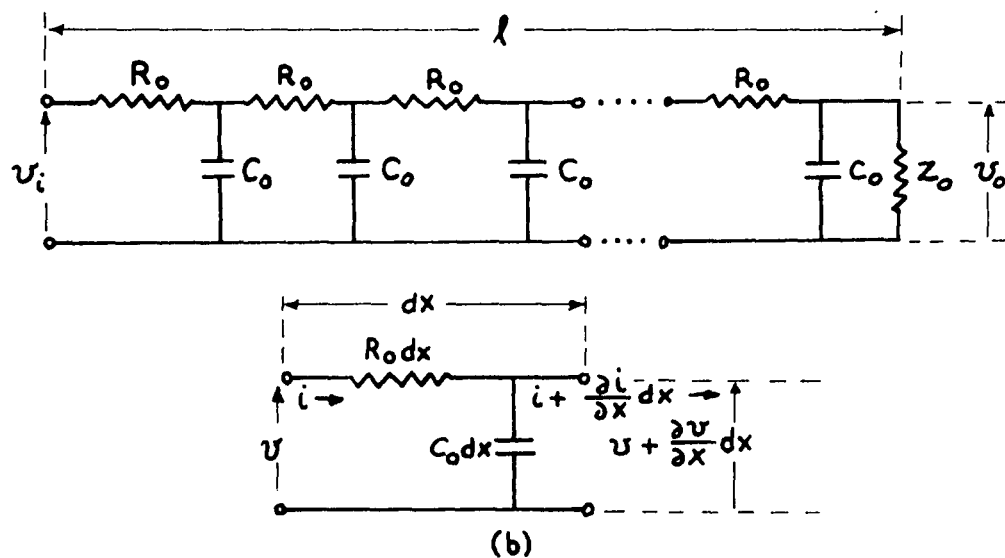
The characteristic equation has an infinite number of roots, which can be obtained by constructing additional branches of the required locus. Figure 3.5.5 shows the second and third branches, as well as the fundamental branch. Again at the points which give the unity value of gain, the second and third pairs of roots are found to be

$$\begin{aligned} \sigma_2 \pm j\omega_2 &= -2.06 \pm j7.56 \\ \sigma_3 \pm j\omega_3 &= -2.65 \pm j13.92 \end{aligned} \quad (3.5.15)$$

In conclusion, the root-locus technique developed by Chu is perhaps the most fruitful of all techniques when designing feedback control systems containing transport lag. The technique, however, is fraught with difficulties when considering high-order systems, or systems where the variable parameter is not a multiplying gain factor in the forward loop.



TRANSMISSION LINE WITH  $L_0 = L/\ell$  AND  $C_0 = C/\ell$



TRANSMISSION LINE (THOMSON CABLE) WITH  $R_0 = R/\ell$   
AND  $C_0 = C/\ell$

Fig. 3.1.1 Distributed Parameter Transmission Lines.

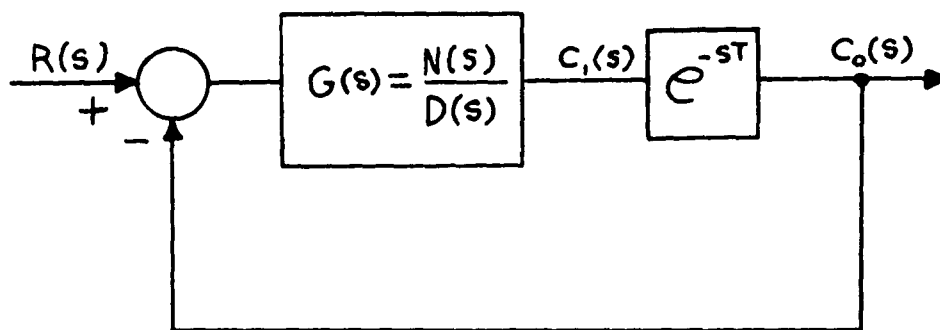


Fig. 3.1.2 Block Diagram of a Feedback Control System With Transport Lag.

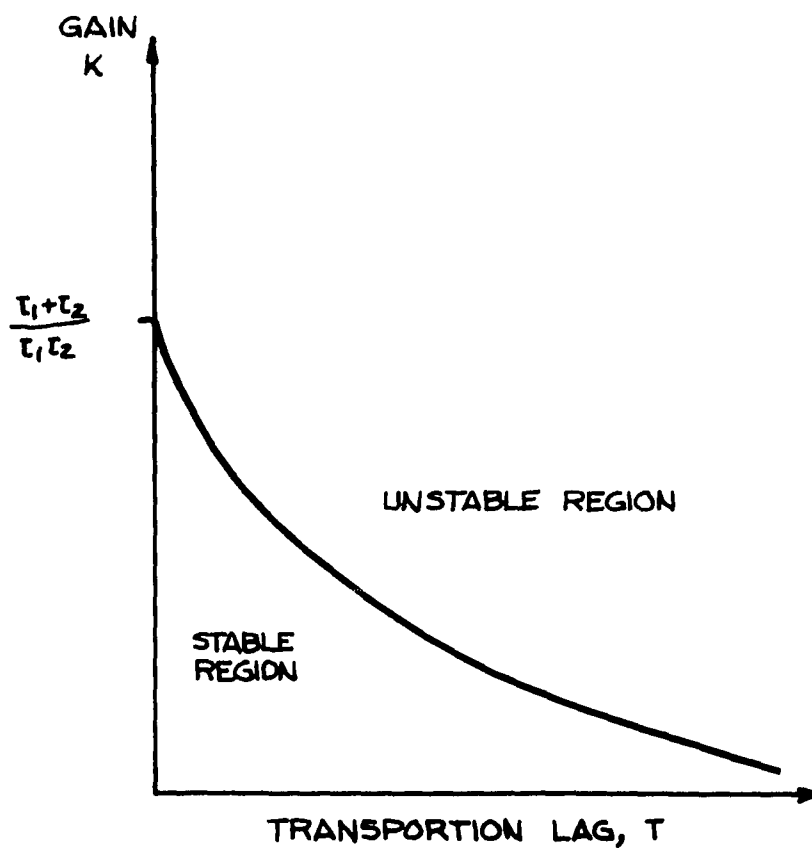
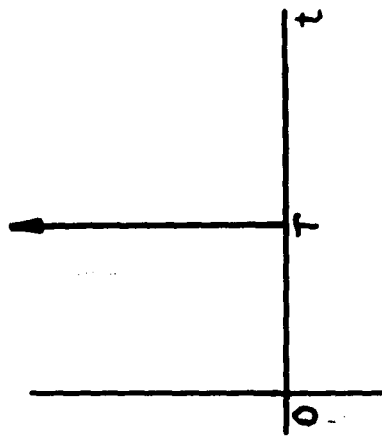
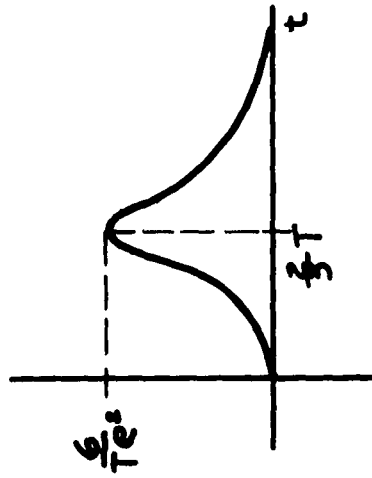


Fig. 3.2.1 Stability Diagram. (From Fig. 8-1 in Del Toro, V., and Parker, S.R., Principles of Control Systems Engineering. New York: McGraw-Hill Book Company, Inc., 1960.)



a. IDEAL RESPONSE FOR TRANSPORTATION LAG



b. RESPONSE OF APPROXIMATION

Fig. 3.2.2 Impulse Response. (From Fig. 9.36 in Ref. 29.)

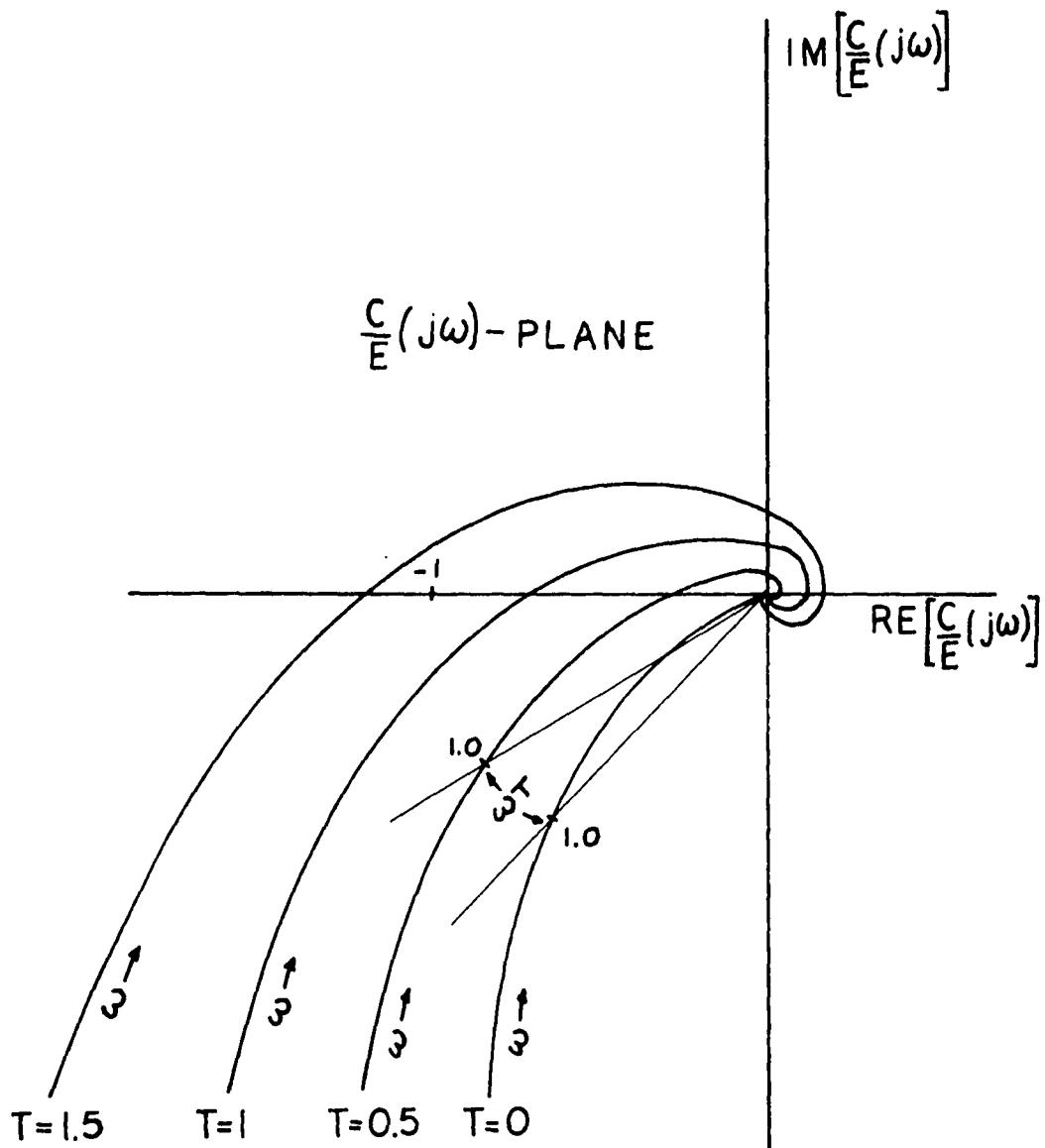


Fig. 3.3.1 Nyquist Diagram of  $G(s)e^{-sT} = \frac{Ke^{-sT}}{s(s+1)}$ . (From Fig. 9.38 in Ref. 29.)

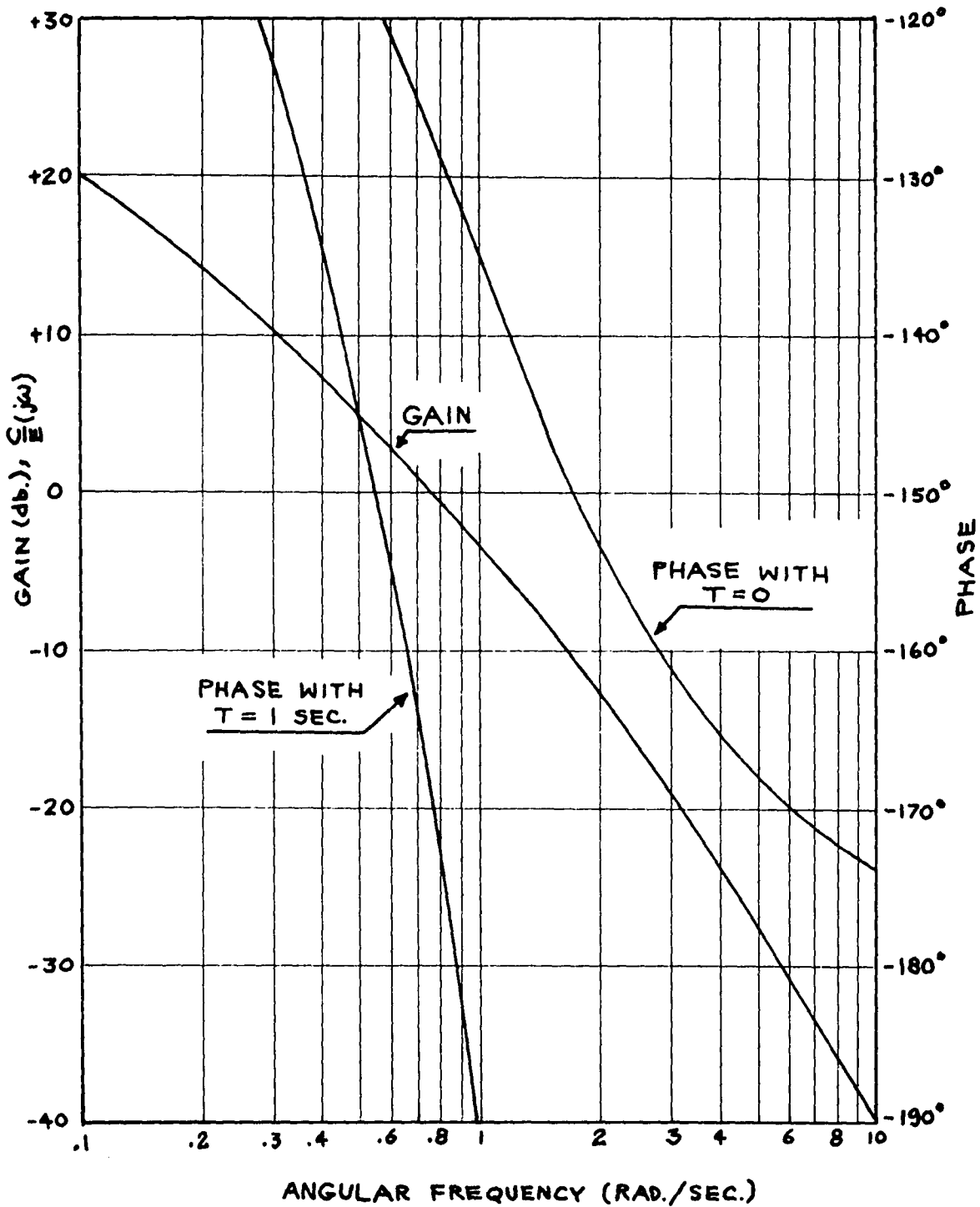


Fig. 3.4.1 Gain and Phase Curve for the Open-Loop Transfer

Function  $\frac{e^{-sT}}{s(s+1)}$ . (From Fig. 9.39 in Ref. 29.)

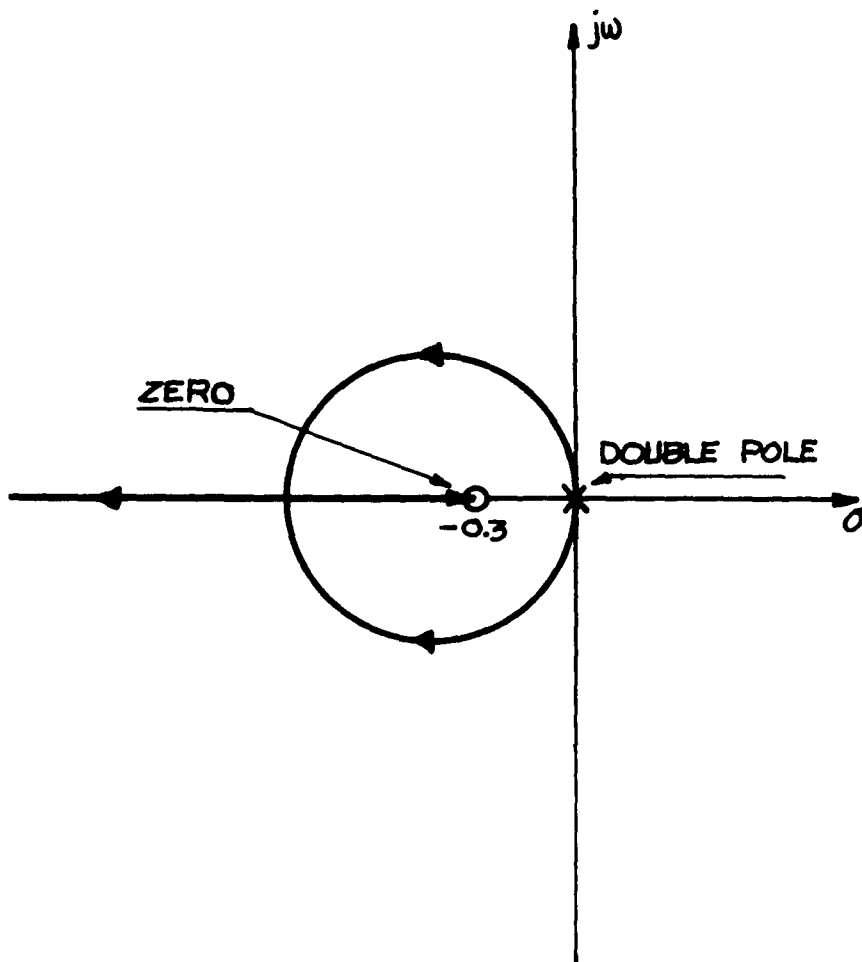


Fig. 3.5.1 The Root-Locus for  $G(s) = \frac{K(s + 0.3)}{s^2}$ .  
(From Fig. 2 in Ref. 2.)



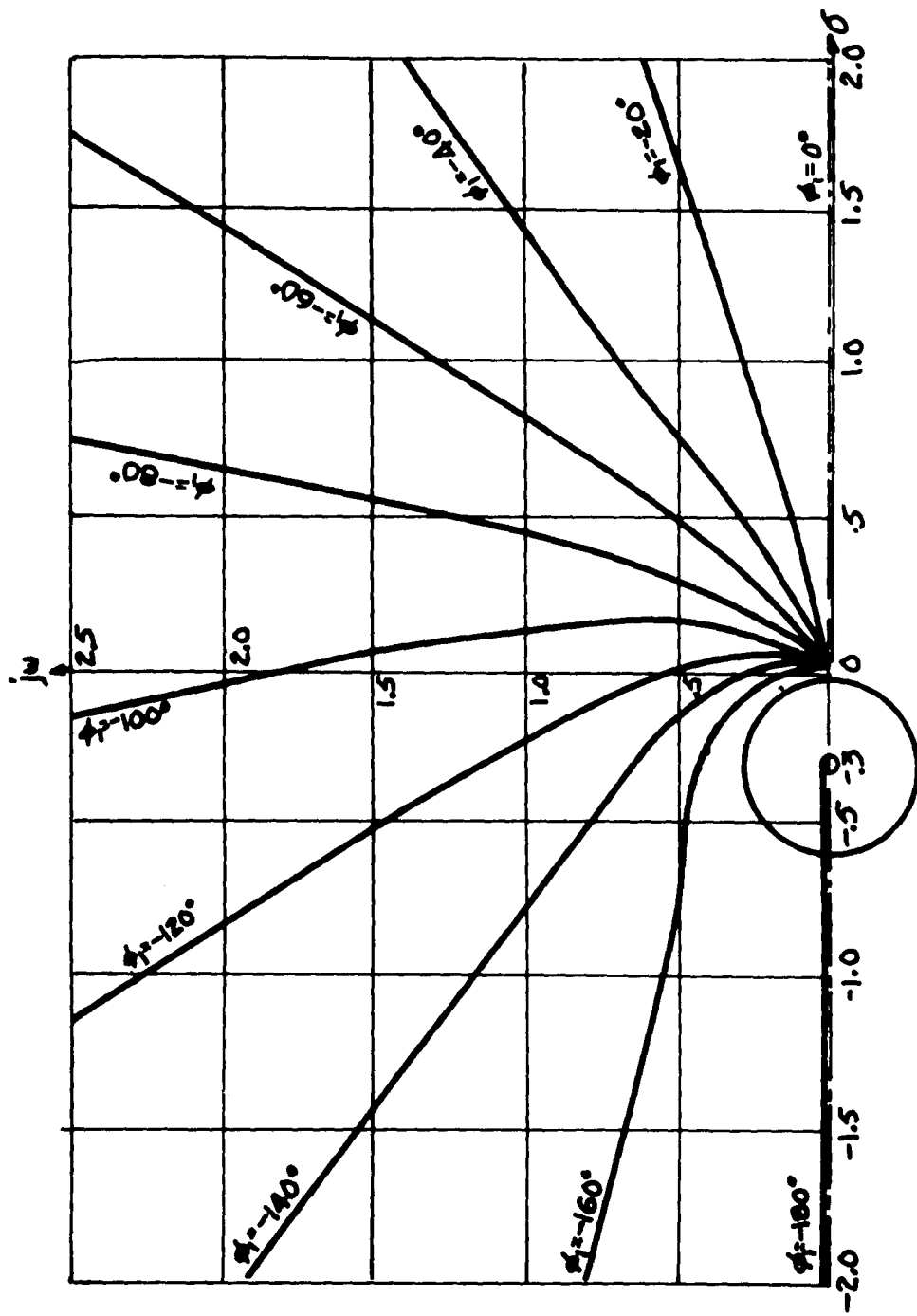


Fig. 3.5.2 phase-Angle Loci for  $\tilde{K}(s) = \frac{\tilde{K}(s + 0.3)}{s^2}$ . (From Fig. 3 in Ref. 2.)

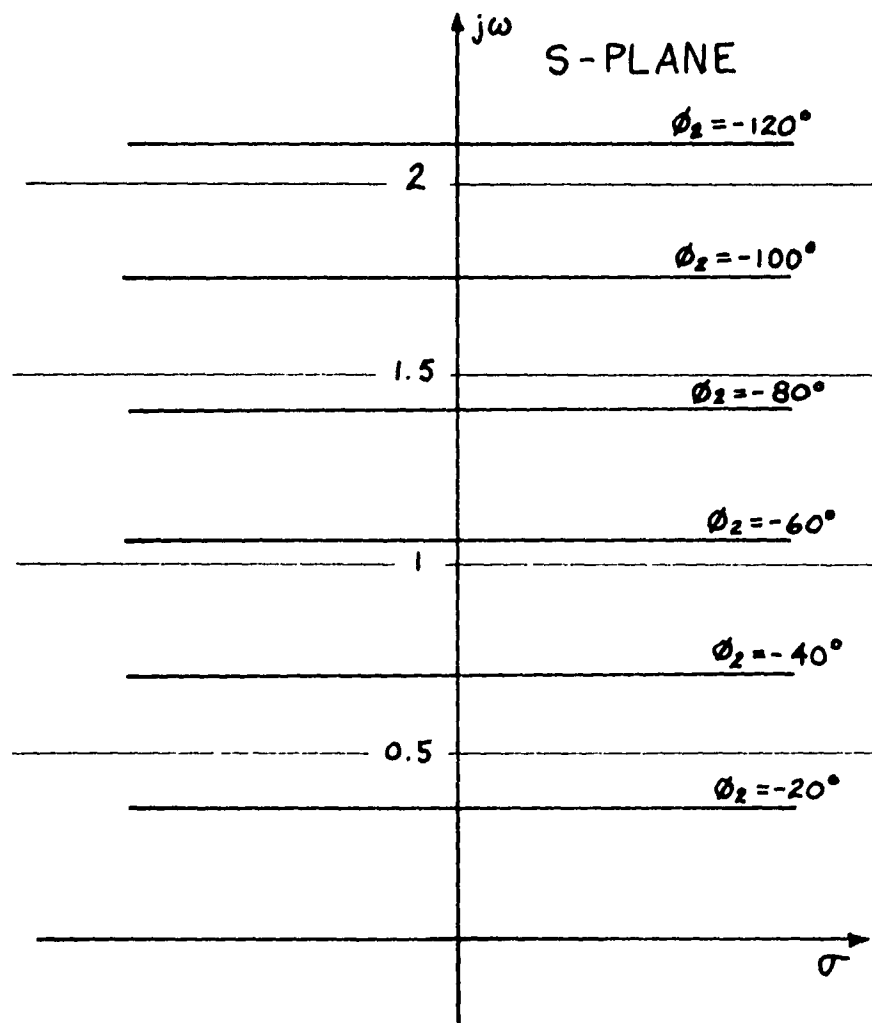


Fig. 3.5.3 Transport Lag Phase-Angle Loci. (From Fig. 5 in Ref. 2.)

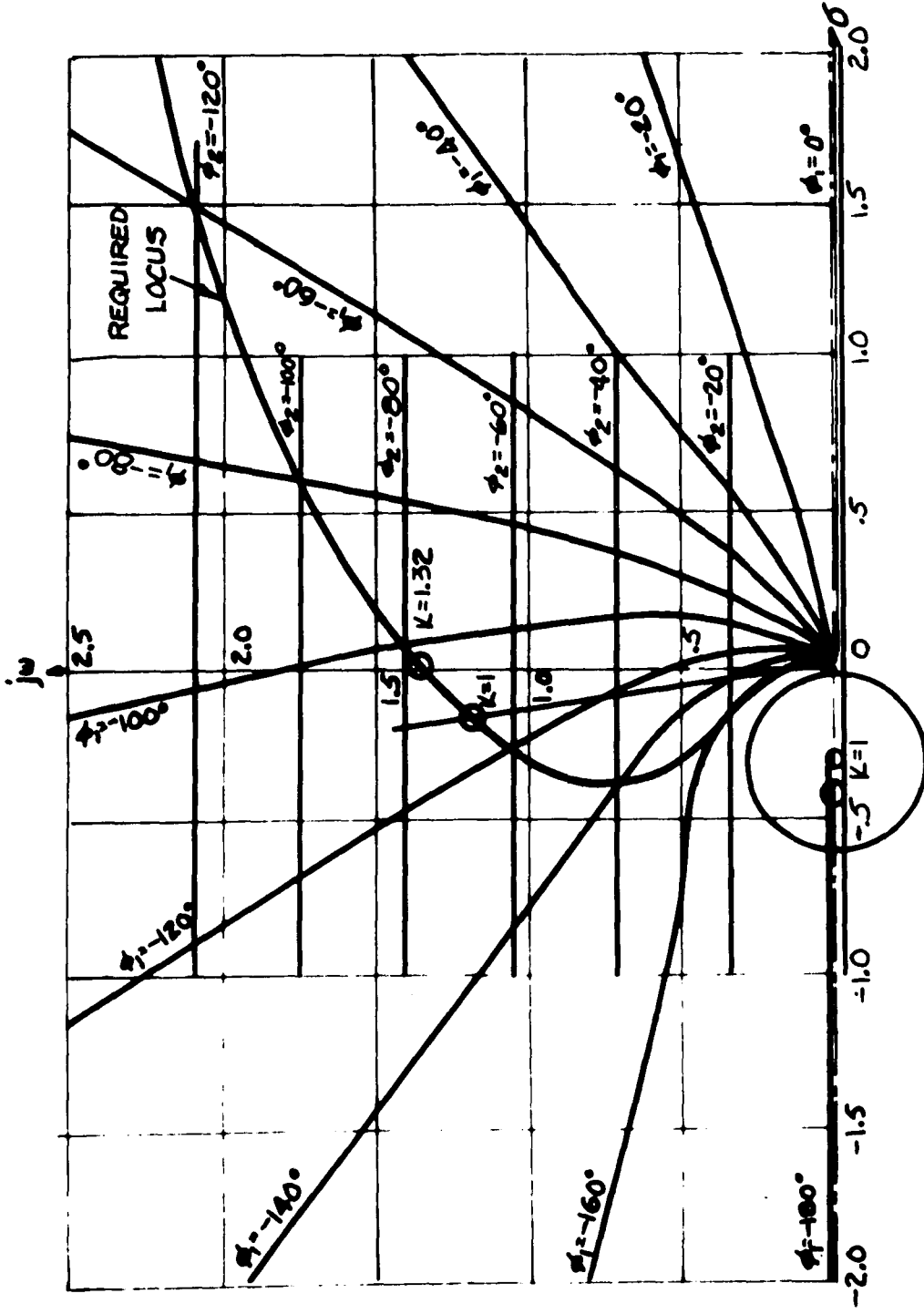


Fig. 3.5.4 Construction of the Required Locus with Transport Lag.  
 (From Fig. 6 in Ref. 2)

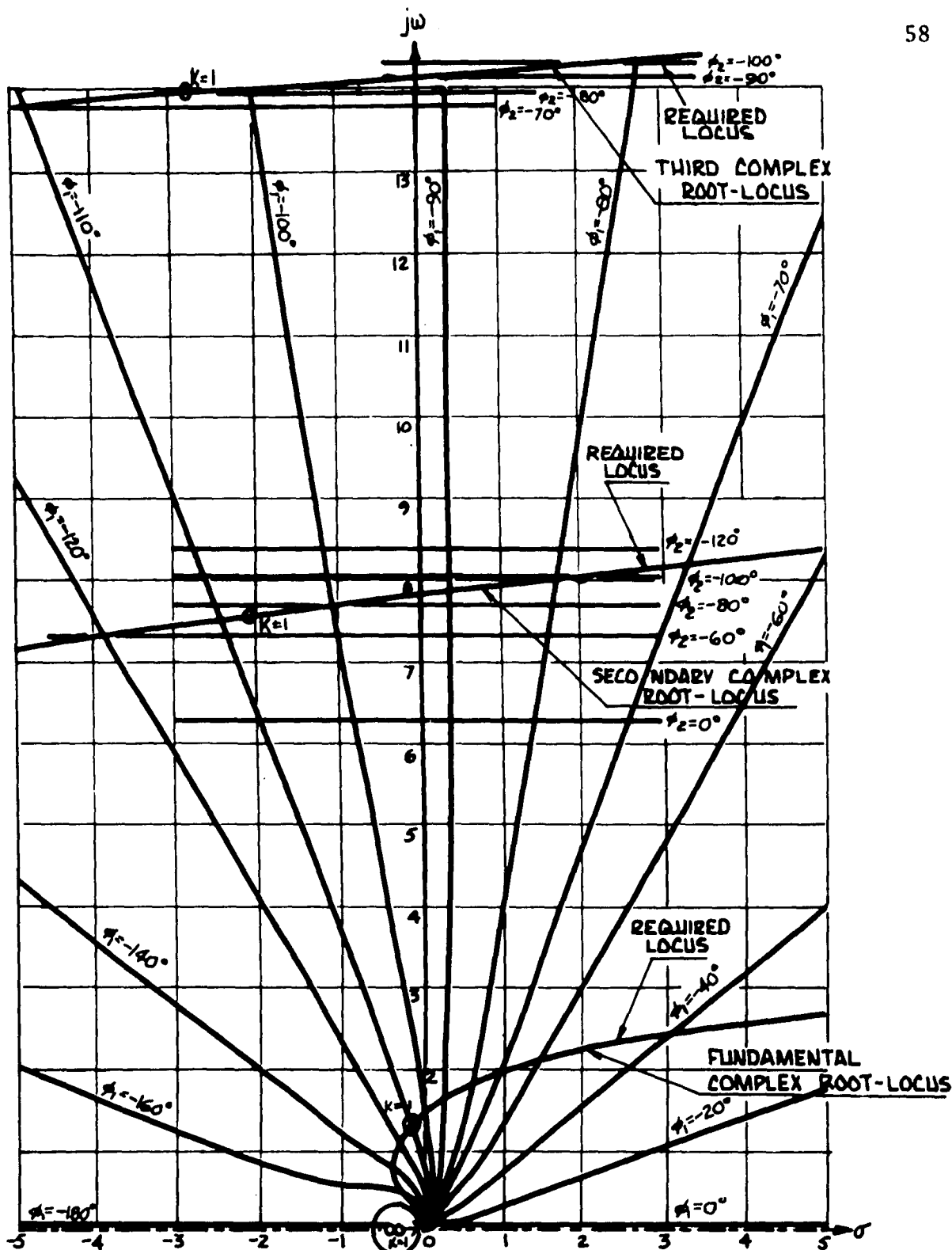


Fig. 3.5.5 Three branches of the Required Locus With Transport Lag.  
 (From Fig. 7 in Ref. 2.)

## CHAPTER 4

### ABSOLUTE AND RELATIVE STABILITY OF SYSTEMS WITH TRANSPORT LAG

#### 4.1 Derivation of Parameter Plane Equations

The fundamental equations and concepts of this dissertation are derived in this chapter and are applied here to the determination of the absolute and relative stability of a linear feedback control system with transport or distributed lag [6].

Consider the linear unity feedback control system with a transport lag in the forward path shown in Figure 4.1.1. The ratio of  $C(s)$  to  $R(s)$  is

$$\frac{C}{R}(s) = \frac{N(s)}{F(s)} = \frac{N(s)}{D(s)e^{sT} + N(s)} \quad (4.1.1)$$

where  $T$  is a constant time delay in seconds and  $s$  is the complex variable

$$s = -\zeta\omega_n + j\omega_n\sqrt{1 - \zeta^2} \quad (4.1.2)$$

Here  $\zeta$  is the dimensionless damping ratio and  $\omega_n$  is the undamped natural frequency in radians per second (see Figure 4.1.2b).

The stability of the system is determined by the locations of the roots of the system characteristic equation  $F(s)$ . Setting  $F(s) = 0$  gives

$$F(s) = D(s)e^{sT} + N(s) = 0 \quad (4.1.3)$$

Note that (4.1.3) will remain unchanged if the transcendental function appears in the feedback path of Figure 4.1.1. Since  $D(s)$  and  $N(s)$  are polynomials in  $s$ , they can be expressed as

$$D(s) = \sum_{k=0}^n q_k s^k, \quad N(s) = \sum_{k=0}^j r_k s^k \quad (4.1.4)$$

where  $q_k$  and  $r_k$  are real and  $j \leq n$  for a practical system configuration. Then from (4.1.3)

$$F(s) = \epsilon^{sT} \sum_{k=0}^n q_k s^k + \sum_{k=0}^j r_k s^k = \sum_{k=0}^n a_k(s) s^k = 0 \quad (4.1.5)$$

Since the  $a_k(s)$  will be a function of  $\epsilon^{sT}$  for  $T \neq 0$  and will contain the system parameters, the  $a_k(s)$  are defined in the following manner in order to include all possible linear combinations of parameters.

$$a_k(s) = \alpha b_k + \alpha c_k \epsilon^{sT} + \beta d_k + \beta e_k \epsilon^{sT} + f_k + g_k \epsilon^{sT} \quad (4.1.6)$$

where  $\alpha$  and  $\beta$  are system parameters that can be chosen or adjusted, i.e. system gains, time constants, etc. The cases in which  $\alpha$  and  $\beta$  appear non-linearly as well as linearly, i.e., as  $\alpha$ ,  $\beta$ ,  $\alpha\beta$ ,  $\alpha^2$ , etc., are not considered.

If

$$s = -\zeta\omega_n + j\omega_n\sqrt{1-\zeta^2}$$

then it can be shown that (see Reference 26)

$$s^k = \omega_n^k [T_k(-\zeta) + j\sqrt{1-\zeta^2} U_k(-\zeta)] \quad (4.1.7)$$

where  $T_k(-\zeta)$  is the Chebyshev function of the first kind, and  $U_k(-\zeta)$  is the Chebyshev function of the second kind. The Chebyshev functions can be constructed by means of the following identities and recursion formulas.

$$T_k(-\zeta) = (-1)^k T_k(\zeta) , \quad U_k(-\zeta) = (-1)^{k+1} U_k(\zeta) \quad (4.1.8a)$$

$$T_{k+1}(\zeta) - 2\zeta T_k(\zeta) + T_{k-1}(\zeta) = 0 \quad (4.1.8b)$$

$$U_{k+1}(\zeta) - 2\zeta U_k(\zeta) + U_{k-1}(\zeta) = 0 \quad (4.1.8c)$$

where

$$T_0(\zeta) = 1 , \quad T_1(\zeta) = \zeta , \quad U_0(\zeta) = 0 , \quad U_1(\zeta) = 1 \quad (4.1.8d)$$

These functions may also be evaluated by means of the following trigonometric definitions (see Tables I and II of Appendix I):

$$T_k(\zeta) = \cos(k \cos^{-1} \zeta) , \quad U_k(\zeta) = \frac{\sin(k \cos^{-1} \zeta)}{\sin(\cos^{-1} \zeta)} \quad (4.1.9)$$

Substituting (4.1.6) and (4.1.7) into (4.1.5) and applying (4.1.8a) gives

$$\begin{aligned} F(\omega_n, \zeta) = & [\alpha B_1(\omega_n, \zeta) + \beta C_1(\omega_n, \zeta) + D_1(\omega_n, \zeta)] \\ & + j[\alpha B_2(\omega_n, \zeta) + \beta C_2(\omega_n, \zeta) + D_2(\omega_n, \zeta)] \quad (4.1.10) \end{aligned}$$

where

$$\begin{aligned}
 B_1 &= \sum_{k=0}^n \omega_n^k \left[ (-1)^k T_k(\zeta) b_k + \varepsilon^{-\phi} c_k \left( (-1)^k T_k(\zeta) \cos \theta - (-1)^{k+1} \sqrt{1-\zeta^2} U_k(\zeta) \sin \theta \right) \right] \\
 C_1 &= \sum_{k=0}^n \omega_n^k \left[ (-1)^k T_k(\zeta) d_k + \varepsilon^{-\phi} e_k \left( (-1)^k T_k(\zeta) \cos \theta - (-1)^{k+1} \sqrt{1-\zeta^2} U_k(\zeta) \sin \theta \right) \right] \\
 D_1 &= \sum_{k=0}^n \omega_n^k \left[ (-1)^k T_k(\zeta) f_k + \varepsilon^{-\phi} g_k \left( (-1)^k T_k(\zeta) \cos \theta - (-1)^{k+1} \sqrt{1-\zeta^2} U_k(\zeta) \sin \theta \right) \right]
 \end{aligned} \tag{4.1.11}$$

$$\begin{aligned}
 B_2 &= \sum_{k=0}^n \omega_n^k \left[ (-1)^{k+1} U_k(\zeta) \sqrt{1-\zeta^2} b_k \right. \\
 &\quad \left. + \varepsilon^{-\phi} c_k \left( (-1)^{k+1} U_k(\zeta) \sqrt{1-\zeta^2} \cos \theta + (-1)^k T_k(\zeta) \sin \theta \right) \right]
 \end{aligned}$$

$$\begin{aligned}
 C_2 &= \sum_{k=0}^n \omega_n^k \left[ (-1)^{k+1} U_k(\zeta) \sqrt{1-\zeta^2} d_k \right. \\
 &\quad \left. + \varepsilon^{-\phi} e_k \left( (-1)^{k+1} U_k(\zeta) \sqrt{1-\zeta^2} \cos \theta + (-1)^k T_k(\zeta) \sin \theta \right) \right]
 \end{aligned}$$

$$\begin{aligned}
 D_2 &= \sum_{k=0}^n \omega_n^k \left[ (-1)^{k+1} U_k(\zeta) \sqrt{1-\zeta^2} f_k \right. \\
 &\quad \left. + \varepsilon^{-\phi} g_k \left( (-1)^{k+1} U_k(\zeta) \sqrt{1-\zeta^2} \cos \theta + (-1)^k T_k(\zeta) \sin \theta \right) \right]
 \end{aligned}$$

In equation (4.1.11) the arguments  $\omega_n$  and  $\zeta$  have been omitted for simplicity, and use has been made of the identity

$$\varepsilon^{ST} = \varepsilon^{-\phi} (\cos \theta + j \sin \theta)$$



where

$$\phi = \zeta \omega_n T \text{ and } \theta = \omega_n \sqrt{1 - \zeta^2} T \quad (4.1.12)$$

Setting  $F(s) = 0$ , or setting the reals and imaginaries of (4.1.10) to zero, yields

$$\begin{aligned} \alpha B_1 + \beta C_1 &= -D_1 \\ \alpha B_2 + \beta C_2 &= -D_2 \end{aligned} \quad (4.1.13)$$

Then<sup>1</sup>

$$\left. \begin{aligned} \alpha &= \frac{C_1 D_2 - D_1 C_2}{\Delta}, & \beta &= \frac{D_1 B_2 - D_2 B_1}{\Delta} \\ \Delta &= B_1 C_2 - C_1 B_2 \end{aligned} \right\} \quad (4.1.14)$$

Equation (4.1.14) for  $\alpha$  and  $\beta$  are parametric equations in  $\omega_n$  and  $\zeta$ , where  $\omega_n$  is the varying parameter and  $\zeta$  is a given constant, or vice versa.

The  $\alpha$ - $\beta$  curves are mappings of curves from the  $s$ -plane, where the characteristic equation is the transformation function, so that

---

<sup>1</sup>The following equations are indeterminate for  $\zeta = \pm 1$ . See Appendix II for a detailed discussion of this point.

care must be taken with respect to which regions of the s-plane map into corresponding regions in the  $\alpha$ - $\beta$  plane. The procedure is as follows. If a curve in the s-plane is shaded as shown in Figure 4.1.2a, then the side to be shaded in the  $\alpha$ - $\beta$  plane is determined by the sign of the Jacobian determinant [14]

$$J = \begin{vmatrix} \frac{\partial X}{\partial \alpha} & \frac{\partial X}{\partial \beta} \\ \frac{\partial Y}{\partial \alpha} & \frac{\partial Y}{\partial \beta} \end{vmatrix} \quad (4.1.15)$$

where the elements of J are the partial derivatives of

$$X = \alpha B_1 + \beta C_1$$

$$Y = \alpha B_2 + \beta C_2$$

Thus from (4.1.15)

$$J = \Delta = \begin{vmatrix} B_1 & C_1 \\ B_2 & C_2 \end{vmatrix} - \begin{vmatrix} B_2 & C_2 \\ B_1 & C_1 \end{vmatrix}$$

and if  $\Delta > 0$  then the curve in the  $\alpha$ - $\beta$  plane should be shaded on the left facing the direction of increasing  $\omega_n$ , and vice versa.

It is important to note that when symmetrically enclosing the entire left-half s-plane or a region therein, it is not necessary to compute values of  $\alpha, \beta$  for  $\omega_n < 0$ . This is because the curves generated in the  $\alpha$ - $\beta$  plane for values of  $\omega_n < 0$  will retrace the curves for  $\omega_n > 0$ . Hence, the curves in the  $\alpha$ - $\beta$  plane would be doubly shaded on

the same side.<sup>2</sup> This assertion will now be proven.

Since all complex roots must appear with conjugates, the real parts of the conjugate roots must be equal. Since  $\text{Re}[s] = \sigma = -\zeta\omega_n$  it follows that if  $\omega_n > 0$  ( $\omega_n < 0$ ) then  $\zeta > 0$  ( $\zeta < 0$ ) in order that  $\sigma = -\zeta\omega_n$ . Substituting  $\omega_n$ ,  $\zeta < 0$  into (4.1.11) and utilizing (4.1.8a) gives the following:

$$B_1(-\omega_n, -\zeta) = B_1(\omega_n, \zeta)$$

$$C_1(-\omega_n, -\zeta) = C_1(\omega_n, \zeta)$$

$$D_1(-\omega_n, -\zeta) = D_1(\omega_n, \zeta)$$

$$B_2(-\omega_n, -\zeta) = -B_2(\omega_n, \zeta)$$

$$C_2(-\omega_n, -\zeta) = -C_2(\omega_n, \zeta)$$

$$D_2(-\omega_n, -\zeta) = -D_2(\omega_n, \zeta)$$

So that from (4.1.14)

$$\Delta(-\omega_n, -\zeta) = -\Delta(\omega_n, \zeta)$$

$$\alpha(-\omega_n, -\zeta) = \alpha(\omega_n, \zeta)$$

$$\beta(-\omega_n, -\zeta) = \beta(\omega_n, \zeta)$$

---

<sup>2</sup>The practical implication of this statement is as follows. If a change in value of a system parameter causes a pair of complex conjugate roots to cross a shaded boundary in the s-plane, this will cause the corresponding point in the  $\alpha$ - $\beta$  plane to cross a doubly shaded boundary.

Thus when traversing the s-plane through values of  $\omega_n, \zeta < 0$  the sign of  $\Delta$  changes but the values of  $\alpha$  and  $\beta$  remain the same. It follows that the  $\alpha$ - $\beta$  curve for  $\omega_n, \zeta < 0$  falls directly over the curve obtained for  $\omega_n, \zeta > 0$  and is shaded on the same side. The result is a doubly shaded  $\alpha$ - $\beta$  curve. This does not limit the procedure in any way since all complex roots must appear with conjugates.

#### 4.2 Distributed Lags

The method described above is directly applicable to systems containing distributed lags. Only minor modifications of the equations derived are necessary. Consider Figure 4.1.1 and assume that the lag is distributed; then the lag term becomes  $e^{-\sqrt{sT}}$ . If

$$s = -\zeta\omega_n + j\omega_n\sqrt{1 - \zeta^2}$$

then

$$\sqrt{sT} = \sqrt{\frac{T}{2}} \left[ \left( (\zeta\omega_n)^2 + \omega_n^2 \right)^{\frac{1}{2}} + \zeta\omega_n \right]^{\frac{1}{2}} + j\sqrt{\frac{T}{2}} \left[ \left( (\zeta\omega_n)^2 + \omega_n^2 \right)^{\frac{1}{2}} - \zeta\omega_n \right]^{\frac{1}{2}} \quad (4.2.1)$$

Defining  $\text{Re}[\sqrt{sT}] = \bar{\phi}$  and  $\text{Im}[\sqrt{sT}] = \bar{\theta}$  it is only necessary to substitute  $\bar{\phi}$  for  $\phi$  and  $\bar{\theta}$  for  $\theta$  in all of the equations of Section 4.1 derived for the transport lag. The ensuing interpretation of the curves in the  $\alpha$ - $\beta$  plane is unchanged.

#### 4.3 Example of Absolute and Relative Stability of a Linear Feedback Control System

An example is now introduced in order to apply the derivation of Section 4.1, and to form a basis for the development of further theory.

Consider the control system<sup>3</sup> of Figure 4.3.1 containing a proportional-integral controller, plant and constant delay, then

$$G(s) = \frac{N(s)}{D(s)} = \frac{K(s + \tau)}{s^2}$$

For a stability investigation of this system form the characteristic equation

$$F(s) = \epsilon^{sT} s^2 + Ks + K\tau = 0$$

define the adjustable parameters to be

$$\alpha = K$$

$$\beta = K\tau$$

then

$$F(s) = \epsilon^{sT} s^2 + \alpha s + \beta = 0 \quad (4.3.1)$$

From (4.1.6)

$$b_0 = 0, \quad c_0 = 0, \quad d_0 = 1, \quad e_0 = 0, \quad f_0 = 0, \quad g_0 = 0$$

$$b_1 = 1, \quad c_1 = 0, \quad d_1 = 0, \quad e_1 = 0, \quad f_1 = 0, \quad g_1 = 0 \quad (4.3.2)$$

$$b_2 = 0, \quad c_2 = 0, \quad d_2 = 0, \quad e_2 = 0, \quad f_2 = 0, \quad g_2 = 1$$

---

<sup>3</sup>This particular system was analyzed in [2] for  $\tau = 0.3$  sec.,  $T = 1$  sec. The technique used was a root-locus method where the *single* parameter  $K$  was varied. Thus, in this example comparisons of data can be made for  $\tau = 0.3$  sec. and  $T = 1$  sec. See Figure 3.5.5 in Chapter 3.

so that from (4.1.11)

$$\begin{aligned}
 B_1 &= -\zeta\omega_n \\
 C_1 &= 1 \\
 D_1 &= \omega_n^2 \varepsilon^{-\phi} ([2\zeta^2 - 1] \cos\theta + 2\zeta\sqrt{1 - \zeta^2} \sin\theta) \\
 B_2 &= \omega_n \sqrt{1 - \zeta^2} \\
 C_2 &= 0 \\
 D_2 &= \omega_n^2 \varepsilon^{-\phi} (-2\zeta\sqrt{1 - \zeta^2} \cos\theta + (2\zeta^2 - 1) \sin\theta)
 \end{aligned} \tag{4.3.3}$$

Substituting (4.3.3) into (4.1.14) gives

$$\begin{aligned}
 \alpha &= \frac{\omega_n \varepsilon^{-\phi}}{\sqrt{1 - \zeta^2}} (2\zeta\sqrt{1 - \zeta^2} \cos\theta + (1 - 2\zeta^2) \sin\theta) \\
 \beta &= \frac{\omega_n^2 \varepsilon^{-\phi}}{\sqrt{1 - \zeta^2}} (\sqrt{1 - \zeta^2} \cos\theta - \zeta \sin\theta) \\
 \Delta &= -\omega_n \sqrt{1 - \zeta^2}
 \end{aligned} \tag{4.3.4}$$

The variables  $\alpha$  and  $\beta$  are now graphed with either  $\omega_n$  or  $\zeta$  as the running parameter. The various regions of the s-plane to be mapped are shown in Figure 4.1.2.

In order to determine the limiting values of  $\alpha, \beta$  for *absolute* stability it is only necessary to set  $\zeta = 0$  in (4.3.4) and let  $\omega_n$

vary from zero to infinity (see Figure 4.1.2a). Recall that values of  $\omega_n < 0$  need not be plotted.

Then from (4.3.4), setting  $\zeta = 0$  gives

$$\begin{aligned}\alpha &= \omega_n \sin \omega_n T \\ \beta &= \omega_n^2 \cos \omega_n T\end{aligned}\quad (4.3.5)$$

A graph of (4.3.5) is shown in Figure 4.3.2 where  $T = 1$  sec. was chosen as the time delay. If, for example,  $\tau = 0.3$  sec. then

$$\beta = K\tau = 0.3K = 0.3\alpha$$

The above equation is a straight line which is also shown in Figure 4.3.2. It follows that the infinite set of frequencies,  $\omega_{n_1}$ ,  $\omega_{n_2}$ ,  $\omega_{n_3}$ , . . . , at which the complex roots cross the imaginary axis are determined by the intersections of the  $\alpha$ - $\beta$  curve and the straight line  $\beta = \tau\alpha$ . Further, dropping a perpendicular from the points labeled  $\omega_{n_1}$ ,  $\omega_{n_2}$ ,  $\omega_{n_3}$ , . . . , to the  $\alpha$  axis gives the gains at which the complex roots cross the imaginary axis. Because the characteristic equation contains a transcendental term there will be an infinite number of such points corresponding to the infinite number of roots of the characteristic equation.

The interpretation given above is deduced from the fact that the entire imaginary axis of the  $s$ -plane of Figure 4.1.2a has been mapped into the  $\alpha$ - $\beta$  locus shown in Figure 4.3.2. The entire left-hand  $s$ -plane has been mapped within the indicated doubly shaded region. Note that

in this example it is always true that  $\Delta = -\omega_n \sqrt{1 - \zeta^2} < 0$ , since  $0 \leq \zeta \leq 1$  and  $\omega_n \geq 0$ , so that the  $\alpha$ - $\beta$  curve is shaded on the right facing the direction of increasing  $\omega_n$ .

The axes of the first quadrant of the  $\alpha$ - $\beta$  plane are singly shaded to include this quadrant since from a practical point of view,  $\alpha$  and  $\beta > 0$ . This divides the first quadrant into regions  $R_1, R_2, R_3, \dots, R_\infty$  where  $R_1 \supset R_2 \supset R_3 \supset \dots \supset R_\infty$ . Only values of  $\alpha$  and  $\beta$  chosen in  $R_1$  will render the system absolutely stable.<sup>4</sup> This is because crossing from a shaded region to an unshaded region in the  $s$ -plane has the same meaning in the  $\alpha$ - $\beta$  plane, and vice versa. Thus, moving from  $R_1$  to  $R_2$  implies that a pair of complex roots has migrated from the left-half  $s$ -plane into the right-half-plane and so on for  $R_2$  to  $R_3$ , etc. Thus, only  $R_1$  can contain all the roots since it is completely closed and contains no subregions.

For example, if a working point  $M(\alpha_1, \beta_1)$  is chosen in  $R_2$ , all the roots of  $F(s)$  will be in the left-half-plane except for one pair that has migrated to the right-half-plane at some frequency  $\omega_{n_1}$ . In this instance the first two conjugate roots can leave  $R_1$  at  $\omega_{n_1} \cong 1.35$  rad./sec. for a system gain of 1.32. Therefore the maximum gain allowable for absolute stability is  $\alpha = K = 1.32$ . Note from Figure 4.3.2 that since  $\omega_n$  continuously increases along the  $\alpha$ - $\beta$  locus, the intersections of the  $\alpha$ - $\beta$  locus and the  $\beta = \tau\alpha$  locus will occur at ever

---

<sup>4</sup>The concept of absolute stability is now slightly modified due to the restriction  $\alpha$  and  $\beta > 0$ . However, in Section 4.7 real root boundaries are introduced and this restriction can be omitted.



larger gains. This continual increase of the  $\alpha$ - $\beta$  locus towards infinity with increasing  $\omega_n$  is easily predicted from (4.3.5); since  $\zeta = 0$ ,  $\epsilon^{-\zeta\omega_n T} = 1$  and the  $\omega_n$  and  $\omega_n^2$  terms of (4.3.5) dominate. These results are easily confirmed by examining the root-locus for this system, shown in Figure 3.5.5 of Chapter 3.

In order to investigate the *relative* stability of the system of Figure 4.3.1 with respect to constant  $\zeta$  lines, the procedure is almost the same as for absolute stability except that values for  $\zeta = \zeta_1$  of Figure 4.1.2b are substituted into (4.3.4)<sup>5</sup>. Figure 4.3.3 shows the  $\alpha$ - $\beta$  curve for  $\zeta = \zeta_1 = 0.2$ . This figure is interpreted the same way as Figure 4.3.2 with respect to shadings. The figure indicates what must be true of all systems with transport lag under the relative stability constraint of  $\zeta = \zeta_1$ . That is, the locus must eventually terminate at the origin due to the existence of the  $\epsilon^{-\zeta\omega_n T}$  term as opposed to the termination of the locus at infinity for  $\zeta = 0$ . Thus, there exists no value of  $\alpha, \beta$  for *all* the roots of the characteristic equation of the system to be within arbitrary radials,  $\zeta = \zeta_1 \neq 0$ , since there will be no region that contains all the roots. In Figure 4.3.3, for example, the relative positions of the complex roots with respect to radials defined by  $\zeta = 0.2$  in the  $s$ -plane is determined as follows.

---

<sup>5</sup>Note that if values of  $\zeta = \zeta_1 < 0$  and  $\omega_n > 0$  are substituted into (4.3.4) the resulting  $\alpha$ - $\beta$  curves yield information about the complex roots in the right-hand  $s$ -plane. The right-hand  $s$ -plane, however, is not of interest since the absolute stability of the system with respect to complex roots can be guaranteed.

The line  $\beta = 0.3\alpha$  is considered to be a reference line L. Note that although the  $\alpha$ - $\beta$  locus is graphed for increasing  $\omega_n$ , it crosses L at frequencies  $\omega_{nA} = 7.75 > \omega_{nB} = 0.95 < \omega_{nC} = 14.2$  rad./sec., etc. Next, define the intersection of L and the  $\alpha$ - $\beta$  locus for smallest  $\omega_n$  as the relative position of the fundamental complex roots, the intersection of L and the locus for the next highest  $\omega_n$  as the relative position of the secondary complex roots, etc. Now we choose a point on L, say  $L_B = \omega_{nB} \equiv M(0.9, 0.3)$ , and investigate the effect of moving from different points on L to  $L_B$  with particular emphasis on the crossings of shaded boundaries. Since  $L_B$  was chosen on the  $\zeta = 0.2$  locus, the values  $\alpha_B = 0.9$  and  $\beta_B = 0.3$  locate the fundamental complex roots on radials of  $\zeta = 0.2$  at a frequency of  $\omega_{nB} = 0.95$  rad./sec. It is easily verifiable from Figure 4.1.2b that the fundamental complex roots are located at the points<sup>6</sup>

$$s_1 = -\zeta\omega_{nB} \pm j\omega_{nB}\sqrt{1 - \zeta^2} \quad (4.3.6)$$

in the s-plane.

Now if the point  $L_A$  moves to  $L_B$  it must cross a doubly shaded boundary from an unshaded side to a shaded side. In the s-plane this means that a pair of complex roots must cross from an unshaded to a shaded side across the boundary  $\zeta = 0.2$ . Thus, the secondary complex

---

<sup>6</sup>This is quite useful as a synthesis technique to place dominant roots at a predetermined location as will be demonstrated later.

roots lie *below* the radials  $\zeta = 0.2$  since the reverse crossing must have occurred for  $L_A$  to be in its present position. If the point  $L_C$  moves to  $L_B$  a doubly shaded boundary is crossed from a shaded side to an unshaded side. Thus, the secondary complex roots lie *above* the radials  $\zeta = 0.2$ . This procedure is continued until the relative location of as many complex roots as desired is determined. For verification of these results see Figure 4.3.4 which was taken from [2].

#### 4.4 Relative Stability with Respect to Finite Semicircular Regions

Consider Figure 4.1.2c where the finite interior of the shaded region in the left-hand  $s$ -plane is to be mapped onto the  $\alpha$ - $\beta$  plane. This mapping is easily facilitated through equations (4.3.4) by first setting  $\zeta = 0$  and allowing  $\omega_n$  to vary from 0 to  $\omega_n'$ , then holding  $\omega_n$  fixed at  $\omega_n'$  and allowing  $\zeta$  to vary between 0 and 1. When  $\omega_n = 0$  or  $\zeta = 1$  the points  $\sigma = 0$  and  $\omega_n'$  respectively are mapped from the  $s$ -plane onto the  $\alpha$ - $\beta$  plane. These  $s$ -plane points are the boundaries across which real roots must cross if they are to leave the finite region under discussion. These points can be mapped onto the  $\alpha$ - $\beta$  plane by substituting  $s = -\sigma$  into equation (4.3.1) and then plotting the resulting  $\alpha, \beta$  locus for  $\sigma = 0$  and  $\sigma = \omega_n'$ . The mapping is singly shaded since crossing this  $\alpha$ - $\beta$  curve corresponds to a single real root leaving the interior of the finite  $s$ -plane region under consideration. The rules for shading (both single and double) the resulting  $\alpha$ - $\beta$  plane curves are unchanged, as are the conditions for  $\omega_n < 0$ .

Suppose that it is desirable to know what values of  $\alpha, \beta$  will cause the roots that lie within the semicircle of radius  $\omega_n' = 5$  rad./sec. to leave this region of the s-plane shown in Figure 4.1.2c. This information can be obtained by superimposing<sup>7</sup> the  $\alpha$ - $\beta$  plane curves for  $\zeta = 0$ , the curve obtained by holding  $\omega_n'$  fixed at  $\omega_n' = 5$  rad./sec. and allowing  $\zeta$  to vary between 0 and 1, and the curves obtained from (4.3.1) where  $s = -\sigma = 0$  and  $\omega_n'$ . The resulting  $\alpha$ - $\beta$  curve is shown in Figure 4.4.1 and is interpreted as follows. The curve corresponding to varying  $\zeta$  never intersects the  $\beta = 0.3\alpha$  line, consequently there is no positive value  $\alpha$  or  $\beta$  such that the existing complex roots in the shaded region of the s-plane can leave this region via the locus of points described by the semicircle. They can, however, leave by crossing the imaginary axis as usual. The singly shaded line corresponding to  $\sigma = -5$  intersects the  $\beta = 0.3\alpha$  line so that a single real root can leave the semicircle in the s-plane by crossing the point  $\sigma = -5$ .

Now we extend the semicircle to a radius  $\omega_n' = 10$  rad./sec. (see Figure (4.4.2)). The portion of the  $\alpha$ - $\beta$  curve corresponding to a variable  $\zeta$  now crosses the  $\beta = 0.3\alpha$  line so it is possible for *one* pair of complex roots to leave the semicircle of radius  $\omega_n' = 10$  rad./sec. Further, the singly shaded line corresponding to  $\sigma = -10$  intersects the  $\beta = 0.3\alpha$  line so that a single real root can leave the

---

<sup>7</sup>In fact, any of the mappings discussed can be superimposed to form new mappings.

semicircle in the s-plane by crossing the point  $\sigma = -10$ . The shading of the curves for varying  $\zeta$  and constant  $\sigma$  are as shown in Figures 4.4.1 and 4.4.2, since this is simply a continuation of the varying  $\omega_n$  curve with respect to shading procedures. These results are clearly verified from the root-locus plot of the system shown in Figure 4.4.3.

Figure 4.4.3 shows the fundamental, secondary and real root-loci for this system where  $T = 1$  sec. and  $\tau = 0.3$  sec., also shown are the finite semicircles of radius  $\omega_n' = 5$  and  $10$  rad./sec. Note that for  $\omega_n' = 5$  rad./sec. the fundamental and secondary root-loci never intersect the semicircle but the locus of the real roots does. When  $\omega_n' = 10$  rad./sec. the secondary root-locus, as well as the real root-locus, does intersect the semicircle so that *one* pair of complex roots and one real root can leave the semicircular region.

#### 4.5 Relative Stability with Respect to Constant Settling Time Lines

The mapping of a constant settling time line as shown in Figure 4.1.2d can be effected by manipulation of  $\alpha$  and  $\beta$  from the original equations (4.3.4). In this instance the mapping traverses a contour of constant  $\sigma = -\zeta\omega_n$ , and the dimensionless damping ratio,  $\zeta$ , is variable. Thus the equations for  $\alpha$  and  $\beta$  can be rearranged such that  $\zeta$  never appears alone, but only in the product  $\sigma = -\zeta\omega_n$ . Rearranging (4.3.4) so that only  $\sigma$  and  $\omega_n$  appear as variables gives

$$\alpha = \frac{e^{-\sigma T}}{\sqrt{\omega_n^2 - \sigma^2}} \left( 2\sigma\sqrt{\omega_n^2 - \sigma^2} \cos\sqrt{\omega_n^2 - \sigma^2}T + (\omega_n^2 - 2\sigma^2) \sin\sqrt{\omega_n^2 - \sigma^2}T \right) \quad (4.5.1)$$

$$\beta = \frac{\omega_n^2 \epsilon^{-\sigma T}}{\sqrt{\omega_n^2 - \sigma^2}} \left( \sqrt{\omega_n^2 - \sigma^2} \cos \sqrt{\omega_n^2 - \sigma^2} T - \sigma \sin \sqrt{\omega_n^2 - \sigma^2} T \right)$$

for  $\omega_n^2 > \sigma^2$ .

Since the mapping is for  $0 \leq \omega_n \leq \infty$  there is a portion of the contour in Figure 4.1.2d where  $\omega_n^2 < \sigma^2$ . In this case (4.5.1) becomes (see Appendix III)

$$\alpha = \frac{\epsilon^{-\sigma T}}{\sqrt{\sigma^2 - \omega_n^2}} \left( 2\sigma \sqrt{\sigma^2 - \omega_n^2} \cosh \sqrt{\sigma^2 - \omega_n^2} T + (\omega_n^2 - 2\sigma^2) \sinh \sqrt{\sigma^2 - \omega_n^2} T \right) \quad (4.5.2)$$

$$\beta = \frac{\omega_n^2 \epsilon^{-\sigma T}}{\sqrt{\sigma^2 - \omega_n^2}} \left( \sqrt{\sigma^2 - \omega_n^2} \cosh \sqrt{\sigma^2 - \omega_n^2} T - \sigma \sinh \sqrt{\sigma^2 - \omega_n^2} T \right)$$

for  $\omega_n^2 < \sigma^2$ .

The singularity occurring when  $\sigma = \omega_n$  implies that  $\zeta = \pm 1$  and is removed as explained in Appendix II.

For example, consider the instance where  $\sigma = -0.5$ . The exponential terms in (4.5.1) and (4.5.2) are fixed at a constant value and the  $\alpha$ - $\beta$  curve must spiral out to infinity and not into the origin as in the case of a constant  $\zeta$  line. Figure 4.5.1 shows the  $\alpha$ - $\beta$  curve obtained and is interpreted as follows. The locus of points where the  $\beta = 0.3\alpha$  line intersects the  $\alpha$ - $\beta$  curve determines the frequencies and gains where the complex roots of the characteristic equation (4.1.5) cross the constant settling time line  $\sigma = -0.5$ . Since the  $\beta = 0.3\alpha$  locus does not enter  $R_1$ , the fundamental complex roots lie to the right of

$\sigma = -0.5$ , and cannot cross this line for any value of gain (see the root-locus plot for Figure 4.4.3). The remaining complex roots all lie to the left of  $\sigma = -0.5$  and would cross this line at frequencies  $\omega_{n_2} = 7.7$ ,  $\omega_{n_3} = 14.1$  rad./sec., . . . , etc. for values of gain equal to  $\alpha_2 = 4.7$ ,  $\alpha_3 = 8.5$ , . . . , respectively. Since a constant  $\sigma < 0$  line can be interpreted as a shifting of the imaginary axis  $\sigma$  units to the left, it is reasonable that the  $\alpha$ - $\beta$  curve should closely resemble the  $\alpha$ - $\beta$  curve for  $\zeta = 0$ . It also follows that the interpretation of both curves are identical.

#### 4.6 Real Roots

The question of the determination of the real roots of the characteristic equation (4.1.5) is now considered. The technique utilized to resolve this question is a natural continuation of previous results since equations (4.1.14) are applicable to any point in the  $s$ -plane. In order to investigate the nature of the real roots of the characteristic equation only the real axis is considered. Substituting  $s = \sigma + j0$  into (4.1.5) gives

$$F(\sigma) = \sum_{k=0}^n \alpha_k(\sigma) \sigma^k = 0 \quad (4.6.1)$$

Then substituting (4.1.6) into (4.6.1) gives

$$\alpha \sum_{k=0}^n \sigma^k (b_k + c_k \epsilon^{\sigma T}) + \beta \sum_{k=0}^n \sigma^k (d_k + e_k \epsilon^{\sigma T}) + \sum_{k=0}^n \sigma^k (f_k + g_k \epsilon^{\sigma T}) = 0 \quad (4.6.2)$$

Thus, for a given value of  $\sigma$ , (4.6.2) represents a straight line in the  $\alpha$ - $\beta$  plane. Note that since a point in the  $s$ -plane maps into a line in the  $\alpha$ - $\beta$  plane the mapping is not conformal. For a given working point  $M(\alpha_1, \beta_1)$  every value of  $\sigma$  that satisfies (4.6.2) is a real root of (4.1.5). These real roots may be determined by graphing (4.6.2) for different values of  $\sigma$  until the straight line passes through the point  $\alpha_1, \beta_1$ . The values of  $\sigma$  that accomplish this condition are real roots of (4.1.5). Since (4.6.2) is the equation of a straight line for a given  $\sigma$ , the graphing is not tedious and interpolation between curves is readily effected. Figure 4.6.1 shows the curves represented by (4.6.2) with various values of  $\sigma$  for the case of Equation (4.3.1). Thus, when  $\alpha = 1, \beta = 0.3$  a real root is determined to be at  $\sigma = -0.413$ .

As an aid in determining the real roots, an alternate procedure can be employed that not only approximately determines the real root values, but also indicates how many real roots exist. The question of the number of real roots is not trivial since the characteristic equation has an infinite number of roots. The procedure is as follows: construct the  $\alpha$ - $\beta$  curves for  $\zeta = \pm 1$  and note the values of frequency,  $\omega_n$ , on these curves. Then draw straight lines through the working point  $M(\alpha_1, \beta_1)$  that are tangent to the  $\zeta = \pm 1$  curve. The number of roots equals the number of tangent lines that can be constructed and the values of these real roots are equal to negative values of the frequencies,  $\omega_{n_1}, \omega_{n_2}, \omega_{n_3}, \dots$ , noted on the  $\zeta = +1$  curve or the positive values of the frequencies noted on the  $\zeta = -1$  curve at these



tangent points. Proof of this statement is given in Appendix IV.

Thus, the values of the real roots are obtained along with the number of real roots.

Using the procedure of Appendix II the equations for the  $\alpha$ - $\beta$  curves for  $\zeta = +1$  become

$$\alpha = \omega_n \varepsilon^{-\omega_n} (2 - \omega_n) , \quad \beta = \omega_n^2 \varepsilon^{-\omega_n} (1 - \omega_n) \quad (4.6.3)$$

and for  $\zeta = -1$  the  $\alpha$ - $\beta$  equations become

$$\alpha = -\omega_n \varepsilon^{\omega_n} (2 - \omega_n) , \quad \beta = \omega_n^2 \varepsilon^{\omega_n} (1 + \omega_n) \quad (4.6.4)$$

Figure 4.6.2 shows these  $\alpha$ - $\beta$  curves and illustrates that there is only one possible straight line that is tangent to the  $\zeta = \pm 1$  curve from the working point  $M(1.0, 0.3)$ . The frequency at this tangent point is  $\omega_n \cong 0.4$  rad./sec. so that there is a single real root of approximate value  $\sigma = -0.4$ . At this point it is pertinent to discuss the nature of the curvature of the  $\zeta = \pm 1$  curve for this example. The slope of the  $\zeta = \pm 1$  curve is determined, from equations (4.6.3) and (4.6.4), to be for  $\zeta = +1$

$$\left( \frac{d\beta}{d\omega_n} \right) \left( \frac{d\omega_n}{d\alpha} \right) = \frac{d\beta}{d\alpha} = \omega_n \quad (4.6.5)$$

and for  $\zeta = -1$

$$\left( \frac{d\beta}{d\omega_n} \right) \left( \frac{d\omega_n}{d\alpha} \right) = \frac{d\beta}{d\alpha} = -\omega_n$$

Thus the slopes of the  $\zeta = \pm 1$  curves increase or decrease monotonically with  $\omega_n$  and it is not possible for these curves to have any points of inflection; this also means that the curves are always either concave upward or concave downward with a discontinuity at the point where the curve changes direction. This clearly shows that a tangent to the curve cannot exist at the points where the curve changes direction, that is, at the tips of the loops in the regions denoted as A and A' on Figure 4.6.2. This point is emphasized since, at first glance, it may not be obvious that a tangent line cannot be drawn to the curve from the point  $M(1.0, 0.3)$  to the discontinuous<sup>8</sup> extreme points in the regions A and A'.

#### 4.7 Real Root Boundaries

$\alpha$ - $\beta$  curves for  $\zeta = \pm 1$  were introduced in the previous section where these curves were used to predict positive and negative real root locations. It will be shown that "real root boundaries" can be defined using the  $\zeta = -1$  curve that will have the same significance as complex root (double shaded) boundaries. These real root boundaries can easily be constructed by noting the regions in the  $\alpha$ - $\beta$  plane from which tangent lines to the  $\zeta = -1$  curve can be constructed. Namely, if a tangent line can be drawn to the  $\zeta = -1$  curve from  $M(\alpha_1, \beta_1)$  then a positive real root exists for the values  $\alpha = \alpha_1, \beta = \beta_1$ .

---

<sup>8</sup>For an excellent discussion on the determination of discontinuities of parametric equations see Chapter 5 of Reference 4.

As an example, consider Figure 4.7.1 which shows the  $\alpha$ - $\beta$  curve for  $\zeta = -1$ . From the slope of the  $\zeta = -1$  curve (recall  $\frac{d\beta}{d\alpha} = -\omega_n$ ) it is obvious that if  $M(\alpha_1, \beta_1)$  lies in region I real positive roots cannot exist. This is because a tangent line cannot be drawn from  $M(\alpha_1, \beta_1)$  to the  $\zeta = -1$  curve. However, a point  $M(\alpha_1, -\beta_1)$  in region II will generate a real positive root so that the  $\alpha \geq 0$  axis is *singly* shaded.<sup>9</sup> Note that the slope of the  $\zeta = -1$  curve at  $\omega_n = 0$  is  $\left. \frac{d\beta}{d\alpha} \right|_{\omega_n=0} = \omega_n = 0$  so that a tangent line can be constructed from the entire  $\alpha \geq 0$  axis. Proceeding in this manner it is obvious that the remaining real root boundary is the  $\zeta = -1$  curve as shown in Figure 4.7.1.

Figure 4.7.2 shows the real root boundary and the complex root boundary for absolute stability ( $\zeta = 0$ ) which is simply the superposition of Figures 4.7.1 and 4.3.2. Note that the restriction that  $\alpha$  and  $\beta$  be positive in order to define regions of stability can be omitted. Thus, conventional regions of stability can be defined. It is noted, however, that  $R_1$  is still the region of *absolute* stability since the real root boundary is the positive  $\alpha$  axis and the singly shaded curve in the second quadrant of Figure 4.7.2.

In conclusion, this chapter has presented an exact method for determining the absolute and relative stability of linear feedback

---

<sup>9</sup>The implication being that crossing a singly shaded boundary in the  $\alpha$ - $\beta$  plane causes a single real root to cross the imaginary axis in the  $s$ -plane.

control systems containing transport or distributed lag. In order to accomplish this it was necessary to determine the locations of the infinite number of roots of the system characteristic equation. A knowledge of the root locations also establishes the nature of the system transient response. Thus, the next logical step is to apply the theory of this chapter to the design of system controllers.

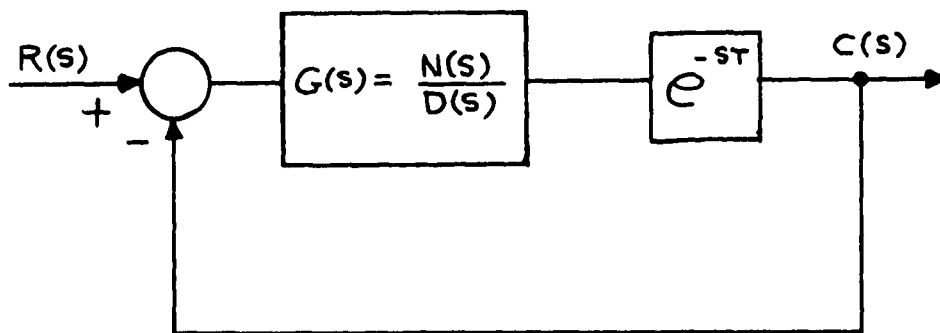


Fig. 4.1.1 Control System With a Transport Lag.

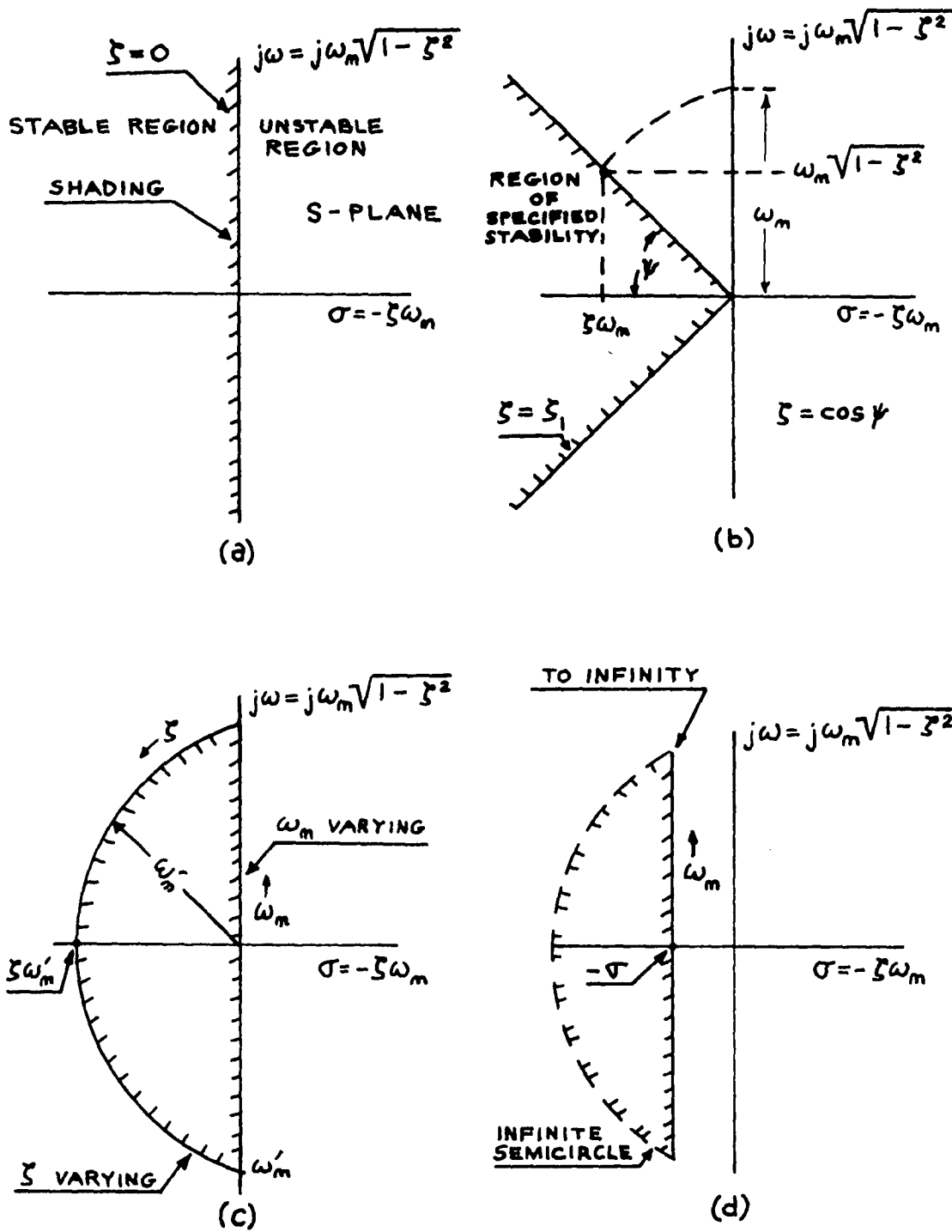


Fig. 4.1.2 s-Plane Contours.

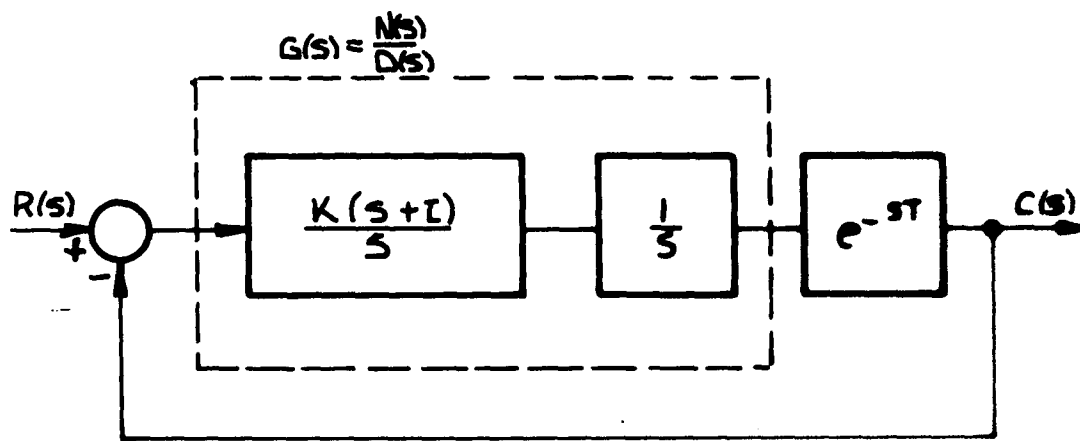


Fig. 4.3.1 Control System with Integral-Proportional Controller

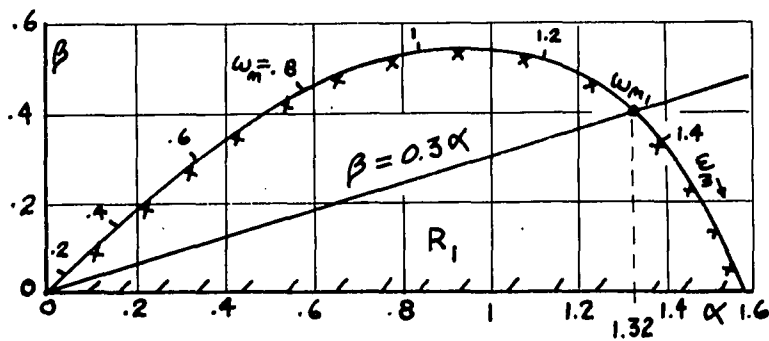
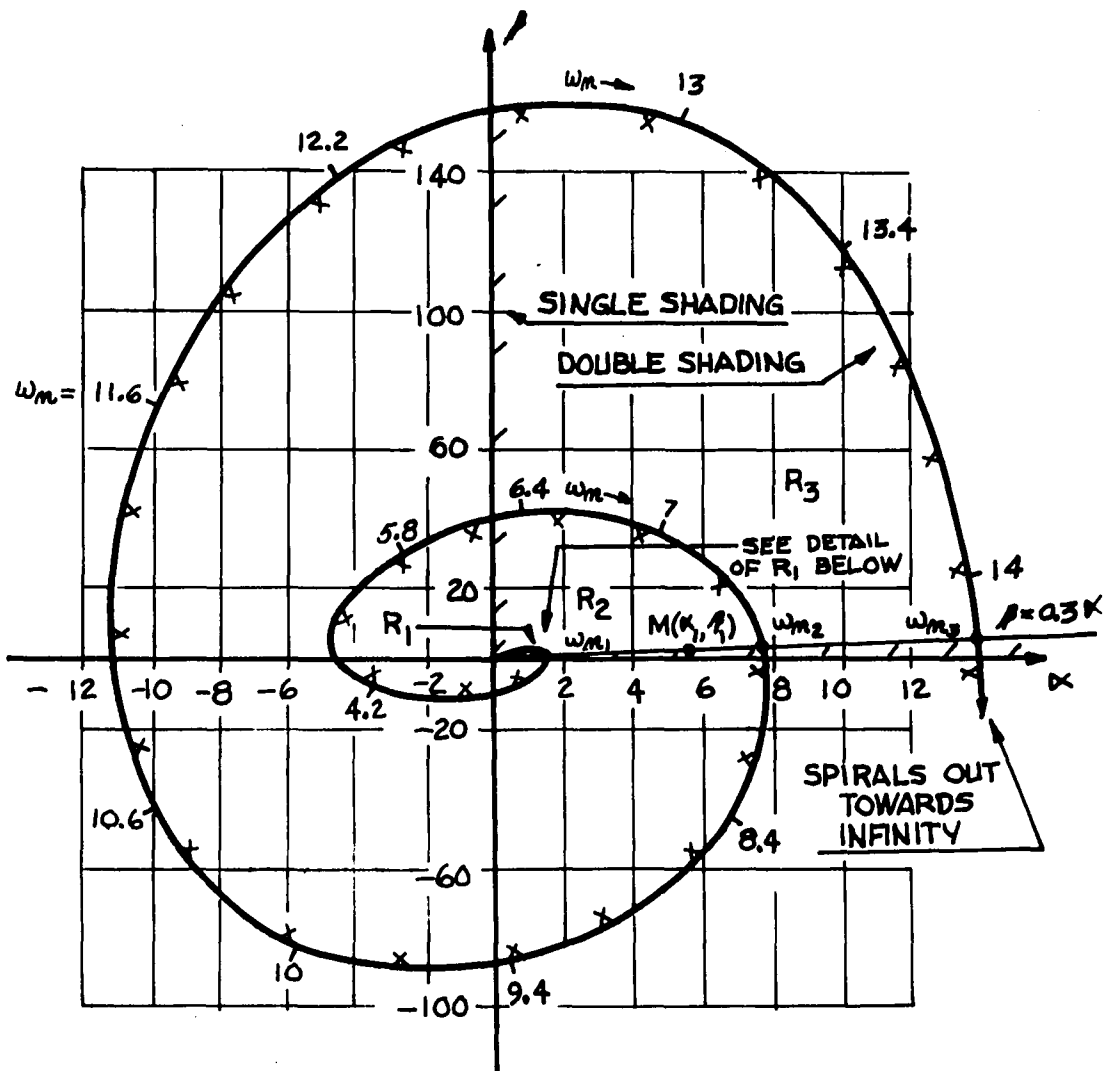


Fig. 4.3.2  $\alpha$ - $\beta$  Plot for  $\zeta = 0$ ,  $T = 1$  sec.



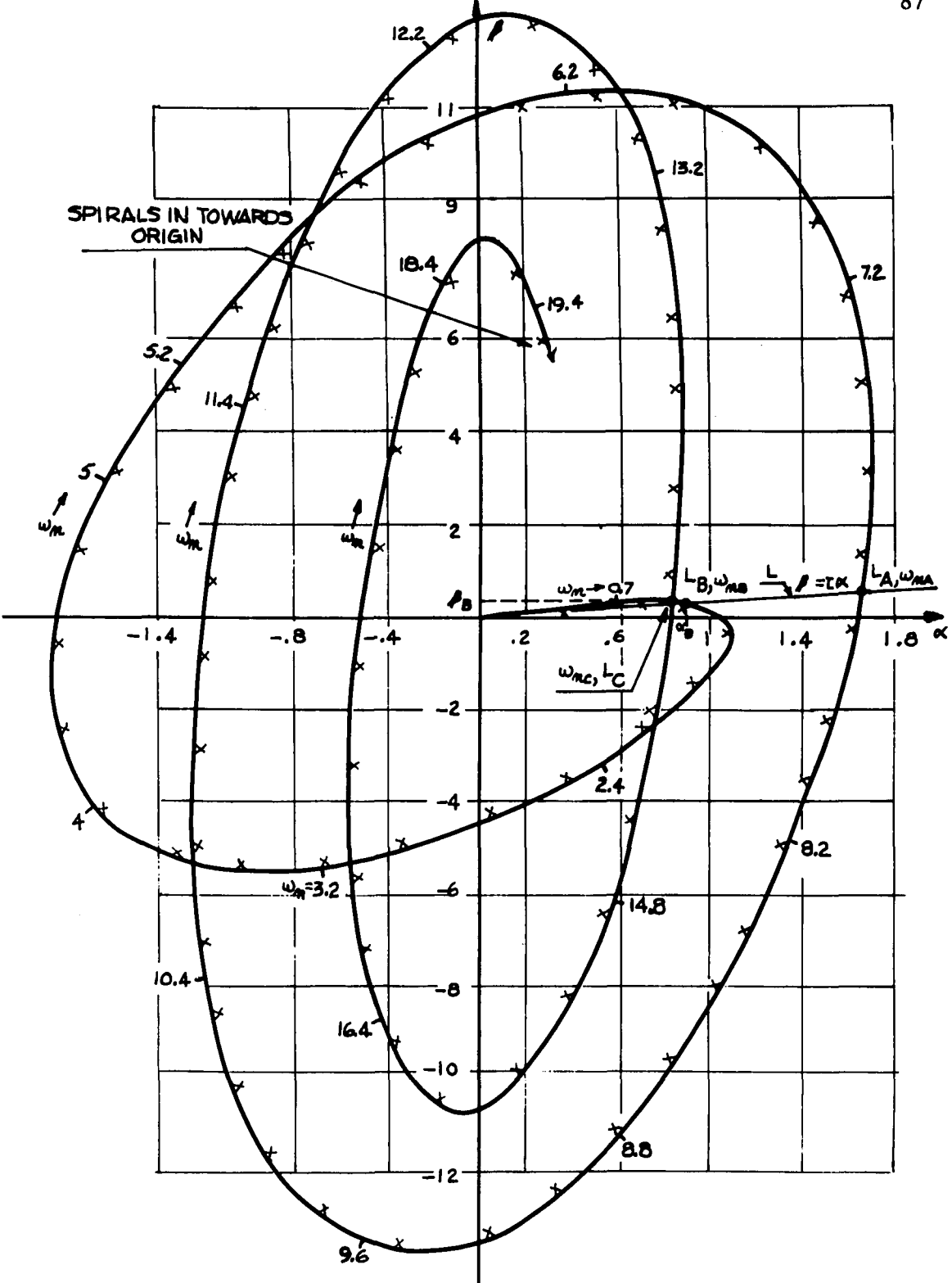


Fig. 4.3.3  $\alpha$ - $\beta$  Plot for  $\zeta = 0.2, T = 1$  sec.

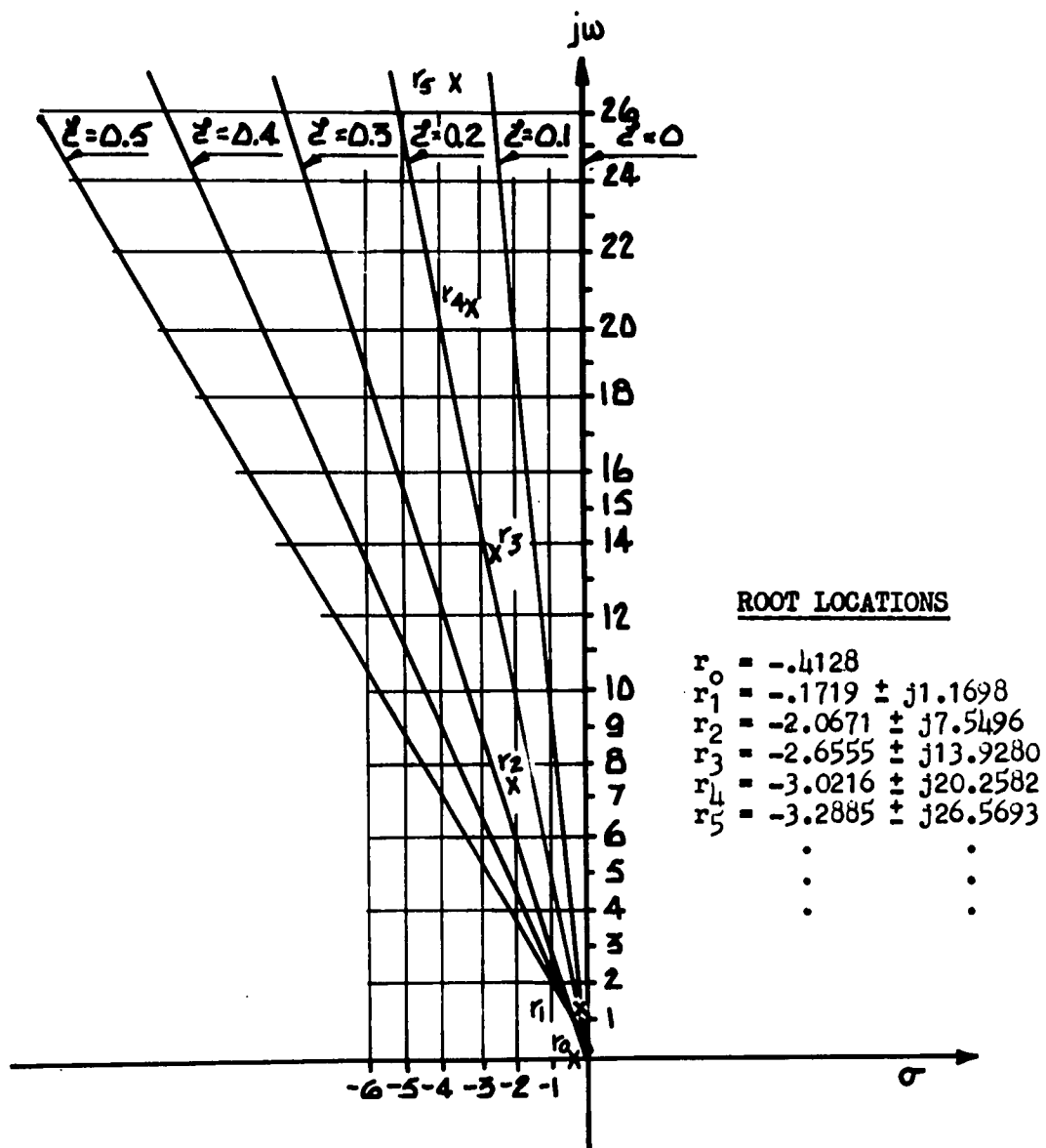


Fig. 4.3.4 Root Locations.

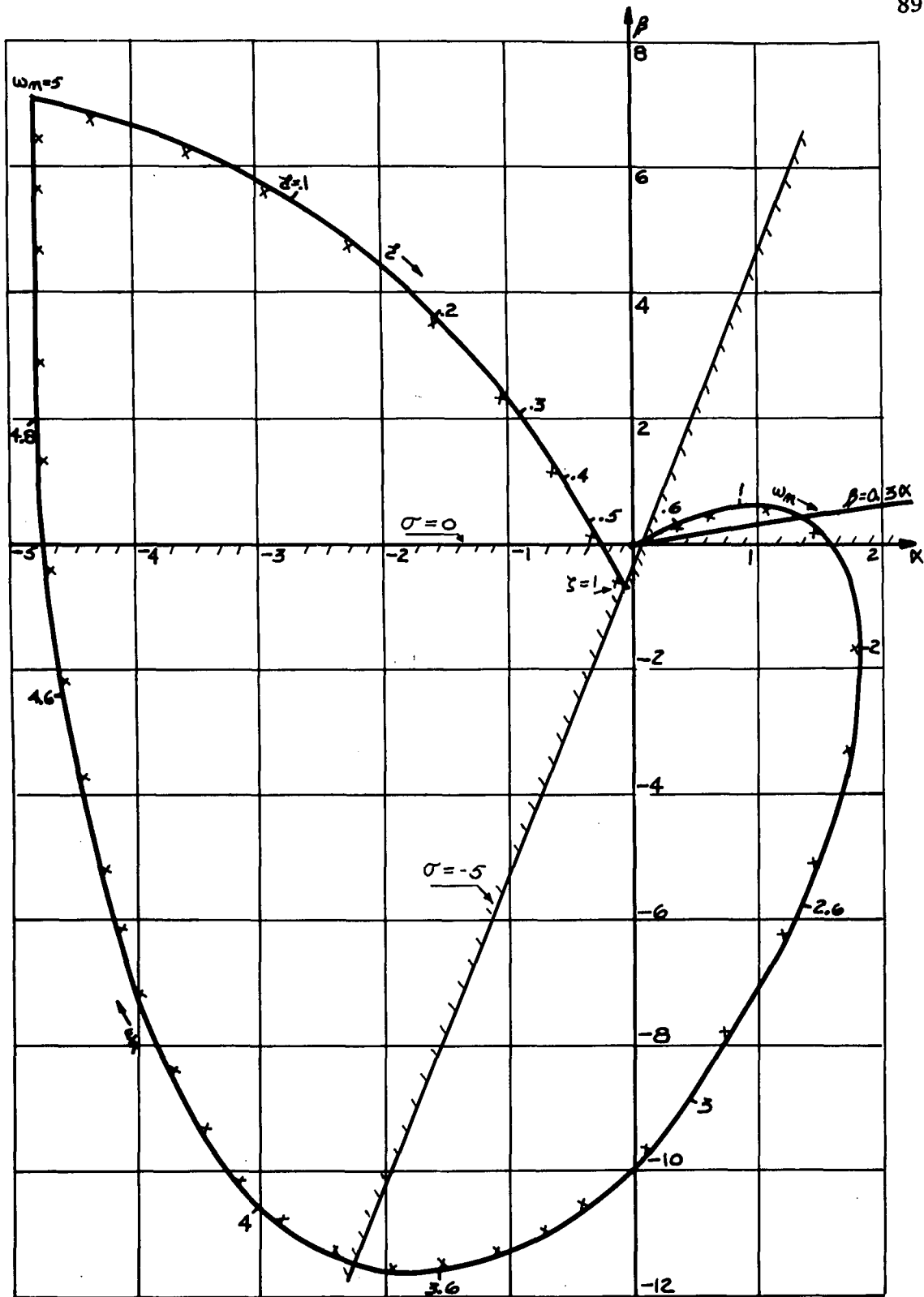


Fig. 4.4.1  $\alpha$ - $\beta$  Plot for a Semicircle of Radius  $\omega_n = 5$  rad./sec.

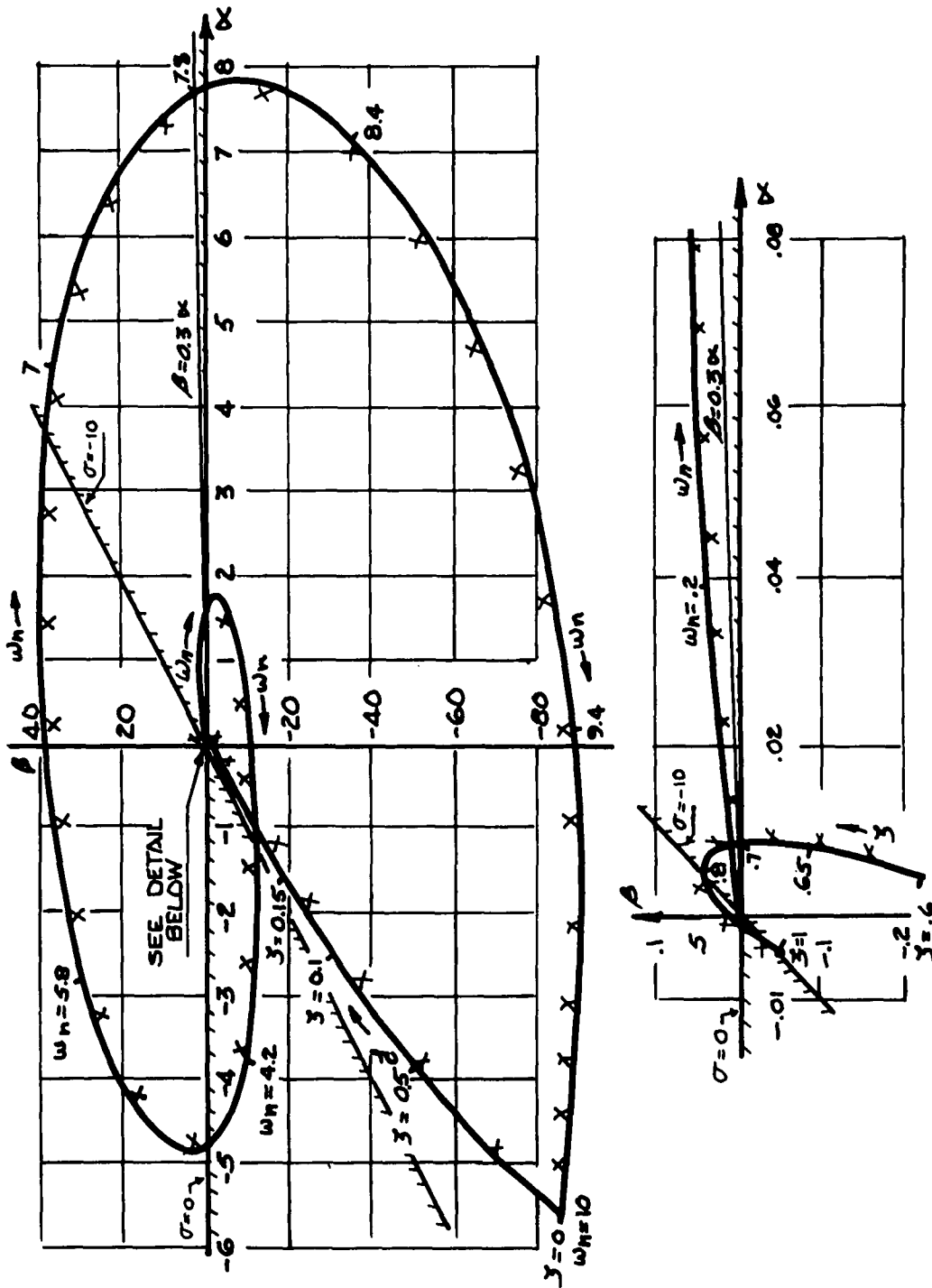


Fig. 4.4.2  $\alpha$ - $\beta$  Plot for a Semicircle  $\omega_n = 10$  rad./sec.

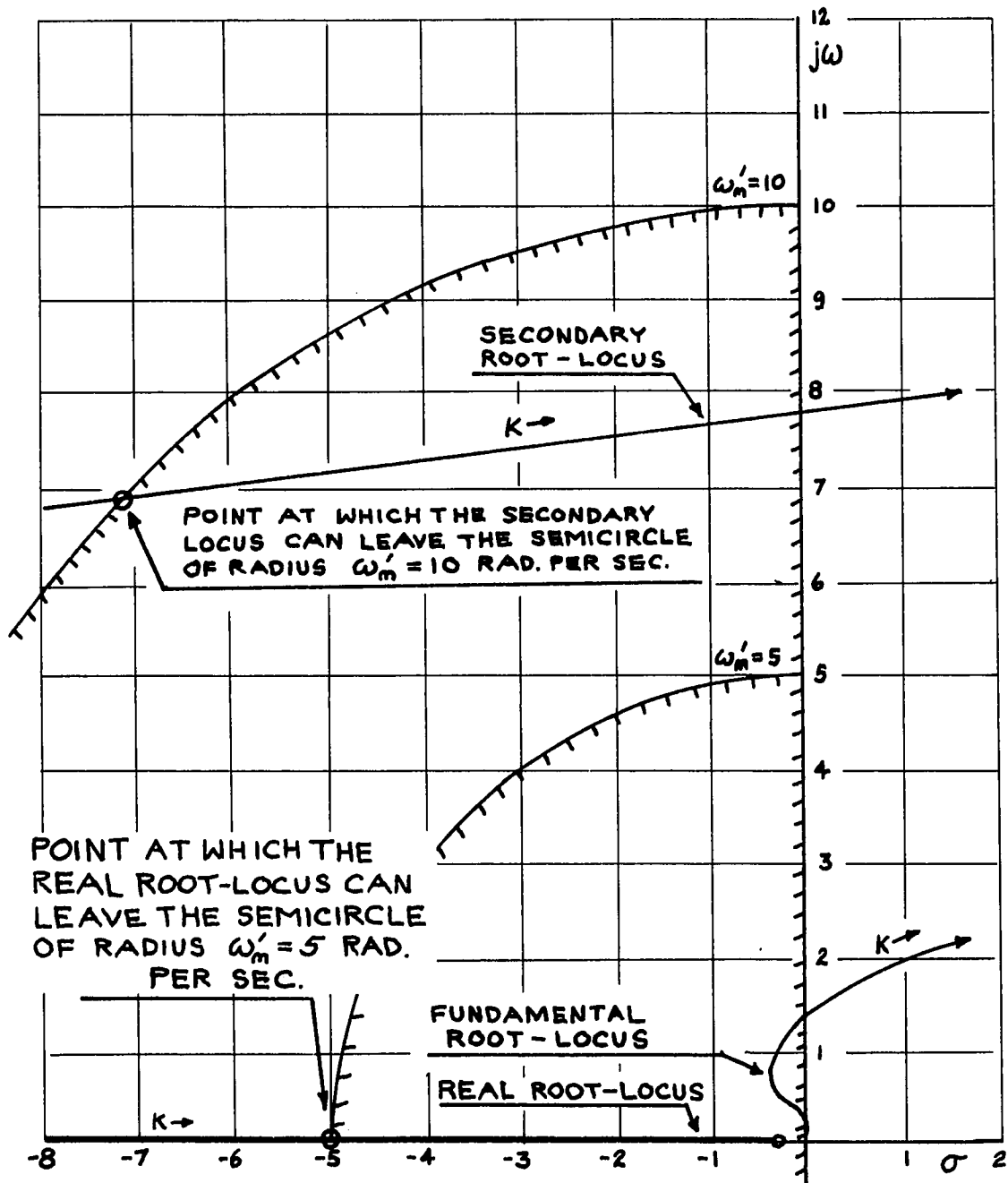


Fig. 4.4.3 Fundamental and Secondary Root-Loci.

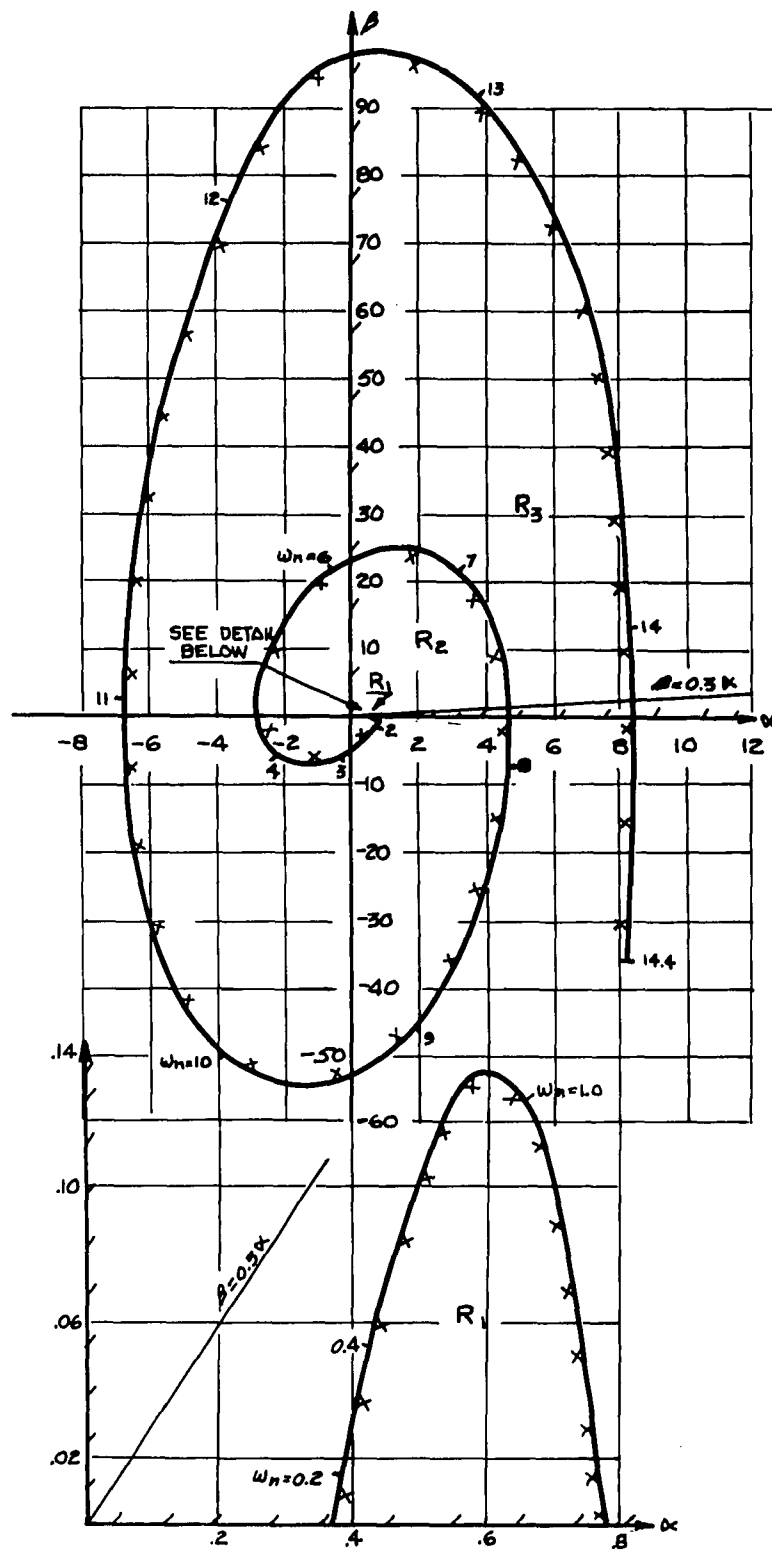


Fig. 4.5.1  $\alpha$ - $\beta$  Plot for a Constant Settling Time Contour of  $\sigma = -0.5$ .

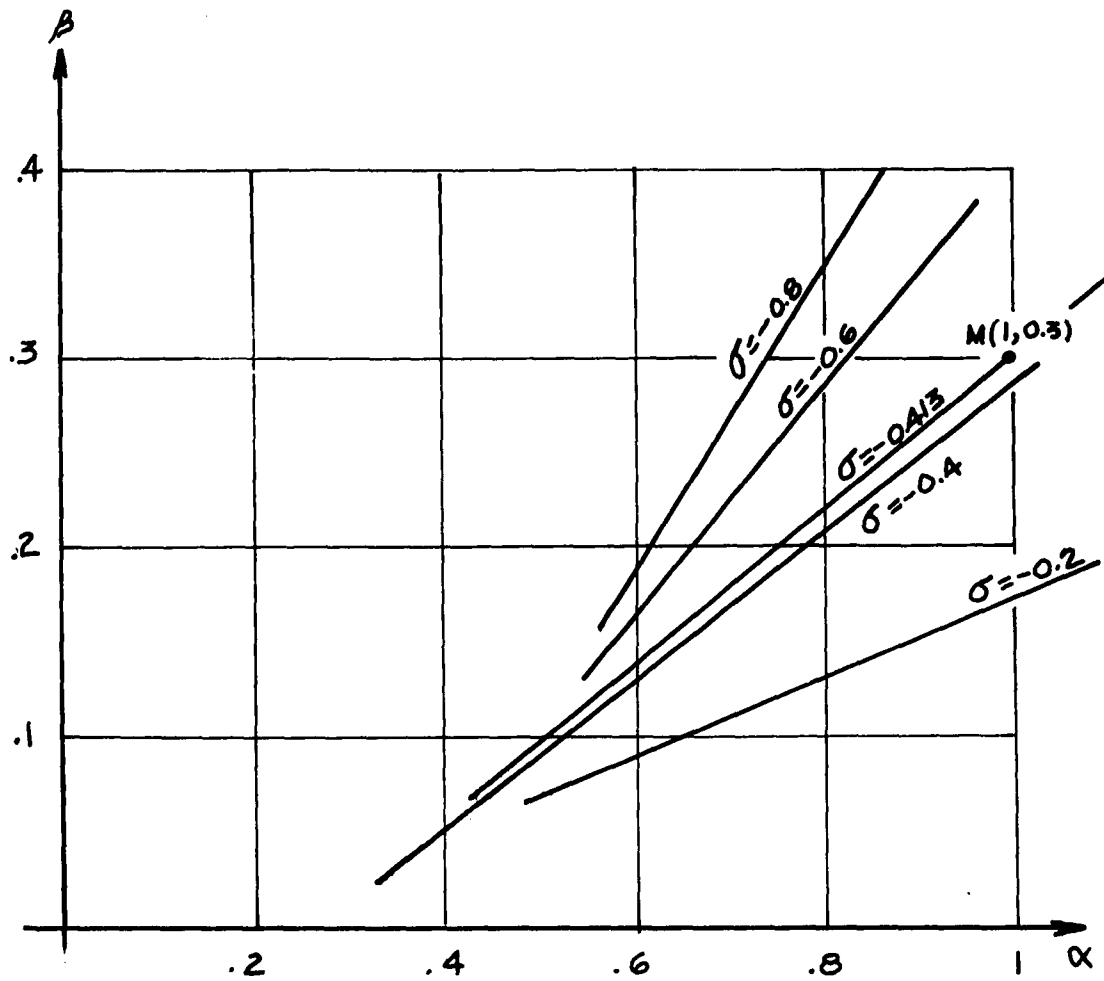


Fig. 4.6.1  $\alpha$ - $\beta$  Plot for Lines of Constant  $\sigma$ .

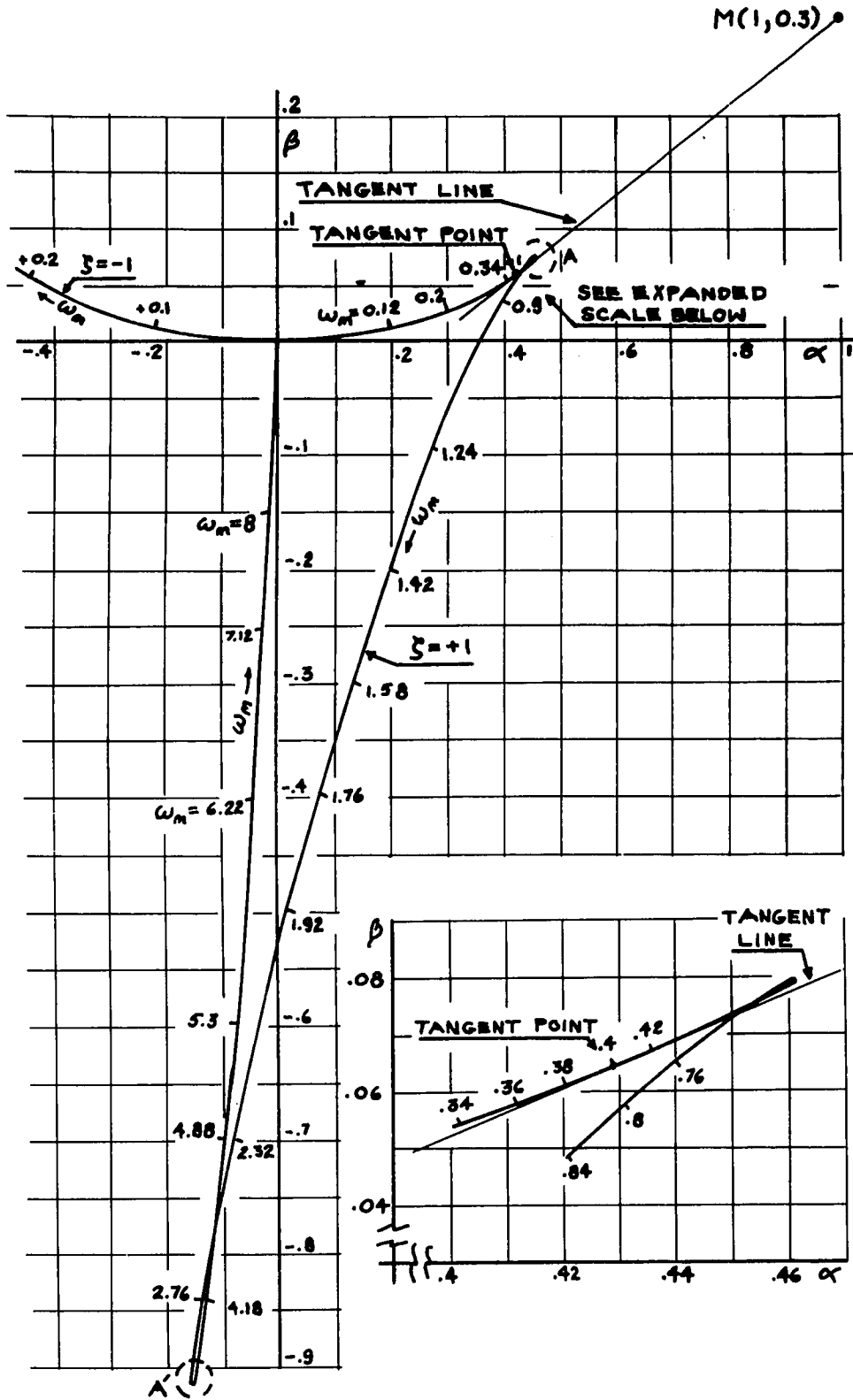


Fig. 4.6.2  $\alpha$ - $\beta$  Plot for  $\zeta = \pm 1, T = 1$  sec.



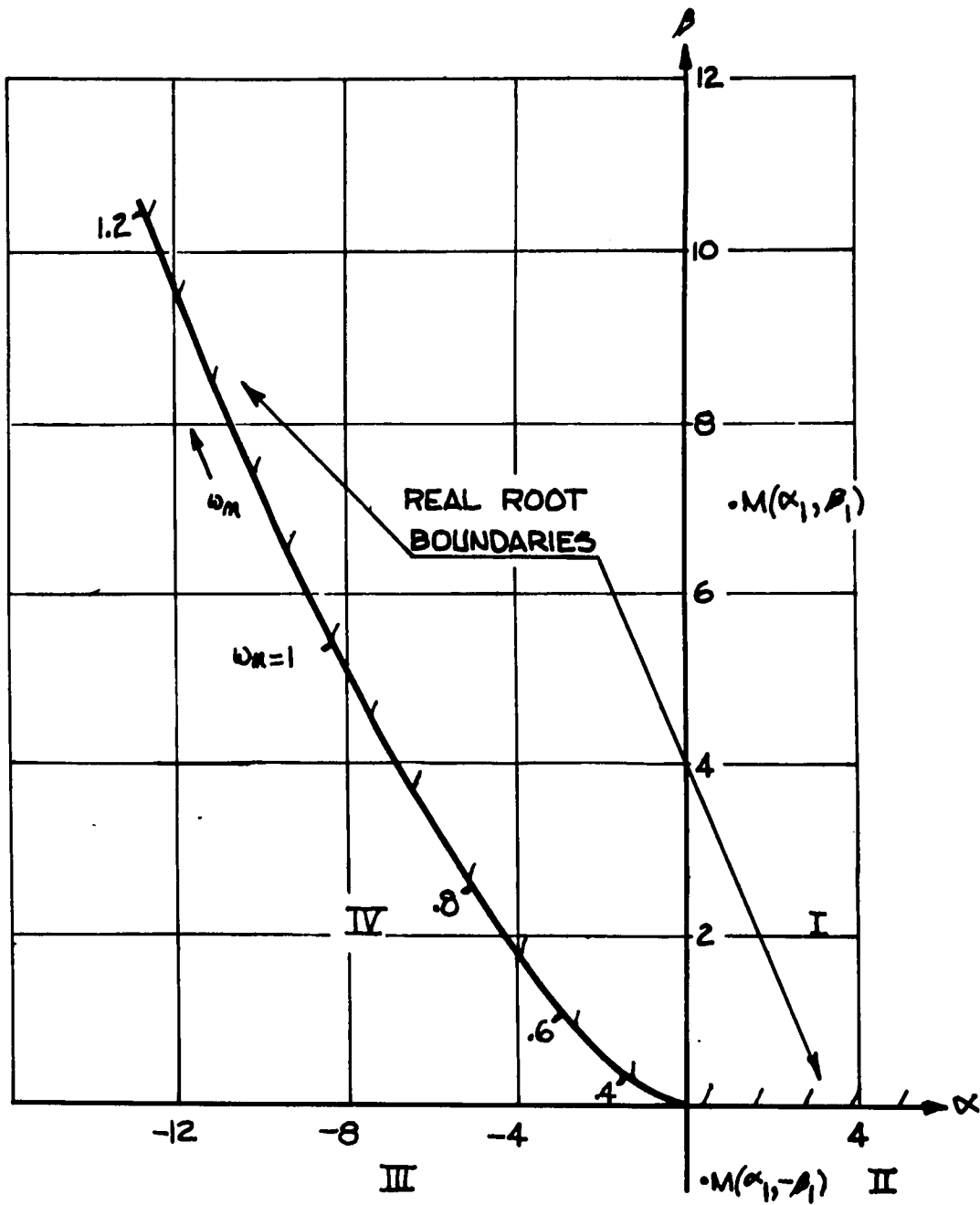


Fig. 4.7.1  $\alpha$ - $\beta$  Plot for  $\zeta = -1, T = 1$  sec.

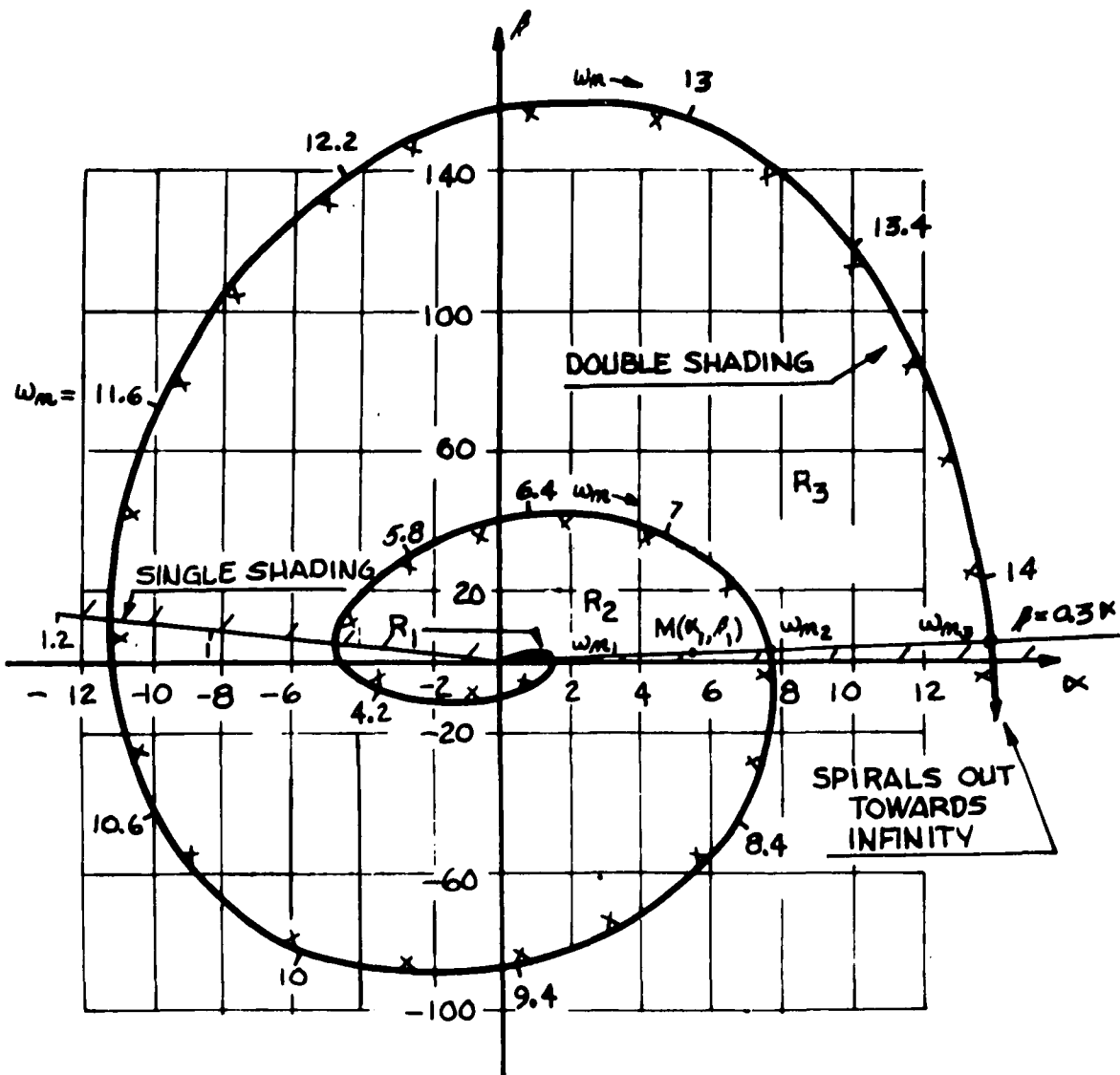


Fig. 4.7.2  $\alpha$ - $\beta$  Plot for  $\zeta = 0$  and  $\zeta = -1$ ,  $T = 1$  sec.

## CHAPTER 5

### CONTROLLER DESIGN FOR SYSTEMS WITH TRANSPORT LAG

#### 5.1 Introduction

The parameter plane method applied to control systems containing transport lag gives the designer a degree of control over the locations of the roots of the characteristic equation. Thus, a detailed discussion of the relationship between the time domain response of a linear feedback control system and the  $s$ -plane root locations is pertinent. In the design of a linear feedback control system the determination of the controller parameters can be guided by the concept of judiciously placing the roots and the zeros of the transfer function in desirable  $s$ -plane locations. Mulligan [17] has shown the response of such a system is very often dominated by a single pair of complex roots of the system characteristic equation. These roots of the characteristic equation, or poles of the transfer function, are termed the "dominant roots" of the system. The modern philosophy of controller design is to choose controller parameters that place the dominant roots in a desirable  $s$ -plane location with respect to the transient and steady state response.

These desirable root locations depend upon the applications of the control system. Simultaneously with this, an attempt is made to place the remaining roots (if there are any) in positions such that the desired dominant roots are indeed dominant. That is, the

remaining roots are placed in regions of the  $s$ -plane where they will have minimal effect on the system response. The location of the dominant roots with respect to the remaining roots and zeros of the system transfer function should be guided by the following considerations:

1. The further to the left in the  $s$ -plane the non-dominant roots are as compared to the dominant pair, the better will be the dominant root approximation.
2. The closer to the real axis the dominant roots are with respect to the non-dominant roots, the better will be the dominant root approximation.
3. There should be no complex zeros too close to the dominant roots.

Thus the design of controllers for a desired time domain response depends upon a convenient and accurate analytical relationship between the roots of the transfer function and the transient response. With this relationship, the transient response can be quickly evaluated without actual computation of the transient solution. In the design of controllers, the input and output are specified, and certain parameters of the system transfer function, related to the open-loop transfer function by the root locations, must be found. Therefore, it is necessary to establish a test input and a resulting output, regarded as known.

Because of the various choices of the accepted input and the desired output, there are different methods of design. In this work, a unit step function is selected as the input. Such an input is a convenient and widely used test signal for linear systems because many other inputs can be closely approximated by a combination of step inputs. For the desired output, a response with a slight oscillation and slight overshoot, as shown in Figure 5.1.1, is selected. The actual desired number of oscillations and actual desired amount of overshoot will be left to be decided in each particular application. Such a desired output is also widely accepted and used.

The desired response, as shown in Figure 5.1.1, requires the existence of a pair of dominant complex roots in the system function, as can be clearly shown on the  $s$ -plane. Figure 5.1.2 shows such a plane, where the pair of dominant complex roots are indicated. Thus, the roots should be chosen through some design method such that their configuration is of the pattern shown in Figure 5.1.2. If the design method does not offer any possibility of such a pattern, such a desired response is unlikely to be obtained. A derivation of the analytical relationships between the  $s$ -plane root locations and the transient response is given in Appendix V.

## 5.2 Controller Design for Systems with Transport Lag

In the case of a feedback control system containing a transport lag, the design of controllers is quite cumbersome and very little work has been done with respect to a formal design technique. This

is especially true where the design is directed towards the concept of *two* free controller parameters. The reason for the difficulty encountered in dealing with feedback control systems containing transport lag is the transcendental nature of the system characteristic equation. Thus, the characteristic equation is of infinite order and has an infinite number of roots. Due to the intractability of this transcendental function with respect to controller parameter values and the resulting root locations, conventional methods of specifying dominant roots and insuring this dominance have not been developed.

In this work the dominant root philosophy is maintained, and the parameter plane concept (as developed here) is applied to systems containing transport lag. Specifically, the dominant roots will be placed in predetermined locations to yield the desired time domain transient response and simultaneous attempts will be made to locate the remaining roots and zeros in s-plane locations that tend to maintain this dominance.

Examples will be given first in which the output specifications are given in the frequency domain. Further examples will be shown in which the specifications are given in the time domain. The specific examples are chosen to show that this method gives the designer *at least* as much control over the system design as would be available if the system did not contain a transport lag. If it is not possible to meet the output specifications the implication are that

- 1) A different type of controller must be utilized.

2) The same controller can possibly be utilized but a more complicated s-plane root-zero configuration is required (without clearly dominant roots) and the secondary effects due to the non-dominant roots must be taken into account.

### 5.3 Integral-Proportional Controller

An example of the procedure for selecting the controller parameters  $K$  and  $\tau$  of an integral-proportional controller is now given. Consider the system shown in Figure 5.3.1 and let the design specifications be for  $T = 1$  sec.

- 1) The dominant roots are to be located at *approximately*<sup>1</sup>  $\zeta_1 = 0.3$  and  $\omega_{n_1} = 1$  rad./sec.
- 2) The controller gain,  $K$ , is to be as large as possible.
- 3) The system is to be absolutely stable, a reasonable specification for systems containing transport lag.

Since the stability of the system was investigated in Chapter 4, the characteristic equation, the  $\alpha$ - $\beta$  equations and some  $\alpha$ - $\beta$  curves are available there and will be referred to or repeated in this section as needed.

The design begins by examining the  $\alpha$ - $\beta$  curve for  $\zeta_1 = 0.3$  shown in Figure 5.3.2 (see equations (4.3.4)). Only the first quadrant of these curves are shown here since for a practical system the gain

---

<sup>1</sup>It is assumed that the designer is aware of the response these dominant roots will yield. Note that the dominant roots reflect the presence of the transport lag so the resulting time domain response must begin at time  $t = 1$  sec.

( $K = \alpha$ ) and the time constant ( $\tau = \beta/\alpha$ ) are both positive. The curves are labeled ①, ②, ③ . . . to indicate the order in which they traverse the origin, that is in the order of increasing  $\omega_n$ . If a point on the  $\zeta_1 = 0.3$  locus is chosen on traversal ① the frequency  $\omega_{n_1}$  can be chosen to be 1 rad./sec., shown as point M. As will be shown below, the fact that traversal ② intersects traversal ① near  $\omega_{n_1} = 1$  rad./sec. will be useful in the design. The choice of  $\omega_{n_1} = 1$  rad./sec. is quite logical since it not only satisfies the first specification of  $\zeta_1 = 0.3$  and  $\omega_{n_1} = 1$  rad./sec., but it also insures that the remaining complex roots will lie above the radials of  $\zeta = 0.3$ . This is easily established by drawing the straight line  $\beta = \tau\alpha$  through the point ( $\zeta = 0.3, \omega_{n_1} = 1$ ), which defines a working point  $M(\alpha, \beta)$  at  $M(0.777, 0.239)$ . As discussed in Section 4.3, since the traversals ②, ③, ④, . . . intersect the line  $\beta = \tau\alpha$  to the left of  $M(0.777, 0.239)$ , the secondary and higher complex roots will lie above the radials  $\zeta_1 = 0.3$ . This insures that all of the non-dominant roots will be well above the dominant roots. In contrast to this, if  $\omega_{n_1} = 0.7$  rad./sec. were chosen, the secondary complex roots would lie below the radials  $\zeta_1 = 0.3$ , since traversal ② would intersect the  $\beta = \tau\alpha$  line to the right of traversal ①. The fact that the secondary roots lie below radials of  $\zeta_1 = 0.3$  does not necessarily mean that they will lie below the dominant roots, but it does mean that they will be closer to the dominant roots in terms of imaginary part separation.



Another point in favor of the initial choice of  $\zeta_1 = 0.3$  and  $\omega_{n_1} = 1$  rad./sec. is that the gain is  $K = \alpha = 0.777$  which is almost the largest gain possible for  $\zeta_1 = 0.3$ . For example, if  $\omega_{n_1}$  were increased to approximately 1.3 rad./sec. along the  $\zeta_1 = 0.3$  locus, the gain could be increased to 0.875. However, this would cause the slope of the  $\beta = \tau\alpha$  line to become excessively small and ensuing difficulties in synthesizing the controller for such small values of  $\tau$  would follow.

The specification that the system be absolutely stable is reconciled next. Figure 5.3.3 shows the first traversal of the  $\alpha$ - $\beta$  curves for  $0 \leq \zeta \leq 1.0$ , as well as the line  $\beta = \tau\alpha$ . Since the locus of points for  $\zeta = 0.3$  is completely contained within the region  $R_1$ , which from Section 4.3 is the region of absolute stability, any working point  $M(\alpha, \beta)$  chosen on the  $\zeta = 0.3$  curve for traversal ① will render the system absolutely stable.<sup>2</sup> At point  $M(0.777, 0.239)$  the value of the controller time constant  $\tau$  is easily determined to be

$$\tau = \frac{\beta}{\alpha} = \frac{0.239}{0.777} = 0.307 \text{ sec.}$$

so that the closed loop transfer function has a real zero at  $\sigma = -0.307$ .

Since values of  $\alpha$  and  $\beta$  have been tentatively chosen, the design is fixed and the following information is known. The dominant roots

---

<sup>2</sup>Note that the maximum gain for absolute stability is  $\alpha = K = 1.31$  from the intersection of the  $\beta = \tau\alpha$  line and the  $\zeta = 0$  curve.

are located in the s-plane at  $\zeta_1 = 0.3$ ,  $\omega_{n1} = \pm 1$  rad./sec., a real zero is located at  $\sigma = -0.307$ , and the controller parameters are  $K = 0.777$  and  $\tau = 0.307$  sec. The numerical values of the dominant roots are easily determined from (4.3.6) which is repeated below

$$s_1 = -\zeta_1 \omega_{n1} \pm j\omega_{n1} \sqrt{1 - \zeta_1^2} = -0.3 \pm j0.955 \quad (4.3.6)$$

It is now necessary to determine the locations of the real roots and the secondary and higher order complex roots.

The secondary complex roots are determined from (4.3.6) by noting which constant  $\zeta$  curve, say  $\zeta_2$ , intersects the point  $M(0.777, 0.239)$  on traversal ② and noting the frequency  $\omega_{n2}$  of this intersection. The third complex roots are determined from traversal ③, etc. It should be pointed out that specification 1) implies a secondary yet important specification. Namely, if *dominant* complex roots are specified, the implication is that the secondary and higher real and complex roots have real parts that are from two to five times or more greater than the real parts of the dominant roots (see Appendix V). This implication was considered in the choice of the working point  $M(0.777, 0.239)$  and will now be explained. The separation between the real part of the dominant roots and the real parts of the remaining complex roots is not as apparent from the  $\alpha$ - $\beta$  curves as the separation along the imaginary axis. However, this separation can be determined as follows. The real part of the  $n^{\text{th}}$  pair of complex roots is given by

$$\sigma_n = \text{Re} \left[ s_n \right] = -\zeta_n \omega_{n_n}$$

Since it is desirable that the ratio of the magnitude of the real parts of the higher order complex roots to the dominant roots be as large as possible, the following inequality is formed:

$$|\sigma_n| = |-\zeta_n \omega_{n_n}| \gg |\sigma_1| = |-\zeta_1 \omega_{n_1}| \quad (5.3.1)$$

Note from Figure 5.3.2 that the working point  $M(0.777, 0.239)$  was chosen such that traversal ② almost passes through this point, indicating that the secondary complex roots lie nearly along radials of  $\zeta = 0.3$ . Then equation (5.3.1) reduces to  $|\omega_{n_2}| \gg |\omega_{n_1}|$  or  $7.9 \gg 1$  (since  $\zeta_2 = \zeta_1$  in this case) which is considered to be a good magnitude separation for the real parts of the roots. A glance at the  $\alpha$ - $\beta$  curves and the  $\beta = \tau\alpha$  line indicates that in general  $\omega_{n_2} \cong 7\omega_{n_1}$ , but if  $\zeta_2 \neq \zeta_1$  the real part of the separation between complex roots will not be as large as it could be while still having the secondary complex roots lying well above the dominant roots. Then the secondary complex roots are located at

$$s_2 = -\zeta_2 \omega_{n_2} + j\omega_{n_2} \sqrt{1 - \zeta_2^2} = -2.37 + j7.15$$

The third pair of complex roots are determined by noting which  $\alpha$ - $\beta$  curve passes through  $M(0.777, 0.239)$  on traversal ③. From Figure 5.3.5 this situation is satisfied for  $\zeta_3 = 0.2$  and  $\omega_{n_3} = 14.15$  rad./sec. so that the real part of the complex roots equals  $-\zeta_3 \omega_{n_3} = -2.83$ , which is to the left of the secondary complex roots.

It is obviously impractical to continue computing the remaining infinite number of complex roots, so the question of how many complex roots to compute is now of interest. The ratio of the real parts of the secondary complex roots to the real parts of the dominant roots is 7.9, and the ratio of the real part of the third complex roots to that of the dominant roots is  $\left| \frac{2.83}{0.3} \right| = 9.43$ , so it is obvious that the effect of the secondary and third complex roots are negligible as compared to the dominant roots. The question is then, do any higher order complex roots exist, the real part of which is less than the real part of the secondary complex roots? If the answer is in the affirmative, then the dominancy of the "dominant roots" is destroyed and these high frequency complex roots have to be accounted for. If the answer is negative, then it is safe to neglect the higher order complex roots. To settle this question it will be proven that, for this system, all of the complex roots with the exception of the dominant and secondary roots have real parts that are greater in magnitude than the real parts of the secondary roots.

Consider the  $\alpha$ - $\beta$  curve, shown in Figure 5.3.6, of the constant settling time contour for  $\sigma = -2.5$  (which is slightly greater than the real part of the secondary roots but less than the real part of the third complex roots). Since the working point  $M(0.777, 0.239)$  lies in  $R_3$  the interpretation is that two pair of complex roots lie to the right of  $\sigma = -2.5$ , since two doubly shaded boundaries must be crossed from  $R_1$  to reach  $R_3$ . Recall from Section 4.3 that since it contains

no sub-regions, only  $R_1$  can contain all of the complex roots. It follows that the remaining complex roots (an infinite number of them) must be to the left of  $\sigma = -2.5$  so the proof is complete.

The real roots are now determined in the manner developed in Section 4.6. That is, the number of real roots and their approximate values are determined from straight lines drawn through the working point  $M(0.777, 0.239)$  that are tangent to the  $\zeta = \pm 1$  curves. Figure 5.3.7 shows the curves for  $\zeta = \pm 1$ . Note that only one tangent is possible to the  $\zeta = +1$  curve, so there is only one negative real root. The value of this root is approximately  $\sigma = -0.5$  since  $\omega_n \approx 0.5$  rad./sec. at the point of tangency. Recall from Section 4.6 that the tips of the  $\zeta = +1$  curve are not points of inflection and tangent lines from  $M(0.777, 0.239)$  cannot be drawn to these tips.

A more accurate value of this root is determined from equation (4.3.1) of Section 4.3 which is repeated here for  $s = -\sigma$  since it is already known that the single real root is negative.

$$\epsilon^{-\sigma} \sigma^2 - \alpha \sigma + \beta = 0 \quad (4.3.1)$$

Graphing this equation for various values of  $\sigma$  indicates that when  $\sigma = -0.51$  the straight line passes through the point  $M(0.777, 0.239)$  (see Figure 5.3.8). Thus the value of the single real root is  $\sigma = -0.51$

Figure 5.3.9 shows the relevant root and zero locations for the transfer function of this feedback control system. Note that the real

root, although close to a zero, is also relatively close to the real part of the dominant roots and therefore should be taken into account (a magnitude separation of 1.7). Further, the real parts of the non-dominant complex roots are relatively far from the real part of the dominant roots.

The zero introduced by the controller is quite close to the real root and will tend to nullify the effect of the real root on the system response and tend to help maintain the dominance of the dominant roots. To see the effect of the real root and the non-dominant roots on the system response, the output response,  $c(t)$ , is shown in Figure 5.3.10.

Figure 5.3.10 shows the output response  $c(t)$  obtained by considering the dominant complex roots as well as the single real root. Also shown in this figure is the exact response  $c(t)$  which was obtained by solving the system differential equation. The system differential equation was solved by using difference equations. The time interval,  $\Delta t$ , was chosen such that the solution is exact to two decimal places. The difference between the exact solution of the system differential equation and the response obtained from the dominant root locations is due to the effect of the non-dominant roots of the system. The salient differences between these responses are indicated on the figure in terms of percentages.

#### 5.4 Proportional Controller

An example of the procedure for the selection of the controller gain  $K$  of a proportional controller is now given. Consider the system

shown in Figure 5.4.1 and let the design specifications be the same as for the integral-proportional controller feedback system of Section 5.3 which are

- 1) The dominant zeros are to be located at *approximately*  $\zeta_1 = 0.3$  and  $\omega_{n_1} = 1$  rad./sec.
- 2) The controller gain  $K$  is to be as large as possible.
- 3) The system is to be absolutely stable.

In Section 5.3 the control of a feedback control system with an integral-proportional controller was investigated. Figure 5.3.1 shows a block diagram of this system. If the controller time constant  $\tau$  is set to zero in Figure 5.3.1 the system reduces to the proportional control system of this section (see Figure 5.4.1). Therefore if a line  $\beta = \tau\alpha = (0)\alpha = 0$  is superimposed on the  $\alpha$ - $\beta$  curves of Section 5.3 the curves can be used where only the  $\alpha$ -axis, corresponding to the  $\beta = 0$  line, has meaning. This is analogous to introducing a dummy variable parameter ( $\tau$ ) into the system transfer function in order to utilize the *two* variable parameter method developed in this work.

Figure 5.3.3 shows the first quadrant of the  $\alpha$ - $\beta$  curves for traversal ① and for  $0 \leq \zeta \leq 1.0$ . It is immediately evident that in order to locate the dominant roots at  $\zeta_1 \cong 0.3$  the gain must be equal to 0.875, since the  $\zeta_1 = 0.3$  locus intersects the  $\beta = 0$  line at  $\alpha = 0.875$ . The value of the frequency at this point is  $\omega_{n_1} = 1.6$  rad./sec. On the other hand, if the gain were reduced to  $\alpha = 0.37$ ,

the frequency  $\omega_{n_1}$  would be 1 rad./sec. but the value for  $\zeta$  would be  $\zeta_1 = 1.0$ . Thus, it is not possible to simultaneously locate the dominant roots at the specified values of  $\zeta = 0.3$  and  $\omega_n = 1$  rad./sec. with an adjustment of only the gain parameter. This is a definite disadvantage of a proportional controller, in contrast to the simultaneous control over both  $\zeta$  and  $\omega_n$  that is possible with a *two* parameter controller.

If it is possible to locate (exactly or approximately) the dominant roots in the specified locations, the design proceeds in a manner similar to the one of the previous section. Note that there is very little flexibility with respect to the assurance that the remaining non-dominant complex roots will lie above or below the specified radials  $\zeta = 0.3$ , or assurance that the magnitude separation of the real parts be large. With only a single parameter control the designer is more or less forced to settle for the remaining complex root locations associated with the specified dominant roots.

In order to determine the real root locations, recourse is made to the  $\zeta = \pm 1$  curves graphed for the integral-proportional controller shown in Figure 5.3.7. That is, a straight line is drawn from the chosen value of  $\alpha = \alpha_1$  (or from the working point  $M(\alpha_1, 0)$ ) that is tangent to the  $\zeta = \pm 1$  curves and the real root value is determined as usual. A more accurate real root value is obtained by substituting  $s = \sigma$  into the system characteristic equation which is from (4.3.1) with  $\tau = 0$  and  $T = 1$  sec.



$$F(\sigma) = \sigma \epsilon^\sigma + \alpha = 0 \quad (5.4.1)$$

The normal procedure is to substitute values of  $\sigma$  into this equation until the equality is satisfied. Note that this procedure is, in fact, the usual graphical technique for finding real roots of polynomials. This is because a proportional controller has only *one* variable parameter and the parameter-plane technique degenerates to standard real root determination techniques.

### 5.5 Derivative-Proportional Controller

The derivative-proportional controller is usually designed in order to obtain a desirable transient response, such as smaller overshoots, faster settling times, etc. For purposes of comparison, a derivative-proportional controller will be designed to control the plant and transport lag previously discussed. Figure 5.5.1 shows this linear feedback control system where the controller has the following transfer function:

$$K(1 + \tau s)$$

Since there is a time delay in the system, the design philosophy will be to quicken the output response in order to overcome the inherent transport lag or delay while still maintaining a reasonable transient response. For this type of response the output specifications are most logically given in the time domain, as opposed to the frequency domain specifications of the last section. Thus, assume that the time

delay  $T = 1$  sec., that the test signal is a unit step, and that the output response specifications to occur *after* one second are<sup>4</sup>:

- 1) The settling time,  $T_s \leq 6$  sec.
- 2) The peak overshoot,  $M \leq 20\%$ .
- 3) The peak time,  $T_p \leq 3$  sec.
- 4) The number of oscillations,  $N \leq 2$ , or one overshoot and one undershoot.

The design begins by forming the system transfer function  $\frac{C}{R}(s)$  from Figure 5.5.1. Then

$$\frac{C}{R}(s) = \frac{N(s)}{F(s)} = \frac{K\tau \left[ s + \frac{1}{\tau} \right]}{(K\tau + \epsilon^S T)s + K} \quad (5.5.1)$$

The characteristic equation,  $F(s)$ , is for  $\alpha = K$ ,  $\beta = K\tau$  and  $T = 1$  sec.,

$$F(s) = (\beta + \epsilon^S)s + \alpha = 0 \quad (5.5.2)$$

The parametric equations for  $\alpha = \alpha(\omega_n)$ ,  $\beta = \beta(\omega_n)$ ,  $\Delta = \Delta(\omega_n)$  and  $\zeta \neq 1$  are determined from (4.1.6), (4.1.11) and (4.1.14) to be

$$\begin{aligned} \alpha &= \frac{\omega_n \epsilon^{-\phi} \sin \theta}{\sqrt{1 - \zeta^2}} \\ \beta &= \frac{\epsilon^{-\phi} (-\sqrt{1 - \zeta^2} \cos \theta + \zeta \sin \theta)}{\sqrt{1 - \zeta^2}} \\ \Delta &= \omega_n \sqrt{1 - \zeta^2} > 0 \end{aligned} \quad (5.5.3)$$

---

<sup>4</sup>See Figure 5.1.1 for the definitions of the following terms.

When  $\zeta = 1$  the  $\alpha$ - $\beta$  equations are

$$\alpha = \omega_n^2 \epsilon^{-\omega_n}, \quad \beta = \epsilon^{-\omega_n} (\omega_n - 1) \quad (5.5.4)$$

and when  $\zeta = -1$  the  $\alpha$ - $\beta$  equations are

$$\alpha = \omega_n^2 \epsilon^{\omega_n}, \quad \beta = -\epsilon^{\omega_n} (\omega_n + 1)$$

The curves representing (5.5.3) and (5.5.4) are shown in Figures 5.5.2 through 5.5.5 where the shading would always be on the left in the direction of increasing frequency, since  $\Delta > 0$ . It is now assumed that values of  $\alpha$  and  $\beta$  can be chosen such that the specifications can be met. This is analogous to placing a pair of dominant roots in a desirable s-plane location while simultaneously placing the remaining roots of the characteristic equation and zeros of the transfer function in positions that have a minimal effect on these dominant roots.

From the specifications and the approximate equations of Appendix V it is seen that from (V.8)

$$\sigma_1 \cong \frac{4}{T_s} = \frac{4}{6} = 0.667 \quad (5.5.5)$$

From (V.9)

$$\omega_{n_1} \cong \frac{\pi \sigma_1 N}{2} = \frac{\pi (0.667) (1.3)}{2} \cong 1.4 \text{ rad./sec.} \quad (5.5.6)$$

So that from (V.10)

$$\zeta_1 = \frac{1}{\sqrt{1 + (\omega_{n_1}/\sigma_1)^2}} = \frac{1}{\sqrt{1 + (1.37/0.667)^2}} = 0.44 \quad (5.5.7)$$

Since the values for  $\omega_{n_1}$  and  $\zeta_1$  are only approximate, their values will be selected after making a quick examination of the  $\alpha$ - $\beta$  curves. Figure 5.5.2 shows that values of  $\alpha$  and  $\beta$  can be easily chosen to yield  $\omega_{n_1} = 1.4$  rad./sec. Further, since a larger value of  $\zeta$  results in a smaller value of peak overshoot, a slightly larger value of  $\zeta$  is considered, say  $\zeta = \zeta_1 = 0.5$ . This slightly larger value of  $\zeta_1 = 0.5$  rather than  $\zeta_1 = 0.44$  is also considered to help offset any secondary effects due to the non-dominant roots. Figure 5.5.7 shows the first quadrant of the  $\alpha$ - $\beta$  plane for the first three traversals of the  $\zeta = 0.5$  locus. It is immediately apparent that if  $\zeta_1 = 0.5$  and  $\omega_{n_1} = 1.4$  rad./sec., the secondary and higher order complex roots will be above the radials of  $\zeta = 0.5$  in the  $s$ -plane. This is because traversals ②, ③, . . . , of the  $\alpha$ - $\beta$  curve will intersect the  $\beta = \tau\alpha$  line to the left of the point  $M(\alpha_1, \beta_1)$ . A final consideration is the absolute stability of the system. Figure 5.5.2 also shows that the  $\zeta = 0.5$  locus is completely contained within the  $\zeta = 0$  locus so that the system will be absolutely stable for this choice of  $\zeta_1$  and  $\omega_{n_1}$ . Thus the choice of dominant roots is that they are located at  $\omega_{n_1} = 1.4$  rad./sec. and  $\zeta_1 = 0.5$ . It immediately follows that the real part of the dominant roots is  $\zeta_1 \omega_{n_1} = -0.7$ , and

from Figure (5.5.2) the values of  $\alpha$  and  $\beta$  are  $\alpha = 0.752$  and  $\beta = 0.095$ .

The remaining roots of the characteristic equation and the zeros of the transfer function are now computed. The transfer function (5.5.1) has a real zero at  $s = -\frac{1}{\tau}$ , and from  $\beta = K\tau = \alpha\tau$  the value of this zero is  $\frac{1}{\tau} = \frac{\alpha}{\beta} = \frac{0.752}{0.095} = 7.92$ . The number of real roots along with their approximate values is determined by placing a working point  $M(0.752, 0.095)$  on the  $\alpha$ - $\beta$  curves for  $\zeta = \pm 1$ . Figure 5.5.5 shows the  $\zeta = \pm 1$  curves and it is apparent that only one tangent can be drawn to this curve from  $M$ . Further, the value of the frequency noted on the  $\zeta = +1$  curve at the point of tangency is approximately  $\omega_n = 8$  rad./sec. so that the system has a single real root located at approximately  $\sigma = -8.0$ . By substituting  $s = -\sigma$  into (5.5.2) (since it is already known that the single real root is negative) and graphing the straight lines for various  $\sigma$ , it is seen that the straight line for  $\sigma = 7.92$  passes through the working point  $M(0.752, 0.095)$  in the  $\alpha$ - $\beta$  plane (see Figure 5.5.6). Thus an accurate value for the real root is  $\sigma = -7.92$  which is the same value as the real zero determined above. At this point it would be fruitful to show, in the same manner as that of Section 4.6, that the point  $A$  on Figure 5.5.5 could not possibly be a tangent point for a line drawn from  $M(0.752, 0.095)$  to the  $\zeta = +1$  curve. From (5.5.4) the slope of the  $\zeta = +1$  curve is

$$\frac{d\beta}{d\alpha} = \frac{1}{\omega_n}$$

so that the curve is either concave upward or concave downward which

proves the assertion.

The secondary complex roots are determined by the intersection of the second traversal of the  $\alpha$ - $\beta$  locus with M. Figure 5.5.3 shows that traversal ② intersects M at a frequency of  $\omega_{n_2} = 8.85$  rad./sec. and  $\zeta_2 = 0.25$  so that the real parts of the secondary roots are  $\zeta_2 \omega_{n_2} = -2.21$ . The third pair of complex roots is determined by the intersection of the third traversal of the  $\alpha$ - $\beta$  curve and the M point. These roots are found to be at  $\omega_{n_3} = 15.4$  rad./sec. and  $\zeta_3 = 0.15$  so that the real part of the third complex roots is  $\zeta_3 \omega_{n_3} = -2.31$  (see Figure 5.5.4). In order to insure that the remaining complex roots have real parts greater than the real part of the secondary roots, the  $\alpha$ - $\beta$  curve for a constant settling time contour of  $\sigma = -2.25$  is graphed. Figure 5.5.8 shows this  $\alpha$ - $\beta$  curve and since the point  $\alpha = 0.752$ ,  $\beta = 0.095$  lies in region  $R_3$  the implication is that four complex roots lie to the right of  $\sigma = -2.25$  (the dominant and secondary roots) and the remainder to the left.

Figure 5.5.9 shows the root-zero locations and the following observations are made: The real zero is well situated since it lies far to the left of the dominant roots and further it also lies on top of the real root thereby cancelling its effect. The real root is well situated since it lies far to the left of the dominant roots, i.e., the ratio of the magnitude separation of the real root and the real part of the dominant roots is  $\left| \frac{7.92}{0.7} \right| = 11.3$ . The magnitude separations between the real parts of the secondary and third complex roots with respect to the real parts of the dominant roots are 3.14 and 3.3 respectively,

which is considered to be a reasonable magnitude separation; and as proven above, the magnitude separation for higher order complex roots is even greater.

In order to see clearly the effect of the non-dominant roots, pertinent portions of the output response are now computed based upon the root-zero locations of the system. Figure 5.5.9 shows these root-zero locations and computations will be based upon this figure. The approximate settling time is computed first from (V.8)

$$T_s \cong \frac{4}{\sigma_1} = \frac{4}{0.7} = 5.7 \text{ sec.} \quad (5.5.8)$$

which is less than the specified settling time of 6 sec. The number of overshoots  $N$  is computed from (V.9)

$$N = \frac{2}{\pi} \frac{\sqrt{1 - \zeta^2}}{\zeta} = 1.23 \quad (5.5.9)$$

which is within the specified  $N \leq 2$ . The time for the output to reach the peak  $T_p$  is computed next from (V.11)

$$T_p = \frac{1}{1.21} \left[ \pi + \frac{\begin{array}{c} \text{due} \\ \text{to real} \\ \text{zero} \end{array} \begin{array}{c} \text{due} \\ \text{to real} \\ \text{root} \end{array} \begin{array}{c} \text{due to} \\ \text{secondary} \\ \text{complex roots} \end{array} \begin{array}{c} \text{due to} \\ \text{third} \\ \text{complex roots} \end{array} \right] \quad (5.5.10)$$

$$T_p = \frac{1}{1.21} \left[ \pi + \frac{(0) + (2.5) + (0.5)}{180/\pi} \right] = 2.64 \text{ sec.}$$

which is less than the specified  $T_p = 3$  sec. Equation (5.5.10) exemplifies the increasingly minor effect of the non-dominant roots on the peak time. It also depicts how the proximity of the real zero to the real root nullifies the effect of the real root. Obviously the inclusion of even more complex roots will have a negligible effect upon  $T_p$ . At this point the inequality (V.7) can be introduced to test whether the dominant roots can be considered dominant, and thus to show the validity of the approximations. Then

$$T_p = 2.64 \geq \frac{3}{\sigma_1} = \frac{3}{2.2} = 1.365$$

shows the validity of the assumption of dominance.

The last specification to be examined, and perhaps the most important one, is the peak overshoot  $M$ . From (V.16)

$$\begin{array}{cccc}
 \begin{array}{c} \text{due to} \\ \text{real} \\ \text{root} \end{array} & \begin{array}{c} \text{due to} \\ \text{secondary} \\ \text{complex root} \end{array} & \begin{array}{c} \text{due to} \\ \text{third} \\ \text{complex roots} \end{array} & \begin{array}{c} \text{due to} \\ \text{real} \\ \text{zero} \end{array} \\
 \swarrow & \swarrow & \swarrow & \swarrow \\
 M = & \left[ \left( \frac{7.92}{7.33} \right) \left( \frac{8.55^2}{(7.41)(9.95)} \right) \left( \frac{15.4^2}{(14.05)(16.55)} \right) \right] \left[ \frac{7.33}{7.92} \right] e^{-(0.7)(2.64)} \\
 \\ 
 M = & \left[ (1.07) \left( \frac{73}{73.9} \right) \left( \frac{237}{232.1} \right) \right] \left[ 0.935 \right] e^{-1.848} \\
 & = \left[ (1.07)(0.99)(1.025) \right] \left[ 0.935 \right] e^{-1.848} \\
 & \\ 
 M = & 0.1605 \\
 & \\ 
 & \text{or } 16.05\% \text{ which is within the specified } M \leq 20\%. \text{ The numerical}
 \end{array}
 \tag{5.5.11}$$

or 16.05% which is within the specified  $M \leq 20\%$ . The numerical



quantities of (5.5.11) are grouped in a manner to point out the effect of the various roots and the single zero on the peak overshoot. Once again it is obvious that the larger magnitude complex roots have little effect upon the peak overshoot and if more complex roots were included their effect would be even less noticeable.

The design of the controller is now considered to be complete, since the design specifications have been met and reasonable controller values of  $K = 0.752$ ,  $\tau = \frac{\beta}{K} = \frac{0.095}{0.752} = 0.1265$  sec. were chosen.

To indicate the validity of the proposed controller design technique, the output response of the system,  $c(t)$ , is shown in Figure 5.5.10. The solid response curve was computed from the root-zero locations of Figure 5.5.9 where only the dominant complex roots and the single real root and zero were considered. The dashed response curve, on the other hand, is the actual output,  $c(t)$ , which was obtained by solving the system differential equations. The system differential equation was solved by using difference equations. The time interval,  $\Delta t$ , was chosen such that the solution is exact to two decimal places.

The difference between the actual and predicted responses is due to the assumption that the effect of the non-dominant roots of the system characteristic equation was negligible. The actual percentage difference between the predicted and actual responses are noted on Figure 5.5.10 and, as can be seen, are quite small.

## 5.6 Tachometric Feedback Control

The effect of output rate damping or "tachometric feedback" on a linear feedback control system with transport lag is now investigated. Tachometric feedback is introduced as a minor feedback loop around the plant, resulting in a multiloop feedback system as shown in Figure 5.6.1. This is a widely used method of control because the derivative action appears in a desirable position with respect to any noise associated with the signal. The signal noise is greatly attenuated by the low pass filter properties of the plant. It should be pointed out that this system is multiloop and normally would be more difficult to design because one of the two free parameters appears in each loop. The parameter plane method, however, is based primarily upon the system characteristic equation and the introduction of additional feedback loops in *no way* complicates the problem.

The system specifications will be the same time domain specifications as given in Section 5.5 for the derivative-proportional controller. These are reasonable specifications for a system containing tachometric feedback because this type of feedback is the counterpart of the derivative-proportional control. This is due to the fact that the latter differentiates the input signal before the plant and the former differentiates the output from the plant and then feeds the output back to the error detector. The similarity between the two controllers is easily seen from the transfer function  $\frac{C}{R}(s)$  for the system containing tachometric feedback. From Figure 5.6.1

$$\frac{C}{R}(s) = \frac{N(s)}{F(s)} = \frac{K_1}{s\epsilon sT + K_T s + K_1} \quad (5.6.1)$$

Defining  $\alpha = K_1$  and  $\beta = K_T$ , the characteristic equation for  $T = 1$  sec. is

$$F(s) = (\epsilon s + \beta)s + \alpha = 0 \quad (5.6.2)$$

Note that the characteristic equations for tachometric feedback (5.6.2) and for derivative-proportional control (5.5.2) are *identical*. The only difference between the two systems is that with derivative-proportional control, the transfer function (5.5.1) contains a real zero located at  $s = -\frac{1}{T}$ , whereas the tachometric feedback transfer function (5.6.1) does not contain any real zeros.

As previously mentioned, controller design via the parameter plane method deals primarily with the system characteristic equation. Therefore, since the design specifications were satisfied for the characteristic equation of this system in the previous section, the next step is to remove the zero from the root-zero plot of Figure 5.5.8 and determine whether the specifications are still satisfied. If they are, it follows that the values of the tachometric feedback controller parameters are  $\alpha = K_1 = 0.752$  and  $\beta = K_T = 0.095$ . Upon removing the real zero from Figure 5.5.7 the following is noted. Equations (5.5.8) and (5.5.9) remain unchanged so that the values of  $T_s$  and  $N$  are unchanged. Removing the  $-9.5^\circ$  contribution of the real

zero from (5.5.10) results in  $T_p = 2.78$  sec. which is 5.04% greater than the  $T_p$  of the derivative-proportional control system. Thus, the peak time is still within the specified  $T_p \leq 3$  sec. The peak overshoot  $M$  is determined from (5.5.11) by removing the term due to the real zero and using the new value for  $T_p$  computed above. This gives the result that the peak overshoot is now  $M = 15.3\%$  which is 4.05% less than the peak overshoot with a derivative-proportional controller. Thus, the peak overshoot is well within the specification of  $M \leq 20\%$ .

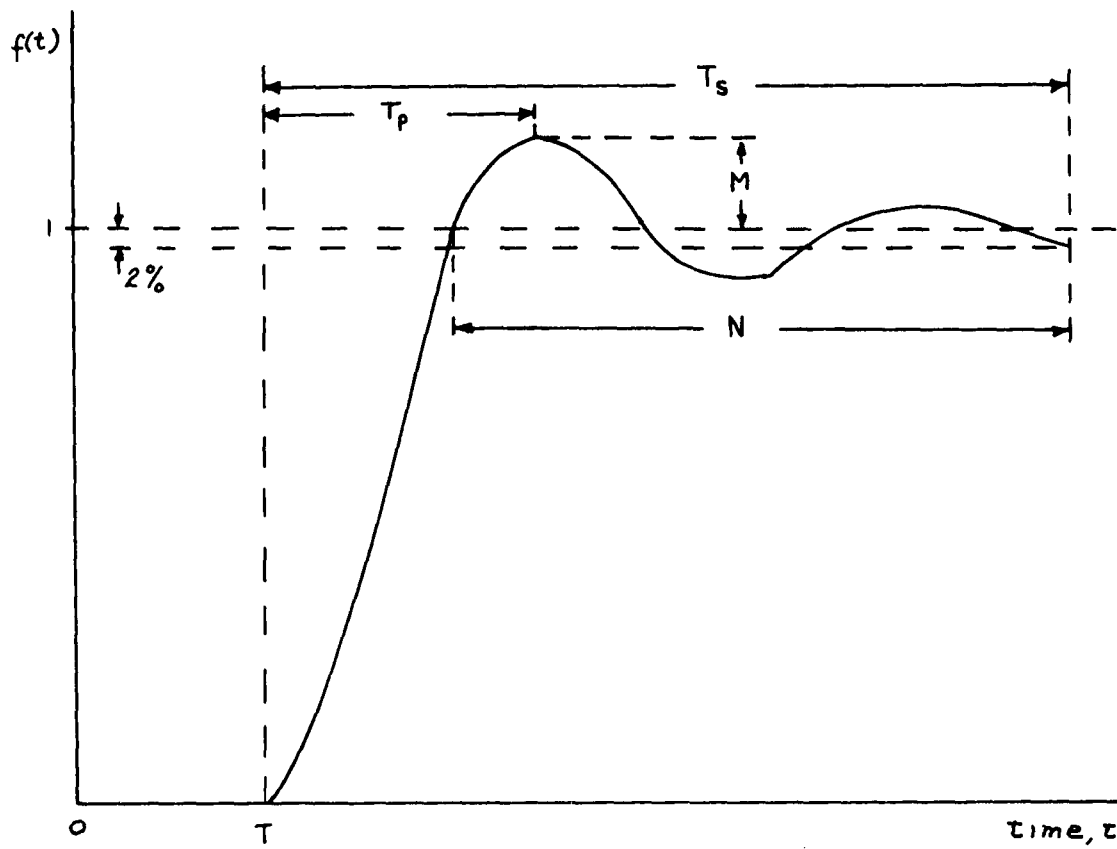


Fig. 5.1.1 The Desired Response.

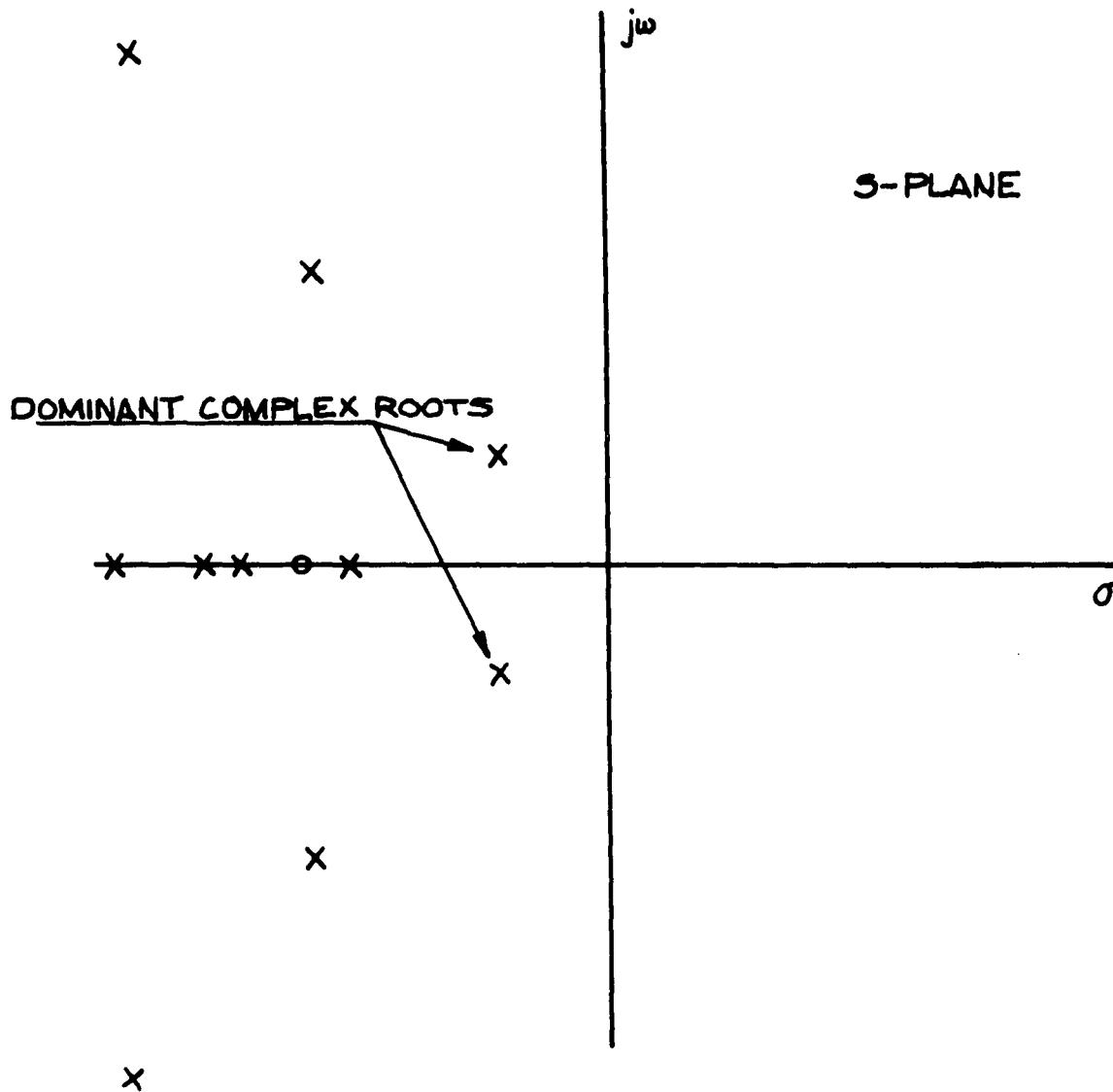


Fig. 5.1.2 Pattern of Root-Zero Configuration of the Desired Response.

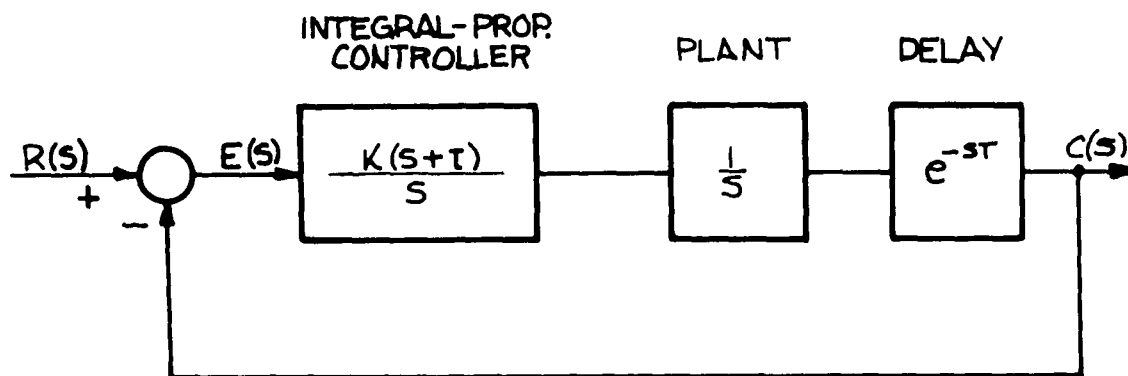


Fig. 5.3.1 Integral-Propotional Controller.

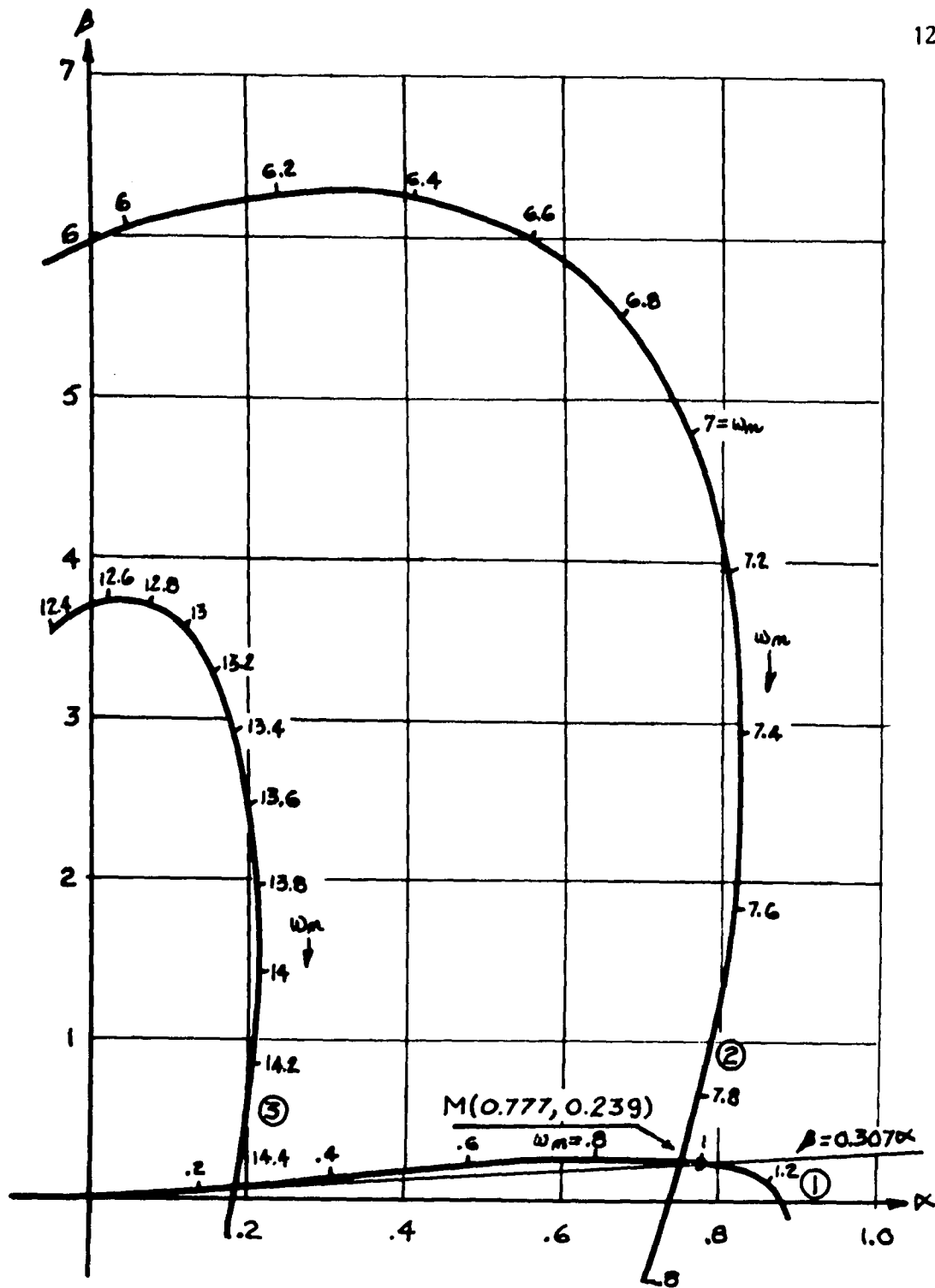


Fig. 5.3.2  $\alpha$ - $\beta$  Plot for  $\zeta = 0.3$ . (First quadrant.)



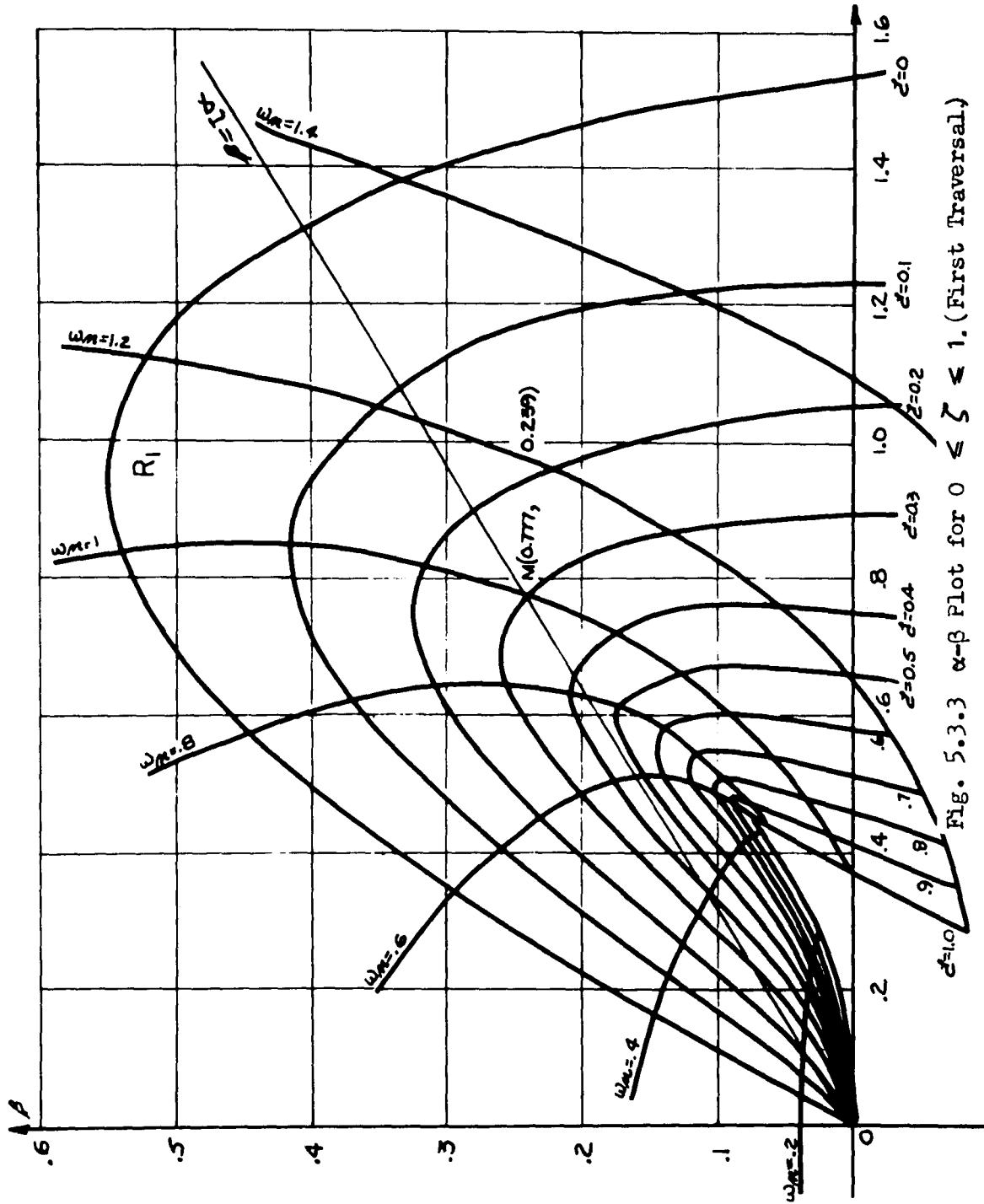


Fig. 5.3.3  $\alpha - \beta$  Plot for  $0 \leq \zeta \leq 1$ . (First Traversal.)

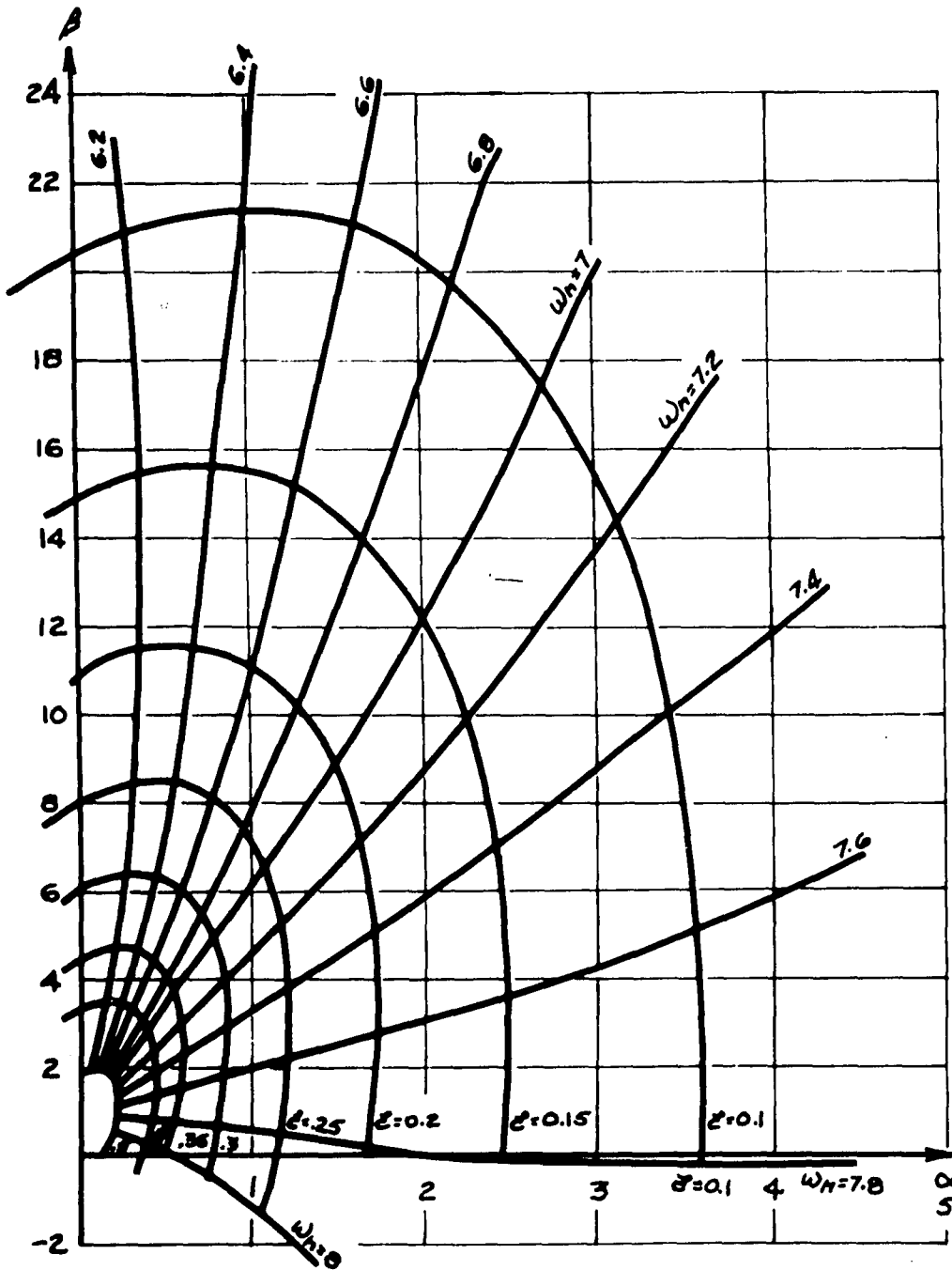


Fig. 5.3.4  $\alpha$ - $\beta$  Plot for  $0 \leq \zeta \leq 0.5$ . (Second Traversal.)

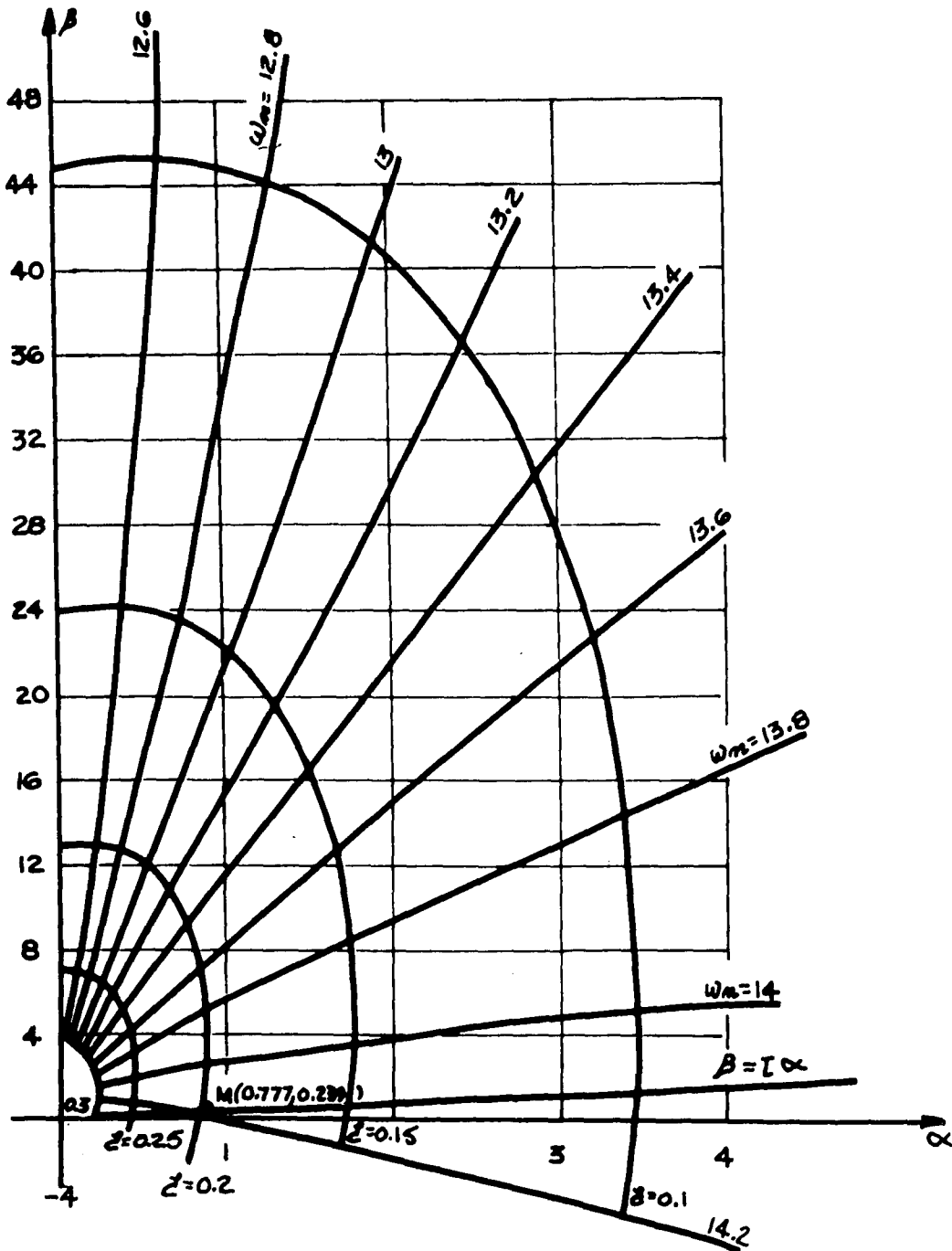


Fig. 5.3.5  $\alpha$ - $\beta$  Plot for  $0.1 \leq \zeta \leq 0.3$ . (Third Traversal.)

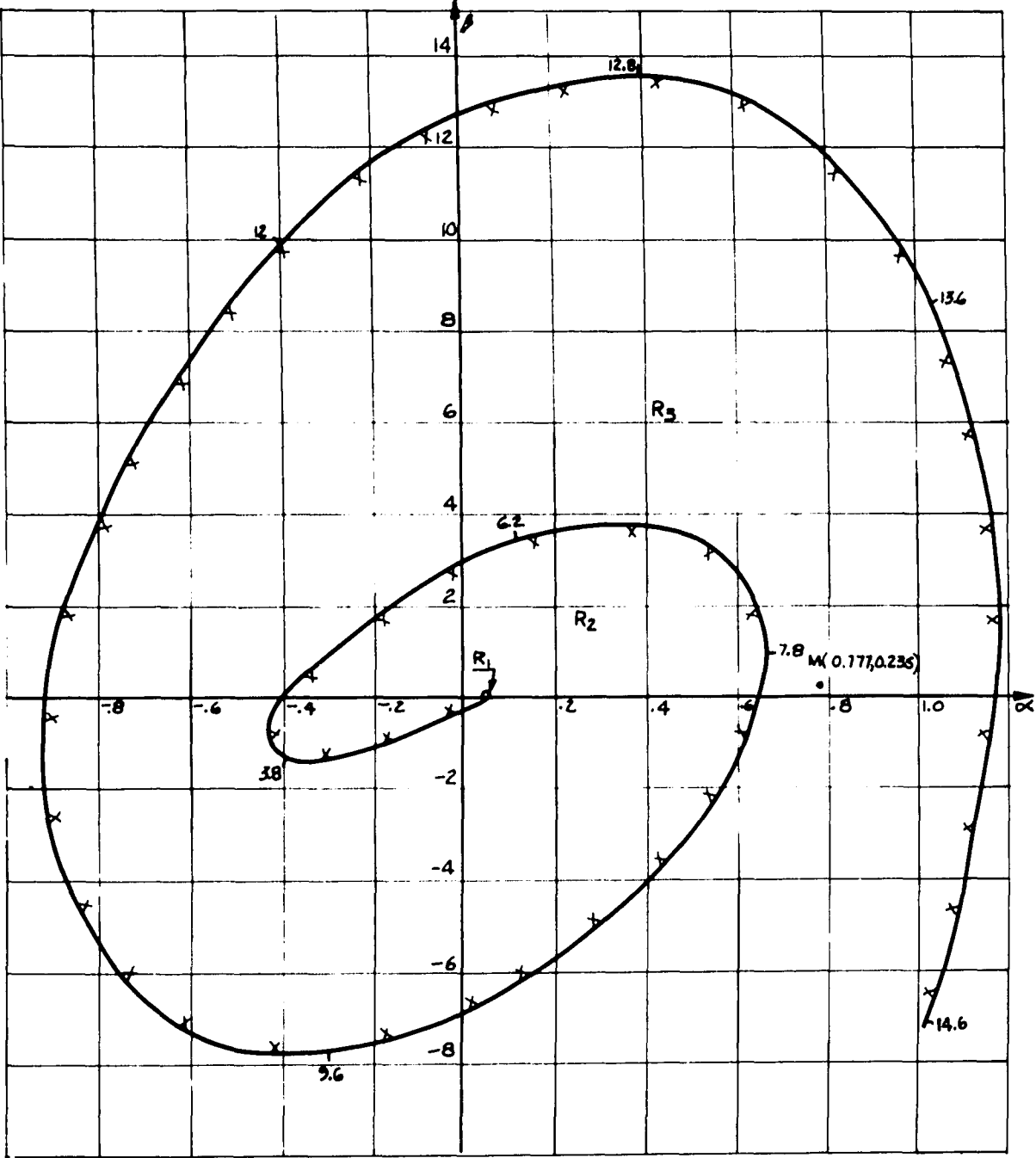


Fig. 5.3.6  $\alpha$ - $\beta$  Plot for a Constant Settling Time Line of  $\sigma = -2.5$ .

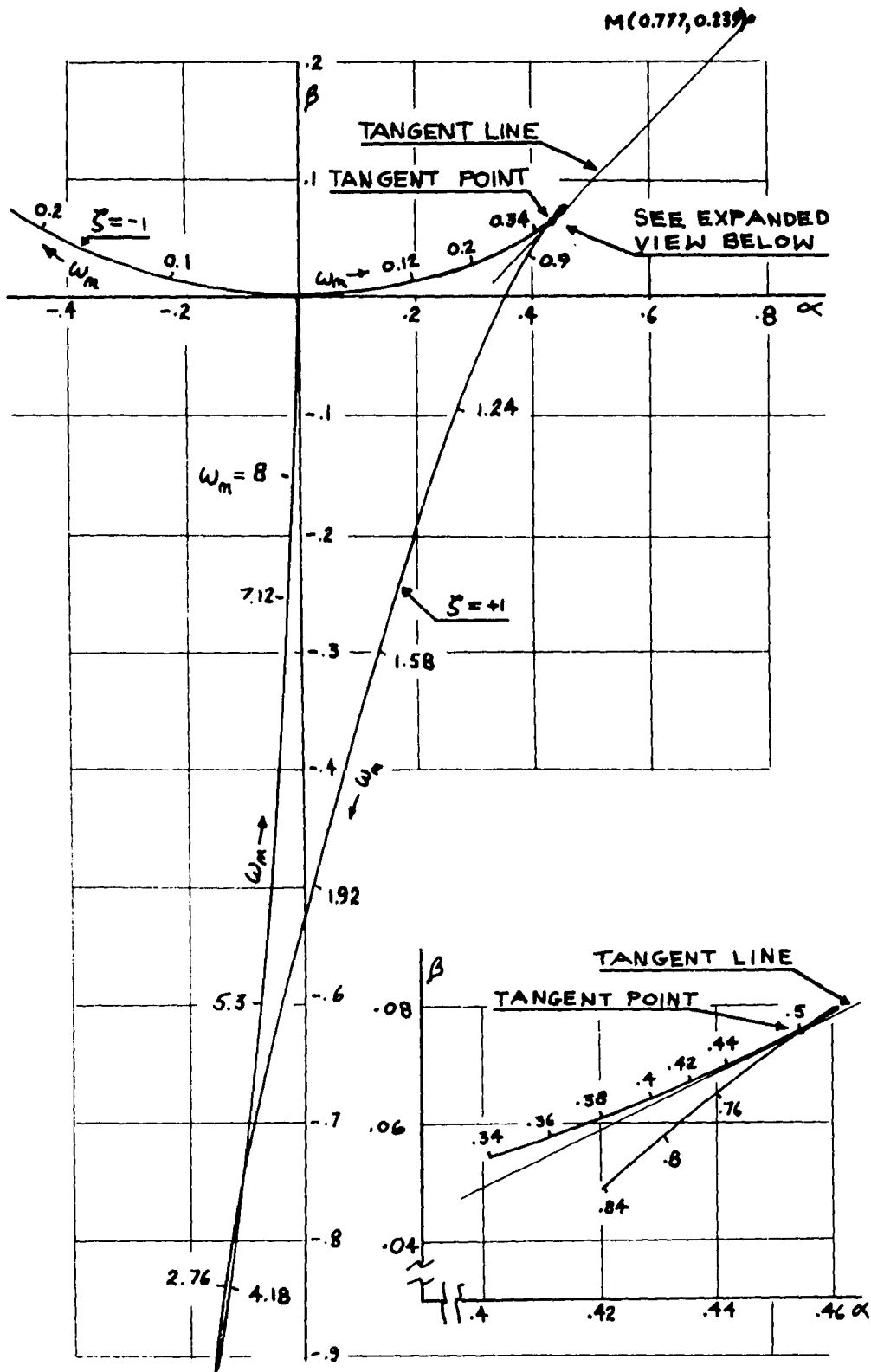


Fig. 5.3.7  $\alpha$ - $\beta$  Plot for  $\zeta = \pm 1$ .

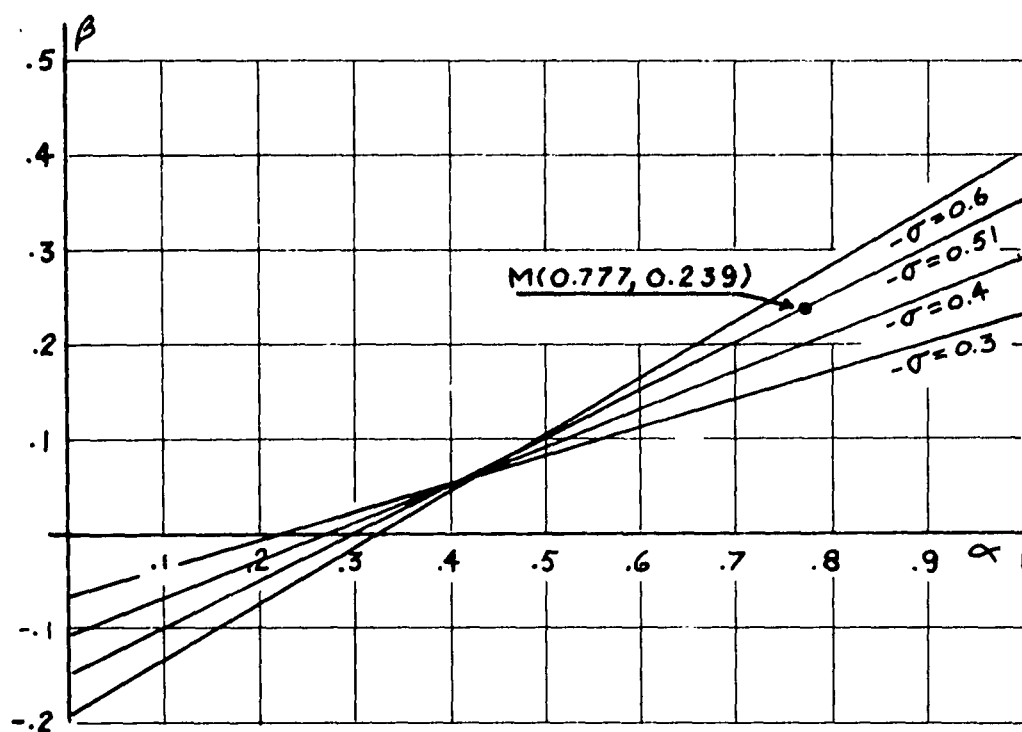


Fig. 5.3.8  $\alpha$ - $\beta$  Plot for Lines of Constant  $\sigma$  .

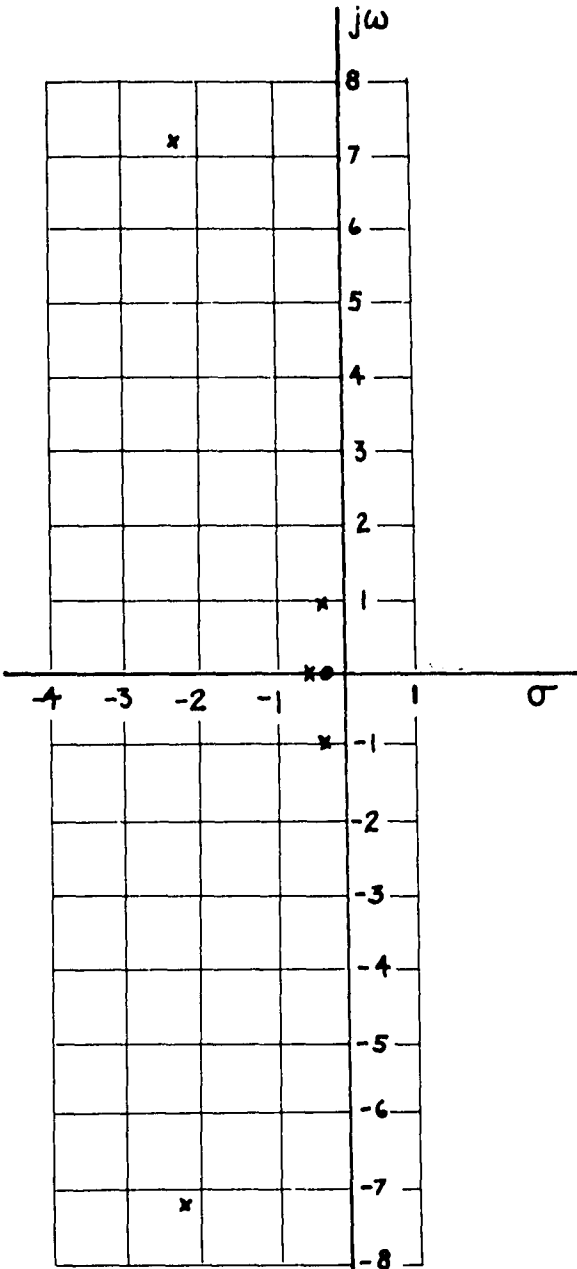


Fig. 5.3.9 Root Zero Locations.

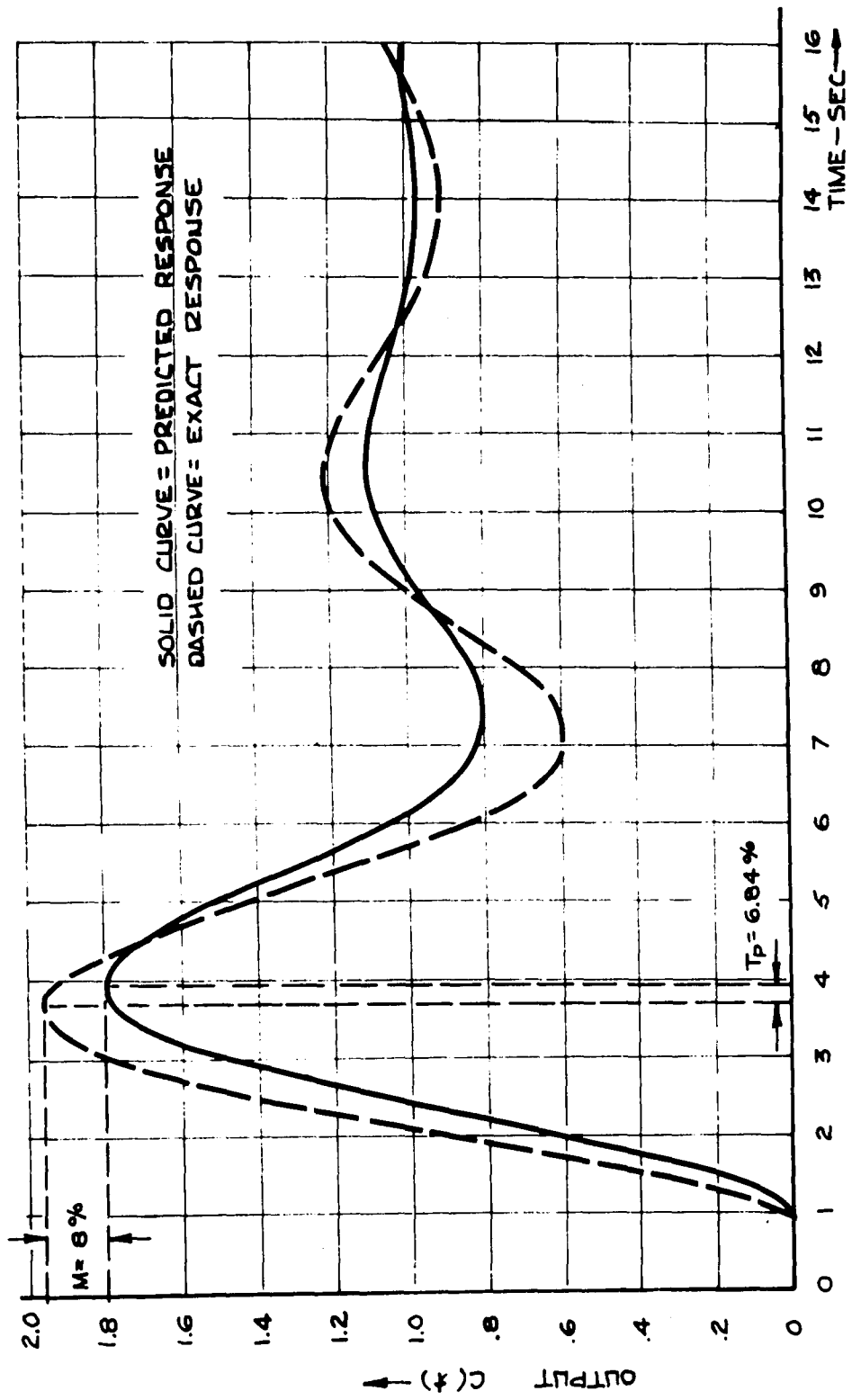


Fig. 5.3.10 Output Response Curves.



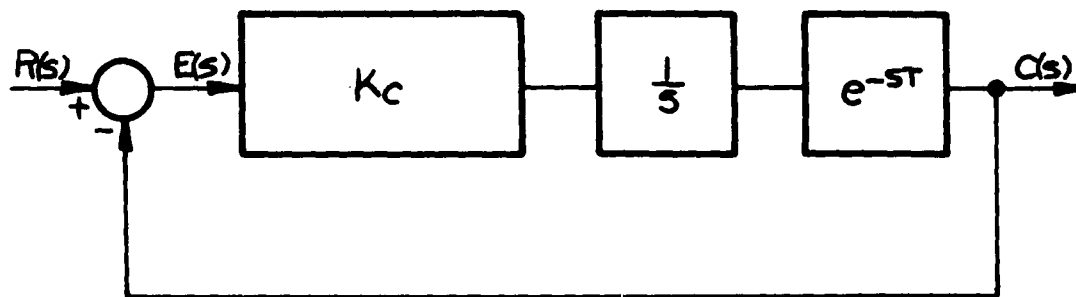


Fig. 5.4.1 Proportional Controller.

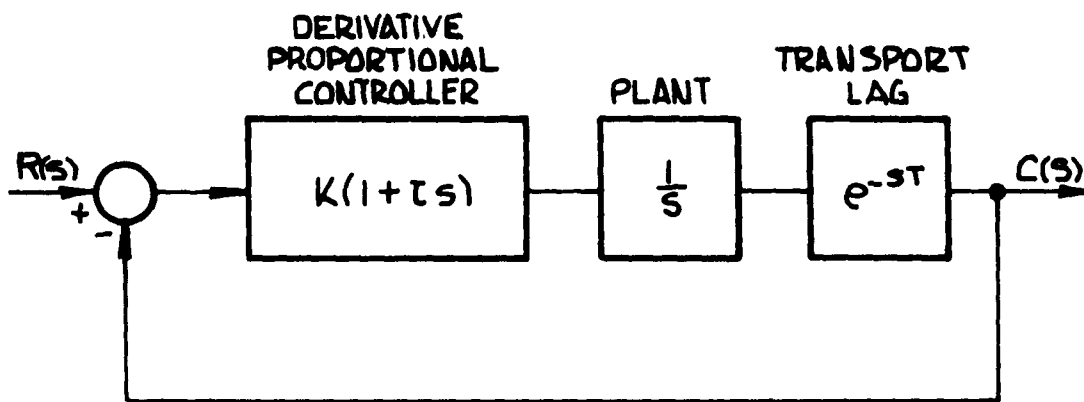


Fig. 5.5.1 Derivative-Proportional Controller.

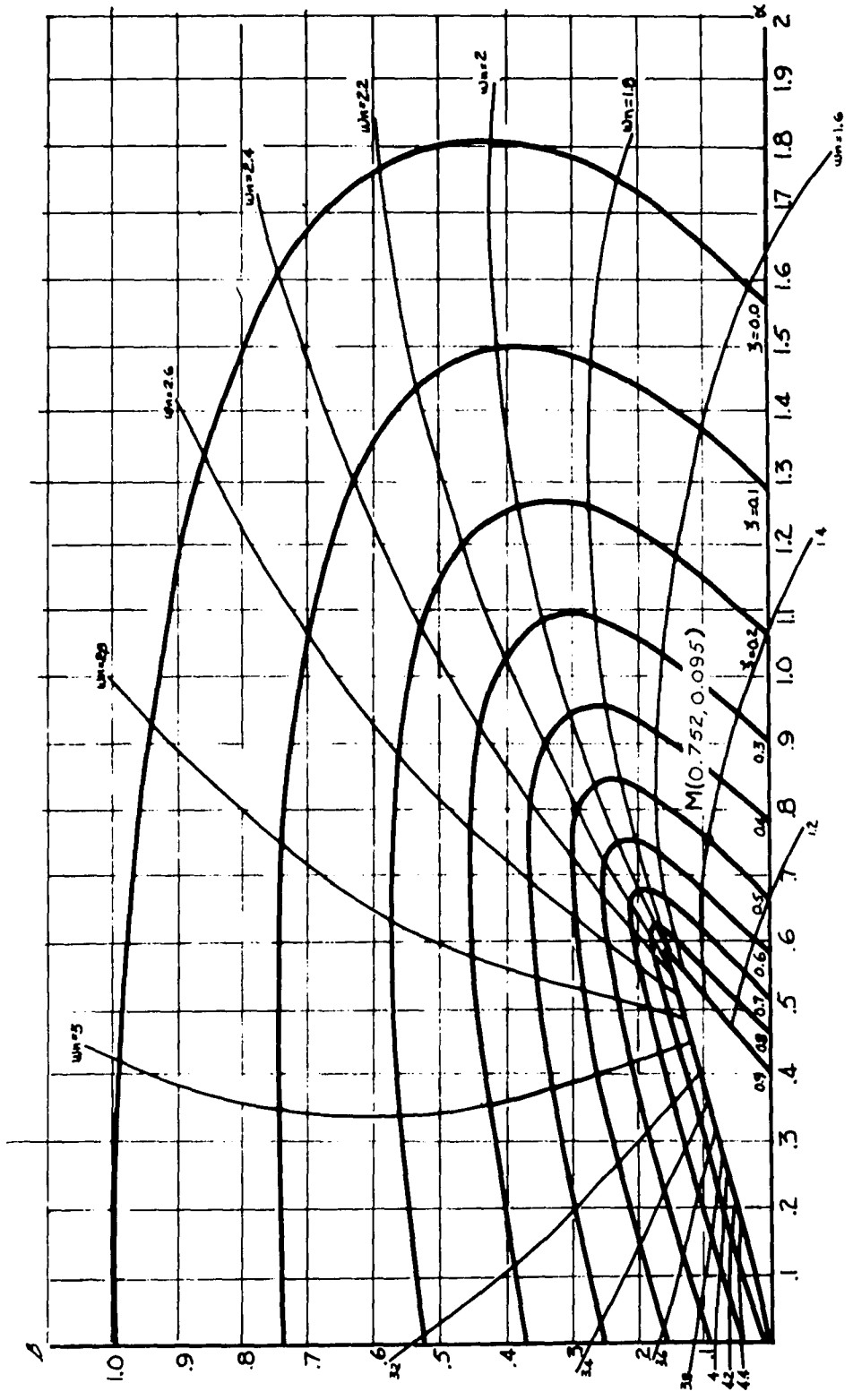


Fig. 5.5.2  $\alpha$ - $\beta$  Plot for  $0 \leq \zeta \leq 0.9$ . (First Traversal.)

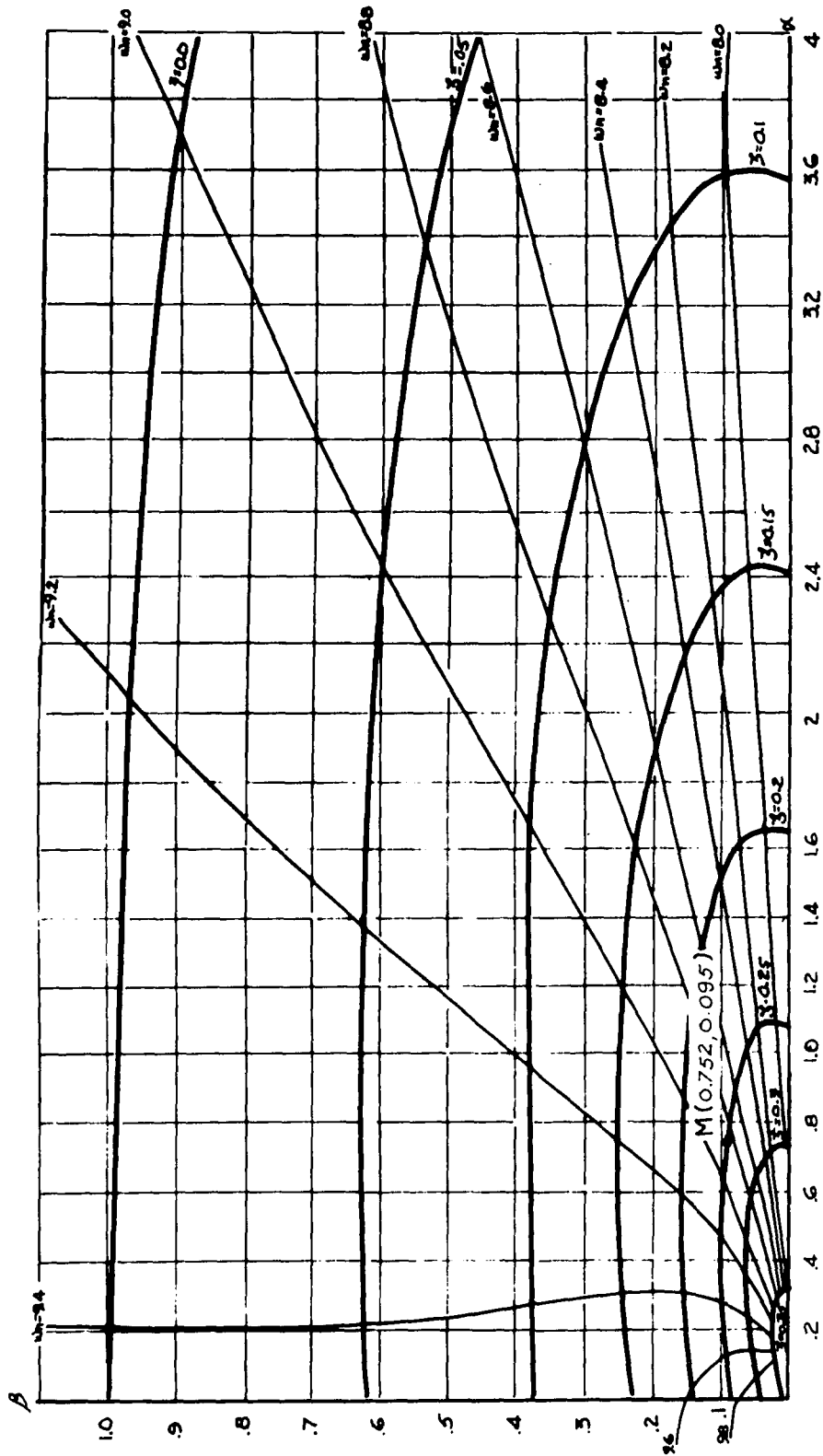


Fig. 5.5.3  $\alpha$ - $\beta$  Plot for  $0 \leq \lambda \leq 0.35$ . (Second Traversal.)

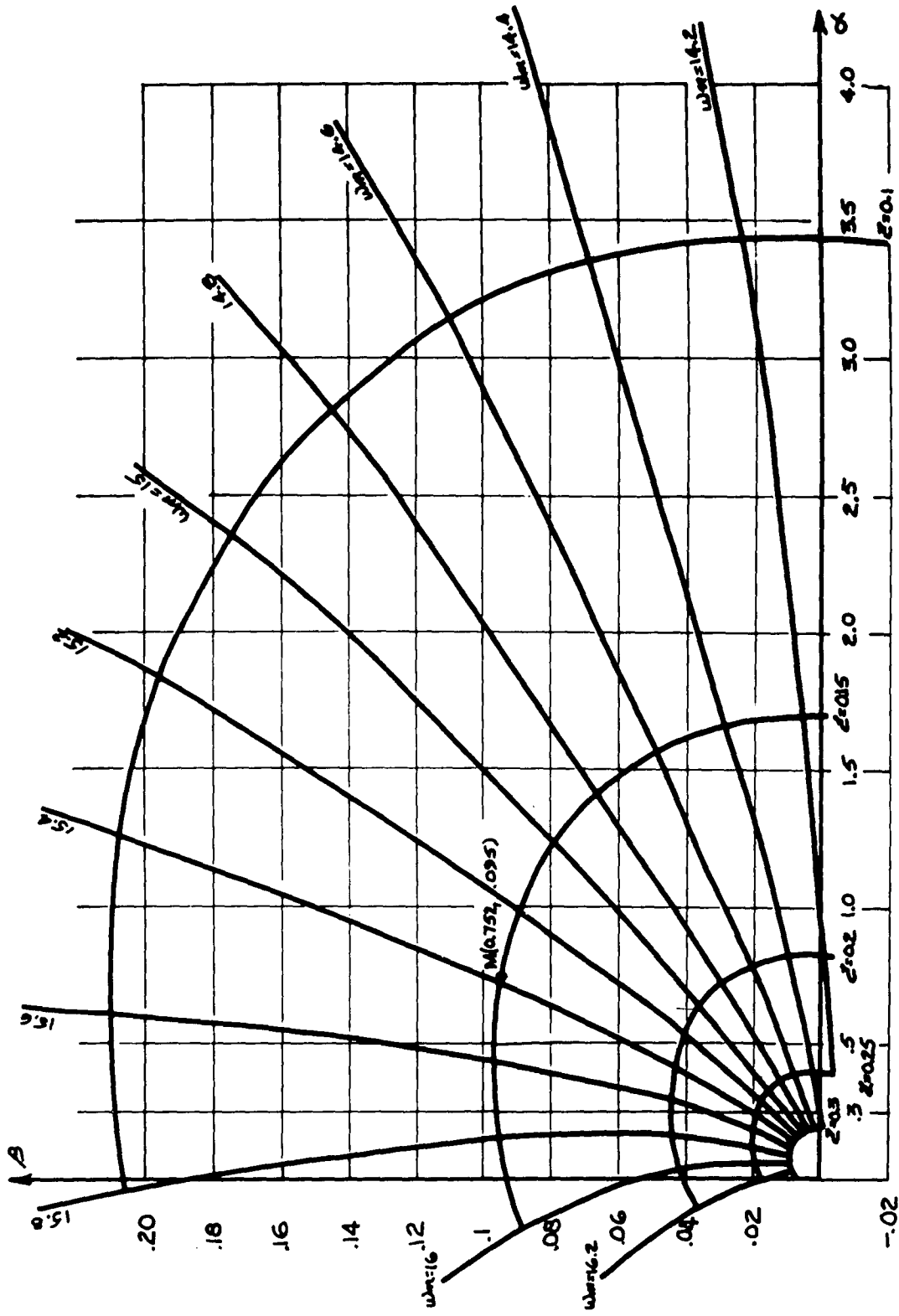


Fig. 5.5.4  $\alpha$ - $\beta$  Plot for  $0 \leq \zeta \leq 0.3$ . (Third Traversal.)

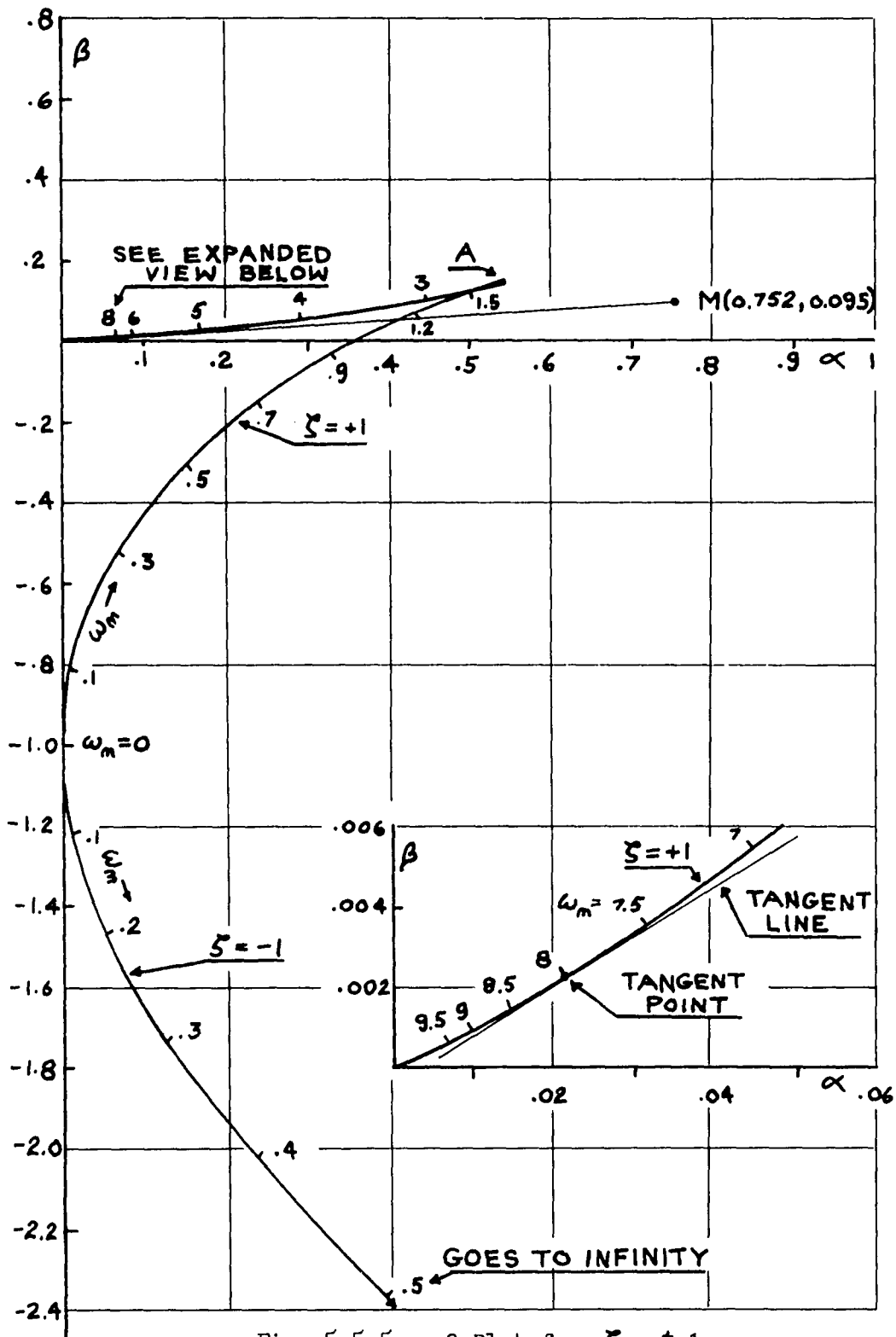
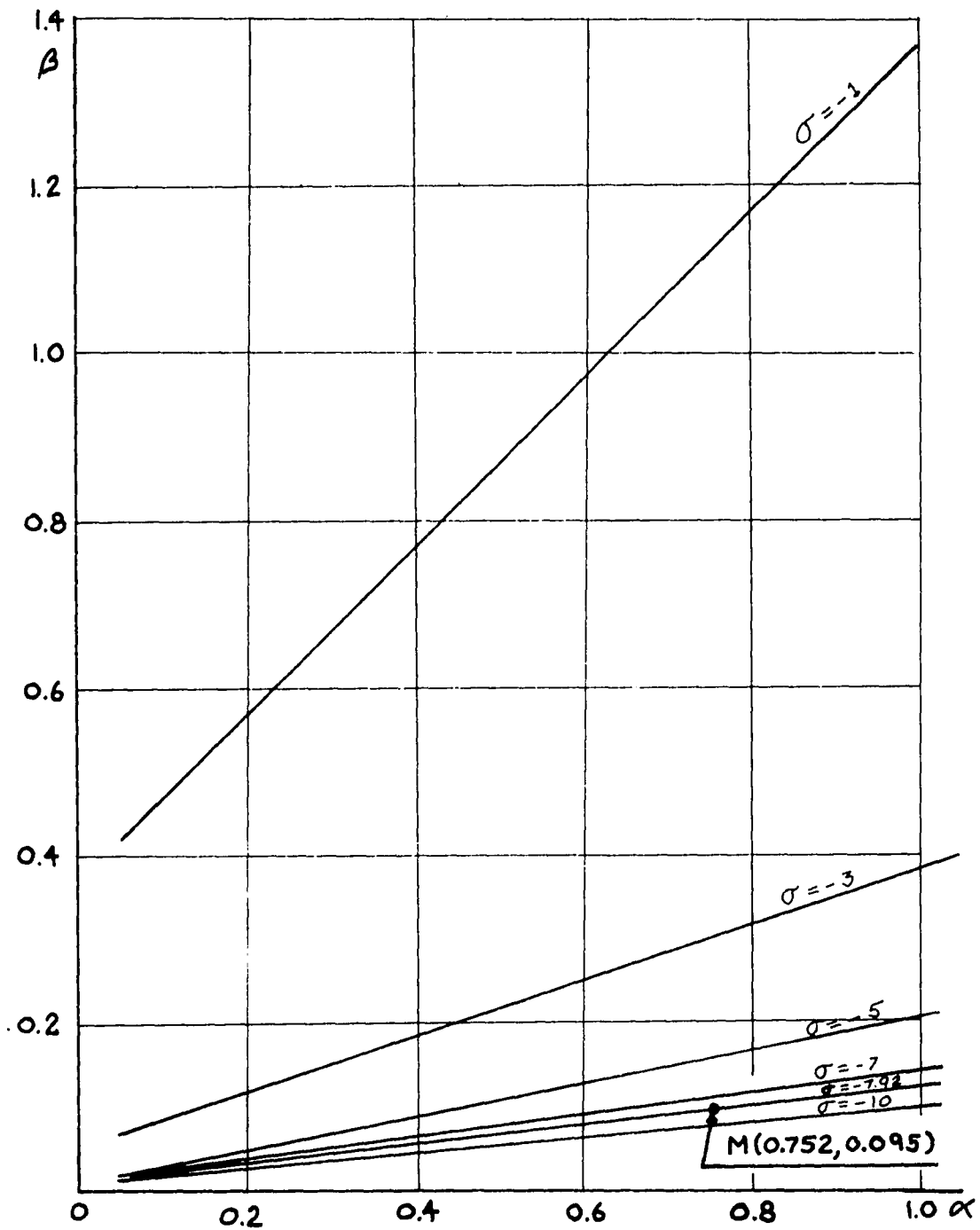


Fig. 5.5.5  $\alpha$ - $\beta$  Plot for  $\zeta = \pm 1$ .

Fig. 5.5.6  $\alpha$ - $\beta$  Plot for Lines of Constant  $\sigma$ .

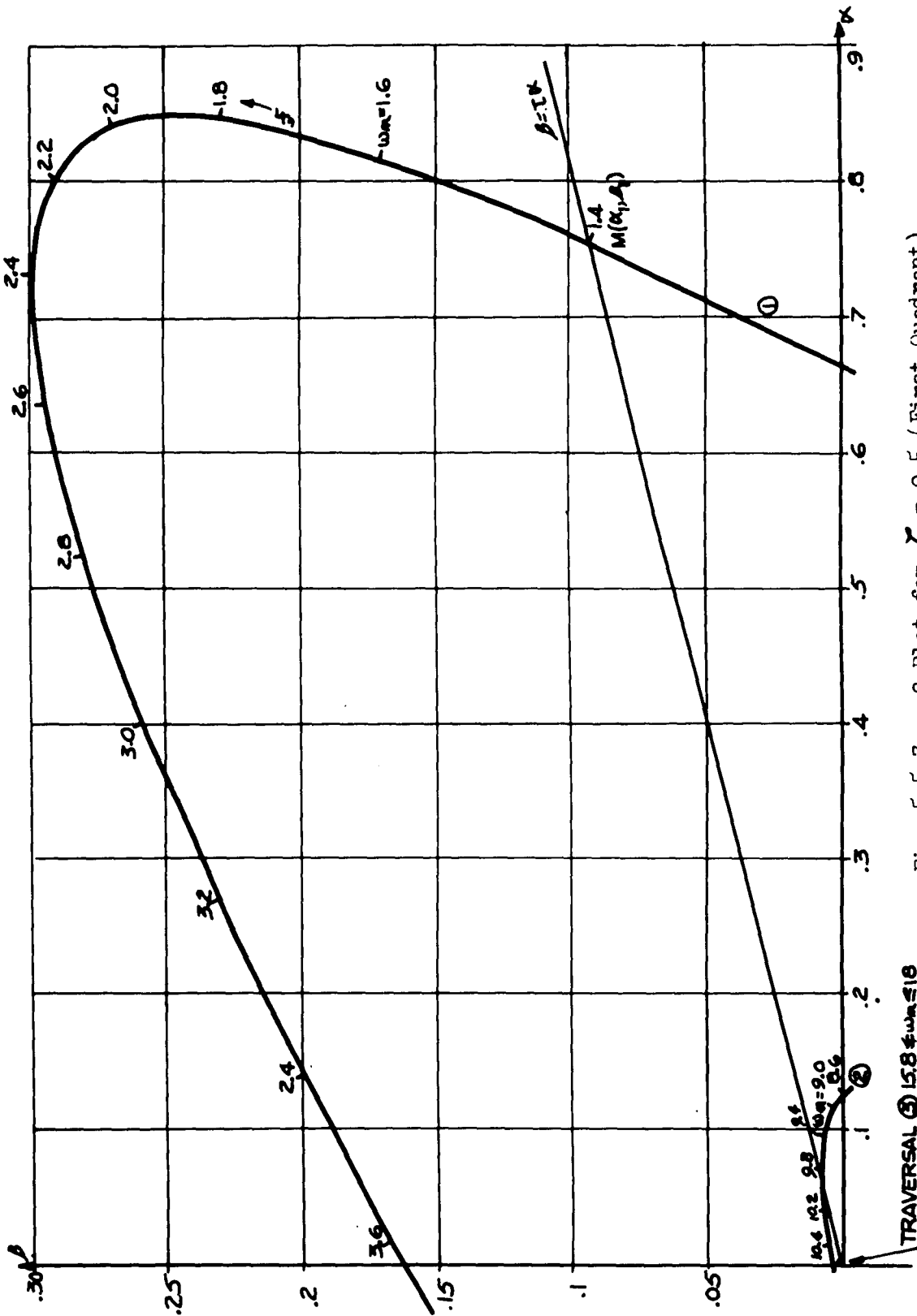


Fig. 5.5.7  $\alpha$ - $\beta$  Plot for  $\zeta = 0.5$ . (First Quadrant.)



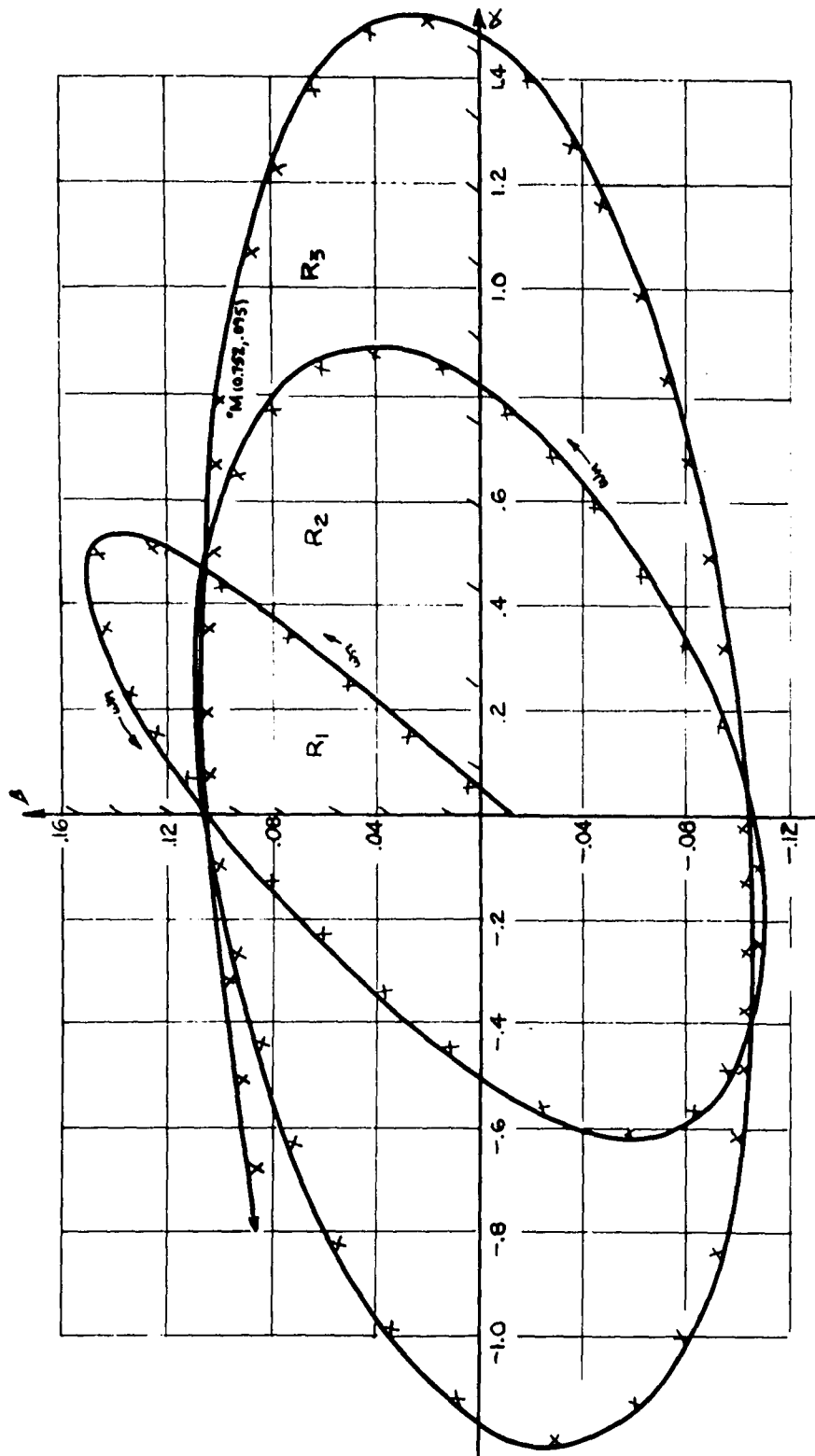


Fig. 5.5.8  $\alpha$ - $\beta$  Plot for a Constant Settling Time Contour of  $\sigma = -2.25$ .

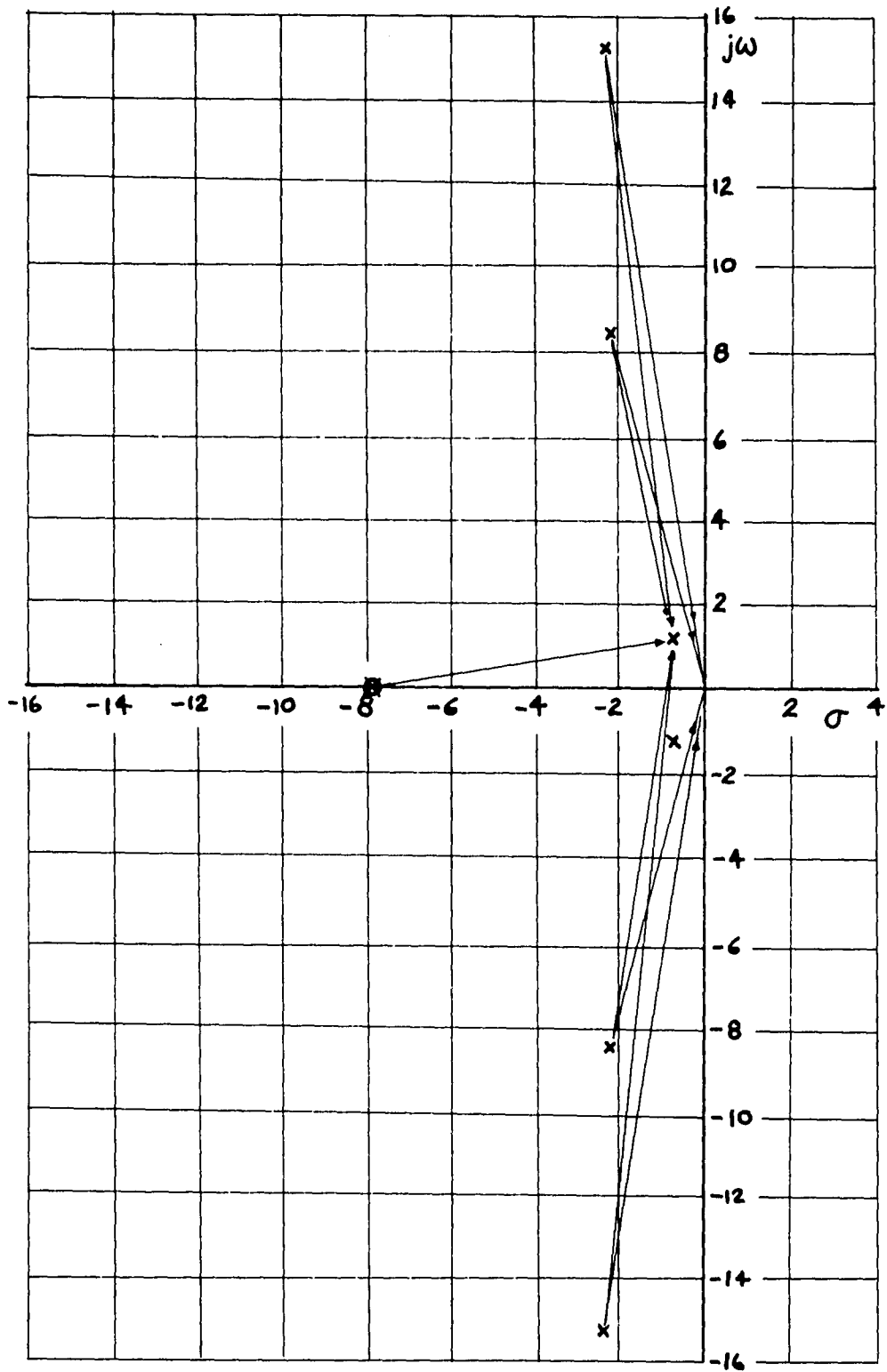
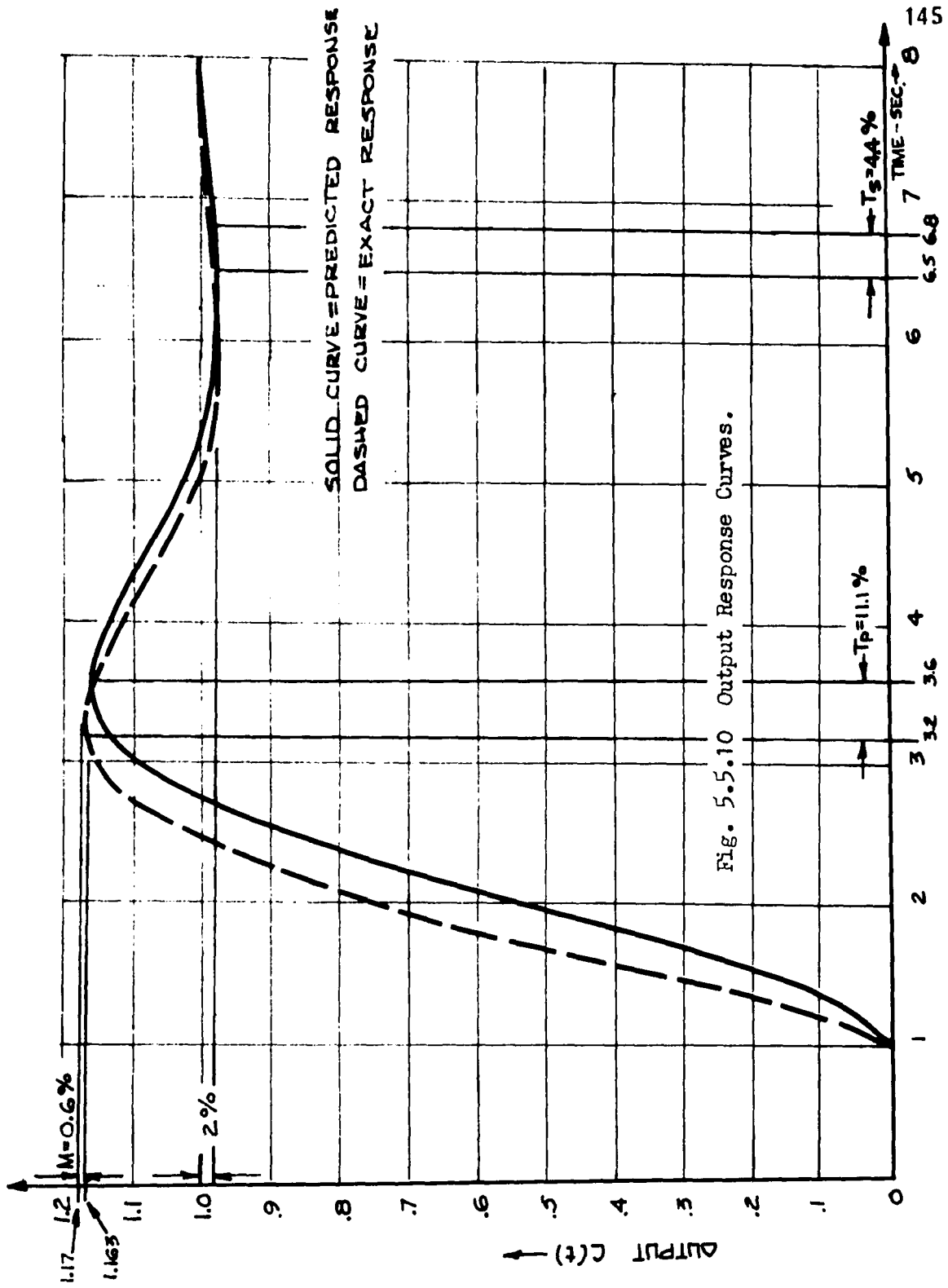


Fig. 5.5.9 Root-Zero Locations.



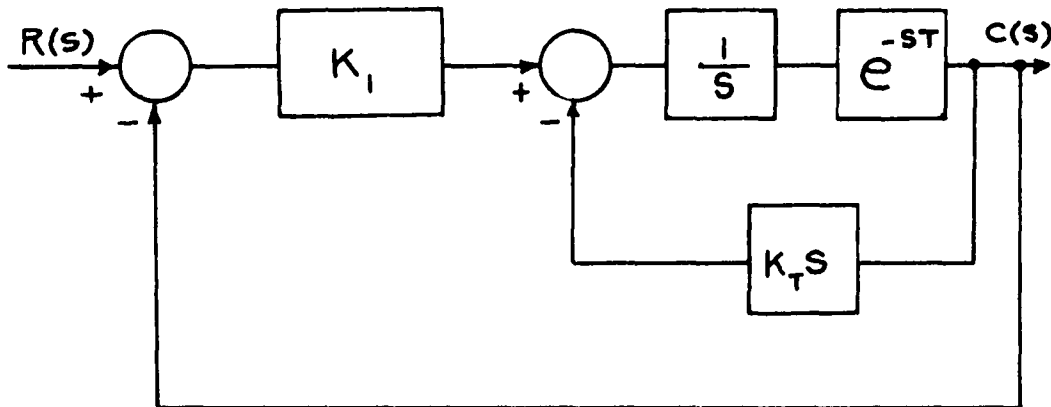


Fig. 5.6.1 Tachometric Feedback Control System.

## CHAPTER 6

### ROOT-LOCUS FOR SYSTEMS WITH TRANSPORT LAG

#### 6.1 Introduction

The parameter plane approach is particularly useful as a means for constructing the root-locus for systems with transport or distributed lag.<sup>1</sup> This method has the following advantages over Chu's method (see Section 3.5).

1. The construction of the root-locus for high order control systems is as easy to perform as for low order control systems.
2. The root-locus is easily constructed for either one of *two* variable parameters in the system.
3. The value of the parameter with respect to which the root-locus is graphed (usually the gain) is immediately available without calculation.
4. If a new value of either of the *two* variable parameters is chosen, the original  $\alpha$ - $\beta$  curves are used to obtain the new root-locus.
5. The root-locus for negative values of the system parameters is also available from the original  $\alpha$ - $\beta$  curves.

---

<sup>1</sup>It must be emphasized that the determination of the system stability, either absolute or relative, as well as the technique developed for controller design, is more expeditiously performed without the construction of the root-locus. However, the conventional root-locus techniques are well known and this chapter is included in order to more closely associate the parameter plane technique with conventional techniques.

## 6.2 Complex Root-Locus

As an example of the application of the parameter plane to the construction of the root-locus of a system, consider the system of Figure 6.2.1. This system was discussed in Section 5.5 in connection with the design of the system controller, so that certain curves and equations are available and will be referred to or repeated here as needed.

The ratio of output to input for this system is

$$\frac{C}{R}(s) = \frac{K(1 + \tau s)}{\epsilon s T s + K + K \tau s} \quad (6.2.1)$$

defining  $\alpha = K$ ,  $\beta = K\tau$ , and setting  $T = 1$  sec. the characteristic equation is

$$F(s) = (\beta + \epsilon s)s + \alpha = 0 \quad (6.2.2)$$

The parametric equations (see Section 4.1) for  $\alpha(\omega_n, \zeta)$  and  $\beta(\omega_n, \zeta)$  are, for  $\zeta \neq 1$ ,

$$\alpha = \frac{\omega_n \epsilon^{-\phi} \sin \theta}{\sqrt{1 - \zeta^2}} \quad (6.2.3)$$

$$\beta = \frac{\epsilon^{-\phi} (-\sqrt{1 - \zeta^2} \cos \theta + \zeta \sin \theta)}{\sqrt{1 - \zeta^2}}$$

for  $\zeta = +1$

$$\alpha = \omega_n^2 \epsilon^{-\omega_n} , \quad \beta = \epsilon^{-\omega_n} (-1 + \omega_n) \quad (6.2.4)$$

and for  $\zeta = -1$

$$\alpha = \omega_n^2 \epsilon^{\omega_n} , \quad \beta = -\epsilon^{\omega_n} (1 + \omega_n) \quad (6.2.5)$$

To determine the locus of the complex roots, equations (6.2.3) are graphed for values of  $0 \leq |\zeta| \leq 0.95$  where  $\omega_n$  is the running parameter. Since the root-locus will be determined from the locus of points described by the constant  $\zeta$  curves (the  $\alpha$ - $\beta$  curves), it is also necessary to graph equations (6.2.3) for values of  $\zeta < 0$ . This is because the complex root locations in the *right-half*  $s$ -plane are characterized by negative values of  $\zeta$  (see Figure 4.1.2b). For example, Figures 6.2.2 and 6.2.3 show the  $\alpha$ - $\beta$  curves for  $\zeta = +0.35$  and  $\zeta = -0.35$  respectively. Note the curve for  $\zeta = +0.35$  spirals into the origin as usual, and for  $\zeta = -0.35$  the curve spirals towards infinity since the exponent of the exponential terms,  $\epsilon^{+\zeta\omega_n}$ , of equations (6.2.3) are now positive.

If only positive values of gain and time constant are considered, it is necessary to graph only positive values of  $\alpha$  and  $\beta$ . Figures 6.2.4 through 6.2.7 show the first quadrants of the first two traversals of the  $\alpha$ - $\beta$  curves for  $0 \leq |\zeta| \leq 0.95$ . When the root-locus is to be determined for a given value of  $\tau$  in (6.2.1) the system gain will be the running parameter on the root-locus. If  $\tau$  is chosen to be equal to say 0.5 sec, then

$$\beta = K\tau = 0.5K = 0.5\alpha \quad (6.2.6)$$

The straight line (6.2.6) is then superimposed on Figures 6.2.4 through 6.2.7 where the intersection of this line and the  $\alpha$ - $\beta$  curves yields the necessary information to construct the first two root-loci for complex roots lying in the upper portion of the  $s$ -plane. For example, the point  $M_1$  in Figure 6.2.4 indicates the existence of a pair of complex roots at  $\zeta = 0.6$ ,  $\omega_n = \pm 0.3$  rad./sec. (recall that the root-loci are symmetrical with respect to the imaginary axis). A gain of  $\alpha = 0.418$  is obtained by dropping a perpendicular from  $M_1$  to the  $\alpha$ -axis. Figure 6.2.8 shows the two complex root-loci obtained in this manner. This procedure is continued until the desired number of root-loci are obtained.

If a new value of  $\tau$  is considered, say  $\tau = \tau_2 = 0.3$  sec., only the slope of the  $\beta = \tau\alpha$  line is changed and the procedure developed above is again performed. This last feature is a distinct advantage over the conventional root-locus technique, since it would normally be necessary to re-graph all of the curves for any change in a parameter value. This latter point is so significant that in instances where the root-locus is desired for feedback control systems that do *not* contain transport lag it may well be advantageous to apply the parameter plane technique to determine the root-locus. This is easily accomplished by setting  $c_k = e_k = g_k = 0$  in equation (4.1.6) of Chapter 4, since this will eliminate the effect of the transport lag term  $\epsilon^{ST}$  in all ensuing equations.

The root-locus for negative values of  $\alpha$  or  $\beta$  are determined from the same  $\alpha$ - $\beta$  curves where the second, third and fourth quadrants are now utilized. For example, for  $\alpha < 0$  and  $\beta > 0$  the  $\beta = -\tau\alpha$  line is drawn in



the second quadrant and the root-locus is constructed from the second quadrant in the manner described above. Further, for  $\alpha < 0$  and  $\beta < 0$  the third quadrant is utilized and for  $\alpha > 0$  and  $\beta < 0$  the fourth quadrant is utilized.

In this example the parameter  $\tau$  was held fixed while the system gain  $\alpha = K$  was the variable parameter with respect to which the root-locus was constructed. If it is desired to construct the root-locus for a fixed value of gain  $\alpha = K_1$ , in which case  $\tau$  is the running parameter, then the  $\beta = \tau\alpha$  line is replaced by the vertical line  $\alpha = K_1$  and the root-locus is constructed as usual.

### 6.3 Real Root-Locus

In order to construct the locus of the real roots recourse is made to the  $\alpha$ - $\beta$  curves for  $\zeta = \pm 1$  shown in Figure 6.3.1. The straight line  $\beta = 0.5\alpha$  is superimposed on the  $\zeta = \pm 1$  curves, and the real root locations for varying  $\alpha$  are determined from straight lines emanating from points  $M(\alpha, \beta)$  on the  $\beta = 0.5\alpha$  line that are tangent to the  $\zeta = \pm 1$  curves. The negative value of the frequency  $\omega_n$  indicated on the  $\zeta = +1$  curve at the point of tangency is the value of a real root; and the value of the frequency  $\omega_n$  indicated on the  $\zeta = -1$  curve at this point is the value of a real root. The value of the gains producing these real root locations are determined by dropping a perpendicular from the points  $M(\alpha, \beta)$  to the  $\alpha$ -axis. In this case the real root locus is from  $s = 0$ , corresponding to the point  $M(0, 0)$  to  $s = -2$ . The real root-locus is also shown on Figure 6.2.3. Note that it is only possible for

one tangent to the  $\zeta = +1$  curve to exist for any point  $M(\alpha_1, \beta_1)$  so that only one real root can exist for a given value of gain. Recall from Section 5.6 that the point A on Figure 6.3.1 is not a point of inflection.

The method discussed above yields the real roots only approximately, because the method is based on a graphical construction of a tangent line to a curve. The origin and termination of the root locus, however, can easily be exactly determined for this example in the following manner. The origin of the locus is exactly  $s = 0$  since a line drawn from  $M(0, 0)$  is tangent to the  $\zeta = \pm 1$  curve at  $\omega_n = 0$ , the point where the  $\zeta = \pm 1$  curve originates. Further, the locus must terminate at a zero of the open-loop transfer function which in this case is  $s = -\frac{1}{\tau} = 2.0$ .

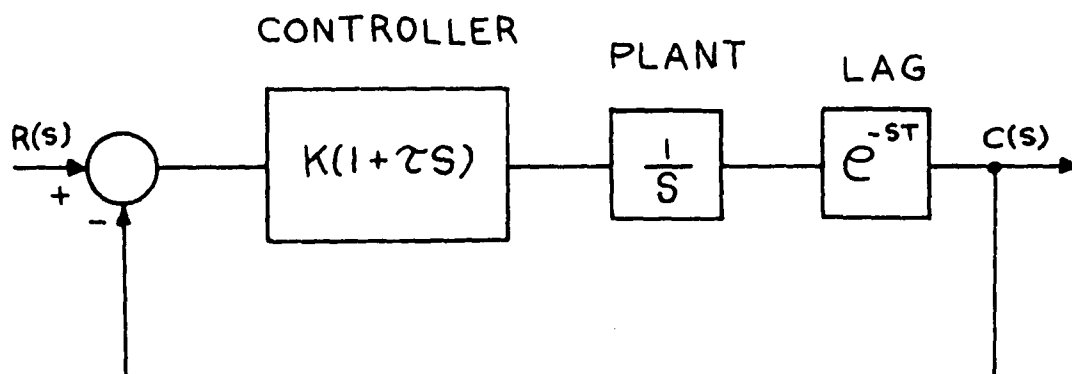


Fig. 6.2.1 Feedback Control System.

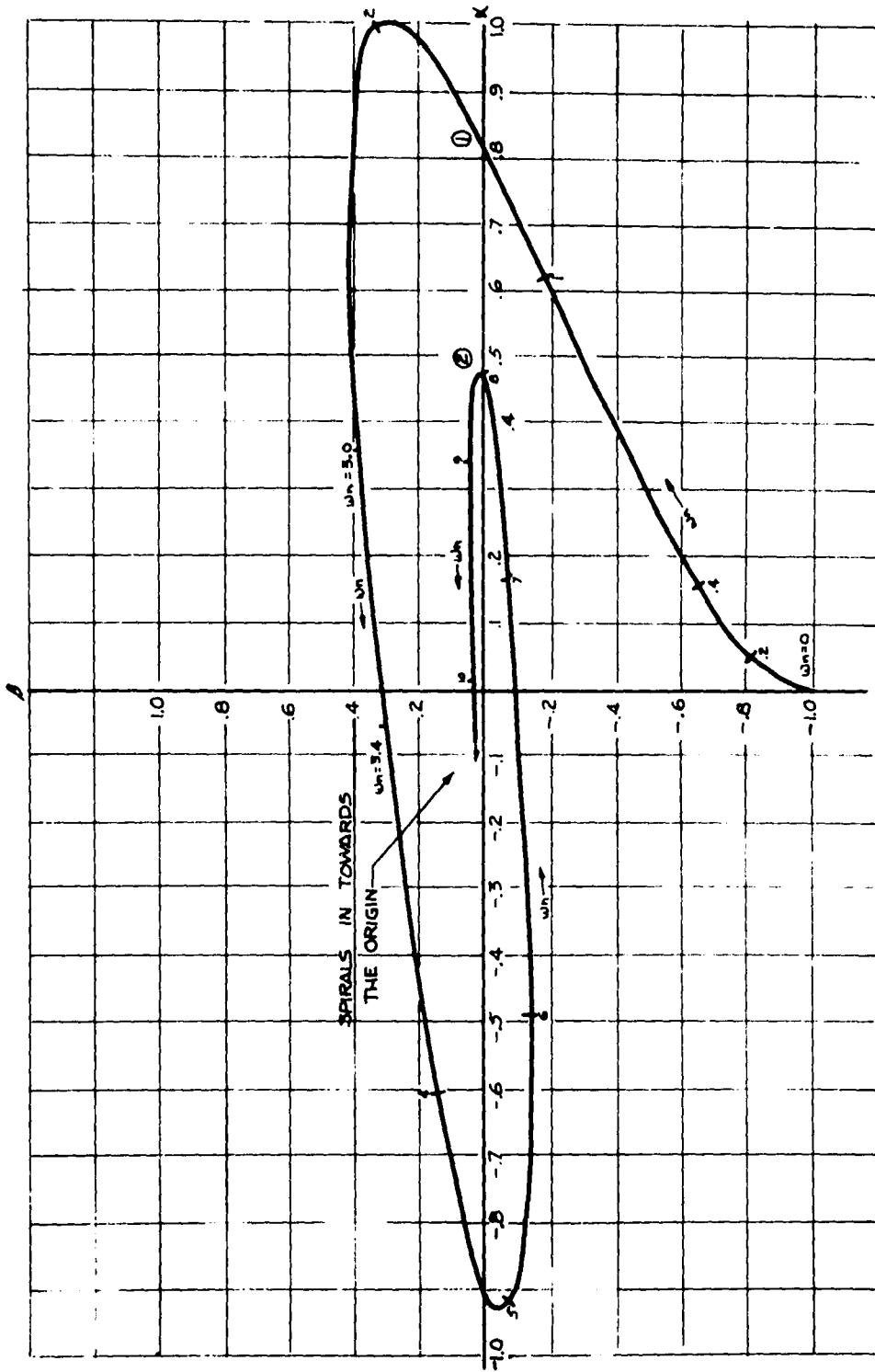


Fig. 6.2.2  $\alpha$ - $\beta$  Plot for  $\zeta = + 0.35$ .

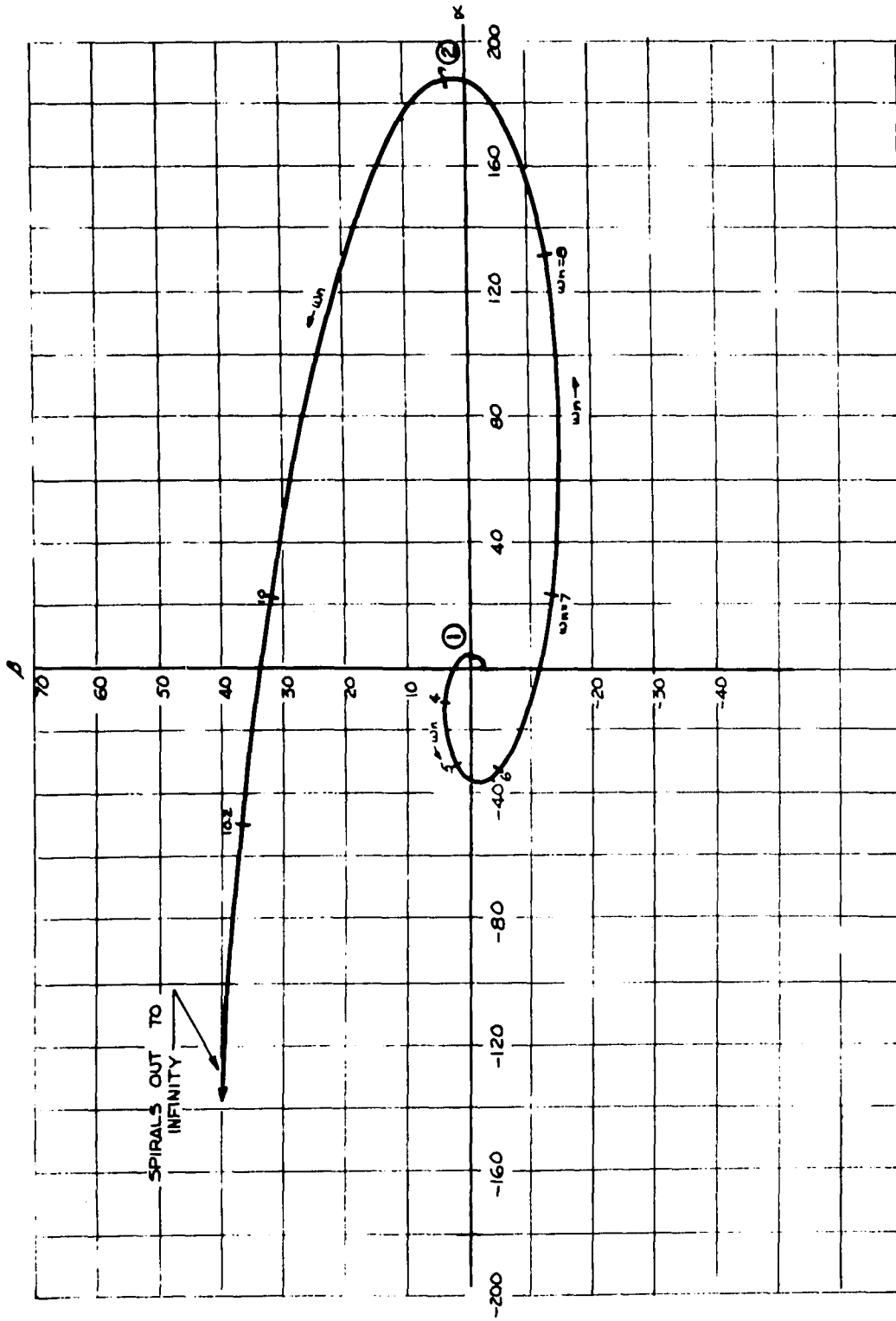


Fig. 6.2.3  $\alpha$ - $\beta$  Plot for  $\zeta = -0.35$ .

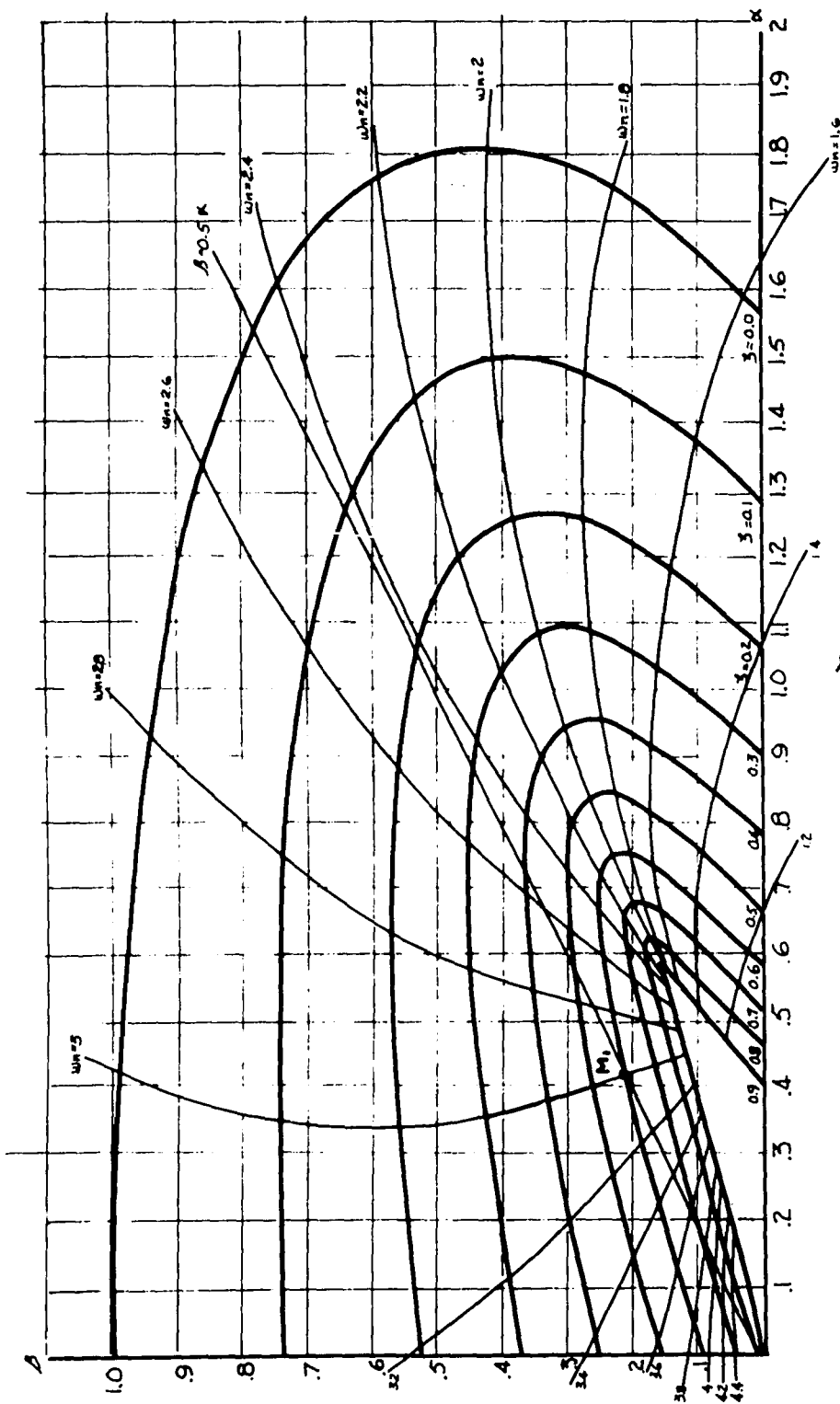


Fig. 6.2.4  $\alpha$ - $\beta$  Plot for  $0 \leq \zeta \leq 0.9$ . (First Traversal)

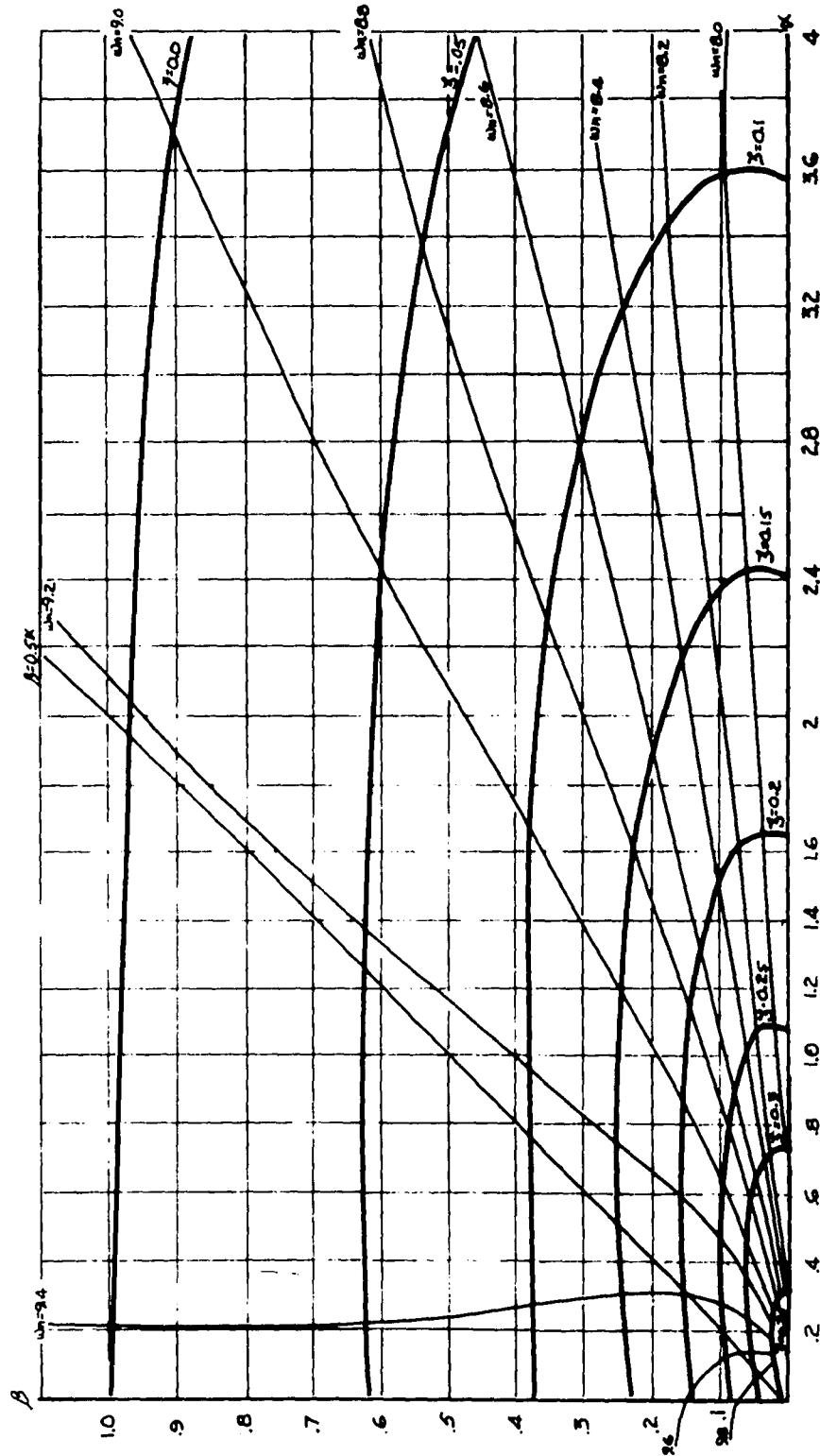


Fig. 6.2.5  $\alpha$ - $\beta$  Plot for  $0 \leq \lambda \leq 0.35$ . (Second Traversal.)

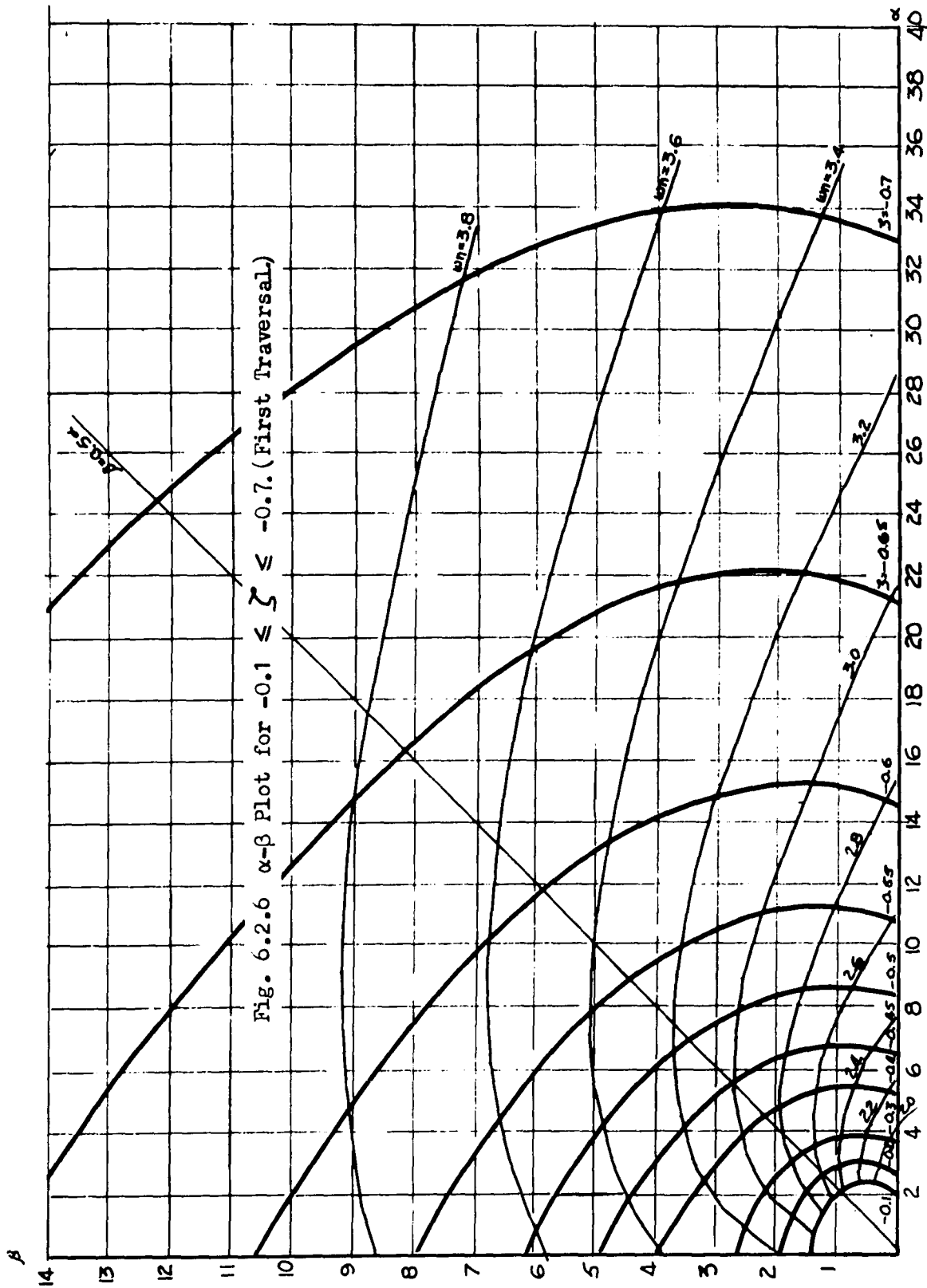


Fig. 6.2.6  $\alpha$ - $\beta$  Plot for  $-0.1 \leq \lambda \leq -0.7$ . (First Traversal)



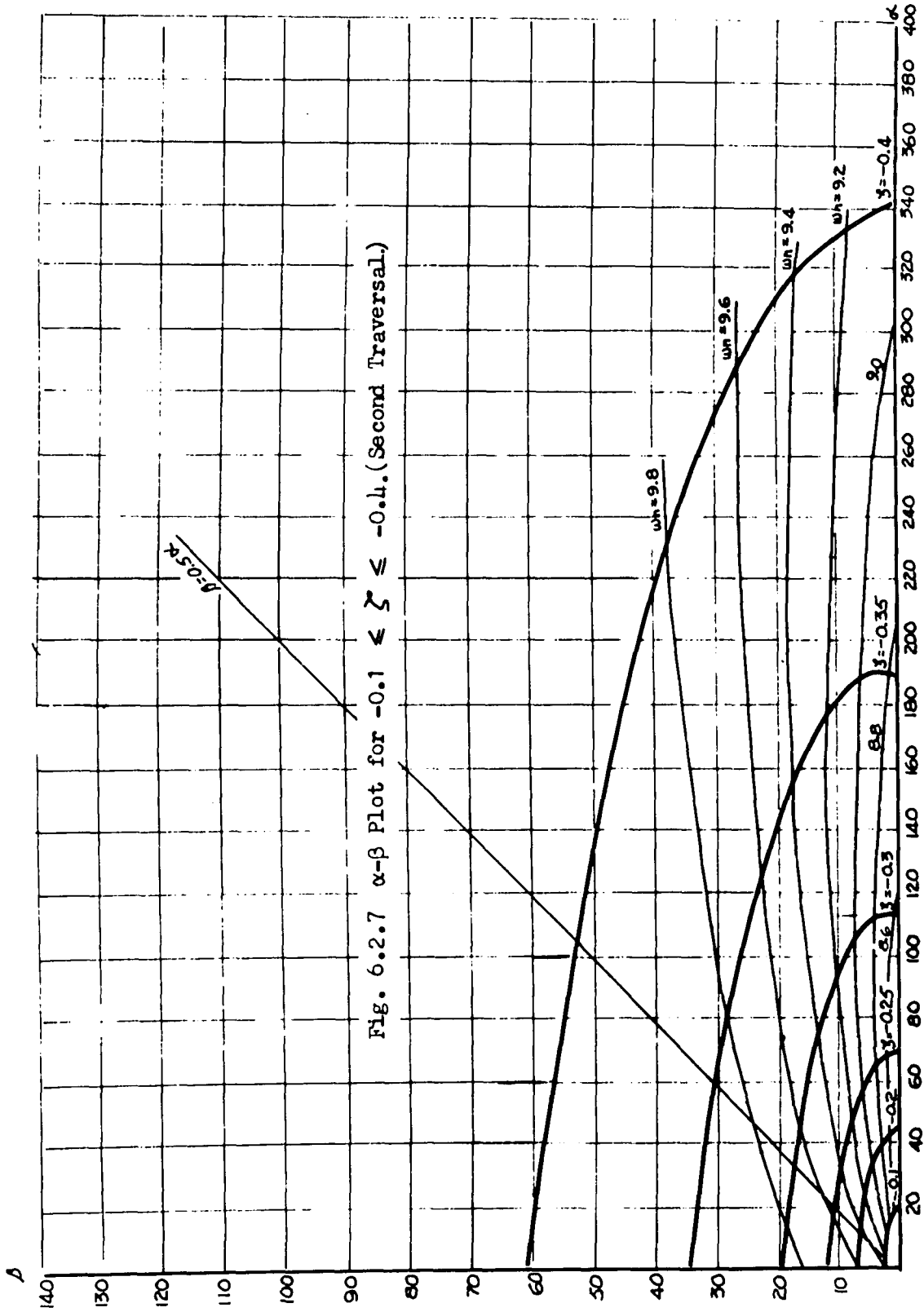


Fig. 6.2.7  $\alpha$ - $\beta$  Plot for  $-0.1 \leq \zeta \leq -0.4$ . (Second Traversal.)

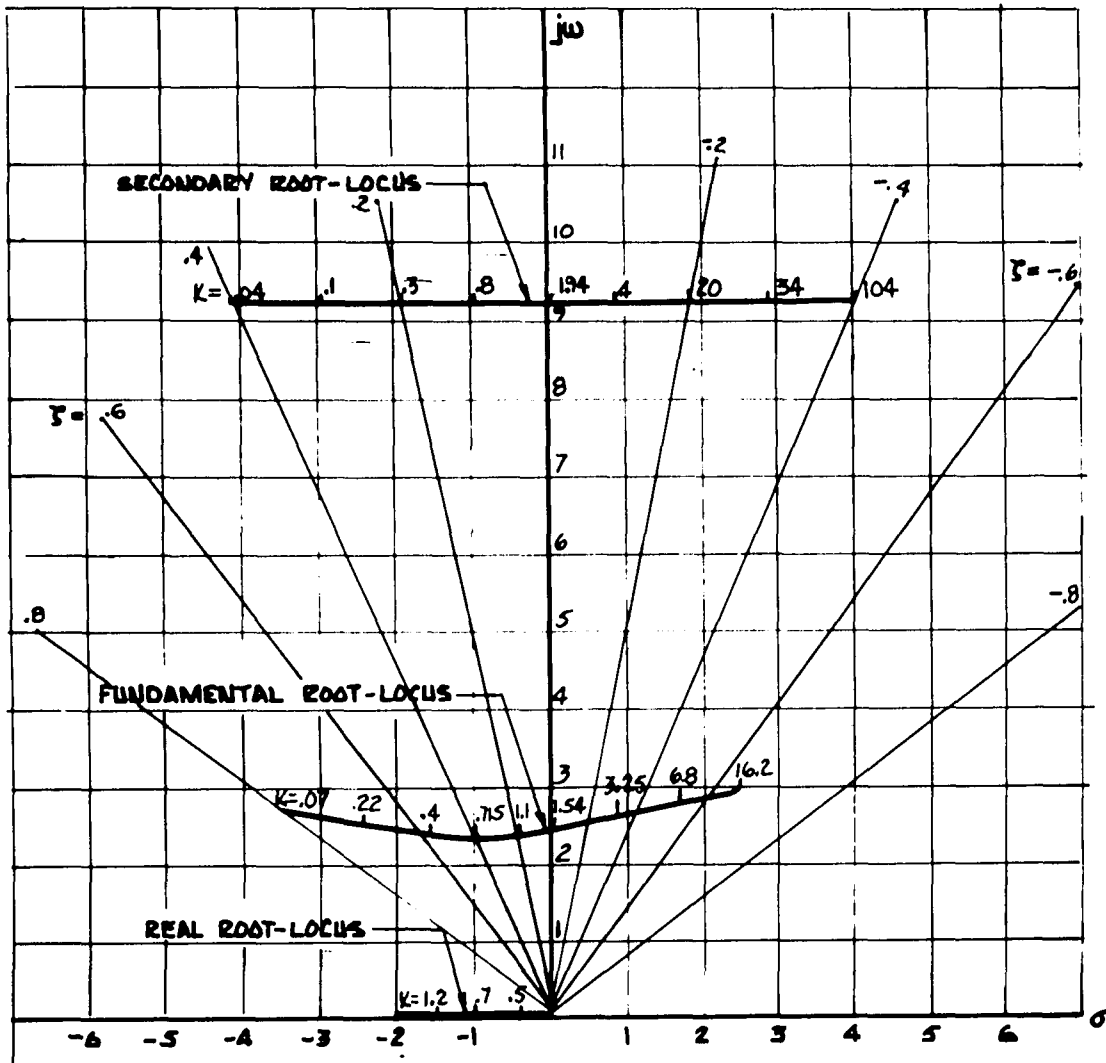


Fig. 6.2.8 Root-Locus for  $\tau = 0.5$  sec.

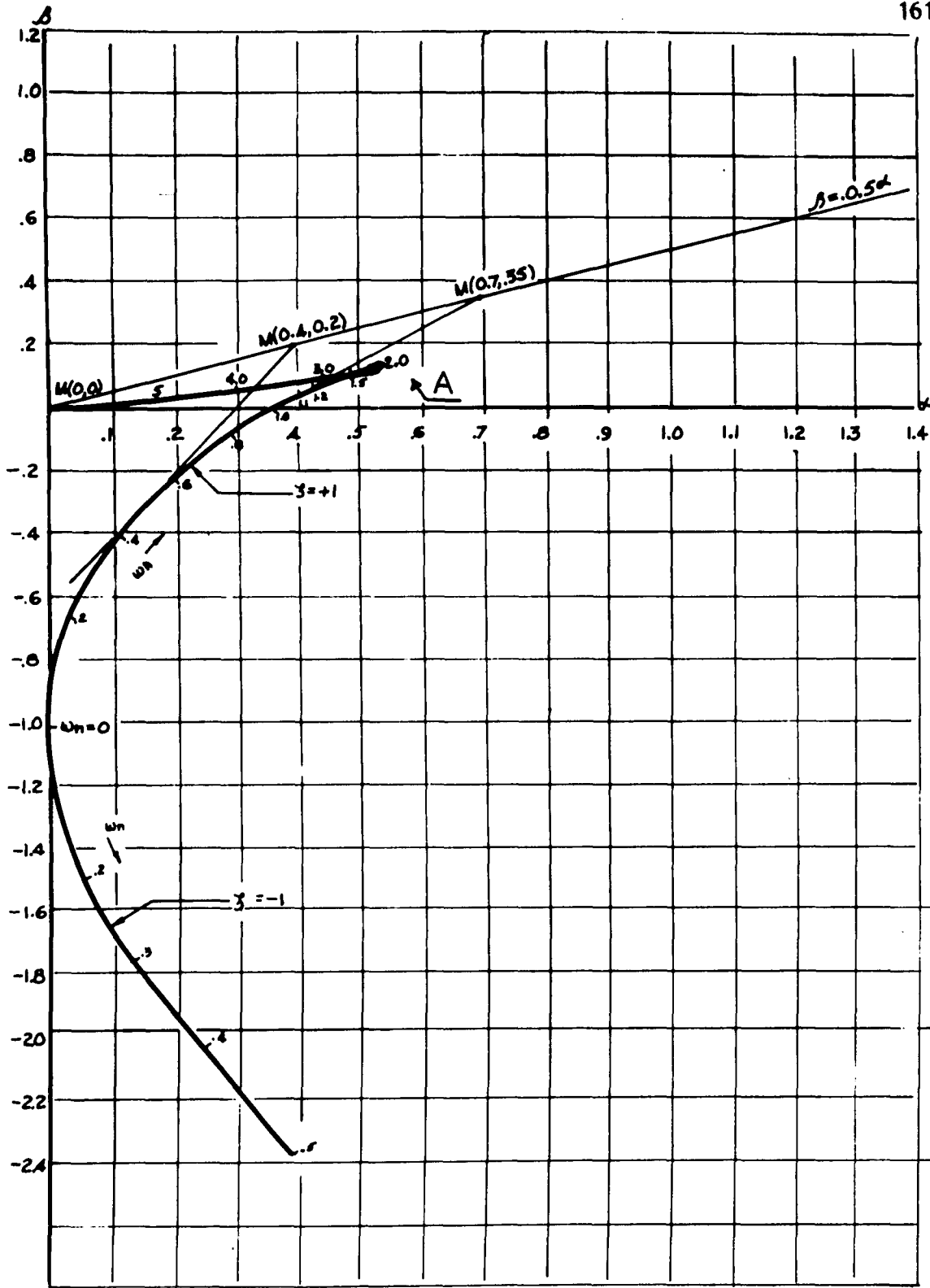


Fig. 6.3.1  $\alpha$ - $\beta$  Plot for  $\zeta = \pm 1$ .

## CHAPTER 7

### NONLINEAR SYSTEMS

#### 7.1 Introduction

In the preceding chapters, the analysis and design techniques discussed were restricted to linear feedback control systems. However, all practical systems are nonlinear to some extent; most physical systems can be considered to be linear only within a limited range of operation. If a feedback control system is designed according to linear theory and methods, it is essential that the components used in the system operate in linear fashions under various operating conditions. If, under certain circumstances, the components are driven into the region of nonlinear characteristics, linear design theory may describe only approximately, or quite often may give a completely erroneous prediction of the system performance. For systems in which the linearity assumption is not valid, nonlinear differential equations must be used to describe system behavior.

The study of nonlinear control systems is difficult because most of the commonly used techniques for linear systems are no longer valid. The transfer function concept of linear systems becomes inapplicable for systems with nonlinear elements; poles and zeros have little meaning in characterizing nonlinear systems. Furthermore, the root-locus diagrams which are so convenient for the study of linear systems are meaningless for nonlinear systems, simply because the characteristic equation is not defined.

## 7.2 Describing Functions

One of the popular techniques used in analyzing the absolute stability of a class of nonlinear systems is the describing function technique as developed by Goldfarb [8] and Kochenburger [10]. The basic philosophy of this approach is to attempt to approximate a non-linearity by a linear function and, in this way, extend the transfer function concepts to nonlinear systems. Therefore, the describing function concept suffers from the immediate limitations associated with all approximate techniques. However, in many practical situations the results, in terms of absolute system stability, are quite accurate. Thus, the concept of the transfer function of a system, along with the system characteristic equation, has been re-introduced. It follows that the theory developed in this work can be applied to nonlinear systems that can be characterized by describing functions.

The describing function method is based on the following assumptions and considerations:

(1) The control system contains only one nonlinear element  $n$ ; a typical form of the nonlinear system under consideration is shown in Figure 7.3.1a.

(2) The input to the nonlinear element  $n$  is assumed to be sinusoidal. The output of the nonlinear element is, in general, not a sinusoidal wave; nevertheless, it is a periodic function, and can be represented by a Fourier series. The describing function analysis assumes that only the fundamental component of the output is significant

when fed back to the input. Actually, if the input to  $n$  is considered to be sinusoidal, the output of  $n$  contains components at the fundamental frequency, and, in general, at all higher harmonic frequencies. It can be shown (Page 567 of Reference 29) that the harmonics in the outputs of most of the common types of nonlinearities in servo systems are often of smaller amplitudes than the amplitudes of the fundamental components. Furthermore, most servo systems act as low pass filters, so that the higher harmonics in the output of the nonlinear elements are attenuated when compared to the fundamental component.

When the basic assumptions listed above are satisfied, the nonlinear element  $n$  can be represented by an equivalent transfer function called the describing function, which is defined as the ratio of the fundamental component of the output to the (sinusoidal) amplitude of the input. Therefore,

Describing function  $N =$

$$\frac{\text{Fundamental component of output from Fourier analysis}}{\text{Amplitude of the sinusoidal input signal}}$$

(7.2.1)

Although the describing function is defined as the ratio of amplitudes of two sinusoidal signals of the same frequency, it is not a linear transfer function. It will be shown that, in general,  $N$  may be a function of the amplitude or the frequency, or both, of the input signal to  $n$ . For instance, the describing functions of simple

amplifier saturation and on-off relays without hysteresis are functions only of the amplitude of the input sinusoid; the describing functions of friction and inertia-controlled gear backlash depend not only on the amplitude but also on the frequency of the input signal. In addition to the above-mentioned properties,  $N$  may be a real number, as in the case of simple amplifier saturation, or ideal relay; or  $N$  may be a complex number, as in the case of a relay with hysteresis.

For the notation of Figure 7.3.1, if the input to the nonlinear element  $n$  is assumed to be

$$x(t) = X \sin \omega t \quad (7.2.2)$$

the output of the nonlinear element  $y(t)$  is a periodic function, and may be represented by the Fourier series

$$y(t) = \sum_{n=1}^{\infty} (A_n \cos n\omega t + B_n \sin n\omega t) , \quad n = 1, 2, 3, \dots \quad (7.2.3)$$

where

$$A_n = \frac{1}{\pi} \int_{-\pi}^{\pi} y(t) \cos n\omega t \, d\omega t$$

$$B_n = \frac{1}{\pi} \int_{-\pi}^{\pi} y(t) \sin n\omega t \, d\omega t \quad (7.2.4)$$

The constant term in the Fourier series has been omitted due to the assumption that the average value of  $y(t)$  is zero; this is true provided that the nonlinear element possesses symmetrical characteristics.

According to the assumptions of the describing function, all higher terms in the Fourier series of equation (7.2.3) may be omitted, leaving only the fundamental component. Thus,

$$\begin{aligned} y(t) \cong y_1(t) &= A_1 \cos \omega t + B_1 \sin \omega t \\ &= \sqrt{A_1^2 + B_1^2} \sin(\omega t + \gamma) = Y_1 \sin(\omega t + \gamma) \end{aligned} \quad (7.2.5)$$

where  $\gamma = \tan^{-1} \left( \frac{A_1}{B_1} \right)$  and  $Y_1 = \sqrt{A_1^2 + B_1^2}$

The describing function is then defined according to equation (7.2.1) as

$$N(X, \omega) = \frac{Y_1}{X} e^{j\gamma} \quad (7.2.6)$$

Therefore,  $N$  is a complex quantity when  $\gamma$  is nonzero. It is a function of input amplitude,  $X$ , and of frequency,  $\omega$ , if  $Y_1$  and/or  $\gamma$  is a function of frequency.

### 7.3 Systems Containing a Single Nonlinearity with a Real Amplitude Dependent Describing Function

Consider the nonlinear feedback control system with transport lag in Figure 7.3.1a where the nonlinearity contains saturation and a dead zone as shown in Figure 7.3.1b. The describing function for this type of nonlinearity is purely real and dependent only upon the amplitude of the input signal to the nonlinearity. Thus,  $N$  appears in the characteristic equation as a gain varying with the amplitude of the input to  $n$  (see page 569 of Reference 29).



As an example, the transfer function  $G(s)$  in Figure 7.3.1a is assumed to be the same one analyzed in Section 5.6 of Chapter 5. This is convenient since the  $\alpha$ - $\beta$  curve for  $\zeta = 0$  is readily available and can be utilized with minor modifications. The characteristic equation for this system is then

$$\frac{C}{R}(s) = \frac{NK(1 + s\tau)}{(\epsilon s^T + NK\tau)s + NK} \quad (7.3.1)$$

Defining

$$\alpha = KN, \quad \beta = K\tau N \quad (7.3.2)$$

The system characteristic equation becomes

$$F(s) = (\epsilon s^T + \beta)s + \alpha = 0 \quad (7.3.3)$$

which is identical to the characteristic equation of Section 5.5 (see (5.5.2)) with the exception of the definitions of  $\alpha$  and  $\beta$ . Thus the  $\alpha$ - $\beta$  curves of Section 5.5 can be used where the ordinate and the abscissa are properly relabeled.

Figure 7.3.2 shows the first quadrant of the  $\alpha$ - $\beta$  curve for  $\zeta = 0$  where  $K = 1$  and the two variable parameters are  $N$  and  $\tau$ . Only the first three traversals are shown where the remaining infinite number of traversals would lie above traversal ③ and intersect the point  $\beta = \tau N = 1$ . Also shown on Figure 7.3.2 are two  $\beta = \tau\alpha$  loci for  $\tau = 0.227$  and  $0.1314$ . Superimposed on each  $\beta = \tau\alpha$  locus are the ratios of the amplitudes to the dead zone,  $\frac{X}{D}$ , for corresponding values of the magnitude of  $N$ .

Other pertinent information relating to the nonlinearity characteristics are shown on Figure 7.3.2. The data to plot the describing function was obtained from standard curves in Reference 29, page 574.

By examining the position of the describing function loci with respect to stable and unstable regions in the  $\alpha$ - $\beta$  plane of Figure 7.3.2 the following properties of the feedback system are evident.

1. When  $\tau = 0.227$ : If the system is at rest, disturbances that result in a magnitude of  $\frac{X}{D} < 2.25$  to the input of the nonlinearity do not lead to instability. If the disturbance is of a magnitude such that  $\frac{X}{D} = 2.25$  sustained oscillations of amplitude  $\frac{X}{D} = 2.25$  and  $\omega = 2$  rad./sec. occur. A slightly larger disturbance, say  $2.25 \leq \frac{X}{D} \leq 8$ , results in a loop gain greater than unity and the oscillations increase until  $\frac{X}{D} = 8$  is reached, at which time equilibrium again exists and sustained oscillations of amplitude  $\frac{X}{D} = 8$  and frequency  $\omega = 2$  rad./sec. occur. A still larger disturbance of magnitude  $\frac{X}{D} > 8$  results in a stable system, with a decay of oscillation amplitude back to  $\frac{X}{D} = 8$ . Thus, the two intersections of the  $\beta = 0.227\alpha$  locus and the  $\zeta = 0$  locus, at amplitudes of  $\frac{X}{D} = 2.25$  and  $\frac{X}{D} = 8$ , represent unstable and stable equilibrium conditions, respectively.

2. When  $\tau = 0.1314$ : If the system is at rest, disturbances at the input to the nonlinearity that result in a magnitude of  $\frac{X}{D} < 10$  do not lead to instability. If the disturbance is of a magnitude such that  $\frac{X}{D} = 10$ , sustained oscillations of amplitude  $\frac{X}{D} = 10$  and  $\omega = 1.8$  rad./sec. occur. A slightly larger disturbance results in a loop gain greater

than unity and the oscillations increase towards  $\frac{X}{D} = \infty$  at a frequency  $\omega = 1.8$  rad./sec. Thus, the intersection of the  $\beta = 0.1314\alpha$  locus and the  $\zeta = 0$  locus, at an amplitude of  $\frac{X}{D} = 10$ , represents an unstable equilibrium condition.

In order to verify these results the inverse Nyquist plot and the negative describing function locus of the system are plotted in Figure 7.3.3. That is, consider the open loop transfer function of Figure 7.3.1a. The limiting values for system stability occur when  $s = j\omega$  and when

$$G(s)\epsilon^{-sT}N = -1 \quad (7.3.4)$$

or when

$$\frac{\epsilon^{sT}}{G(s)} = -N \quad (7.3.5)$$

Setting  $s = j\omega$  yields

$$\frac{\epsilon^{j\omega T}}{G(j\omega)} = -N \quad (7.3.6)$$

Figures 7.3.3 and 7.3.4 show Re vs. Im plots of equation (7.3.6) for  $\tau = 0.227$  and  $0.1314$  respectively. Note that these polar plots both continually encircle the origin due to the existence of the transport lag which contributes an infinite amount of phase lag as  $\omega \rightarrow \infty$ . By noting the intersections of the  $\frac{\epsilon^{j\omega T}}{G(j\omega)}$  plot and the  $-N$  plot it can be

seen that the interpretation of system stability given above is verified. For example, in Figure 7.3.3 the  $-N$  locus intersects the  $\frac{\epsilon^{j\omega T}}{G(j\omega)}$  locus at the frequency  $\omega = 2$  rad./sec. for values of  $\frac{X}{D}$  equal to 2.25 and 8 as predicted from the  $\alpha$ - $\beta$  plot and  $-N$  locus of Figure 7.3.2. Similarly, the critical point of Figure 7.3.4 corresponds to the intersection of the  $\beta = 0.1314\alpha$  locus and the  $\zeta = 0$  locus shown on Figure 7.3.2.

In order to further verify the results predicted above, the control system of Figure 7.3.1 was simulated on a digital computer. The system differential equation was solved by using finite differences and all results are accurate to one decimal place. Figure 7.3.5 shows the input waveform to the nonlinearity for  $\tau = 0.227$  and  $\frac{X}{D} = 1.5$ , which is less than the critical value of  $\frac{X}{D} = 2.25$ . From Figure 7.3.5 it is seen that the system is stable. Figure 7.3.6 shows the steady state input waveform to the nonlinearity for  $\frac{X}{D}$  equal to 3 and 10. The values  $\frac{X}{D} = 3$  and 10 both result in oscillations of amplitude  $\frac{X}{D} = 8.6$  and frequency  $\omega = 2$  rad./sec. The percentage difference between the predicted and actual amplitudes and frequencies for  $\tau = 0.227$  are noted on Figure 7.3.6 and, as can be seen are quite small.

When the system was simulated for  $\tau = 0.1314$  the result was a stable system when the input to the nonlinearity was  $\frac{X}{D} < 10$ . For values of  $\frac{X}{D} > 10$  oscillations were noted at a frequency of  $\omega = 1.84$  rad./sec. (a difference of 2.18% from the predicted value) that increased indefinitely in amplitude. It was further determined that the value of  $\frac{X}{D}$  at the unstable equilibrium point is between  $9.65 \leq \frac{X}{D} \leq 9.67$  since the

waveform decayed for  $\frac{X}{D} = 9.65$  and increased in amplitude towards infinity for  $\frac{X}{D} = 9.67$ . The difference is then approximately 3.4% from the predicted amplitude of oscillations.

Thus, the digital computer simulation further verifies the predicted results obtained from the  $\alpha$ - $\beta$  plane. The percentage differences in both cases ( $\tau = 0.227$  and  $0.1314$ ) can be attributed to the error inherent in the approximations associated with the concept of describing functions.

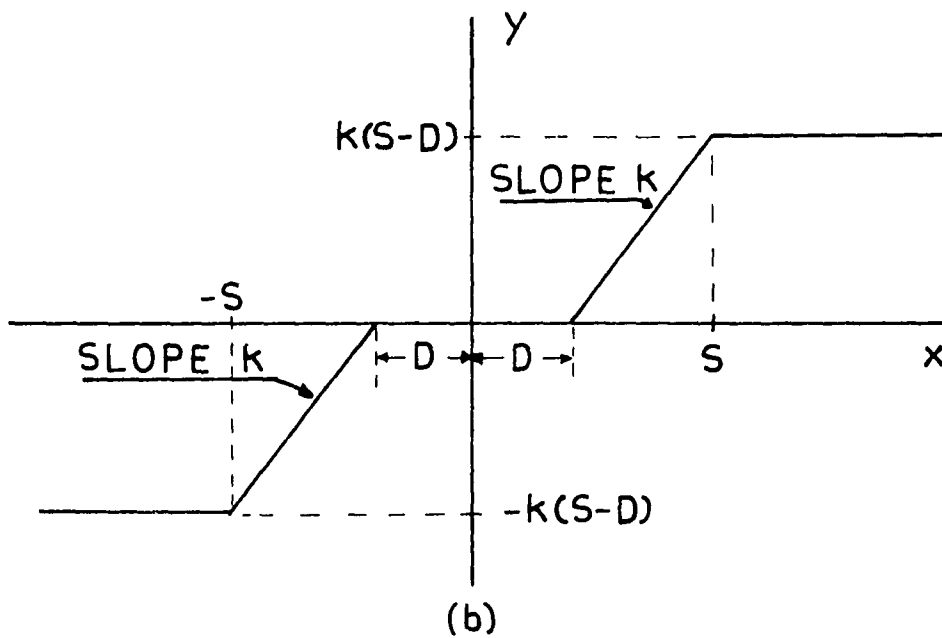
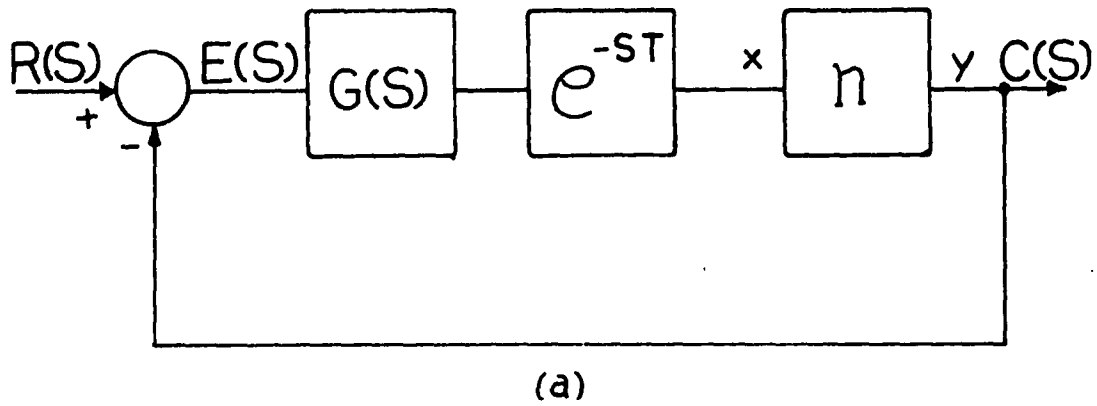


Fig. 7.3.1 A Nonlinear Feedback Control System With Transport Lag.

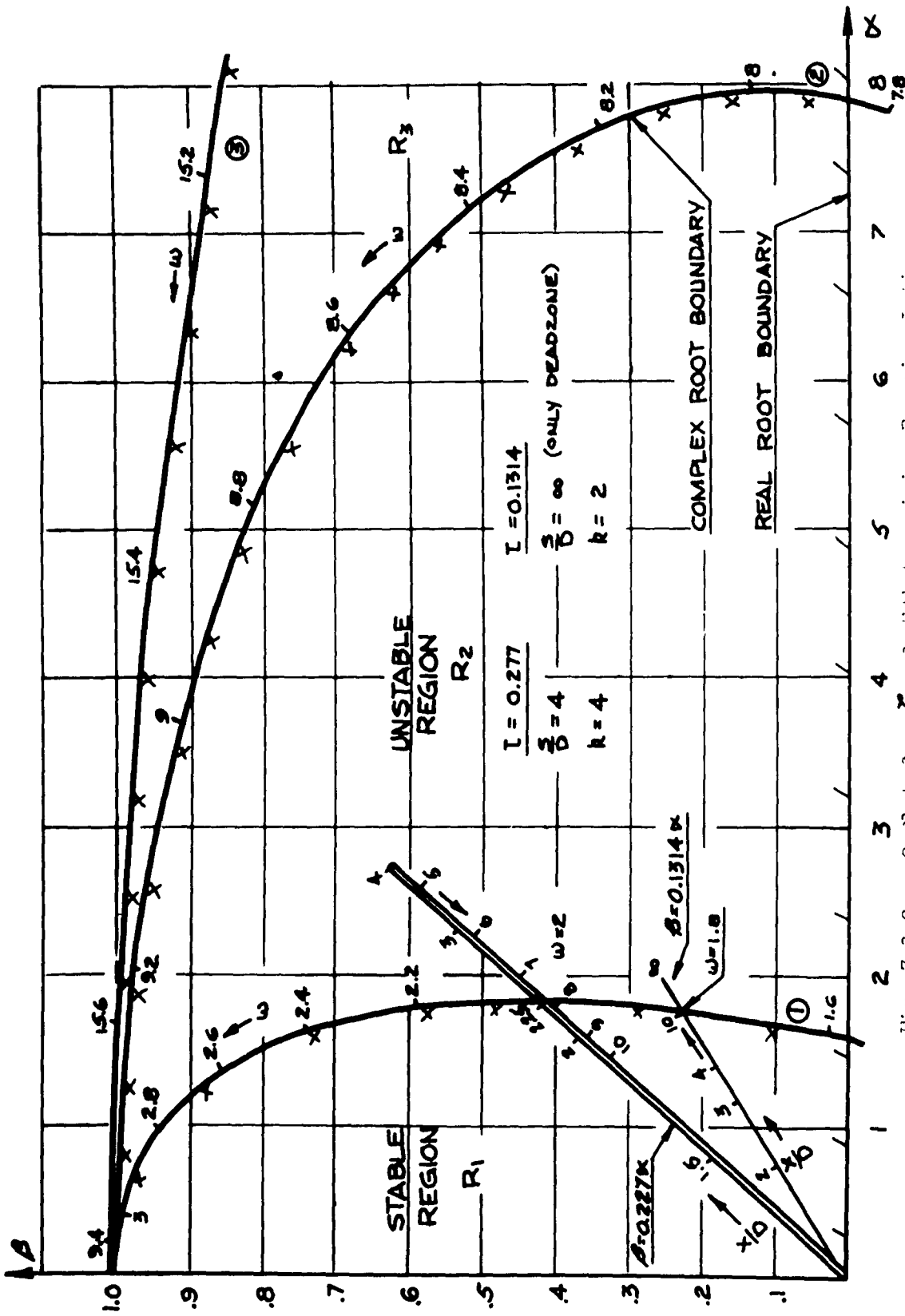


Fig. 7.3.2  $\alpha$ - $\beta$  Plot for  $\zeta = 0$  with Describing Function Loci.

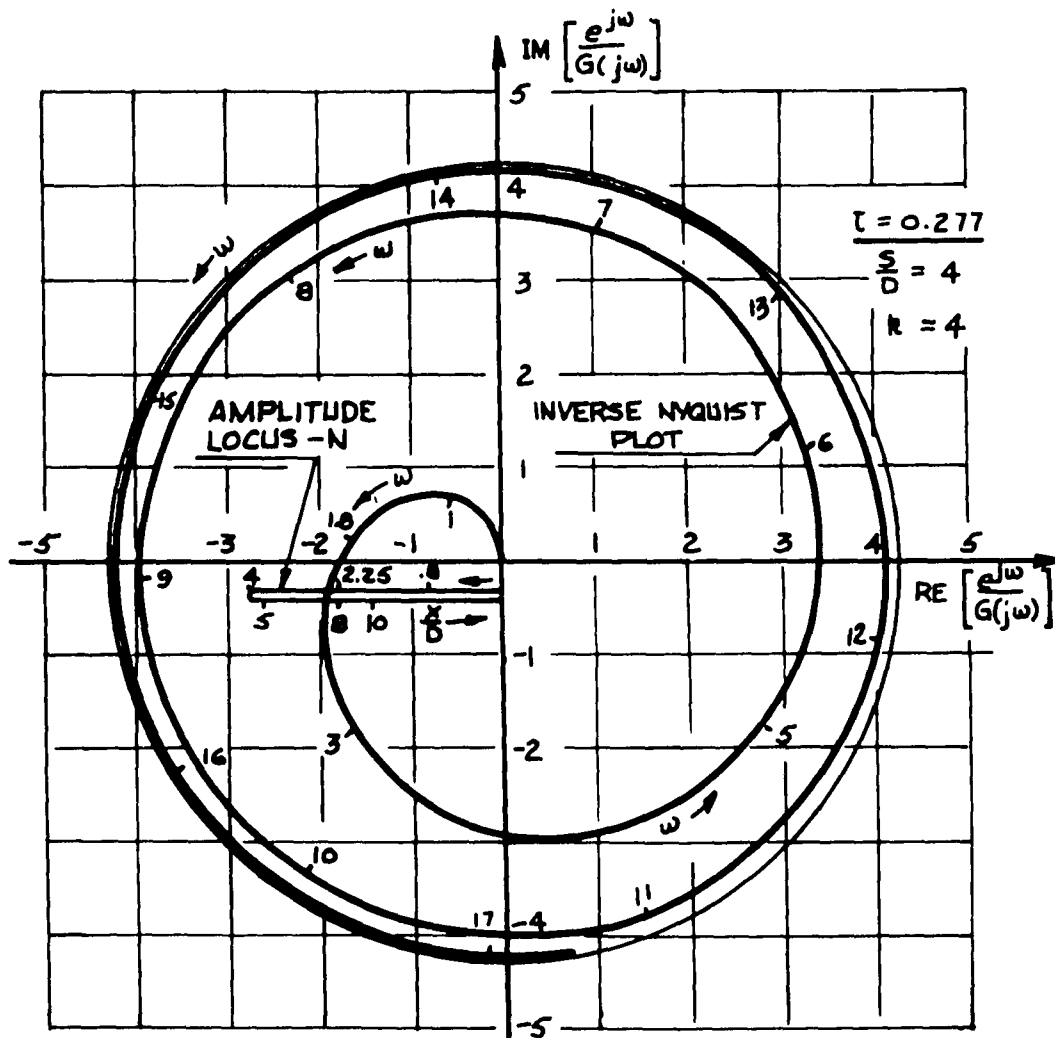


Fig. 7.3.3 Inverse Nyquist Plot and Describing Function Locus for  $\tau = 0.227$ .



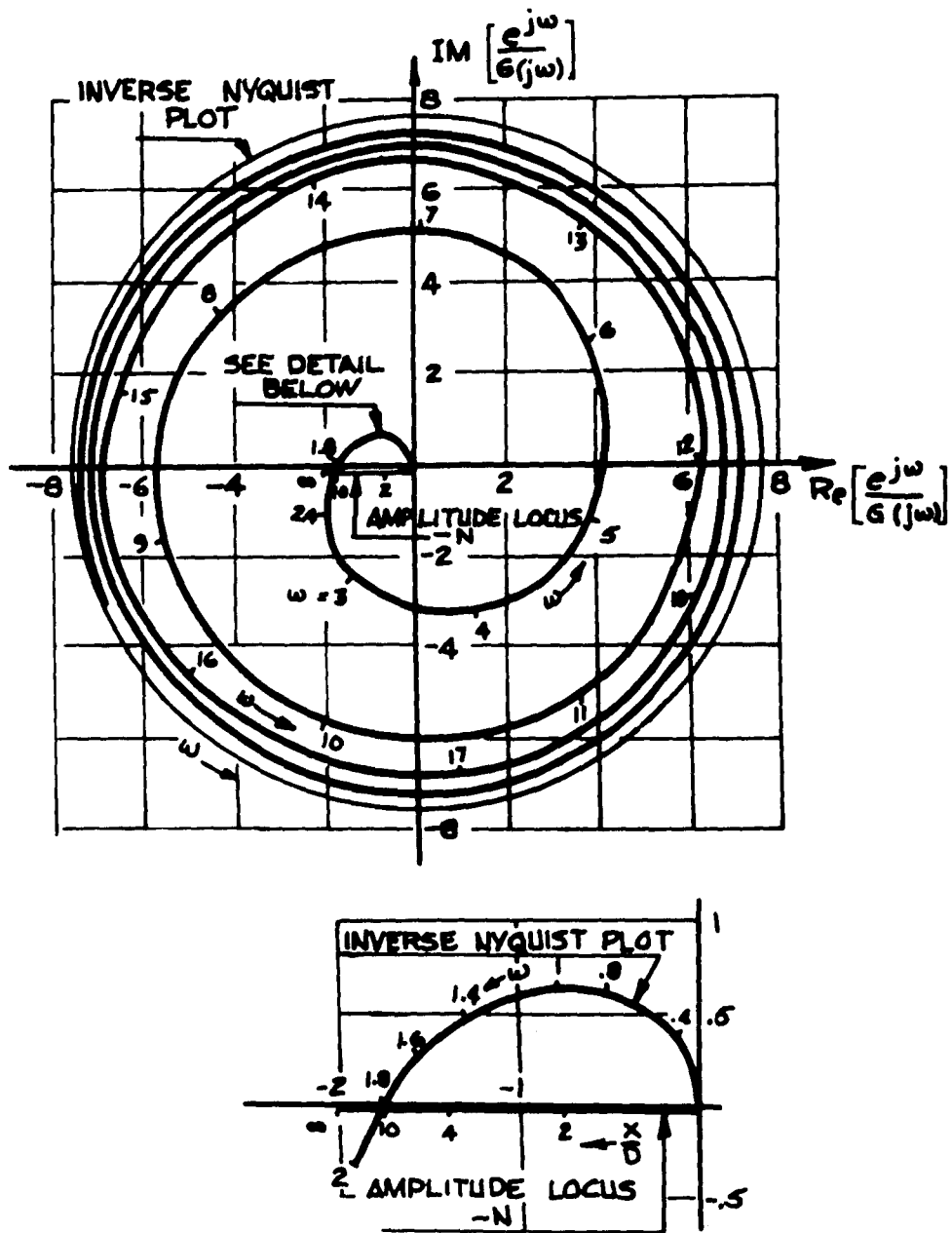


Fig. 7.3.4 Inverse Nyquist Plot and Describing Function Locus for  $\tau = 0.1314$ .

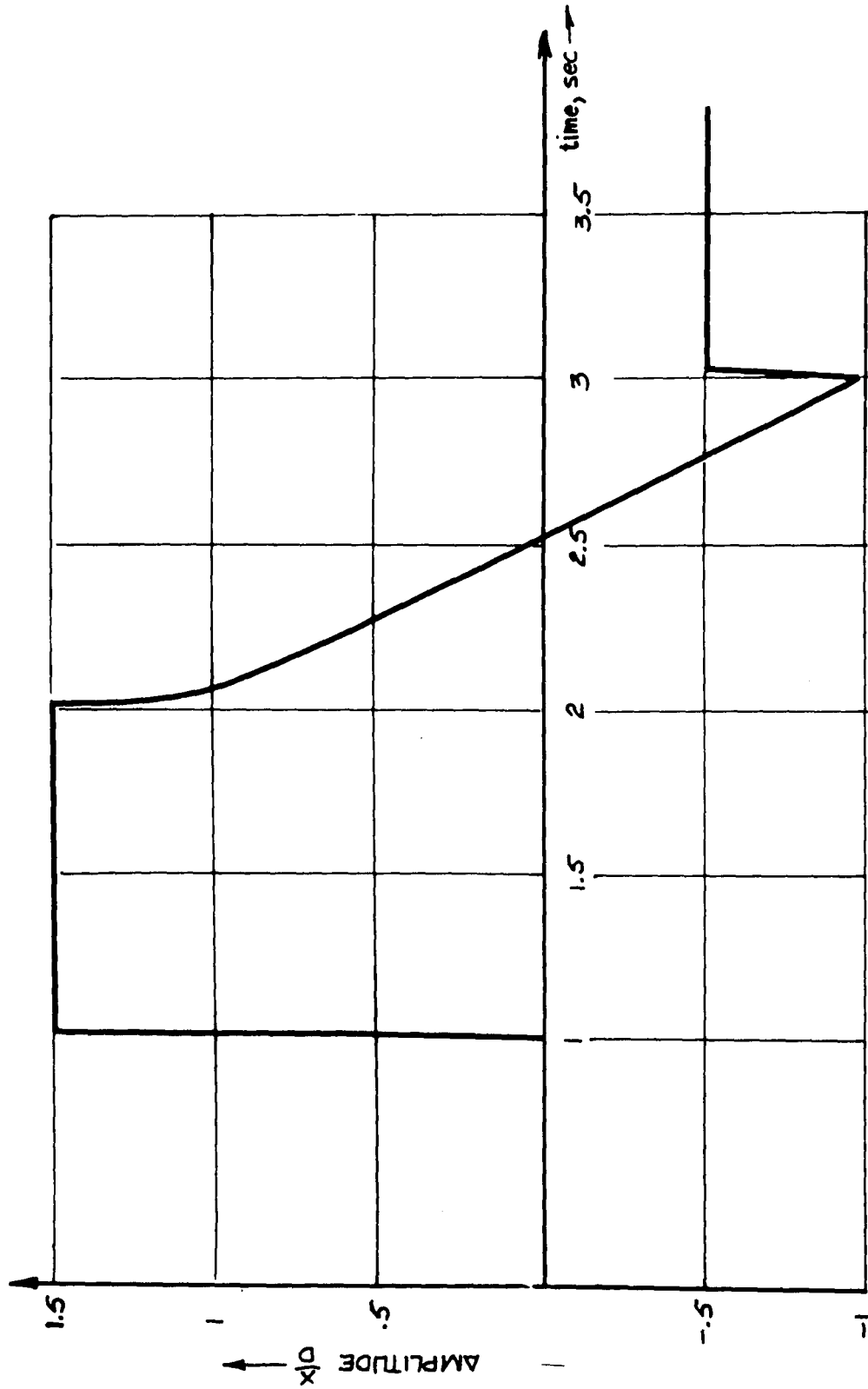
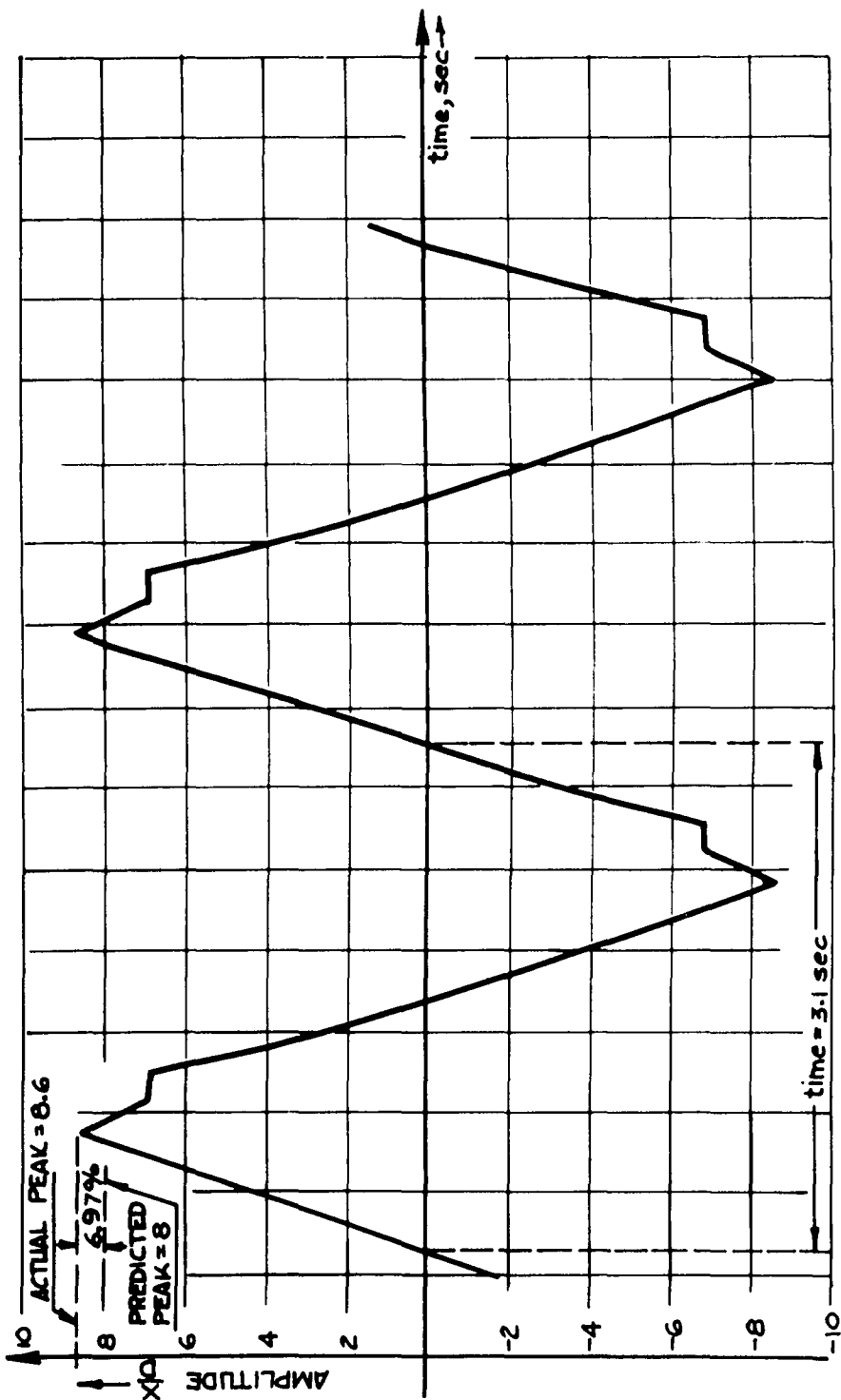


Fig. 7.3.5 Input waveform to the nonlinearity for  $\tau = 0.227$   
and disturbance  $\frac{X}{D} = 1.5$ .



ACTUAL  $\omega = 2.02$  rad./sec.  
 PREDICTED  $\omega = 2.0$  rad./sec.  
 DIFFERENCE = 0.99 %

Fig. 7.3.6 Steady State Input Waveform to the Nonlinearity for

$$\tau = 0.227 \text{ and Disturbance } \frac{X}{D} = 3 \text{ and } 10.$$

## CHAPTER 8

### CONCLUSIONS

A method is presented for the exact determination of absolute and relative stability of linear feedback control systems containing transport or distributed lag. All results are in terms of two variable system parameters, whereas contemporary techniques determine only absolute stability with respect to only one variable system parameter. The method utilizes an extension of parameter plane techniques as developed by Vishnegradski [30], Neimark [18], Mitrović [16], and Siljak [26].

The method is then applied to the design of controllers in linear systems containing transport lag. A design technique is proposed that allows for the systematic determination of two variable controller parameters in order to meet frequency or time domain design specifications. The design technique is formulated in terms of the familiar "dominant root" concept. The proposed design technique gives the system designer "at least" as much control over the system response as he obtains with conventional design procedures for systems without transport lag.

The investigation of absolute and relative stability, as well as the proposed method for controller design, is no more complicated for multiloop feedback control systems than for single loop systems. This

is because the characteristic equation of the closed-loop system transfer function is utilized rather than the conventional open-loop methods. Further, if a digital computer is used, high-order systems are dealt with as easily as low-order systems.

A method for constructing the root-locus of systems containing transport lag is then proposed so that this familiar engineering tool can be used in conjunction with the proposed analysis and design technique. The root-locus technique proposed here has the following advantages over the conventional method of Chu [2].

- 1) The locus can easily be constructed from the parameter plane curves for either one of two variable system parameters. Further, the value of the variable parameter is immediately available without computation.
- 2) The system can be multiloop and if a digital computer is utilized the order of the system does not complicate the root-locus construction.

Finally, the method is applied to nonlinear systems containing transport lag where describing function analysis is applicable. It is shown that the amplitude and frequency of limit cycles can be predicted where the describing function is real and is dependent upon the amplitude of the input signal to the nonlinearity.

## CHAPTER 9

### SUGGESTIONS FOR FUTURE INVESTIGATION

A further area of investigation is the application of the theory developed in this dissertation to the "identification" of high-order linear systems. A definite characteristic of high-order stable system responses is the relatively long time required to reach a peak value, followed by periodic variations. Such a response can be approximated by the response of a low-order system (say second-order) containing a transport lag. Figure 9.1 shows a typical response of a high-order system and the suggested approximation by the response of a second-order system with transport lag.

Another area of investigation that should prove fruitful is the further application of this theory to nonlinear systems with transport lag. The success of this investigation would probably depend upon the specific type of nonlinearity involved. The author has initiated further work in this area for the cases where the describing function can be

1. complex and dependent upon amplitude
2. real and dependent upon amplitude and frequency
3. a combination of two real amplitude-dependent describing functions.

The results have been encouraging and further work in this area is contemplated.

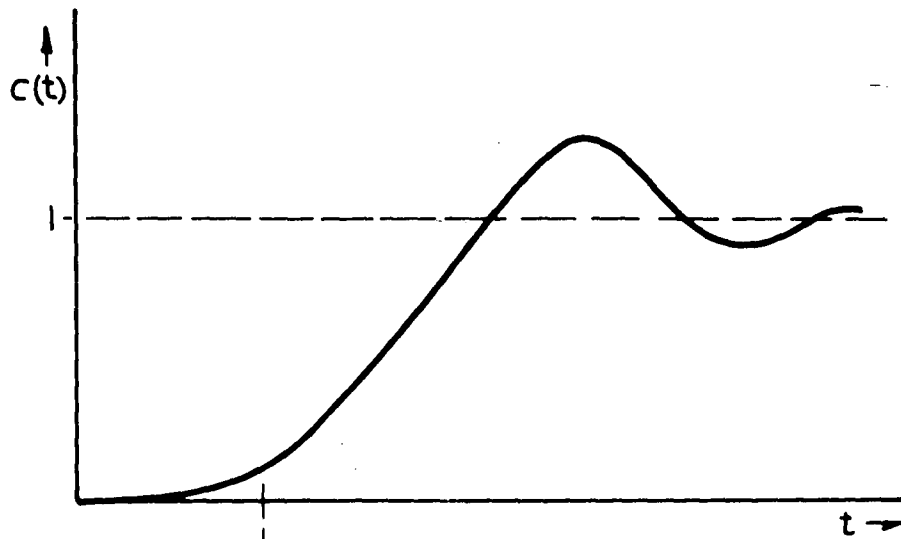
The concept of "root location sensitivity" with respect to parameter variations for systems with transport lag seems feasible. This question

can possibly be resolved by studying the parameter plane sensitivity relationships previously developed by Kokotović and Siljak [11].

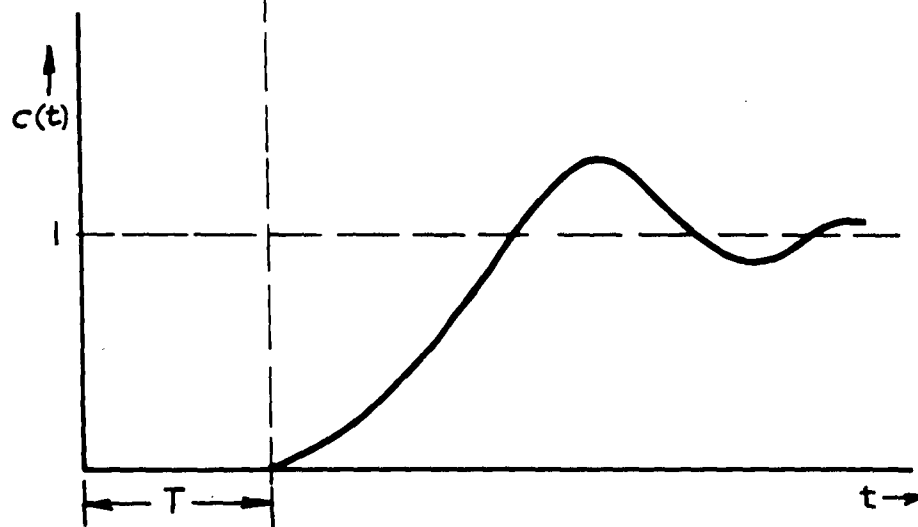
Finally, problems related to the "predictor method" of compensation of linear systems with transport lag can be investigated through parameter plane techniques. The predictor method [27] utilizes the feedback arrangement shown in Figure 9.2. The purpose is to make the input to the controller appear as if the system had no transport lag. If the controller lag,  $\epsilon_a^{-sT}$ , is identical to the actual lag,  $\bar{\epsilon}^{sT}$ , then the system transfer function is

$$\frac{C}{R}(s) = \frac{G_1(s)G_2(s)}{1 + G_1(s)G_2(s)}$$

which is independent of the transport lag. Since it is not possible to perfectly synthesize  $\epsilon_a^{-sT}$  in the controller, perfect cancellation of  $\bar{\epsilon}^{sT}$  in the plant is not possible. However,  $\epsilon_a^{-sT}$  can be approximated and the resulting system transfer function, although still in terms of  $\bar{\epsilon}^{sT}$ , is amenable to parameter plane methods of analysis and design. The author has done some preliminary work in this area and the results are encouraging.



(a) HIGH-ORDER SYSTEM RESPONSE



(b) SECOND-ORDER SYSTEM RESPONSE  
WITH TRANSPORT LAG

Fig. 7.1 Comparison of a High-Order System Response to a Second-Order Response With Transport Lag.



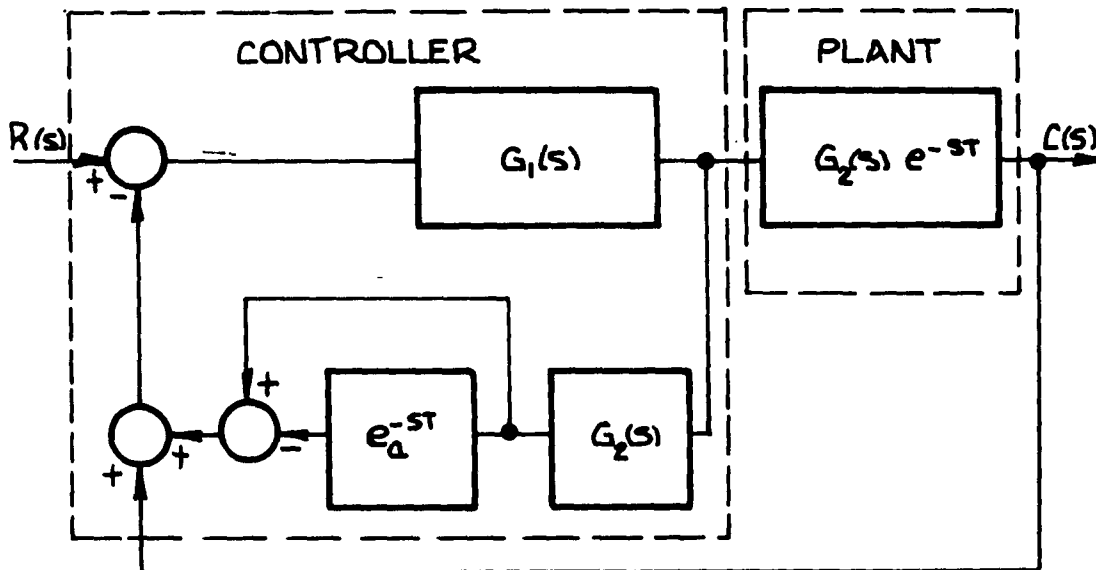


Fig. 9.2 Predictor Method of Control.

5

## APPENDICES

APPENDIX I

TABLES OF  $T_k(\tau)$  AND  $U_k(\tau)$

Table I.

$\tau$	$T_0$	$T_1$	$T_2$	$T_3$	$T_4$	$T_5$	$T_6$	$T_7$	$T_8$	$T_9$	$T_{10}$
0.00	0.00	-1.000	0.00000	0.00000	0.00000	-1.00000000	0.00000000	0.00000000	1.00000000	0.00000000	-1.0000000000
0.05	0.05	-0.985	0.01495	0.00005	0.347505	-0.04203495	-0.04203495	0.00000000	0.00000000	0.00000000	0.0000000000
0.10	0.10	-0.980	0.02980	0.02080	0.480160	-0.04511360	-0.04511360	0.00000000	0.00000000	0.00000000	0.0000000000
0.15	0.15	-0.985	0.04365	0.04005	0.6189355	-0.04819225	-0.04819225	0.00000000	0.00000000	0.00000000	0.0000000000
0.20	0.20	-0.920	0.05680	0.05280	0.815120	-0.0517920	-0.0517920	0.00000000	0.00000000	0.00000000	0.0000000000
0.25	0.25	-0.875	0.06875	0.06125	0.931125	-0.0549875	-0.0549875	0.00000000	0.00000000	0.00000000	0.0000000000
0.30	0.30	-0.820	0.07920	0.07480	0.998840	-0.0582940	-0.0582940	0.00000000	0.00000000	0.00000000	0.0000000000
0.35	0.35	-0.755	0.0785	0.07535	0.14005	0.543245	-0.0596785	-0.0596785	0.00000000	0.00000000	0.0000000000
0.40	0.40	-0.680	0.0440	0.07520	0.883840	0.7822720	-0.05802240	-0.05802240	0.00000000	0.00000000	0.0000000000
0.45	0.45	-0.595	0.0855	0.29185	0.722745	0.9424205	0.12513345	-0.05000000	0.00000000	0.00000000	0.0000000000
0.50	0.50	-0.500	-1.00000	0.50000	0.500000	1.00000000	1.00000000	0.00000000	0.00000000	0.00000000	0.0000000000
0.55	0.55	-0.395	0.0845	0.08795	0.9384805	0.80457355	0.80457355	0.00000000	0.00000000	0.00000000	0.0000000000
0.60	0.60	-0.280	0.04360	0.04320	0.7521920	0.97817040	0.97817040	0.00000000	0.00000000	0.00000000	0.0000000000
0.65	0.65	-0.155	0.04315	-0.03195	-0.3896035	0.4501045	0.97117085	0.00000000	0.00000000	0.00000000	0.0000000000
0.70	0.70	0.020	0.07280	0.09920	0.0596660	0.5986660	0.96801280	0.00000000	0.00000000	0.00000000	0.0000000000
0.75	0.75	0.125	0.05925	0.06875	0.80625	0.33984375	0.875953125	0.00000000	0.00000000	0.00000000	0.0000000000
0.80	0.80	0.280	0.03520	0.04320	0.987120	0.7521920	0.20638720	0.00000000	0.00000000	0.00000000	0.0000000000
0.85	0.85	0.445	0.00435	0.00395	0.93215	0.9825155	-0.7379135	0.00000000	0.00000000	0.00000000	0.0000000000
0.90	0.90	0.620	0.2160	0.23120	0.032160	-0.9066880	-0.99987840	0.00000000	0.00000000	0.00000000	0.0000000000
0.95	0.95	0.805	0.3795	0.29605	-0.017005	-0.3283595	-0.6087805	0.00000000	0.00000000	0.00000000	0.0000000000
1.00	1.00	1.000	1.00000	1.00000	1.000000	1.00000000	1.00000000	0.00000000	0.00000000	0.00000000	0.0000000000

Table II.

$\tau$	$U_0$	$U_1$	$U_2$	$U_3$	$U_4$	$U_5$	$U_6$	$U_7$	$U_8$	$U_9$	$U_{10}$
0.00	0.00	0.00	0.000	0.000	0.00000	0.000000	0.000000	0.000000	0.000000	0.000000	0.00000000
0.05	0.01	-0.89	0.000	0.199	0.29501	0.000000	-1.000000	0.000000	0.000000	0.000000	0.00000000
0.10	0.2	-0.86	-0.392	0.392	0.56832	0.29501	-0.010489	0.000000	0.000000	0.000000	0.00000000
0.15	0.3	-0.84	-0.573	0.573	0.79443	0.56832	-0.078336	0.000000	0.000000	0.000000	0.00000000
0.20	0.4	-0.84	-0.736	0.736	0.95424	0.79443	-0.163904	0.000000	0.000000	0.000000	0.00000000
0.25	0.5	-0.75	-0.875	0.875	0.3125	1.03125	0.203125	-0.1980016	0.000000	0.000000	0.00000000
0.30	0.6	-0.64	-0.964	0.964	0.0466	1.01376	0.558676	-0.9296875	0.000000	0.000000	0.00000000
0.35	0.7	-0.51	-0.957	0.957	0.2299	0.89107	0.857149	-0.2900657	0.000000	0.000000	0.00000000
0.40	0.8	-0.36	-0.988	0.988	0.5104	0.67968	1.034144	-0.1636532	0.000000	0.000000	0.00000000
0.45	0.9	-0.19	-0.971	0.971	0.7739	0.37449	1.10941	0.6253569	0.000000	0.000000	0.00000000
0.50	1.0	0.00	-1.000	1.000	0.00000	0.000000	1.000000	0.000000	0.000000	0.000000	0.00000000
0.55	1.1	0.21	-0.869	1.059	-0.41349	0.711061	1.1976371	0.60416181	0.000000	0.000000	0.00000000
0.60	1.2	0.44	-0.672	1.2464	-0.82368	0.257984	1.332908	1.10192895	0.000000	0.000000	0.00000000
0.65	1.3	0.69	-0.403	1.2139	-1.17507	0.313691	0.7072717	1.3114421	0.000000	0.000000	0.00000000
0.70	1.4	0.96	-0.0596	1.0384	-1.39776	-0.018464	0.119104	1.07513859	0.000000	0.000000	0.00000000
0.75	1.5	1.25	0.375	0.6875	-1.40825	-1.421875	0.7265925	0.33203125	0.000000	0.000000	0.00000000
0.80	1.6	1.56	0.896	-0.1264	-1.09824	-1.630784	-0.5110144	-0.78683004	0.000000	0.000000	0.00000000
0.85	1.7	1.89	1.513	0.6821	-0.35343	-1.282931	-1.8255227	-1.82360859	0.000000	0.000000	0.00000000
0.90	1.8	2.24	2.232	3.2021	0.90768	-0.035776	-1.8255227	-1.82196224	0.000000	0.000000	0.00000000
0.95	1.9	2.61	3.059	3.2021	3.02469	2.545381	1.9112339	-2.247455232	0.000000	0.000000	0.00000000
1.00	2.0	3.00	4.000	5.0000	6.00000	7.000000	8.0000000	9.00000000	0.000000	0.000000	0.00000000

NOTE: These tables were compiled from pp. 451-452 of Reference 26.

## APPENDIX II

### $\alpha$ - $\beta$ Curves for $\zeta = \pm 1$

As mentioned in Section 4.1, care must be exercised when computing values of  $\alpha$  and  $\beta$  for  $\zeta = \pm 1$ . If  $\zeta = \pm 1$  is substituted into (4.1.14) the resulting equations are indeterminate. Specifically, substitution of  $\zeta = \pm 1$  into (4.1.11) gives

$$B_1(\pm 1, \omega_n) = \sum_{k=0}^n (-1)^k \omega_n^k (b_k + \epsilon^{\mp} \omega_n^T c_k) T_k(\pm 1)$$

$$C_1(\pm 1, \omega_n) = \sum_{k=0}^n (-1)^k \omega_n^k (d_k + \epsilon^{\mp} \omega_n^T e_k) T_k(\pm 1)$$

$$D_1(\pm 1, \omega_n) = \sum_{k=0}^n (-1)^k \omega_n^k (f_k + \epsilon^{\mp} \omega_n^T g_k) T_k(\pm 1)$$

$$B_2(\pm 1, \omega_n) = C_2(\pm 1, \omega_n) = D_2(\pm 1, \omega_n) = 0$$

Thus, from (4.1.14), the  $\alpha$ - $\beta$  curves are indeterminate due to a singularity for  $\zeta = \pm 1$ . To remove this singularity define

$$\begin{aligned} \bar{B}_2 &= B_2(\pm 1, \omega_n) / \sqrt{1 - \zeta^2} \\ \bar{C}_2 &= C_2(\pm 1, \omega_n) / \sqrt{1 - \zeta^2} \\ \bar{D}_2 &= D_2(\pm 1, \omega_n) / \sqrt{1 - \zeta^2} \end{aligned} \tag{II.1}$$

Further define

$$\bar{\alpha} = \frac{C_1 \bar{D}_2 - D_1 \bar{C}_2}{B_1 \bar{C}_2 - C_1 \bar{B}_2}, \quad \bar{\beta} = \frac{D_1 \bar{B}_2 - \bar{D}_2 B_1}{B_1 \bar{C}_2 - C_1 \bar{B}_2} \tag{II.2}$$

Substituting (II.1) into (II.2) gives

$$\bar{\alpha} = \frac{C_1 \bar{D}_2 - D_1 \bar{C}_2}{B_1 \bar{C}_2 - C_1 \bar{B}_2} = \frac{C_1 D_2 - D_1 C_2}{B_1 C_2 - C_1 B_2} = \alpha$$

$$\bar{\beta} = \frac{D_1 \bar{B}_2 - \bar{D}_2 B_1}{B_1 \bar{C}_2 - C_1 \bar{B}_2} = \frac{D_1 B_2 - D_2 B_1}{B_1 C_2 - C_1 B_2} = \beta$$

so that  $\bar{\alpha} = \alpha$  and  $\bar{\beta} = \beta$ , and it remains to show that the singularity can be removed by using  $\bar{B}_2$ ,  $\bar{C}_2$ ,  $\bar{D}_2$ . Note that

$$\bar{B}_2(\pm 1, \omega_n), \quad \bar{C}_2(\pm 1, \omega_n), \quad \bar{D}_2(\pm 1, \omega_n)$$

reduce to

$$\begin{aligned} \bar{B}_2(\pm 1, \omega_n) &= \sum_{k=0}^n (-1)^{k+1} \omega_n^k U_k(\pm 1) (b_k + \epsilon^{\mp \omega_n T} c_k) + \\ &\quad \epsilon^{\mp \omega_n T} \frac{\sin \omega_n \sqrt{1 - \zeta^2} T}{\sqrt{1 - \zeta^2}} \sum_{k=0}^n (-1)^k c_k \omega_n^k T_k(\pm 1) \\ \bar{C}_2(\pm 1, \omega_n) &= \sum_{k=0}^n (-1)^{k+1} \omega_n^k U_k(\pm 1) (d_k + \epsilon^{\mp \omega_n T} e_k) + \\ &\quad \epsilon^{\mp \omega_n T} \frac{\sin \omega_n \sqrt{1 - \zeta^2} T}{\sqrt{1 - \zeta^2}} \sum_{k=0}^n (-1)^k e_k \omega_n^k T_k(\pm 1) \end{aligned} \quad (\text{II.3})$$

$$\begin{aligned} \bar{D}_2(\pm 1, \omega_n) &= \sum_{k=0}^n (-1)^{k+1} \omega_n^k U_k(\pm 1) (f_k + \epsilon^{\mp \omega_n T} g_k) + \\ &\quad \epsilon^{\mp \omega_n T} \frac{\sin \omega_n \sqrt{1 - \zeta^2} T}{\sqrt{1 - \zeta^2}} \sum_{k=0}^n (-1)^k g_k \omega_n^k T_k(\pm 1) \end{aligned}$$

Attention is now focused on the singular term of (II.3) when  $\zeta = \pm 1$ .

Namely, consider

$$\lim_{\zeta \rightarrow \pm 1} f(\zeta) = \lim_{\zeta \rightarrow \pm 1} \frac{\sin \omega_n \sqrt{1 - \zeta^2} T}{\sqrt{1 - \zeta^2}} \quad (\text{II.4})$$

and make the substitution  $x = \sqrt{1 - \zeta^2}$  so that

$$\lim_{\zeta \rightarrow \pm 1} f(\zeta) = \lim_{x \rightarrow 0} \frac{\sin \omega_n T x}{x} = \omega_n T$$

which is easily verified by taking a Taylor series expansion of (II.4).

Thus equations (II.3) become

$$\begin{aligned} \bar{B}_2(\pm 1, \omega_n) &= \sum_{k=0}^n (-1)^{k+1} \omega_n^k U_k(\pm 1) (b_k + \bar{\epsilon} \omega_n^T c_k) + \\ &\quad \omega_n T \bar{\epsilon} \bar{\omega}_n^T \sum_{k=0}^n (-1)^k c_k \omega_n^k T_k(\pm 1) \\ \bar{C}_2(\pm 1, \omega_n) &= \sum_{k=0}^n (-1)^{k+1} \omega_n^k U_k(\pm 1) (d_k + \bar{\epsilon} \omega_n^T e_k) + \\ &\quad \omega_n T \bar{\epsilon} \bar{\omega}_n^T \sum_{k=0}^n (-1)^k e_k \omega_n^k T_k(\pm 1) \\ \bar{D}_2(\pm 1, \omega_n) &= \sum_{k=0}^n (-1)^{k+1} \omega_n^k U_k(\pm 1) (f_k + \bar{\epsilon} \omega_n^T g_k) + \\ &\quad \omega_n T \bar{\epsilon} \bar{\omega}_n^T \sum_{k=0}^n (-1)^k g_k \omega_n^k T_k(\pm 1) \end{aligned} \quad (\text{II.5})$$

and the singularity has been removed. Thus, the  $\alpha$ - $\beta$  equations for

$\zeta = \pm 1$  are determined from (4.1.14) where  $B_2$ ,  $C_2$  and  $D_2$  are replaced by  $\bar{B}_2(\pm 1, \omega_n)$ ,  $\bar{C}_2(\pm 1, \omega_n)$  and  $\bar{D}_2(\pm 1, \omega_n)$  of (II.3).

## APPENDIX III

### CONSTANT SETTLING TIME LINES

To show that the algebraic manipulations resulting in (4.5.1) and (4.5.2) can always be effected, a formal derivation is offered that yields explicit equations for  $\alpha(\sigma, \omega_n^2)$  and  $\beta(\sigma, \omega_n^2)$ .

Since the contour of Figure 4.1.2c is mapped for a given value of  $\sigma = -\zeta\omega_n$  as  $\omega_n$  varies from zero to infinity,  $\zeta$  is a variable for this contour, but the product  $\sigma = -\zeta\omega_n$  is not. Thus rewrite from (4.1.12)

$$\phi = \zeta\omega_n T = \sigma T$$

$$\theta = \omega_n \sqrt{1 - \zeta^2} T = \sqrt{\omega_n^2 - \sigma^2} T$$

$$\sqrt{1 - \zeta^2} = \frac{1}{\omega_n} \sqrt{\omega_n^2 - \sigma^2}$$

Since the Chebyshev functions are functions of  $\zeta$  they are rewritten as

$$P_k(\sigma, \omega_n^2) = (-1)^k \omega_n^k T_k(\zeta)$$

$$Q_k(\sigma, \omega_n^2) = (-1)^{k+1} \omega_n^{k-1} U_k(\zeta)$$

Where the  $P_k$  and  $Q_k$  may be obtained from the following recursion formulae [26]

$$P_{k+1}(\sigma, \omega_n^2) + 2\sigma P_k(\sigma, \omega_n^2) + \omega_n^2 P_{k-1}(\sigma, \omega_n^2) = 0$$

$$Q_{k+1}(\sigma, \omega_n^2) + 2\sigma Q_k(\sigma, \omega_n^2) + \omega_n^2 Q_{k-1}(\sigma, \omega_n^2) = 0$$



Where

$$P_0 = 1, \quad P_1 = -\sigma, \quad Q_0 = 0, \quad Q_1 = 1$$

Equations (4.1.11) can now be expressed as, for  $\omega_n^2 > \sigma^2$

$$\begin{aligned} B_1(\sigma, \omega_n^2) &= \sum_{k=0}^n [P_k b_k + \epsilon^{-\phi} (P_k c_k \cos \theta - \sqrt{\omega_n^2 - \sigma^2} Q_k c_k \sin \theta)] \\ C_1(\sigma, \omega_n^2) &= \sum_{k=0}^n [P_k d_k + \epsilon^{-\phi} (P_k e_k \cos \theta - \sqrt{\omega_n^2 - \sigma^2} Q_k e_k \sin \theta)] \\ D_1(\sigma, \omega_n^2) &= \sum_{k=0}^n [P_k f_k + \epsilon^{-\phi} (P_k g_k \cos \theta - \sqrt{\omega_n^2 - \sigma^2} Q_k g_k \sin \theta)] \end{aligned} \quad (\text{III.1})$$

$$\begin{aligned} B_2(\sigma, \omega_n^2) &= \sum_{k=0}^n [Q_k b_k \sqrt{\omega_n^2 - \sigma^2} + \epsilon^{-\phi} (Q_k c_k \sqrt{\omega_n^2 - \sigma^2} \cos \theta + P_k c_k \sin \theta)] \\ C_2(\sigma, \omega_n^2) &= \sum_{k=0}^n [Q_k d_k \sqrt{\omega_n^2 - \sigma^2} + \epsilon^{-\phi} (Q_k e_k \sqrt{\omega_n^2 - \sigma^2} \cos \theta + P_k e_k \sin \theta)] \\ D_2(\sigma, \omega_n^2) &= \sum_{k=0}^n [Q_k f_k \sqrt{\omega_n^2 - \sigma^2} + \epsilon^{-\phi} (Q_k g_k \sqrt{\omega_n^2 - \sigma^2} \cos \theta + P_k g_k \sin \theta)] \end{aligned}$$

Equations (III.1) are valid for  $\omega_n^2 > \sigma^2$ ; however, the mapping of constant settling time contours is for  $0 \leq \omega_n \leq \infty$  so that there are values of  $\omega_n$  and  $\sigma$  where  $\omega_n^2 < \sigma^2$ . Thus

$$\sqrt{\omega_n^2 - \sigma^2} = j\sqrt{\sigma^2 - \omega_n^2}$$

In this instance (III.1) becomes, upon using the identities

$$\cos j\sqrt{\sigma^2 - \omega_n^2} = \cosh \sqrt{\sigma^2 - \omega_n^2}$$

$$\sin j\sqrt{\sigma^2 - \omega_n^2} = j \sinh\sqrt{\sigma^2 - \omega_n^2}$$

for  $\omega_n^2 < \sigma^2$

$$B_1(\sigma, \omega_n^2) = \sum_{k=0}^n \left[ P_k b_k + \varepsilon^{-\phi} (P_k c_k \cosh\sqrt{\sigma^2 - \omega_n^2} T + \sqrt{\sigma^2 - \omega_n^2} Q_k c_k \sinh\sqrt{\sigma^2 - \omega_n^2} T) \right]$$

$$C_1(\sigma, \omega_n^2) = \sum_{k=0}^n \left[ P_k d_k + \varepsilon^{-\phi} (P_k e_k \cosh\sqrt{\sigma^2 - \omega_n^2} T + \sqrt{\sigma^2 - \omega_n^2} Q_k e_k \sinh\sqrt{\sigma^2 - \omega_n^2} T) \right]$$

$$D_1(\sigma, \omega_n^2) = \sum_{k=0}^n \left[ P_k f_k + \varepsilon^{-\phi} (P_k g_k \cosh\sqrt{\sigma^2 - \omega_n^2} T + \sqrt{\sigma^2 - \omega_n^2} Q_k g_k \sinh\sqrt{\sigma^2 - \omega_n^2} T) \right]$$

(III.2)

$$\bar{B}_2(\sigma, \omega_n^2) = \sum_{k=0}^n \left[ Q_k b_k + \varepsilon^{-\phi} (Q_k c_k \cosh\sqrt{\sigma^2 - \omega_n^2} T + P_k c_k \frac{\sinh\sqrt{\sigma^2 - \omega_n^2} T}{\sqrt{\sigma^2 - \omega_n^2}}) \right]$$

$$\bar{C}_2(\sigma, \omega_n^2) = \sum_{k=0}^n \left[ Q_k d_k + \varepsilon^{-\phi} (Q_k e_k \cosh\sqrt{\sigma^2 - \omega_n^2} T + P_k e_k \frac{\sinh\sqrt{\sigma^2 - \omega_n^2} T}{\sqrt{\sigma^2 - \omega_n^2}}) \right]$$

$$\bar{D}_2(\sigma, \omega_n^2) = \sum_{k=0}^n \left[ Q_k f_k + \epsilon^{-\phi} (Q_k g_k \cosh \sqrt{\sigma^2 - \omega_n^2} T + P_k g_k \frac{\sinh \sqrt{\sigma^2 - \omega_n^2} T}{\sqrt{\sigma^2 - \omega_n^2}}) \right]$$

where

$$\bar{B}_2(\sigma, \omega_n^2) = \frac{B_2(\sigma, \omega_n^2)}{j\sqrt{\sigma^2 - \omega_n^2}}, \text{ etc.}$$

Recall from Appendix II that introducing  $\bar{B}_2$ ,  $\bar{C}_2$  and  $\bar{D}_2$  into (4.1.14) does not alter these equations. Further, the singularities that appear in (III.2) when  $\sigma^2 = \omega_n^2$  are easily removed as shown in Appendix II.

## APPENDIX IV

### REAL ROOT DETERMINATION

It will now be shown that the number of real roots equals the number of straight lines drawn through a working point  $M(\alpha_1, \beta_1)$  that are tangent to the  $\zeta = +1$   $\alpha$ - $\beta$  curve; and that the values of these real roots equals the negative of the frequencies,  $\omega_{n_1}, \omega_{n_2}, \omega_{n_3}, \dots$ , at the tangent points on the  $\zeta = +1$  curve. The argument is the following: any value of  $\sigma$  that satisfies (4.6.2) for a given value of  $\alpha = \alpha_1$  and  $\beta = \beta_1$  is a real root. Then if the slope of the  $\zeta = +1$  curve is the same as the slope of (4.6.2), the value of the slope of the  $\zeta = +1$  curve where it is tangent to (4.6.2) is also a real root. Consider (4.6.2), which is the equation for the mapping of the real axis, and determine its slope for a point on the negative real axis, i.e., substitute  $s = -\sigma$  into (4.6.2). Then,

$$\alpha \sum_{k=0}^n (-1)^k \sigma^k (b_k + c_k \epsilon^{-\sigma T}) + \beta \sum_{k=0}^n (-1)^k \sigma^k (d_k + e_k \epsilon^{-\sigma T}) + \sum_{k=0}^n (-1)^k \sigma^k (f_k + g_k \epsilon^{-\sigma T}) = 0$$

The slope for a given working point  $M(\alpha_1, \beta_1)$  is

$$\frac{d\beta_1}{d\alpha_1} = - \frac{\sum_{k=0}^n (-1)^k \sigma^k (b_k + c_k \epsilon^{-\sigma T})}{\sum_{k=0}^n (-1)^k \sigma^k (d_k + e_k \epsilon^{-\sigma T})} \quad (\text{IV.1})$$

Now consider (4.1.14) which are the parametric equations for  $\alpha$  and  $\beta$  and determine

$$\left. \frac{d\beta}{d\alpha} \right]_{\zeta} = +1$$

Note that when  $\zeta = +1$  (which corresponds to the negative real axis)

$$s = [-\zeta\omega_n + j\omega_n\sqrt{1 - \zeta^2}]_{\zeta = +1} = -\omega_n = \sigma$$

and the real root equals the negative of the frequency on the  $\zeta = +1$  curve. Then from (4.1.14) and (II.1)

$$\begin{aligned} \frac{d\beta}{d\sigma} = & [(B_1\bar{C}_2 - C_1\bar{B}_2)(D_1\bar{B}'_2 + \bar{B}_2D'_1 - \bar{D}_2B'_1 - B_1\bar{D}'_2) - \\ & (D_1\bar{B}_2 - \bar{D}_2B_1)(B_1\bar{C}'_2 + \bar{C}_2B'_1 - C_1\bar{B}'_2 - \bar{B}_2C'_1)] / \Delta^2 \end{aligned}$$

and

$$\begin{aligned} \frac{d\alpha}{d\sigma} = & [(B_1\bar{C}_2 - C_1\bar{B}_2)(C_1\bar{D}'_2 + \bar{D}_2C'_1 - D_1\bar{C}'_2 - \bar{C}_2D'_1) - \\ & (C_1\bar{D}_2 - D_1\bar{C}_2)(B_1\bar{C}'_2 + \bar{C}_2B'_1 - C_1\bar{B}'_2 - \bar{B}_2C'_1)] / \Delta^2 \end{aligned}$$

where  $B'_1, B'_2, \dots$ , etc. denotes differentiation with respect to  $\sigma$ . It can be shown after some manipulation that

$$B'_1 = -\sigma\bar{B}_2, \quad C'_1 = -\sigma\bar{C}_2, \quad D'_1 = -\sigma\bar{D}_2$$

so that  $d\beta/d\alpha$  reduces to

$$\frac{d\beta}{d\alpha} = \left( \frac{d\beta}{d\sigma} \right) \left( \frac{d\sigma}{d\alpha} \right) = \frac{B_1 \left[ \bar{B}'_2(\bar{C}_2D_1 - \bar{D}_2C_1) + \bar{C}'_2(\bar{D}_2B_1 - D_1\bar{B}_2) + \bar{D}'_2(C_1\bar{B}_2 - B_1\bar{C}_2) \right]}{C_1 \left[ \bar{B}'_2(\bar{D}_2C_1 - D_1\bar{C}_2) + \bar{C}'_2(\bar{B}_2D_1 - \bar{D}_2B_1) + \bar{D}'_2(B_1\bar{C}_2 - C_1\bar{B}_2) \right]}$$

or

$$\frac{d\beta}{d\alpha} = -\frac{B_1}{C_1} = -\frac{\sum_{k=0}^n (-1)^k \sigma^k (b_k + c_k \epsilon^{-\sigma T})}{\sum_{k=0}^n (-1)^k \sigma^k (d_k + e_k \epsilon^{-\sigma T})}$$

Thus, the slope at any point on the  $\alpha$ - $\beta$  curve for  $\zeta = +1$  is the slope for the straight line obtained when mapping a point on the negative real axis (see equation IV.1). In order to prove the proposition for  $\zeta = -1$ , the argument is the same except  $\zeta = -1$  is substituted in the above derivation. If the working point  $M(\alpha_1, \beta_1)$  is chosen on the  $\zeta = \pm 1$  curve a double real root exists of magnitude  $\mp \omega_n$  denoted on the curve. This is because the  $\zeta = \pm 1$  line in the  $s$ -plane is the limiting case of complex conjugate roots coalescing on the real root axis as  $\zeta \rightarrow \pm 1$ .

## APPENDIX V

### RELATIONSHIPS BETWEEN ROOT LOCATIONS AND SYSTEM RESPONSE

The desired output established in Section 5.1 can be represented in the  $s$ -plane by the configuration of roots and zeros of the system function as shown in Figure 5.1.2. The next step in the process of establishing the necessary relationships is to relate quantitatively this configuration with the transient response. This relation is the general transient solution. Because of the complexity of this general solution, approximating relations have been formulated by Chu<sup>1</sup>. These approximating relations along with their significance are the subject of this appendix.

For a given linear feedback control system without transport lag (Figure 4.1.1 with  $T=0$ ) the system transfer function  $\frac{C}{R}(s)$  is

$$\frac{C}{R}(s) = \frac{G(s)}{1 + G(s)} = K \frac{N(s)}{F(s)} \quad (V.1)$$

where

$$N(s) = \prod_{j=1}^m (s - z_j), \quad F(s) = \prod_{k=1}^n (s - q_k)$$

In this expression it is assumed no multiple roots exist and the order of  $N(s)$  is smaller than that of  $F(s)$ . These two assumptions are true in most applications, and in the case of systems with transport lag in the

---

<sup>1</sup>The material contained in this appendix is a slightly modified version of a portion of a derivation contained in Reference 3.

forward loop the existence of the term  $\epsilon^{sT}$  in  $F(s)$  (see equation 4.1.1) guarantees that the order of  $N(s)$  is smaller than that of  $F(s)$ . Further, since the designer has control over the  $s$ -plane root locations it is a simple matter to ensure the existence of no multiple roots.

The values of  $z_j$  and  $q_k$  may either be real or complex. By using the Laplace inverse transformation, the transient solution of (V.1) for a unit step input with zero initial conditions may be expressed as

$$c(t) = K \frac{N(0)}{F(0)} + \sum_{k=1}^n K \frac{N(q_k)}{q_k F'(q_k)} \epsilon^{q_k t} \quad (V.2)$$

If the complex roots are combined, it may be written as

$$c(t) = K \frac{N(0)}{F(0)} + \sum_{q_k = \text{real}}^n \frac{KN(q_k)}{q_k F'(q_k)} \epsilon^{q_k t} + \sum_{q_k = \sigma_k + j\omega_k}^n 2 \left| \frac{KN(q_k)}{q_k F'(q_k)} \right| \epsilon^{\sigma_k t} \cos \left[ \omega_k t + \frac{N(q_k)}{q_k} - \frac{1}{F'(q_k)} \right] \quad (V.3)$$

This is the general transient solution within the limits of the assumptions (note that for a system with transport lag equation (V.3) has an infinite number of terms). The output response is the *summation* of all real modes due to the real roots and of all complex modes due to complex roots in addition to a constant term. The following assumption is now made in order to reach a simple but practical result: It is assumed all the modes of (V.3) may be neglected except the first constant term and those due to



the pair of dominant roots. With such an assumption, equation (V.3) becomes approximately

$$c(t) \cong K \frac{N(0)}{F(0)} + 2 \left| K \frac{N(S_1)}{S_1 F'(S_1)} \right| \epsilon^{-\sigma_1 t} \cos \left[ \omega_1 t + \angle N(S_1) - \angle S_1 - \angle F'(S_1) \right] \quad (V.4)$$

where  $s_1 = -\sigma_1 \pm j\omega_1$  are the dominant roots. By differentiating the output with respect to time and equating the result to zero, the time to reach the peak of the first overshoot, called  $T_p$ , is found to be

$$T_p \text{ (peak time)} = \frac{1}{\omega_1} \left[ \frac{\pi}{2} - \angle N(S_1) + \angle F'(S_1) \right] \quad (V.5)$$

The amount of the first overshoot,  $M$ , is

$$M \text{ (peak overshoot)} = \frac{2\omega_1}{\sigma_1 + \omega_1} \left| \frac{KN(S_1)}{F'(S_1)} \right| \epsilon^{-\sigma_1 T_p} \quad (V.6)$$

obtained from the difference between the output at  $T_p$  and the steady state value of the output. Equations (V.5) and (V.6) are two approximate equations to be discussed below.

The *accuracy* of the assumption resulting in these two approximate equations can be estimated readily. A certain simple mode  $K_2 \epsilon^{-\sigma_2 t}$  is considered from the exact solution, equation (V.3). This mode will decay to 5 per cent of its initial value when  $t$  is equal to  $3/\sigma_2$ . If  $T_p$  is larger than this value, that is

$$T_p \geq \frac{3}{\sigma_2} \text{ or } \sigma_2 \geq \frac{3}{T_p} \quad (V.7)$$

the effect of this simple mode is small even though  $K_2$  may be reasonably

large. It has been shown [29] that the value of the coefficient  $K_2$  is small if this root  $s = -\sigma_2$  is not too close to the other roots, if no zero very close to the origin on the  $s$ -plane exists, or if a real zero is very close to this root. Thus, equation (V.7) shows the minimum value above which the approximate equations will give quite accurate results. It also may be applied to the case of a complex mode, where  $\sigma_2$  is then the real part of the complex roots. In case a certain mode must be accounted for, the magnitude of this mode at  $T_p$  can be evaluated from the proper term of the general equation (V.3) and can be added to the result of equation (V.6) as a second approximation.

Simple yet accurate relationships between the transient response and the chosen roots are now developed. The desired response (as shown in Figure 5.1.1) is specified by the following four quantities:

1) The settling time,  $T_s$ , the time at which the response reaches a certain percentage of its final value. A commonly accepted value for  $T_p$  is 2 per cent.

2) The number of oscillations,  $N$ , for the interval up to the settling time.

3) The peak time,  $T_p$ , the time to reach the peak of the first overshoot.

4) The peak overshoot,  $M$ , the amount of the first overshoot.

With these four quantities, together with the pattern of the chosen

root-configuration (Figure 5.1.2), the desired response is virtually known without its actual calculations. The first two quantities,  $T_s$ , and  $N$ , can be computed from the dominant pair of roots, which are  $-\sigma_1 \pm j\omega_1 = -\zeta_1 \omega_{n_1} \pm j\omega_{n_1} \sqrt{1 - \zeta_1^2}$ . The settling time is from (V.4)

$$T_s = \frac{4}{\sigma_1} = \frac{4}{\zeta_1 \omega_{n_1}} \quad (\text{V.8})$$

for a 2% deviation from the steady state value. The number of oscillations may be calculated approximately as follows

$$N = \frac{\text{settling time}}{\text{period of damped oscillations}} = \frac{2\omega_1}{\pi\sigma_1} = \frac{2}{\pi} \frac{\sqrt{1 - \zeta_1^2}}{\zeta_1} \quad (\text{V.9})$$

Solving for  $\zeta_1$  from the two right hand relationships above yields the useful result that

$$\zeta_1 = \frac{1}{\sqrt{1 + (\omega_1/\sigma_1)^2}} \quad (\text{V.10})$$

The third quantity,  $T_p$ , the time to reach the peak of the first overshoot, is calculated from the approximate equation (V.5). This can be expressed in the following form

$$T_p = \frac{1}{\omega_1} \left[ \pi/2 - (\text{sum of angles from zeros to the dominant root } -\sigma_1 + j\omega_1) + (\text{sum of angles from the other roots to the dominant root } -\sigma_1 + j\omega_1) \right] \quad (\text{V.11})$$

Thus, it may be concluded that zeros decrease  $T_p$  and additional roots increase  $T_p$ . If the system is known to be approximately second order

and without any zeros, then the peak time from equation (V.11) is

$$T_p = \frac{\pi}{\omega_1} \quad (V.12)$$

Because of the relation  $\omega_1 = \omega_{n_1} \sqrt{1 - \zeta_1^2}$ , another conclusion from equation (V.11) is the peak time is inversely proportional to the undamped natural frequency  $\omega_{n_1}$  of the dominant roots.

The last quantity,  $M$ , the amount of the first overshoot, is calculated from the approximate equation (V.6). It is the product of the following two terms

$$(a) \quad e^{-\sigma_1 T_p} \quad (\text{this quantity is always less than unity as } \sigma_1 \text{ and } T_p \text{ are positive)} \quad (V.13)$$

$$(b) \quad \frac{K}{\omega_{n_1}^2} \times \frac{(\text{product of distances from zeros to the dominant root } -\sigma_1 + j\omega_1)}{(\text{product of distance from all roots to the dominant root } -\sigma_1 + j\omega_1 \text{ excluding the distance between the two dominant roots})} \quad (V.14)$$

It is obvious from the first term (a) that the smaller the  $T_p$  the larger the  $M$ ; thus the choice of  $T_p$  and  $M$  requires a compromise. The effect of the second term (b) on the magnitude of  $M$  depends on  $K$ , usually a controller parameter to be chosen. For a zero displacement error system,  $K$  must have the following value (from equation (V.1)).

$$K = \frac{\prod_{k=1}^n q_k}{\prod_{j=1}^m Z_j} = \frac{(\text{product of distances from all roots to the origin})}{(\text{product of distances from all zeros to the origin})} \quad (V.15)$$

This is due to the fact that the output is equal to the input at steady state for a step input in such a system. By substituting equations (V.15) and (V.14) into (V.6), the result is

$$M = \frac{\text{(product of distances from all roots to the origin excluding distances from the two dominant roots to the origin)}}{\text{(product of distances from all roots to the dominant root } -\sigma_1 + j\omega_1 \text{ excluding the distance between the dominant roots)}} \times \quad (V.16)$$

$$\frac{\text{(product of distances from zeros to the dominant root } -\sigma_1 + j\omega_1 \text{)}}{\text{(product of distance from all zeros to origin)}} \times e^{-\sigma_1 T_p}$$

## REFERENCES

## REFERENCES

- [1] Bode, W. Hendrik, *Network Analysis and Feedback Amplifier Design*. New York: D. Van Nostrand Company, Inc., 1945.
- [2] Chu, Yaohan, "Feedback Control Systems with Dead-Time Lag or Distributed Lag by Root-Locus Method," *AIEE Transactions, Applications and Industry, Part II*, vol. 71, November, 1952, pp. 291-296.
- [3] \_\_\_\_\_, "Synthesis of Feedback Control Systems by Phase-Angle Loci," *AIEE Transactions, Applications and Industry, Part II*, vol. 71, November, 1952, pp. 330-338.
- [4] Courant, R., *Differential and Integral Calculus*, vol. I, Translated by E. J. McShane, New York: Interscience Publishers, Inc., Second edition, 1937, pg. 485.
- [5] Eisenberg, Lawrence, "Approximate Roots of  $n^{\text{th}}$  Order Polynomials," *IEEE Transactions on Automatic Control*, vol. AC-10, no. 3, July, 1965, pp. 354-356.
- [6] \_\_\_\_\_, "Stability of Linear Systems with Transport Lag," *IEEE Transactions on Automatic Control*, to be published in April, 1966.
- [7] Evans, W. R., "Analysis of Control Systems," *AIEE Transactions, Part II*, vol. 67, 1948, pp. 547-551.
- [8] Goldfarb, L. C., "On Some Non-Linear Phenomena in Regulatory Systems," *Avtomatika i Telemekhanika*, vol. 8, no. 5, 1947, pp. 349-383.
- [9] Hurwitz, A., "The Conditions Under which an Equation has only Roots with Negative Real Parts," *Mathematische Annalen*, vol. 46, 1895, pp. 273-284.
- [10] Kochenburger, R. J., "A Frequency Response Method for Analyzing and Synthesizing Contactor Servomechanisms," *AIEE Transactions, Part I*, vol. 69, 1950, pp. 270-284.
- [11] Kokotović, P. and D. D. Siljak, "The Sensitivity Problem in Continuous and Sampled-Data Linear Control Systems by Generalized Mitrović's Method," *IEEE Transactions on Applications and Industry*, vol. 83, no. 74, September, 1964, pp. 321-324.

- [12] Leonhard, A., "Relative Damping as a Criterion for Stability and as an Aid in Finding the Roots of a Hurwitz Polynomial," *Automatic and Manual Control--Papers Contributed to the Conference at Cranfield, 1951*, London: Butterworths Scientific Publications, 1952, pp.25-35.
- [13] Meerov, M. V., *Introduction to the Dynamics of Automatic Regulating of Electrical Machines*. Translated by J. S. Shapiro, London: Butterworths, 1961.
- [14] Miller, R. Aloysius, "Parameter Plane Analysis of Sampled Data Systems (With Extensions for Continuous System Applicability)," Ph.D. Thesis in Electrical Engineering, United States Naval Postgraduate School, Monterey, California, 1965, pp.29-36.
- [15] Mishkin, Eli and Ludwig Braun, Jr., *Adaptive Control Systems*. New York: McGraw-Hill Book Company, Inc., 1961, pp. 101-103.
- [16] Mitrović, Dusan, "Graphical Analysis and Synthesis of Feedback Control Systems I--Theory and Analysis," *AIEE Transactions, Applications and Industry, Part II*, vol. 77, 1958, pp. 476-487.
- [17] Mulligan, J. H. Jr., "The Effect of Pole and Zero Locations on the Transient Response of Linear Dynamic Systems," *Proceedings of the I. R. E.*, vol. 37, May, 1949, pp. 516-529.
- [18] Neimark, J. I., "About Determination of Parameter Values Which Insure Stability of Automatic Control Systems," *Avtomatika i Telemekhanika*, no. 3, 1948.
- [19] Numakura, T. and T. Miura, "A New Stability Criterion of Linear Servomechanisms by a Graphical Method," *AIEE Transactions, Applications and Industry, Part II*, vol. 76, March, 1957, pp. 40-48.
- [20] Nyquist, H., "Regeneration Theory," *Bell System Technical Journal*, vol. 11, 1932, pp. 126-147.
- [21] Oldenbourg, R. C. and H. Sartorius, *The Dynamics of Automatic Control*. Translated by H. L. Mason, New York: American Society of Mechanical Engineers, 1948.
- [22] Polak, E., "A Note on D-Decomposition Theory," *IEEE Transactions on Automatic Control*, vol. AC-9, no. 1, January, 1964, pp. 107-109.



- [23] Popov, E. P., *The Dynamics of Automatic Control Systems*. Reading, Massachusetts: Addison-Wesley Publishing Company, Inc., 1962, pp.436-444.
- [24] Routh, E. J., "Dynamics of a System of Rigid Bodies," *Adams Prize Essay*, London: MacMillan, 1877.
- [25] Siljak, D. D., "Generalization of Mitrović's Method," *IEEE Transactions on Applications and Industry*, vol. 83, no. 74, September, 1964, pp. 314-320.
- [26] \_\_\_\_\_, "Analysis and Synthesis of Feedback Control Systems in the Parameter Plane," *IEEE Transactions on Applications and Industry*, vol. 83, no. 75, November, 1964, pp. 449-466.
- [27] Smith, J. M. Otto, *Feedback Control Systems*. New York: McGraw-Hill Book Company, Inc., 1958.
- [28] Thaler, J. George and R. G. Brown, *Analysis and Design of Feedback Control Systems*. New York: McGraw-Hill Book Company, Inc., 1960.
- [29] Truxal, G. John, *Automatic Feedback Control Systems*. New York: McGraw-Hill Book Company, Inc., 1955.
- [30] Vishnegradski, I. A., "On Direct Action Regulators," *News of the St. Petersburg Technological Institute*, 1877. pp. 21-62.

## VITA

Lawrence Eisenberg was born in New York City, New York on June 9, 1933. He received his B.S. degree in Electrical Engineering from Fairleigh Dickinson University, Teaneck, New Jersey in 1960. In 1961 he received an M.S. degree in Mathematics from New York University, New York, N. Y. From 1960 to 1961 he was a Systems Engineer with the Systems Development Corporation, Paramus, New Jersey. From 1961 to 1965 he was an Instructor at the Newark College of Engineering, Newark, New Jersey. He has had summer positions as an electrical engineer with International Telegraph and Telephone Corporation, Nutley, New Jersey; General Precision Aerospace, Inc., Little Falls, New Jersey; and Electronics Associates Inc., Princeton, New Jersey.

Since June, 1965, he has been on a leave of absence from the Newark College of Engineering in order to carry out his doctoral dissertation research. This research was performed at the Newark College of Engineering with the support of a National Science Foundation Faculty Fellowship.